

# **Thaumasite Sulfate Attack in Cement Mortars Exposed to Sulfate and Chloride and Implications to Rebar Corrosion**



A thesis submitted for the degree of Doctor of Philosophy in the Faculty of Engineering of the University of Sheffield

**By:**

**Ashraf H M Abdalkader**

**Supervised by:**

**Dr Cyril Lynsdale & Dr John Cripps**

THE UNIVERSITY OF SHEFFIELD  
DEPARTMENT OF CIVIL AND STRUCTURAL ENGINEERING

**July 2014**

---

To

My Family

# **Declaration**

Ashraf Abdalkader certifies that all material contained within this document is his own work except where it is clearly referenced to others.

# Abstract

Although field cases reported the presence of chloride in situations in which concrete suffered from the thaumasite form of sulfate attack (TSA), few laboratory studies have been carried out into the impact of chloride ions on TSA. In fact the literature contains contradictory results with some studies indicating that chloride reduces TSA, while others show the opposite and, moreover, no published experimental data have been found that address the role of chloride ions on the extent of thaumasite formation, the effect of thaumasite formation on cement chloride binding capacity or chloride induced corrosion of steel reinforcement in conditions conducive to thaumasite formation. Thus, the aim of this study was to investigate these issues with respect to the performance of standard Portland Cement (PC) and Portland Limestone Cement (LF) mortars and other binders based on blends of PC with pulverised fuel ash (PFA) or ground granulated blast furnace slag (GGBS) that potentially may be more resistant to TSA. Siliceous fine aggregate and a water to binder ratio of 0.6 were used to cast specimens that, following curing, were exposed to various solutions containing sulfate and / or chlorides at 5°C and at approximately 20°C for a period of up to 630 days.

The performance of the samples was assessed by regular visual inspections and mass changes together with measurements of length, porosity and oxygen permeability. The pH and chemistry of the test solutions were monitored and the deterioration products were investigated using XRD, IRS and SEM/EDX techniques. The effect of chloride concentration on the solubility of calcite and gypsum was also investigated. Water soluble chloride was evaluated in order to measure free chloride of powdered samples taken from different depths into the specimens. Linear polarization resistance and visual observations were used to monitor the corrosion of steel reinforcement in the experiments and the degree of carbonation in selected specimens was also evaluated.

All specimens stored at 5°C, except those stored in the combined sulfate and 2.0% chloride solution, suffered from TSA, where the greatest deterioration occurred to LF mortars. The extent of thaumasite degradation was concentration sensitive, where damage was accelerated at 0.5% and mitigated at 2% in the conditions investigated, where this mitigation effect is attributed to pH increase, Friedel's salt deposition, increased gypsum solubility and reduced calcite solubility. At low concentrations, corrosion risk increases due to the reduction of chloride binding capacity of thaumasite-affected areas of the cement.

The use of slag and fly ash as cement replacements delayed sulfate attack, probably due to the consumption of calcium hydroxide and improved pore structure. However, mortars made with these cements and exposed to DS4 (BRE Ground aggressivity Class) magnesium sulfate at low temperature suffered conventional sulfate attack. The presence of chloride in solution led to further enhancement of sulfate resistance of fly ash mortars, probably due to the positive effect of high chloride binding capacity. However, it enhanced lime leaching in GGBS mortar which would provide more calcium ions required for gypsum precipitation. At high chloride concentration (2.0%) and due to high gypsum solubility, no gypsum was formed.

The non chloride binding capacity of thaumasite means that where TSA occurred, the reinforcement was increasingly vulnerable to damage. An additional implication of poor binding capacity of thaumasite is that because C-S-H can be

transformed to thaumasite, physically adsorbed chloride on C-S-H would be released into the pore solution which would tend to increase corrosion risk.

## **Acknowledgements**

First, I would like to express my deepest gratitude and love to my wife, Asma and my children Sharifa, Rana and Fadlalla for their patience.

I would also like to express my sincere gratitude to my supervisors Dr. Cyril Lynsdale and Dr. John Cripps for their guidance and friendship during my study.

My special thanks to all the technicians of the civil and structural engineering department at Sheffield University. I appreciate all the help and support given by my friends Jumma and Farhat, who helped and encouraged me to achieve my study. I would also like to acknowledge the help provided by Ruben Borg (University of Malta) who performed SEM/EDX determinations on some of the deteriorated materials. I would like to acknowledge the financial support provided by Ministry of Higher Education of Libya for this research.

Finally, I just want to thank my family in Libya for all the support given during this time.

# Contents

|  |            |
|--|------------|
| <b>Contents .....</b>                                  | <b>vi</b>  |
| <b>List of Tables.....</b>                             | <b>xi</b>  |
| <b>List of Figures .....</b>                           | <b>xii</b> |
| <b>List of Abbreviations and Nomenclature .....</b>    | <b>xx</b>  |
| <b>1. Introduction.....</b>                            | <b>1</b>   |
| <b>1.1 Background.....</b>                             | <b>1</b>   |
| <b>1.2 Research Questions:.....</b>                    | <b>3</b>   |
| <b>1.3 Aim and Objectives .....</b>                    | <b>4</b>   |
| <b>1.4 Structure of the thesis .....</b>               | <b>4</b>   |
| <b>2. Literature review.....</b>                       | <b>6</b>   |
| <b>2.1 Introduction .....</b>                          | <b>6</b>   |
| <b>2.2 Sulfate attack of concrete .....</b>            | <b>6</b>   |
| <b>2.3 Conventional form of sulfate attack.....</b>    | <b>6</b>   |
| <b>2.4 Thaumasite form of sulfate attack.....</b>      | <b>7</b>   |
| <b>2.5 Mechanism of thaumasite formation .....</b>     | <b>8</b>   |
| <b>2.6 Factors affecting thaumasite formation.....</b> | <b>9</b>   |
| 2.6.1 Source of silicate .....                         | 9          |
| 2.6.2 Source of sulfate .....                          | 9          |
| 2.6.3 Source of carbonate.....                         | 9          |
| 2.6.4 Source of water .....                            | 10         |
| 2.6.5 Effect of temperature.....                       | 10         |
| 2.6.6 The role of pH.....                              | 11         |
| <b>2.7 Degradation mode of thaumasite .....</b>        | <b>12</b>  |
| <b>2.8 Identifications of thaumasite .....</b>         | <b>13</b>  |
| <b>2.9 The role of chloride in sulfate attack.....</b> | <b>14</b>  |

|             |  |           |
|-------------|--|-----------|
| 2.9.1       | Conventional form of sulfate attack .....  | 14        |
| 2.9.2       | Thaumasite form of sulfate attack .....  | 15        |
| <b>2.10</b> | <b>Using slag and fly ash to avoid or mitigate thaumasite sulfate attack</b>                               | <b>16</b> |
| 2.10.1      | Pulverized Fly Ash (PFA) .....   | 16        |
| 2.10.2      | Ground granulated blast furnace slag (GGBS) .....  | 17        |
| <b>2.11</b> | <b>Chloride transport into concrete subjected to sulfate attack.....</b>                                   | <b>18</b> |
| <b>2.12</b> | <b>Chloride binding capacity of cement .....</b>   | <b>19</b> |
| <b>2.13</b> | <b>Factors affecting chloride binding .....</b>  | <b>19</b> |
| 2.13.1      | Chloride concentration .....   | 19        |
| 2.13.2      | Supplementary cementitious materials .....   | 19        |
| 2.13.3      | Temperature.....   | 20        |
| <b>2.14</b> | <b>Chloride binding capacity of cement subjected to sulfate attack .....</b>                               | <b>20</b> |
| <b>2.15</b> | <b>Chloride induced corrosion of steel rebars in concrete/mortar<br/>subjected to sulfate attack .....</b> | <b>21</b> |
| 2.15.1      | Background .....   | 21        |
| 2.15.2      | Laboratory studies .....   | 22        |
| 2.15.3      | Field investigations related to TSA .....  | 23        |
| <b>2.16</b> | <b>Concluding remarks .....</b>  | <b>24</b> |
| <b>3.</b>   | <b>Experimental programme .....</b>  | <b>25</b> |
| <b>3.1</b>  | <b>Introduction .....</b>  | <b>25</b> |
| <b>3.2</b>  | <b>Materials.....</b>  | <b>26</b> |
| 3.2.1       | Cement (CEMI 52.5N) .....  | 26        |
| 3.2.2       | Limestone Filler (LF) .....  | 26        |
| 3.2.3       | Ground Granulated Blast Furnace Slag (GGBS).....   | 26        |
| 3.2.4       | Pulverized Fly Ash (PFA) .....   | 26        |
| 3.2.5       | Aggregate .....  | 26        |
| 3.2.6       | Water .....  | 26        |
| <b>3.3</b>  | <b>Mixing and casting of mortars .....</b>   | <b>27</b> |



|            |  |           |
|------------|--|-----------|
| <b>3.4</b> | <b>Test solutions .....</b>  | <b>29</b> |
| <b>3.5</b> | <b>Curing regime .....</b>   | <b>29</b> |
| 3.5.1      | Initial curing .....   | 29        |
| 3.5.2      | Long term exposure to sulfate/chloride solutions .....   | 29        |
| <b>3.6</b> | <b>Test method.....</b>  | <b>31</b> |
| 3.6.1      | Visual observations assessment .....   | 31        |
| 3.6.2      | Mass measurement .....   | 31        |
| 3.6.3      | Length change.....   | 31        |
| 3.6.4      | Sample preparation for X-ray diffraction (XRD) and infrared spectroscopy (IRS) .....               | 32        |
| 3.6.5      | X-ray diffraction (XRD) .....  | 32        |
| 3.6.6      | Infrared spectroscopy (IRS).....   | 32        |
| 3.6.7      | Scanning electron microscopy (SEM) and energy dispersive X-ray analysis (EDX).....                 | 33        |
| 3.6.8      | Chemical analysis of test solutions .....  | 34        |
| 3.6.9      | pH measurement of test solutions .....   | 34        |
| 3.6.10     | Calcite and gypsum solubility .....  | 34        |
| 3.6.11     | Open porosity.....   | 35        |
| 3.6.12     | Oxygen permeability .....  | 35        |
| 3.6.13     | Chloride content and diffusion .....   | 36        |
| 3.6.14     | Carbonation depth by phenolphthalein.....  | 38        |
| 3.6.15     | Corrosion evaluation .....   | 38        |
| A.         | Linear polarisation technique.....   | 39        |
| B.         | Visual assessment of steel surface area .....  | 41        |
| <b>4.</b>  | <b>Performance of cement mortars subjected to sulfate and chloride exposure at 5 and 20°C.....</b> | <b>42</b> |
| <b>4.1</b> | <b>Introduction .....</b>  | <b>42</b> |
| <b>4.2</b> | <b>Visual observation assessment .....</b>   | <b>42</b> |

|             |   |            |
|-------------|---|------------|
| 4.2.1       | Visual assessment after 90 days.....  | 43         |
| 4.2.2       | Visual assessment after 180 days.....   | 45         |
| 4.2.3       | Visual assessment after 360 days.....   | 49         |
| 4.2.4       | Visual assessment after 630 days.....   | 50         |
| <b>4.3</b>  | <b>Mass change up to 630 days.....</b>  | <b>53</b>  |
| <b>4.4</b>  | <b>Length change up to 630 days.....</b>  | <b>58</b>  |
| <b>4.5</b>  | <b>Mineralogy of deteriorated materials.....</b>  | <b>59</b>  |
| 4.5.1       | X-ray diffraction (XRD).....  | 59         |
| 4.5.2       | Analysis by infrared spectroscopy.....  | 73         |
| <b>4.6</b>  | <b>Scanning electron microscopy (SEM) and energy dispersive X-ray (EDX) analysis.....</b>                             | <b>79</b>  |
| <b>4.7</b>  | <b>Chemical analysis of test solutions.....</b>   | <b>104</b> |
| <b>4.8</b>  | <b>pH measurement of test solutions:.....</b>   | <b>118</b> |
| <b>4.9</b>  | <b>The effect of chloride concentration on solubility of calcite and gypsum.....</b>                                  | <b>125</b> |
| <b>4.10</b> | <b>Summary.....</b>   | <b>127</b> |
| <b>5.</b>   | <b>Corrosion behaviour of steel rebars embedded in cement mortars subjected to sulfate and chloride exposure.....</b> | <b>132</b> |
| <b>5.1</b>  | <b>Introduction.....</b>  | <b>132</b> |
| <b>5.2</b>  | <b>Visual assessment of mortars after 900 days of exposure.....</b>   | <b>132</b> |
| <b>5.3</b>  | <b>Open porosity and Oxygen permeability measurements.....</b>  | <b>135</b> |
| <b>5.4</b>  | <b>Determination of carbonation depth.....</b>  | <b>138</b> |
| <b>5.5</b>  | <b>Chloride diffusion into mortars subjected to sulfate and chloride exposure.....</b>                                | <b>140</b> |
| 5.5.1       | Chloride content:.....  | 140        |
| 5.5.2       | Chloride diffusion:.....  | 147        |
| <b>5.6</b>  | <b>X-ray diffraction of steel-mortar interface samples.....</b>   | <b>152</b> |
| <b>5.7</b>  | <b>SEM/EDX of steel-mortar interface samples.....</b>   | <b>155</b> |
| <b>5.8</b>  | <b>Linear Polarization Resistance (LPR).....</b>  | <b>158</b> |

|  |            |
|--|------------|
| <b>5.9 Visual assessment of steel rebar .....</b>  | <b>164</b> |
| <b>5.10 Summary .....</b>  | <b>167</b> |
| <b>6. TSA and related corrosion risk in the presence of chloride: Overall</b>                              |            |
| <b>Discussions .....</b>   | <b>171</b> |
| <b>6.1 TSA in presence of chloride: .....</b>  | <b>171</b> |
| 6.1.1 Diffusion of sulfate, chloride, magnesium ions, CH leaching and pH change: 172                       |            |
| 6.1.2 Friedel's salt formation .....   | 173        |
| 6.1.3 Gypsum formation .....   | 174        |
| 6.1.4 C-S-H decalcification .....  | 175        |
| 6.1.5 CaCO <sub>3</sub> solubility .....   | 176        |
| 6.1.6 Thaumasite formation.....  | 176        |
| <b>6.2 The effect of TSA on chloride binding capacity of cement and related corrosion risk.....</b>        | <b>181</b> |
| <b>6.3 The use of fly ash and slag as cement replacement to prevent TSA in presence of chloride: .....</b> | <b>183</b> |
| <b>7. Conclusions and recommendations.....</b>   | <b>186</b> |
| <b>7.1 Overall Conclusions.....</b>  | <b>186</b> |
| <b>7.2 Implications of Results for Research and Engineering.....</b>                                       | <b>189</b> |
| <b>7.3 Recommendations for Future Work .....</b>   | <b>190</b> |
| <b>References .....</b>  | <b>192</b> |
| <br>   |            |
| <b>Appendix .....</b>  | <b>250</b> |

## List of Tables

|   |     |
|---|-----|
| Table 2.1. Chemical composition of ettringite and thaumasite (Eden, 2003).....  | 14  |
| Table 3.1. Chemical and mineralogical composition of cement, LF, PFA and GGBS (XRF analyses performed at Leicester University)..... | 27  |
| Table 3.2 Chemical composition and physical properties of concrete sand, as provided by the supplier.....                           | 27  |
| Table 3.3. Mortar mixtures.....   | 28  |
| Table 3.4. Chemical compositions of steel rebar (wt. %), as provided by the supplier. ....  | 28  |
| Table 3.5 Compositions of test solutions. ....  | 29  |
| Table 4.1. Summary of visual assessment for 50mm mortar cubes.....  | 43  |
| Table 4.2. Peaks for various phases.....  | 60  |
| Table 5.1. Summary of air permeability and open porosity measurements. ....   | 136 |
| Table 5.2. Summary of chloride contents at different depths. ....   | 141 |
| Table 5.3. Chloride diffusion coefficient and surface concentrations (least squares best fit). ....                                 | 148 |
| Table 5.4. Variations in corrosion measurements. ....   | 159 |

## List of Figures

|  |    |
|--|----|
| Figure 3.1. Schematic view of experimental programme.....  | 25 |
| Figure 3.2. Mortar specimens in air curing (~20°C-room temperature).....                                   | 30 |
| Figure 3.3 Containers in 5°C temperature tanks. ....   | 30 |
| Figure 3.4 Containers at 20°C in laboratory room.....  | 31 |
| Figure 3.5. Schematic diagram for diffusion. ....  | 37 |
| Figure 3.6 Grinding equipment used to collect powders.....   | 38 |
| Figure 3.7. Corrosion equipment. ....  | 40 |
| Figure 3.8. Set up of corrosion measurements by LPR. ....  | 41 |
| Figure 4.1. 20mm mortar cubes of CEMI-LF mortar stored for 74 days in SC5 at 5°C. ....                     | 44 |
| <b>Figure 4.2.</b> 20mm cubes of CEMI and CEMI-LF stored for 90 days at 5°C.....                           | 45 |
| Figure 4.3. CEMI and CEMI-LF mortar stored for 180 days at 5°C.....  | 47 |
| Figure 4.4. General view of 20mm of CEMI-LF specimens stored for 180 days at 5°C. ....                     | 48 |
| <b>Figure 4.5.</b> 20 mm CEMI-PFA mortar cubes stored for 180 days in S at 5°C. ....                       | 48 |
| <b>Figure 4.6.</b> 20mm CEMI-GGBS mortar cubes stored for 180 days in SC5 at 5°C..                         | 49 |
| <b>Figure 4.7.</b> CEMI and CEMI-LF mortar specimens stored for 360 days at 5 and 20°C. ....               | 50 |
| <b>Figure 4.8.</b> CEMI and CEM-LF mortar specimens stored for 630 days in solutions at 5 and 20°C.....    | 51 |
| <b>Figure 4.9.</b> PFA and GGBS mortar specimens stored for 630 days in solutions at 5 and 20°C.....       | 52 |
| <b>Figure 4.10.</b> General view of CEMI and CEMI-LF mortar in containers stored for 630 days at 5°C. .... | 53 |
| <b>Figure 4.11.</b> Mass changes for CEMI mortar cubes stored 630 days at 5°C.....                         | 54 |
| <b>Figure 4.12.</b> Mass changes for CEMI-LF mortar cubes stored 630 days at 5°C....                       | 55 |
| Figure 4.13. Mass changes for CEMI mortar cubes stored for 630 days at 20°C...55                           |    |
| Figure 4.14. Mass changes for CEMI-LF mortar cubes stored 630 days at 20°C...56                            |    |
| <b>Figure 4.15.</b> Mass changes for CEMI-PFA mortar cubes stored 630 days at 5°C. .56                     |    |
| <b>Figure 4.16.</b> Mass changes for CEMI-PFA mortar cubes stored 630 days at 20°C. ....                   | 57 |

|  |    |
|--|----|
| Figure 4.17. Mass changes for CEMI-GGBS mortar cubes stored 630 days at 5°C.   | 57 |
| .....  |    |
| <b>Figure 4.18.</b> Mass changes for CEMI-GGBS mortar cubes stored 630 days at 20°C.   | 58 |
| .....  |    |
| Figure 4.19.Length change variations for CEMI and CEMI-LF mortars stored for 630 days at 5 and 20°C.   | 59 |
| .....  |    |
| Figure 4.20. XRD patterns of CEMI samples stored for 630 days at 5°C.  | 62 |
| .....  |    |
| Figure 4.21.XRD patterns of CEMI-LF samples stored for 630 days at 5°C.  | 63 |
| .....  |    |
| Figure 4.22. XRD patterns of CEMI samples stored for 630 days at 20°C.   | 63 |
| .....  |    |
| Figure 4.23. XRD patterns of CEMI-LF samples stored for 630 days at 20°C.  | 64 |
| .....  |    |
| Figure 4.24. XRD patterns for degraded surface and sound core samples for CEMI-LF specimens stored 630 days in sulfate only solution at 5°C. | 65 |
| .....  |    |
| Figure 4.25. XRD patterns for degraded surface and sound core samples for CEMI-LF specimens stored 630 days in SC5 at 5°C.                   | 65 |
| .....  |    |
| Figure 4.26. XRD patterns for sound surface and core samples for CEMI-LF specimens stored 630 days in SC20 at 5°C.                           | 66 |
| .....  |    |
| Figure 4.27. XRD patterns for CEMI-PFA samples stored for 630 days at 5°C.   | 67 |
| .....  |    |
| Figure 4.28. XRD patterns for CEMI-PFA samples stored for 630 days at 20°C.  | 68 |
| .....  |    |
| Figure 4.29.XRD patterns for CEMI-GGBS samples stored for 630 days at 5°C.   | 70 |
| .....  |    |
| Figure 4.30. XRD patterns for CEMI-GGBS samples stored for 630 days at 20°C.   | 70 |
| .....  |    |
| <b>Figure 4.31.</b> XRD patterns for CEMI-PFA samples stored for 180 days at 5°C.  | 72 |
| .....  |    |
| Figure 4.32. XRD patterns for CEMI-GGBS samples stored for 180 days at 5°C.  | 73 |
| .....  |    |
| Figure 4.33. Infrared spectra for CEMI degraded samples at 5°C.  | 75 |
| .....  |    |
| Figure 4.34. Infrared spectra for CEMI-LF degraded samples stored at 5°C.  | 75 |
| .....  |    |
| Figure 4.35. Infrared spectra for CEMI and CEMI-LF surface samples stored in SC20 at 5°C.  | 76 |
| .....  |    |
| Figure 4.36.Infrared spectra for surface samples of CEMI-LF stored at 20°C.  | 76 |
| .....  |    |
| Figure 4.37. IR spectra for CEMI-PFA sample stored 180 days in sulfate only solution at 5°C.   | 78 |
| .....  |    |
| Figure 4.38. IR spectra for CEM-GGBS sample stored 180 days in sulfate only solution at 5°C.   | 78 |
| .....  |    |
| Figure 4.39. IR spectra for CEMI-GGBS sample stored 180 days in SC5 at 5°C.  | 79 |
| .....  |    |
| Figure 4.40. Morphology of degraded surface of CEMI-LF mortar stored 360 days in sulfate only solution at 5°C.                               | 80 |
| .....  |    |

|   |    |
|---|----|
| Figure 4.41. Morphology of degraded surface of CEMI-LF mortar stored 360 days in SC5 at 5°C.....  | 80 |
| Figure 4.42. Morphology of degraded surface of CEMI-LF mortar stored 360 days in SC10 at 5°C..... | 80 |
| Figure 4.43. EDX of the needles (thaumasite-ettringite solid solution) in Figure 4.41.....        | 80 |
| Figure 4.44. SEM image of CEMI sample stored 450 days in sulfate only solution.....               | 81 |
| Figure 4.45. EDX of cracked light grey area (with Al:Si >1) in Figure 4.44.....                   | 82 |
| Figure 4.46. EDX of dark grey area (with Al: Si <1) in Figure 4.44.....                           | 82 |
| Figure 4.47. EDX of light grey area (gypsum) in Figure 4.44.....                                  | 82 |
| Figure 4.48. SEM image of CEMI-LF sample stored 450 days in sulfate only solution.....            | 83 |
| Figure 4.49. EDX of point shown in Figure 4.48.....   | 83 |
| Figure 4.50. SEM image of CEMI-LF sample stored for 450 days in SC5.....                          | 85 |
| Figure 4.51. Detail 1 in Figure 4.50.....   | 85 |
| Figure 4.52. Details 2 (Thaumasite needles) in Figure 4.51.....                                   | 85 |
| Figure 4.53. EDX of dark grey area in Figure 4.51.....  | 85 |
| Figure 4.54. SEM image of CEMI sample stored 450 days in SC5.....                                 | 86 |
| Figure 4.55. SEM image of CEMI sample stored for 450 days in SC5.....                             | 86 |
| <b>Figure 4.56.</b> EDX of (Thaumasite-ettringite solid solution) in Figure 4.54.....             | 86 |
| Figure 4.57. EDX of (Mg-C-S-H) in Figure 4.55.....  | 86 |
| Figure 4.58. SEM image of CEMI sample stored 450 days in SC10.....                                | 87 |
| Figure 4.59. EDX of thaumasite -ettringite solid solution in Figure 4.58.....                     | 87 |
| Figure 4.60. EDX of Friedel's salt in Figure 4.58.....  | 87 |
| Figure 4.61. SEM image of CEMI-LF sample stored 450 days in SC10.....                             | 88 |
| Figure 4.62. EDX for the point in Figure 4.61.....  | 88 |
| Figure 4.63. SEM image of CEMI sample stored 450 days in SC20.....                                | 89 |
| Figure 4.64. EDX for 2 in Figure 4.63.....  | 89 |
| Figure 4.65. EDX Friedel's salt in Figure 4.63.....   | 89 |
| Figure 4.66. SEM image of CEMI-LF sample stored 450 days in SC20.....                             | 90 |
| Figure 4.67. EDX of cracked material in Figure 4.66.....  | 90 |
| Figure 4.68. EDX of Friedel's salt in Figure 4.66.....  | 90 |
| Figure 4.69. SEM image of CEMI-LF sample stored 630 days in sulfate only solution at 20°C.....    | 91 |

|  |     |
|--|-----|
| Figure 4.70. Detail 1 in Figure 4.69.....  | 92  |
| Figure 4.71. EDX of cracked material in Figure 4.70. ....  | 92  |
| Figure 4.72. SEM image of degraded CEMI-LF sample stored in 630 days in SC5 at 20°C. ....                    | 92  |
| Figure 4.73. Detail 1 in Figure 4.72.....  | 92  |
| Figure 4.74. EDX of dark grey area in Figure 4.72.....   | 92  |
| Figure 4.75. SEM image of CEMI-LF sample stored 630 days in SC20 at 20°C.....                                | 93  |
| Figure 4.76. EDX of Friedel's salt in Figure 4.75.....   | 93  |
| Figure 4.77. SEM image of CEMI-PFA sample stored 630 days in sulfate only solution at 5°C. ....              | 95  |
| Figure 4.78. EDX of cracked material in Figure 4.77. ....  | 95  |
| Figure 4.79. SEM image of CEMI-PFA sample stored 630 days in SC5 at 5°C. ....                                | 95  |
| Figure 4.80. EDX of dark area (Mg rich phase) in Figure 4.79.....  | 95  |
| Figure 4.81. SEM image of CEMI-PFA sample stored 630 days in SC20 at 5°C. ...                                | 96  |
| Figure 4.82. EDX of dark grey area (Mg rich phase) in Figure 4.81. ....                                      | 96  |
| Figure 4.83. SEM image of CEMI-GGBS sample stored 630 days in sulfate only solution at 5°C.....              | 98  |
| Figure 4.84. EDX of dark grey area in Figure 4.83.....   | 98  |
| Figure 4.85. EDX of light grey area (gypsum) in Figure 4.83. ....  | 98  |
| Figure 4.86. SEM image of CEMI-GGBS sample stored 630 days in SC5 at 5°C. ..                                 | 99  |
| Figure 4.87. EDX of 1 (Cracked area) in Figure 4.86.....   | 99  |
| Figure 4.88. EDX of 2 (C-S-H) gel with Ca/Si =0.5) in Figure 4.86. ....                                      | 99  |
| Figure 4.89. SEM image of CEMI-GGBS sample stored 630 days in SC20 at 5°C. ....                              | 100 |
| Figure 4.90. EDX of 1 in Figure 4.89. ....   | 100 |
| Figure 4.91. EDX of 2 in Figure 4.89. ....   | 100 |
| Figure 4.92. SEM of CEMI-GGBS sample stored 180 days in sulfate only at 5°C. ....                            | 102 |
| Figure 4.93. EDX of 1 in Figure 4.92.....  | 102 |
| Figure 4.94. EDX of 2 in Figure 4.92.....  | 102 |
| Figure 4.95. SEM images of CEMI-GGBS samples stored 180 days in SC5 at 5°C. ....                             | 103 |
| Figure 4.96. EDX of prismatic crystals and light grey area around aggregate particles in Figure 4.95-D. .... | 104 |
| Figure 4.97. EDX of dark area (M-S-H) in Figure 4.95-D.....  | 104 |



|  |     |
|--|-----|
| Figure 4.98. Variation of sulfate ion in test solutions at 5°C. ....   | 106 |
| Figure 4.99. Variation of calcium ion in test solution at 5°C. ....  | 107 |
| Figure 4.100. Variation of magnesium ion in test solution at 5°C. ....   | 107 |
| Figure 4.101. Variation of chloride concentration in composite solutions at 5°C.<br>.....  | 108 |
| Figure 4.102. Variation of sulfate ion in test solutions at 20°C. ....   | 109 |
| Figure 4.103. Variation of calcium ion in test solutions at 20°C.....  | 110 |
| Figure 4.104. Variation in magnesium ion in test solutions at 20°C.....  | 110 |
| Figure 4.105. Variation of chloride concentration in test solutions at 20°C. ....  | 111 |
| Figure 4.106. Concentration of sulfate, magnesium and calcium in CEMI solutions<br>after 180 days at 5 and 20C. ....   | 112 |
| Figure 4.107. Variation of calcium level in CEMI-LF solutions stored 180 days at<br>5°C. ....  | 113 |
| <b>Figure 4.108.</b> Variation of sulfate level in CEMI-LF solutions stored for 180 days<br>at 5°C. ....   | 114 |
| Figure 4.109. Variation of magnesium level of CEMI-LF solutions stored 180 days<br>at 5°C. ....  | 114 |
| Figure 4.110. Concentration of sulfate, magnesium and calcium ions in CEMI-LF<br>solutions stored 180 days at 20°C. ....   | 115 |
| Figure 4.111. Variation of sulfate, magnesium and calcium ions in CEMI-GGBS<br>solutions after 180 days at 5°C. ....   | 116 |
| Figure 4.112. Variation of sulfate, magnesium and calcium ions in CEMI-GGBS<br>solutions after 180 days at 20°C. ....  | 116 |
| Figure 4.113. Variation of sulfate, magnesium and calcium ions in CEMI-PFA<br>solutions after 180 days at 5°C. ....  | 117 |
| Figure 4.114. Variations of sulfate, magnesium and calcium ions in CEMI-PFA<br>solutions after 180 days at 20°C. ....  | 118 |
| Figure 4.115. pH change in CEMI-LF stored for 180 days at 5°C. ....  | 120 |
| Figure 4.116. pH change in CEMI-LF stored for 180 days at 20°C. ....   | 121 |
| Figure 4.117. pH change in CEMI-GGBS solutions stored for 180 days at 5°C...   | 123 |
| Figure 4.118. pH change of CEMI-GGBS solutions stored for 180 days at 20°C.  | 123 |
| Figure 4.119. pH change in CEMI-PFA solutions stored for 180 days at 5°C. ....   | 124 |
| Figure 4.120. pH change of CEMI-PFA solutions stored for 180 days at 20°C. ...   | 125 |
| Figure 4.121. Calcium ion levels of CaCO <sub>3</sub> -NaCl-MgSO <sub>4</sub> -H <sub>2</sub> O-CO <sub>2</sub> and CaSO <sub>4</sub> -NaCl-<br>MgSO <sub>4</sub> -H <sub>2</sub> O-CO <sub>2</sub> schemes at 5°C. .... | 126 |

|   |     |
|---|-----|
| <b>Figure 5.1.</b> Mortar specimens stored for 900 days in SC5 at 5°C. ....   | 133 |
| Figure 5.2. Mortar specimens stored 900 days in SC5 at 20°C.....  | 133 |
| Figure 5.3. Mortar specimens stored for 900 days in SC20 at 5°C. ....   | 134 |
| Figure 5.4. Mortar specimens stored for 900 days in SC20 at 20°C.....   | 134 |
| Figure 5.5. Degraded part of CEMI mortar at 5°C shown in Figure 5.1.....  | 135 |
| Figure 5.6. Drilled core for permeability test after 900 days of exposure. ....   | 137 |
| Figure 5.7. Variation in oxygen permeability for mortar samples made with<br>different binders.....   | 137 |
| Figure 5.8. Changes of open porosity for mortars stored in SC5 at 5°C. ....   | 138 |
| Figure 5.9. Open porosity vs. oxygen permeability for mortars with different<br>binders. ....   | 138 |
| Figure 5.10. Typical treated mortar by phenolphthalein solution. ....   | 140 |
| Figure 5.11. Chloride contents for CEMI mortars stored 90 and 270 days at 5°C.<br>.....   | 143 |
| Figure 5.12. Chloride contents for CEMI mortars stored 90 and 270 days at 20°C.<br>.....  | 143 |
| Figure 5.13. Chloride contents for CEMI-LF mortars stored 90 and 270 days at<br>5°C. ....   | 144 |
| Figure 5.14. Chloride contents for CEMI-LF mortars stored 90 and 270 days at<br>20°C. ....  | 144 |
| Figure 5.15. Chloride contents for CEMI-PFA mortars stored 90 and 180 days at<br>5°C. ....  | 145 |
| Figure 5.16. Chloride contents for CEMI-PFA mortars stored 90 and 180 days at<br>20°C. ....   | 145 |
| Figure 5.17. Chloride contents for CEMI-GGBS mortars stored 90 and 180 days at<br>5°C. ....   | 146 |
| Figure 5.18. Chloride contents for CEMI-GGBS mortars stored 90 and 180 days at<br>20°C. ....  | 146 |
| Figure 5.19. Chloride profile for CEMI mortars stored 90 days in SC20 at 5°C...   | 147 |
| Figure 5.20. Chloride diffusion coefficients for mortars with different binder. ....  | 148 |
| Figure 5.21. Chloride diffusion coefficient for CEMI and CEMI-LF mortars stored<br>90 and 270 days in chloride only (C20) and composite sulfate and 2.0% chloride<br>(SC20) solutions at 5 and 20°C. .... | 150 |

Figure 5.22. Chloride diffusion coefficient for CEMI-PFA mortars stored for 90 and 180 days in chloride only (C20) and composite sulfate and 2.0% chloride (SC20) solutions at 5 and 20°C..... 151

Figure 5.23. Chloride diffusion coefficient for CEMI-GGBS mortars stored in chloride only (C20) and composite sulfate and 2.0% chloride (SC20)..... 152

Figure 5.24. XRD pattern for CEMI-LF interface samples stored in SC5 at 5°C (Top, red) and 20°C (Bottom, blue). ..... 153

Figure 5.25. XRD pattern for CEMI-PFA interface samples stored in SC5 at 5 °C (Top) and 20°C (Bottom). ..... 154

Figure 5.26. XRD patterns for CEMI-GGBS interface samples stored in SC5 at 5 °C (Top) and 20°C (Bottom). ..... 155

Figure 5.27. SEM image for SC5 steel-mortar interface sample stored 900 days at 5°C. .... 156

Figure 5.28. Detail 1 in Figure 5.27..... 157

Figure 5.29. EDX for 1 (Iron oxide) in Figure 5.27. .... 157

Figure 5.30. EDX for 2 in Figure 5.27..... 157

Figure 5.31. SEM image for SC5 interface sample after 900 days at 20°C. .... 158

Figure 5.32. Variations in corrosion current densities for steel rebars in CEMI and CEMI-LF mortars stored in SC5 and SC20 at 5 and 20°C..... 161

Figure 5.33. Corrosion current density ( $I_{corr}$ ) vs. diffusion coefficient (D) for CEMI and CEMI-LF specimens stored in SC20 at 5 and 20°C (Diffusion was calculated after 270 days of exposure, whereas corrosion was measured after 900 days)... 162

Figure 5.34. Variations of corrosion current densities for steel rebars in CEMI-PFA and CEMI-GGBS mortars stored in SC5 at 5 and 20°C..... 163

Figure 5.35. Variations of corrosion current densities for steel rebars in CEMI-PFA and CEMI-GGBS mortars stored in SC20 at 5 and 20°C..... 164

Figure 5.36. Surface of steel bars in mortar specimens stored 900 days in SC5 at 5°C. .... 165

Figure 5.37. Surface of steel bars in mortar specimens stored 900 days in SC5 at 20°C. .... 166

Figure 5.38. Surface of steel bars in mortar specimens stored 900 days in SC20 at 5°C ..... 166

Figure 5.39. Surface of steel bars in mortar specimens stored 900 days in SC20 at 20°C ..... 167

Figure 6.1. Evaluation of damage degree as indicated by visual appearance of mortar specimens. [0= No visible damage, 1= minor cracking to corners and edges, 2= moderate damage at corners and edges, 3= severe attack at corners, 4= cracking and spalling, 5= swelling of surfaces, and 6=extensive cracking and swelling].....179

Figure 6.2. Effect of chloride level on initial pH change and later severity of TSA of CEMI-LF stored 630 days in solutions at 5°C. ....179

Figure 6.3. Scheme for sulfate interaction between limestone cement components and magnesium sulfate solution at 5°C (A modified schematic proposed by Bonen and Cohen (1992)).....180

Figure 6.4. Scheme for sulfate and chloride interaction between limestone cement components and composite sulfate and 0.5% chloride solution at 5°C. ....180

Figure 6.5. Scheme for sulfate and chloride interaction between limestone cement components and composite sulfate and 2.0% chloride at 5°C. ....181

Figure 6.6. Severity of TSA (By mass loss) and relative peak hight of Friedel's salt (FS) in surface materials for CEMI-LF mortars stored 630 days at 5°C. (Scale of relative peak intensity for FS: 1= low or absence; 2=moderate; and 3= high). ....182

Figure 6.7. Calcium concentration in different solutions after 7 days exposure at 5°C. ....185

## List of Abbreviations and Nomenclature

|           |  |
|-----------|--|
| PFA       | Pulverized Fuel Ash                                    |
| GGBS      | Ground Granulated Blast furnace Slag                   |
| LF        | Limestone Filler                                       |
| W/B       | Water to binder ratio                                  |
| SEM       | Scanning electron microscopy                           |
| EDX       | Energy dispersive x-ray analysis                       |
| XRD       | X-ray diffraction                                      |
| XRF       | X-ray fluorescence                                     |
| IR        | Infra red spectroscopy                                 |
| DS4       | BRE ground aggressivity Class (Design Sulfate Class 4) |
| LPR       | Linear polarization resistance                         |
| TF        | Thaumasite formation                                   |
| TSA       | Thaumasite sulfate attack                              |
| CH        | Calcium hydroxide                                      |
| C-S-H     | Calcium silicate hydrate                               |
| CEMI-LF   | CEMI replaced by 10% LF                                |
| CEMI-PFA  | CEMI replaced by 50% PFA                               |
| CEMI-GGBS | CEMI replaced by 70% GGBS                              |
| OPC       | Ordinary Portland cement                               |
| S         | 0.6% sulfate only solution                             |
| SC5       | 0.6% sulfate plus 0.5% chloride solution               |
| SC10      | 0.6% sulfate plus 1.0% chloride solution               |
| SC20      | 0.6% sulfate plus 2.0% chloride solution               |
| C20       | 2.0% chloride only solution                            |
| FS        | Friedel's salt   |
| TEG       | Thaumasite Expert Group                                |
| BRE       | Building Research Establishment                        |
| SRPC      | Sulfate resistance Portland cement                     |
| ASTM      | American Society for Testing and Materials             |

# 1. Introduction

## 1.1 Background

Exposure of concrete structure components to external sulfates leads to deterioration owing to the formation of expansive phases, such as ettringite, gypsum and thaumasite, depending on the exposure conditions. The thaumasite form of sulfate attack (TSA) has been receiving great attention from researchers and engineers since it was discovered in a number of concrete bridge structures in the UK in 1998 (Thaumasite Expert Group, 1999). According to Crammond (2003) for thaumasite to form sulfate, calcium, carbonate and silicate in the presence of water are required in low temperature conditions (5 to 15°C). It is generally accepted that for extensive thaumasite formation to occur, low temperature conditions are necessary, various researchers, including Irassar et al. (2005), Martinez-Ramirez et al. (2011), Abubaker et al. (2013) and, Hartshorn et al. (2002) point out the possibility of its formation at higher temperature (e.g. 15-20°C). The main risk factors leading to TSA have been reported by the Thaumasite Expert Group (1999), established by the UK Government to consider the risks, diagnosis, remedial works and guidance on new construction, after identification of TSA in degraded foundation concrete of 10 motorway bridges on the M5 motorway near Cheltenham in the west of England in 1998.

TSA can lead to severe degradation of concrete. The deterioration can be much more severe than inflicted by the conventional form of sulfate attack. This is because as it is associated with the degradation of the calcium silicate hydrate (C-S-H) gel, the main binding phase of the cement (Macphee and Diamond, 2003, Glasser et al., 2008), particularly when sulfates are associated with the magnesium ions and low pH as both contribute to the decomposition of C-S-H (Hobbs, 2003).

There are two different proposed mechanisms leading to thaumasite formation, known as the direct route and the woodfordite route. In the direct route, thaumasite results from reactions between C-S-H, calcium sulfate, calcium carbonate and water (Heinz and Urbonas, 2003). In the woodfordite route (Bensted, 2003b), it is proposed that thaumasite forms as a result of reaction

between ettringite, C–S–H and carbonate ions in the presence of excess water. It has also been proposed that thaumasite formation can occur through the heterogeneous nucleation of thaumasite on the surface of ettringite when the disintegration of C–S–H takes place in cement paste (Köhler et al., 2006).

In recent years, the employment of limestone blended cements is gaining popularity due to their technical, economic, and environmental benefits. Many of the recent studies on this topic concluded that cementitious materials incorporating limestone filler are more susceptible to thaumasite attack due to the presence of carbonate ions. The damage of mortar and concrete made with Portland-limestone cement due to the formation of thaumasite during sulfate attack at low temperatures is well documented (Torres et al., 2003, Torres et al., 2006, Irassar, 2009b).

Several field cases (Slater et al., 2003, Eden, 2003) reported the presence of chloride in medium where concrete suffered from TSA. Chloride may also be present accompanied by sulfate ions, particularly in concrete structure near the sea, where ground water, becomes mixed with seawater or is contaminated with sea spray. In addition, significant amounts of chloride and sulfate ions may be present as a result of the use of de-icing salt during winter time, where concentration will vary according to run-off. The current view reported by TEG (1999), is that for concrete placed in an aggressive environment, the presence of chloride mitigates or reduces the concrete's vulnerability to sulfate attack.

Previous studies by Zuquan et al. (2007) and Ekolu et al. (2006) have shown that the presence of chloride ions in association with sulfate delays or mitigates the conventional form of sulfate attack, where ettringite is the main deterioration product. However, Torres (2004) and Sotiriadis et al. (2012) note that there is very little information available about vulnerability to the thaumasite form of sulfate attack of concrete/mortar simultaneously exposed to both chloride and sulfate solutions at low temperature. However, according to an experimental study carried out at Sheffield University by Torres (2004), the extent of deterioration due to thaumasite formation in 20 mm mortar cubes depended on chloride concentration in solutions where 1 and 2.0% chloride present in solutions resulted in accelerated attack. Samples made with Portland cement blended with 15% limestone filler that were immersed in sulfate solution containing 2.0% Cl<sup>-</sup> displayed damage similar to that for pure sulfate solution. Less damage occurred to samples immersed in sulfate and 0.5% Cl<sup>-</sup> solution, whereas more severe damage was observed in samples

immersed in sulfate plus 1.0%Cl<sup>-</sup>. On the other hand, according to a recent study (Sotiriadis et al., 2012), in which a 2.1% chloride concentration and 100 mm concrete cubes were used; TSA was mitigated. The lack of published detailed information regarding the effect of chloride on thaumasite sulfate attack emphasises the importance of such investigation.

An additional aspect associated with the presence of chloride ions is higher risk of corrosion of steel reinforcement. Based on the observations made during inspection and analysis of the structures examined by the Highways Agency, Wimpenny and Slater (2003) pointed out that the increased risk of chloride induced corrosion can be lead by higher concentration at the depth of the reinforcement as a consequence of TSA development. Chloride binding capacity of cement matrix was reported by Torres (2004) to be affected by TSA. No experimental work has been reported in the published literature investigating the effect of thaumasite related damage of mortar/concrete cover on corrosion resistance of steel reinforcement; hence, it would be also of great interest to investigate the impact of TSA on corrosion resistance of steel reinforcement.

The use of mineral admixtures such as PFA and GGBS are reportedly (Tsvivilis et al., 2003, Skaropoulou et al., 2013, Skaropoulou et al., 2009, Hill et al., 2003) effective in preventing TSA at 5°C; however, the presence of chloride alongside sulfate at low temperature was found to have a negative effect on the performance of concrete made with these components (Sotiriadis et al., 2013).

## **1.2 Research Questions:**

The main research questions that will be addressed in this investigation are:

- What role can chloride have on TSA, and how does this vary with chloride concentration?
- To what extent chloride mitigates or accelerates TSA?
- Is TSA sensitive to chloride concentration?
- What is the mechanism for any effect played by chloride?
- What is the implication of TSA in the presence of chloride on rebar corrosion risk?
- How chloride affects the performance of fly ash and slag cements in environment prone to thaumasite formation?
- What effect thaumasite formation (TF) has on chloride binding capacity?



### 1.3 Aim and Objectives

The aim of this research is to clarify the effects of chlorides on thaumasite form of sulfate attack (TSA) in mortars with different binder compositions and implications on corrosion of steel reinforcement.

In order to achieve this aim, a numbers of objectives were identified, as follows:

- To investigate the role of chloride and its concentration on thaumasite sulfate attack.
- To investigate the mechanism for any effect played by chloride.
- To investigate the impact of TF on chloride binding capacity.
- To investigate the implications of TSA in the presence of chloride on rebar corrosion risk.
- To study the effect of chloride on performance of fly ash and slag cements in environment prone to thaumasite formation.

### 1.4 Structure of the thesis

This thesis is organised into seven chapters as follows:

**Chapter 1:** Background and justification for the study

**Chapter 2:** Review of available literature related to TSA, factors affecting thaumasite formation, the role of chloride on sulfate attack, the role of pH on thaumasite formation, the role of temperature on thaumasite formation, the use of pulverised fly ash and ground granulated blast-furnace as cement replacement in controlling TSA, the corrosion resistance of steel reinforcement simultaneously subjected to sulfate and chloride environment;

**Chapter 3:** Description of the materials and test methods adopted in the laboratory study;

**Chapter 4:** Results of the assessment of the effect of chloride concentration and temperature on performance of cement mortars subjected to sulfate exposure;

**Chapter 5:** Results of the assessment of corrosion resistance of steel rebars embedded in cement mortars subjected to composite sulfate and chloride solutions;

**Chapter 6:** A discussion of the results obtained in the research;

**Chapter 7:** Overall conclusions, the implications of the research for engineering and recommendations for future research work.

## **2. Literature review**

### **2.1 Introduction**

This Chapter presents a review of available literature related to thaumasite sulfate attack (TSA), factors affecting thaumasite formation, the role of chloride on sulfate attack, the role of pH on thaumasite formation, the role of temperature on thaumasite formation, the use of pulverised fly ash (PFA) and ground granulated blast-furnace slag (GGBS) as cement replacement in controlling TSA, and the corrosion resistance of steel reinforcement simultaneously subjected to sulfate and chloride environment.

### **2.2 Sulfate attack of concrete**

Deleterious changes that occur in cementitious materials as a consequence of the chemical interactions between sulfate ions and hydrated cement paste is known as sulfate attack (Neville, 1995). There are now considered to be two main types of sulfate attack, which are described below. In the conventional form of sulfate attack, formation of ettringite ( $3\text{CaO}\cdot\text{Al}_2\text{O}_3\cdot 3\text{CaSO}_4\cdot 32\text{H}_2\text{O}$ ) and gypsum ( $\text{CaSO}_4\cdot 2\text{H}_2\text{O}$ ) which result in expansive degradation of the concrete, whereas in the thaumasite form of sulfate attack the main product is thaumasite ( $\text{CaSiO}_3\cdot\text{CaCO}_3\cdot\text{CaSO}_4\cdot 15\text{H}_2\text{O}$ ), which is a soft, weak materials that possesses no capacity for binding the aggregate particles together (Thaumasite Expert Group,1999), which of these to occur depends mainly upon the environment of the exposure conditions.

### **2.3 Conventional form of sulfate attack**

Until the identification of thaumasite form of sulfate attack, the conventional type of sulfate attack was the only widely known type of degradation when cementitious materials were subjected to sulfate solution. This form of attack depends on the cation (s) present (Neville, 1995), where calcium and sulfate ions react with  $\text{C}_3\text{A}$  to form ettringite. Sodium and sulfate ions react with the calcium aluminate hydrates to form ettringite and with the portlandite to form gypsum.

Magnesium and sulfate ions react with portlandite, and calcium silicate hydrates, to precipitate brucite. The brucite can react further with the calcium silicate hydrates to form magnesium silicate hydrates, which result in non-cohesive products. Due to the low solubility of brucite, these reactions can continue to completion, giving greater deterioration of the cement paste than is the case for other sulfate solutions (Bonen and Cohen, 1992). The mechanism of attack is still not completely clear.

## **2.4 Thaumasite form of sulfate attack**

Crammond (2003) reported that for thaumasite to form, reactions of calcium, sulfate, carbonate and silicate ions should occur in wet, cold (favourably less than 15°C) conditions. The first case of thaumasite in concrete was reported in the United States in 1965, and several other field cases have since been reported elsewhere in European countries, Canada, Africa and United States (Crammond, 2002). However, it did not receive any considerable thought in the UK until the observation in 1998 of ten cases in the foundations of over-bridges along the M5 motorway in Gloucestershire, UK (Crammond, 2003). A Thaumasite Expert Group was immediately established by the UK Government to consider the risks, diagnosis, remedial works and guidance on new construction. The first report of Thaumasite Expert Group (1999) confirmed that the deterioration in the concrete was due to the presence of thaumasite.

Since 1999, degradation due to thaumasite formation has been recognised as a new form of sulfate attack, which has the potential to impact adversely on a wide range of elements and a variety of building materials (Crammond, 2002). Two classifications to thaumasite have been given by the Thaumasite Expert Group (1999). The first classification is the 'Thaumasite form of Sulfate Attack' (TSA) where considerable attack of the concrete/mortar matrix has taken place as a consequence of transformation of cement hydrates to thaumasite, in which the attack is characteristic by a white soft, mushy mass. The second term is 'Thaumasite Formation' (TF) in which thaumasite formed precipitates in pre-existing voids and cracks without causing damage to the concrete/mortar.

The primary risk factors for thaumasite formation as pointed by Crammond (2003) are:

- A presence of sulfates and/or sulfides in the ground;
- Availability of carbonate;
- Availability of silicate;

- Availability of mobile groundwater, and
- Low temperatures (Lower than 5°C).

Crammond (2002) points out that TSA is the main damaging mechanism relating to the incidence of thaumasite in new constructions. It was detected in high-quality, buried concretes made with limestone aggregate and subjected to sulfate-bearing groundwater. It is suggested by Crammond (2003) that, TSA is not a new incident and took place previously, but was not detected probably for the following reasons:

- Failure to identify thaumasite in standard sulfate resistance examinations
- Developed methodical technique
- Buried concrete elements are not usually examined
- Post-construction improvement of sulfate levels in the ground; and
- Use of limestone filler in OPC.

## **2.5 Mechanism of thaumasite formation**

Bensted (2003a) suggests two possible formation routes for thaumasite, the direct route and the woodfordite route. In the Direct route, thaumasite forms by the general reaction of sulfate with carbonate, silicate and excess water in the presence of calcium ions. In the woodfordite route, thaumasite and ettringite form as last products from a solid solution, which takes place during the reaction between ettringite, silicate and carbonate in the presence of surplus water. It is suggested that the rate of thaumasite formation increases as it is formed. Bensted (2003) notes that both reactions are slow.

Crammond (2003) suggests that thaumasite may also form through a solution mechanism in which sulfate attack occurs in the conventional way until the alumina is consumed and ettringite stops to precipitate. This leaves sulfate ions in solution that then will lead to seek for a new sulfate-bearing host, such as the portlandite. If carbonate/bicarbonate ions are available, the end product formed will be thaumasite rather than gypsum.

An investigation by Köhler et al. (2006) showed that thaumasite is not formed through the woodfordite route and the direct route is very slow. They suggest that thaumasite forms through a heterogeneous nucleation of thaumasite on the ettringite surface when the breakdown of C-S-H occurs in the cement matrix.

## **2.6 Factors affecting thaumasite formation**

A number of factors are implemented in thaumasite formation, including silicate, sulfate, carbonate, pH, temperature and wet environment.

### **2.6.1 Source of silicate**

The required silicate for thaumasite originates from the silicate containing phases in the cement paste, mainly the C-S-H phases which are the main binding phase in cement. Residue unhydrated clinker grains such as alite ( $C_3S$ ) and belite ( $C_2S$ ) are a secondary silicate bearing phase (Crammond, 2003)

### **2.6.2 Source of sulfate**

The external available sulfate-ions in the soil can be present in a variety of different sulfur minerals either already as sulfates or as sulfides which are able to become converted to sulfate-ions. Sulfates arise mainly in soils as calcium sulfates. However, other secondary elements such as magnesium sulfate and sodium sulfate may also be present (Crammond, 2003)

The presence of sulfides, which are usually found in usual ground as the mineral pyrite and other less frequent minerals such as marcasite and pyrrhotite, can contribute to the source of sulfate ions (Longworth, 2003). Sulfide-bearing clays contain in their un-weathered state a negligible amount of sulfate-bearing phases but considerable amounts of pyrite. Such clay had been categorised as harmless regarding sulfate attack in the past (Crammond, 2003). Hobbs and Taylor (2000) pointed out that oxidation of pyrite to sulfate can increase significantly the sulfate level in the ground and this reaction has been described by Longworth (2003) and many others.

Other sources of sulfate-bearing material in ground or in contact with the structure are in failure materials such as cinder and ash waste products, furnace bottom ash, spoil from mining of oil shale and coal which are found around old industrial areas as well as seabed (Crammond, 2003), (Crammond, 2002). Aggregates, cements and cement products as well as sulfate-based binders such as plaster and cement renders are potential source of sulfate that provide a basis partly for the formation of thaumasite in above ground constructions (Sims and Huntley, 2004).

### **2.6.3 Source of carbonate**

Carbonate is a necessary component for thaumasite to form. The main sources of carbonate ions are likely to be internal, from limestone aggregates or cement

filler (Crammond, 2003), (Irassar, 2009a), where part of the cement is replaced by finely ground limestone.

Limestone fillers are considered, by BRE (2005), to be the most susceptible binder for the formation of TSA with attack extent increasing with the amount of limestone added. This has been confirmed by Hartshorn et al. (1999), Justnes (2003), Torres et al. (2004a) and Skaropoulou et al. (2012). Current UK and European Portland cements (CEM I), BS EN 197-1:2011 are allowed to include up to 5% limestone filler as a small addition. According to Torres et al. (2006), this can result in even higher vulnerability to thaumasite.

It was thought that only fine dust carbonate particles would contribute to TSA but investigations on affected concretes in the laboratory and field have shown that good quality carbonate aggregates are also able to initiate deterioration (Crammond, 2003), however, smaller limestone particles are the more reactive according to Crammond (2003).

A secondary internal source is the carbonated layer in concrete, which is formed on the concrete surface by reaction with atmospheric CO<sub>2</sub>. It was concluded by Sims and Huntley (2004), Collett et al. (2004), Gaze and Crammond (2000), Eden (2003), Thomas et al. (2003), and Torres et al. (2006) in which concrete were made without carbonate containing materials, that atmospheric carbon dioxide and the consequent carbonation of concrete/mortar would have been the only available carbonate source contributing to TSA.

#### **2.6.4 Source of water**

Water is required for sulfate attack, providing transfer means for the sulfates and supporting the chemical interactions. The supply of water in regarding TSA in buried concretes is mobile groundwater, which arises naturally. The quantity of water is often subject to increase during the construction phase when the overburden is removed and the ground undergoes swelling. The formation of a sump during foundation works, or later damage in drainage are also possible causes for this increase (Crammond, 2003), (Loudon, 2003).

#### **2.6.5 Effect of temperature**

It has been reported in many investigations including Bensted (1999), Crammond et al. (2003), Pipilikaki et al. (2008), Skaropoulou et al. (Skaropoulou et al., 2012) that the most favourable temperature for thaumasite to form is 5°C. However, evidence of thaumasite formation was reported in

warm climates by Diamond (2003), Martinez-Ramirez et al. (2011), Irassar et al. (2005), Lee et al. (2008), Blanco-Varela et al.(2006), and Hartshorn et al. (2002). Hartshorn et al. (2002) also reported the formation of thaumasite in 35% limestone filler specimens stored in magnesium sulfate solution at 20°C after a year, but the degree of attack was less than at 5°C.

According to Crammond (2003) thaumasite is possibly formed at lower temperatures for four reasons:

- The decrease in thaumasite solubility;
- The increase in stability of  $\text{Si(OH)}_6$ ;
- The increase in  $\text{CO}_2$  solubility; and
- The increase in portlandite solubility.

### **2.6.6 The role of pH**

Since the stability of thaumasite phase is pH sensitive, many investigations have been conducted to examine the role of pH on thaumasite formation. Hobbs and Taylor (2000) suggested that thaumasite was formed in the M5 bridge structure as a result of sulfuric acid attack, during the oxidation of pyrite. Hill et al. (2003) found that when concretes containing carbonate aggregates were cured in high levels of sulfuric acid, the degradation product was gypsum rather than thaumasite. Zhou et al. (2006) reported that the presence of acid does not encourage thaumasite formation, since the observed deterioration of the concrete detected in acid conditions was due to gypsum precipitation rather than thaumasite.

Jallad et al. (2003) reported that the change in the pH value of the surrounding environment influenced the stability of thaumasite. At pH lower than 11, thaumasite reacted with the ions present in the solutions, and some transformation to calcium phosphate, calcium silicate and calcium carbonate was observed. At pH levels higher than 11, small quantities of calcium carbonate were observed, while thaumasite showed stability in conditions where pH equal to 13 was present.

Both Hartshorn et al.(1999) and Tsivilis et al.(2003) concluded that in the reaction to form thaumasite, portlandite is a reactant, which also implies that the conditions in which thaumasite will form must be alkaline. Crammond (2003) suggested that when the pH decreases towards 7, hydroxyl ions are consumed in the immediate vicinity of the thaumasite forming, leading to the dissolution of more portlandite which will initially maintain a high pH. Once this portlandite is consumed, the pH can only remain high as a result of more



hydroxyl ions diffusing in from other parts of the cement paste. As these hydroxyl ions are also consumed, the pH eventually decreases, and the thaumasite becomes less stable, and dissociates, forming calcium carbonate and releasing calcium and sulfate ions.

The type of sulfate solution plays a role in modifying pH which results in changing the main phases of sulfate attack. Magnesium sulfate solution may be buffered at pH close to 7 due to the low solubility of brucite as Lawrence (1992) states. The replenishment of test solution can control this change of pH as reported by Higgins and Crammond (2003), Justnes (2003), Bellmann and Stark (2007), Lee et al. (2008), Barker and Hobbs (1999), Hartshorn et al. (1999), Torres et al. (2006), Vuk et al. (2002). Increasing the volume of solution to volume of the specimen ratio is another approach which can be used to avoid changing in pH in solution as reported in a review paper by Irassar (2009).

Gaze and Crammond (2000) pointed out that the thaumasite would only form when pH value is higher than 10.5 and as soon as it is formed; it is very stable even at low pH.

The following explanation was suggested by Collett et al. (2004) with regard to the role of pH on thaumasite formation; at pH below 10.55 and due to equilibrium of carbonate ions at the pH value around 10.55 when the temperature drop to 5°C, more bicarbonates ions would convert into carbonic acid, which would result in fewer free carbonate ions being available for thaumasite formation.

## **2.7 Degradation mode of thaumasite**

The conditions leading to TSA in concrete are described in Section 2.6. The destruction and consumption of cement matrix, namely C-S-H phase during formation of thaumasite results in formation of white mushy materials on surface and within the body of concrete or mortar.

Based on field observation, Hobbs and Taylor (2000) suggest that the formation of ettringite and thaumasite are expansive reactions and control of this expansion by the undamaged part of concrete results in fine cracks parallel to the face of concrete component. Ramezani-pour and Hooton (2013) reported that the expansion of mortar bars started as a result of ettringite and gypsum

formation and expanded greatly and finally collapsed due to the formation of thaumasite.

In investigation carried out by Slater et al. (2003) for Highways Agency on the trunk roads in Gloucestershire, UK, the typical attack pattern to the buried vertical concrete elements was softening accompanied by greatest degree of expansion at the face of the concrete.

According to a research carried out by Smallwood et al. (2003) there was differences in the nature of deterioration of the concrete exposed to sulfate solution at 5°C and that exposed to sulfatic clay at 5°C. In the solution, materials resulting from chemical reactions constantly spalls from the outer part of specimens which keep them constantly exposed to the aggressive solution.

Based on a long-term investigation into chemical degradation vulnerability of different types of concrete that were exposed to pyrite rich clay reported by Abubaker et al. (2014), the deterioration due to thaumasite attack characterised by formation of white mushy material, spalling, loss of edge, exposure of aggregate and loss of cementitious matrix.

## **2.8 Identifications of thaumasite**

The identification of TSA and its reaction products can be unmistakably achieved using a combination of techniques, i.e. X-ray diffraction (XRD) and scanning electron microscopy (SEM) (Skaropoulou, 2006, Pouya, 2007). A combination of XRD and SEM with energy dispersive X-ray analysis (EDX) can also be used for the identification of TSA reaction products (Freyburg and Berninger, 2003). Infrared spectroscopy (IR) is also a powerful technique which can be used besides SEM/EDX and XRD to identify the solid solutions between thaumasite and ettringite (Barnett et al., 2002), (Pipilikaki et al., 2009).

Before the development of these techniques, it was very difficult to distinguish the main reaction products of the classical and the thaumasite form of sulfate attack and misidentification was common (Crammond, 2003). Ettringite and thaumasite have very close similarities in their atomic structure and differ principally in the aluminium and silicon content (See Table 2.1), but they are very difficult to be distinguished using XRD.

**Table 2.1.** Chemical composition of ettringite and thaumasite (Eden, 2003).

|                                | Ettringite | Thaumasite |
|--------------------------------|------------|------------|
| SiO <sub>2</sub>               | 0.00       | 19.4       |
| Al <sub>2</sub> O <sub>3</sub> | 15.0       | 00.0       |
| CaO                            | 49.5       | 54.5       |
| SO <sub>3</sub>                | 35.5       | 26.1       |

## 2.9 The role of chloride in sulfate attack

### 2.9.1 Conventional form of sulfate attack

Many studies have shown that the presence of combined chloride and sulfate result in mitigating sulfate attack. BEN-YAIR (1967 ) observed less expansion in Portland cement immersed in combined sulfate and chloride compared to specimens placed in pure sulfate solution of the same concentration. The positive impact of chloride ions in delaying the expansion due to sulfate attack was also observed by Al-Amoudi et al. (1995).

Al-Amoudi et al.(1995) investigated the effect of cation type related to the sulfate on concrete damage due to sulfate attack and the effect of chloride on sulfate attack in OPC and blended cements. They found that the presence of chloride tends to mitigate sodium sulfate attack. They attributed this to the solubility enhancement of gypsum and ettringite in presence of chloride. In magnesium sulfate environments, the chloride also mitigates the gypsum attack, but the chloride ions did not greatly affect the attack of magnesium sulfate on C-S-H.

Santhanam et al. (2006) investigated the performance of mortar samples made with OPC cement that were exposed to simulated seawater and groundwater solutions at about 21°C. The chloride ion concentration of seawater used was 19.09 g/l compared to only 1.04 g/l for groundwater. Similar concentration of sulfate ions (2233 mg/l as SO<sub>3</sub>) was used. The restriction of expansive ettringite formation and the protection provided by brucite formation against the further ingress of the solution into the mortar seems to be main reasons for mitigation effect of chloride in case of seawater, according to the author.

Dehwah (2007) did not note deterioration in OPC and blended cement concrete samples placed in sodium chloride and sodium sulfate solutions even in 4% SO<sub>4</sub><sup>-2</sup>. However, in magnesium sulfate solutions, surface deterioration was noted in OPC and PFA concrete when the sulfate level was 2.5% and more.

GGBS concrete showed deterioration when the magnesium sulfate level was as low as 1%.

A study conducted by Zuquan et al. (2007) also indicated that the availability of chloride in solution with sulfate delayed sulfate attack in concretes and the author attributed this behaviour to the following: (I) lower diffusion rate of sulfate in combined solution compared with sulfate only solution. (II) Higher rate of chloride diffusion than sulfate. Factor would result in rapid reaction between chloride ions and  $C_3A$  to form Friedel's salt ( $3CaO \cdot Al_2O_3 \cdot CaCl_2 \cdot 10H_2O$ ), which will lessen the formation of gypsum and ettringite. (III) The increase in sulfate product solubility.

### **2.9.2 Thaumassite form of sulfate attack**

Several field cases have shown that chloride was present when concrete suffered attack by thaumasite. In investigation carried out by Slater et al. (2003) for Highways Agency on the trunk roads in Gloucestershire, UK in which concrete structures suffered severe deterioration. Rust staining and chloride contamination related to steel corrosion were also present in thaumasite affected structures several metres under ground level.

According to an examination by Eden (2003) on many cores taken from bridge foundations throughout the UK, high chloride concentrations were also found in the cement paste of TSA degraded concrete.

An experimental study carried out at Sheffield University by Torres (2004) aimed to investigate the role of chloride ions on thaumasite formation. Three levels of chloride concentration (0 %  $Cl^-$ , 0.5%  $Cl^-$ , 1.0%  $Cl^-$  and 2%  $Cl^-$ ) as sodium chloride were added to 0.6%  $SO_4^{2-}$  as magnesium sulfate. 20 mm mortar cubes made with ordinary Portland cement (OPC) and different replacement of limestone fillers (0%, 5% and 15%) and water to binder ratio of 0.5 were placed in water, pure sulfate solution, combined sulfate and chloride solutions up to 12 months. It was concluded that the role of chloride ions on sulfate attack depends on the temperature and found that it mitigated the conventional sulfate attack at 20°C but it increased the TSA at 5°C. It was also found that the effect of chloride concentration on the performance of the mortar in magnesium sulfate depended on temperature and cement composition. No clear trend was observed to the damage of the samples with 15% limestone filler and with regard to chloride concentration at 5°C. Samples immersed in sulfate and 2.0%  $Cl^-$  showed similar damage to those immersed in pure sulfate. The least damage occurred to samples immersed in sulfate and 0.5%  $Cl^-$ ,

whereas the greatest damage was observed in samples immersed in sulfate and 1.0%Cl<sup>-</sup>.

Contradictory to the above observations, recent published study by Sotiriadis et al. (2012) and Sotiriadis et al. (2013) in which a 2.1% chloride concentration and 100 mm limestone concrete cubes were used; TSA was mitigated and high potential of thaumasite solubility in presence of chloride is suggested by the authors for this mitigation effect of composite solution.

## **2.10 Using slag and fly ash to avoid or mitigate thaumasite sulfate attack**

It is reported by Bellmann and Stark (2007) that thaumasite formation can be prevented, if an adequate amount of pozzolanic admixtures is used as much as to guarantee the consumption of portlandite and the Ca/Si ratio in the produced C-S-H phases is decreased. They suggested that cement structure with low Ca/Si ratio should be produced in the binder to avoid the thaumasite formation at low temperatures. However, in magnesium sulfate solution the produced C-S-H possessed low Ca/Si ratio of PFA was reported to be subjected to attack by magnesium and sulfate ions. One reason for this may be the low pH nature of pore solution in PFA mortars.

### **2.10.1 Pulverized Fly Ash (PFA)**

Part of a study by Tsivilis et al. (2003) aimed to examine the role of fly ash on formation of thaumasite in limestone cement mortar. Mortar specimens were prepared with limestone cement containing 15 percent and 30 percent fly ash replacement of cement. The specimens were stored in a 1.8% magnesium sulfate solution and cured at 5°C and 25°C. It was concluded that the inclusion of fly ash retarded the thaumasite formation.

A result of further 3-year investigation by Skaropoulou et al. (2013) and (2009) indicated that the performance of limestone cement concrete against sulfate attack was improved when fly ash used as cement replacement.

Concrete incorporating fly ash was studied as a part of long term durability work conducted by Hill et al. (2003). Test results indicated that fly ash concrete was attacked by ettringite, rather than thaumasite sulfate attack. Concretes incorporating 30% or more fly ash did not show degradation when subjected to

tidal marine environment, and no evidence of thaumasite formation was seen by Thomas et al. (2003).

However, Mulenga et al. (2003) reported that either mitigation or promotion of thaumasite formation when using high replacement level of fly ash will depend on the type of cement used. Deterioration of specimens as a result of thaumasite formation was observed in mixtures of sulfate resisting Portland cement (SRPC) with 50% fly ash addition. Thaumasite was also detected in mixtures prepared with SRPC without fly ash but without deterioration. Blends of Portland limestone cement with 40% fly ash showed restricted formation of thaumasite while blending by 50% resulted in no thaumasite formation at all. It was concluded that thaumasite can also be formed in mixtures including fly ash.

### **2.10.2 Ground granulated blast furnace slag (GGBS)**

Higgins and Crammond (2003) investigated the role of slag replacement (70% GGBS/30PC) in concrete placed in sulfate solution at 5°C and 20°C. The results indicated that slag replacement produced high resistance to TSA and their general sulfate resistance was significantly improved in mix where carbonate was present.

Hill et al. (2003) found that slag concrete was more resistant to TSA and did not show evidence of thaumasite formation. It was also reported by Tsivilis et al. (2003) that the inclusion of slag resulted in enhanced the sulfate attack resistance of limestone cement. They reported that the slow reaction of pozzolans seem to be unable to offer efficient resistance to sulfate attack if the concrete is exposed to sulfates prior to the beginning action of pozzolanic reaction. A part of five years study by Skaropoulou et al. (2009), also show that the inclusion of slag significantly enhanced the resistance of the limestone cements against sulfate attack.

Brown et al. (2003) investigated samples stored in magnesium sulfate solution in a laboratory for 4 years. They concluded that the replacement of OPC cement by slag results in sulfate resistance similar to that of concrete made with sulfate resistance-Type V cement. They noted that the reduction in permeability is more significant in enhancing sulfate resistance than is compositional control.

According to a long term laboratory investigation by Abubaker et al. (2014) on the performance concrete made with different binders immersed in clay, 25% replacement with fly ash concrete was found to be susceptible to TSA.

Based on thermodynamic model, Juel et al. (2003) found that as a result of their high aluminate contents, slag and fly ash cements should provide greater resistance to thaumasite form of sulfate attack. However, a recent laboratory investigation by Sotiriadis et al. (2013) reported that the presence of chloride in sulfate solutions accelerated thaumasite sulfate attack of slag and fly ash concretes due to thaumasite formation. 30% PFA and 50% GGBS replacement of limestone cement were used in this study.

### **2.11 Chloride transport into concrete subjected to sulfate attack**

Zuquan et al. (2007) investigated the damage process caused by the presence of combined sulfate and chloride solutions on plain and fly ash (20% and 30%) concretes subjected to conventional form of sulfate attack, using 3.5% sodium chloride and 5% sodium sulfate solutions. The experimental results showed that the presence of sulfate in combined solution enhanced the resistance to chloride penetration into concretes at early stage of exposure, but the reverse trend was found at a later period. According to the authors, this may be related to the development of ettringite formation. It was also reported that fly ash increased the penetration of chloride into concretes at the early stage but reduced it at later age. The authors explain this by the lower hydration rate of fly ash at early ages.

The benefit of using fly ash in reducing the chloride ingress was also confirmed by Thomas and Matthews (2004) who conducted a study on concrete subjected to a marine environment for 10 years old. They concluded that chloride concentration was reduced significantly in the fly ash concretes compared with cement only, and they found increasing fly ash content resulted in lower chloride levels within the concrete.

Santhanam et al. (2006) states that the presence of a thick layer of brucite, which results from the reaction between magnesium sulfate and chloride ions, on the surface of mortar samples immersed in seawater solution could have resulted in improving the resistance against the further ingress of aggressive solution into mortar.

Based on field investigation, reported by Slater et al. (2003) thaumasite affected areas offered little resistance to chloride penetration as a result of open cracks which provided access in the damaged areas.

## **2.12 Chloride binding capacity of cement**

Chloride binding is the term used when chlorides react chemically with tricalcium aluminate ( $C_3A$ ) or its hydrates to form calcium chloro-aluminate,  $C_3A \cdot CaCl_2 \cdot 10H_2O$ , known as Friedel's salt, and can also physically bind due to its adsorption on the surface of C-S-H.

Chloride binding is important for evaluating the service life of concrete; according to Yuan et al. (2009) for the following reasons: (1) lessening of the free chlorides levels in the surrounding area of the steel rebar; (2) removal of chloride from the diffusion flux, so delaying the access of chloride to reach the steel surface, (3) The consequent reduction in structure pores and the transport of chloride ion as Friedel's salt is formed.

## **2.13 Factors affecting chloride binding**

### **2.13.1 Chloride concentration**

Higher levels of chloride binding when using higher chloride concentration have been reported. Arya et al. (1990) examined the effect of different chloride concentrations on binding capacity of OPC cement paste with water to cement ratio of 0.5. They found that the bound chloride increased with increasing chloride level in solution. Loser et al. (2010) also found that chloride binding for CEMI, estimated by the difference between total and free chloride, depends on the chloride level in the pores.

### **2.13.2 Supplementary cementitious materials**

Dhir et al. (1997) investigated the impact of PFA replacement at 0, 17, 33, 50 and 67% on chloride binding of cement paste for a W/B ratio of 0.55. The results indicated that the capacity of chloride binding increases with the increase in PFA replacement up to 50%, and then decreases at 67%. The authors suggested the following reasons for this behaviour: the reduction in the calcium hydroxide content of 50% PFA levels did not reach a level that affects the stability of Friedel's salt and its ferrite analogue, but beyond this level it does. Enhancement in binding of chloride due to the replacement of fly ash was also reported by Arya et al. (1990), Arya and Xu (1995).



According to Dhir and Jones (1999), higher binding capacity in PFA cement may be primarily attributed to the high alumina content in fly ash, which leads to the formation of more Friedel's salt. However, reductions of chloride binding when 30% of cement replaced with fly ash was reported by Nagataki (1993). Loser et al.(2010) explain a variable influence of PFA on binding capacity of cement due to the variation of fly ashes used.

It have been also shown that replacement of cement with slag increases the chloride binding in external chlorides as reported by Nagataki (1993), Arya et al. (1990) and Dhir et al.(1997)) as well as internal chlorides as reported by Luo et al. (2003) , Arya et al. (1990) and Arya and Xu (1995). The high alumina content and the consequent Friedel's salt formation is considered to be the main reason according to Dhir et al. (1996) and (1997). The high level of chloride binding of slag may be also attributed to the increase in adsorbed chlorides, according to Arya et al. (1990). Xu (1997) studied chloride binding in cement paste with admixed chloride, and found that the higher binding capacity of slag-cement paste moved out when the sulfate ion in slag-cement paste is increased to the same level as cement paste. He attributed the higher binding capacity of slag-cement to the dilution effects of sulfate ions.

However, it is also found by Mohammed and Hamada (2003) that increased slag replacement led to a reduction in the chloride-binding ability. Loser et al. (2010) points out that whether the addition of slag or fly ash will increase chloride binding or not depends to large extent on the reactivity of mineral admixture used.

### **2.13.3 Temperature**

In a study carried out by Arya et al. (1990) it was found that chloride binding increases as curing temperature increases when chlorides were introduced internally into the mix made with OPC and water to cement ratio of 0.5. The authors attributed this to the rapid reaction rate as temperature increases

## **2.14 Chloride binding capacity of cement subjected to sulfate attack**

The chloride binding capacity of cement under conventional sulfate attack has been investigated by several researchers. In general, the presence of sulfate found to reduce chloride binding capacity as reported by Xu (1997), Ehtesham Hussain et al.(1994) and Xu et al.(2013). According to Ehtesham Hussain et al.

(1994) this is probably due to the faster interaction of sulfate than chloride with  $C_3A$  when they both present. It was also reported by Xu et al. (2013) that during the sulfate attack, Friedel's salt can be transformed into ettringite, which contributes to the release of bound chloride.

With regard to thaumasite, a study carried out by Torres (2004) on mortar samples made with Ordinary Portland Cement containing 15% limestone filler and placed in combined chloride and sulfate solution at 5°C for 12 months found that Friedel's salt was absent in TSA affected materials which was attributed by the author to the instability of Friedel's salt in presence of thaumasite. It could not be established whether the chloride binding capacity of the cement matrix was reduced since Friedel's salt was absent within the corroded material where thaumasite was abundant, as explained by the author.

## **2.15 Chloride induced corrosion of steel rebars in concrete/mortar subjected to sulfate attack**

### **2.15.1 Background**

Chloride induced corrosion is one of the main causes for the reduction in the surface life of concrete structures. Besides internal sources, chloride can penetrate into concrete from different external sources such as seawater, soil, ground water and de-icer salts.

Due to high alkalinity of pore solution of concrete, thin protective layer forms on the steel rebar surface and consequently the steel is protected from corrosion. The stability of this layer is affected by the change in the pH of the surrounding environment. The formation of CH during the hydration of cement results in environment with high alkalinity (Mehta, 2006 ). However, according to Mehta (2006), the protective layer may be destroyed as a result of the decrease in the alkalinity of the pore solution due to carbonation, or by the ingress of chlorides to the interface region.

In the presence of chloride ions, depending on the  $Cl^-/OH^-$  ratio, it is reported that the protective layer is damaged even at high pH. According to Mehta (2006 ), it is reported that with a  $Cl^-/OH^-$  ratio higher than 0.6, rebar will not be protected against corrosion probably due to either increase in permeability or instability of the protective film under these circumstances.

### 2.15.2 Laboratory studies

Several studies have been conducted into the effect on the corrosion rate of steel rebar of sulfate ions alone and concomitant with chloride. Al-Tayyib et al. (1988) studied the effect of sulfate ions on rebar corrosion using simulated concrete pore solution. In this study, carbon steel specimens were placed in saturated CH solutions containing different levels of sulfate and the corrosion rate was evaluated by linear polarization resistance (LPR) and A.C. impedance. The results indicated that in the presence of sulfate and at 22°C, active corrosion was caused by change in the nature of iron oxide film.

In further investigations, Al-Tayyib and S Khan (1991) compared the corrosive resistance of steel in actual concrete subjected to sulfate ions with that with chloride ions. Reinforced concrete specimens introduced with equal amounts of sulfate and chloride ions were stored in potable water for up to 808 days and then in 3%  $\text{SO}_4^{2-}$  and 3%  $\text{Cl}^-$  solutions for a period of 60 days. Half-cell potential and corrosion rate measurements were made during the entire exposure period of 868 days. It was concluded that the sulfate ions were corrosive to the rebar but in less activity than chloride.

A study carried out by Cheng et al. (1990) using AC impedance technique show that the role of chloride and sulfate ions on the electrochemical properties and corrosion activity of steel bar in concrete made with either ASTM-Type I or sulfate resisting-Type V cements were different. They observed that sulfate ions could significantly change the mechanistic parameters of surface layer, and the sulfate-induced corrosion might be more aggressive.

Al-Amoudi (1993) studied the impact of sulfate ions, combined effect of chlorides and sulfates, on rebar in cement paste for 500 days. The steel corrosion was assessed by corrosion potentials and linear polarization resistance techniques. Results indicated that the corrosion was negligible in specimens stored in sulfate only solution. The corrosion activity was higher in specimens stored in composite solutions compared to those stored in chloride only solution. The author explained the increased corrosion in combined chloride and sulfate solution by the reaction of sulfate and chloride ions with the metal surface as compared to corrosion of rebar in the presence of chloride ions only.

Further investigation conducted by Al-Amoudi (1995) examined the corrosion activity of steel embedded in concrete in a mixed magnesium-sodium sulfate

solution. Type I, Type II and Type V, PFA, silica fume (SF) and GGBS and two water-to-binder ratios (0.5 and 0.35) were used in the study. Corrosion behaviour was monitored using corrosion potentials and polarization resistance. The results of the investigation indicated that plain cement concretes made with Type I cement could not protect the rebar from corrosion. PFA and GGBS concretes showed higher extents of corrosion. SF concrete showed the greatest corrosion resistance. Within the initial 500 days of monitoring, all samples showed passivity. According to the author, this may be due to the low diffusivity of sulfate ions to the steel surface.

Jarrah et al. (1995) investigated the electrochemical activities of rebar in OPC and blended cement concrete placed in only sulfate, only chloride and composite sulfate and chloride solutions. Their results indicated that the combined sulfate and chloride did not considerably affect the corrosion initiation time but the corrosion rate was considerably increased by the amount of sulfate ions related to the chloride ions.

Saleem et al. (1996) conducted a study to estimate the role of combined chloride and sulfate solution on the electrical resistivity of concrete. Reduction in electrical resistivity of concrete was observed as a result of sulfate contamination which increases the corrosion rate in carbonated concrete.

Sakr, (2005) reported that the existence of chloride and sulfate solutions in the surrounding environment generally decreased the negative effects of sulfate ions on steel rebar. According to Sakr (2005) the high solubility of the component part of cement and of hydro-sulpho-aluminate due to the presence of chloride ions in sulfate solution was the main reason.

### **2.15.3 Field investigations related to TSA**

It has been suggested by Slater et al.(2003) that thaumasite affected areas offered little resistance to chloride diffusion, due to the damage inflicted in the matrix that results in the opening cracks and flows. Also, it has been reported that the concentration of chloride was reduced at the surface and increased at the reinforcement-matrix interface (Eden, 2003). Based on the observations made during inspection and analysis of the M5 structures operated by the Highways Agency, Wimpenny and Slater (2003) proposed what may have happened during sulfate attack. They looked at four stages of reaction. The first stage was when the surface of the concrete was just starting to react with chemicals in the surrounding ground, progressing to stage four when all the

concrete, up to the depth of the reinforcement bars, had been affected, to some degree, by the ingress and subsequent reaction of the concrete with the external chemical species. They pointed out that the increased risk of chloride induced corrosion is probably related to concentration at the depth of the reinforcement as a consequence of TSA development.

## **2.16 Concluding remarks**

Based on the literature review, it is concluded that there has been limited data available dealing with the role of contamination effect of chloride and sulfate ions on the performance of concrete and the majority of these data have been obtained under conventional form of sulfate attack. Although, extensive work has been found dealing with the performance of concrete/mortar made with supplementary materials and the effect of temperature and the role of pH on thaumasite formation, very limited data are available dealing with the role of chloride ions on thaumasite form of sulfate attack and different points view are present. Moreover, no published laboratory work has been found dealing with the chloride binding capacity and chloride induced corrosion under thaumasite form of sulfate attack, In addition, there is no enough data available dealing with the role of chloride ions on performance of fly ash and slag cements in environment prone to thaumasite formation. Therefore, laboratory work is required to cover all of these aspects of chloride ions present in medium where concrete is prone to thaumasite form of sulfate attack.

### 3. Experimental programme

#### 3.1 Introduction

This chapter details the materials, equipment and the experimental work carried out to study the performance against thaumasite form of sulfate attack of mortar mixes made with different cements exposed to sulfate only and composite sulfate and chloride solutions. The cements used were CEMI, CEMI blended with 10%LF (CEMI-LF), CEMI blended with 50%PFA (CEMI-PFA) and CEMI blended with 70%GGBS (CEMI-GGBS). Details of the materials, mortar mixtures, stored temperature, test solutions and test methods, as summarised in Figure 3.1, are described below.

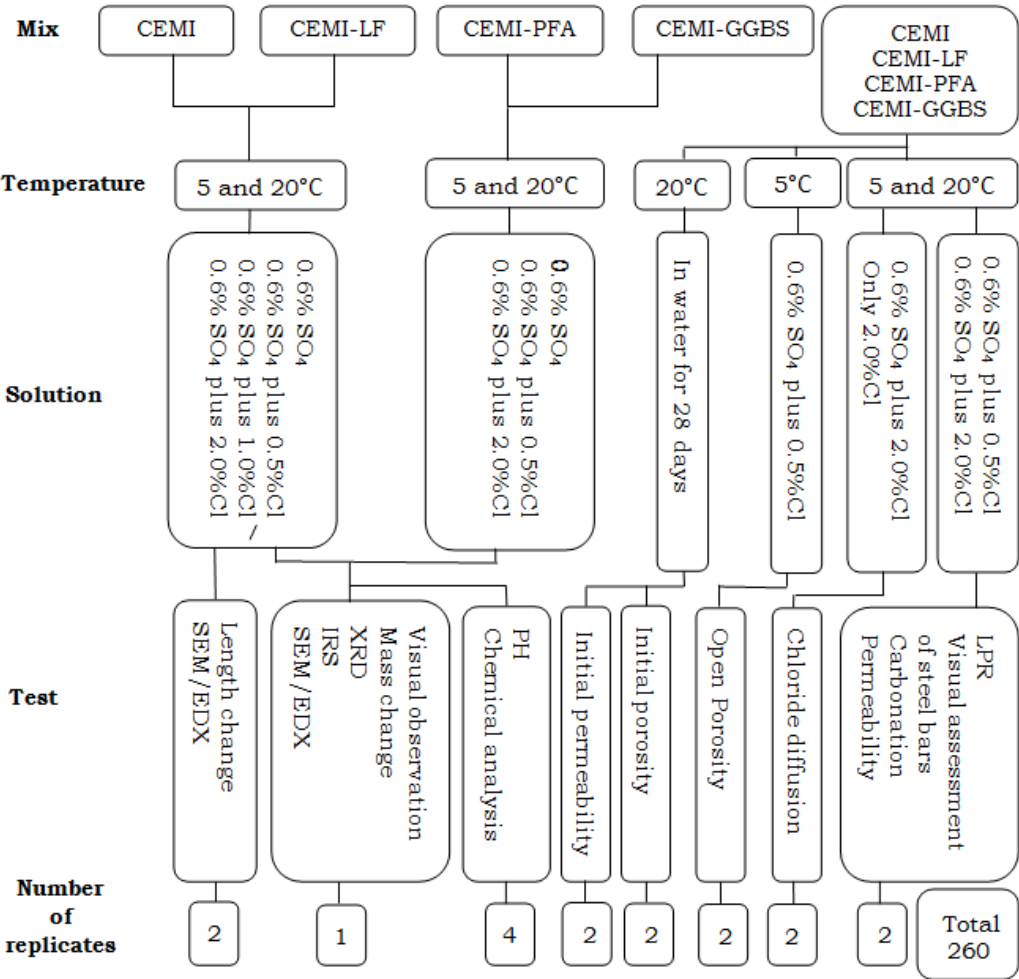


Figure 3.1. Schematic view of experimental programme.

## **3.2 Materials**

### **3.2.1 Cement (CEMI 52.5N)**

Commercial CEMI 52.5N cement manufactured by Paragon Industries, conforming to the requirements of BS EN 197-1:2011, the chemical and mineralogical compositions of which are given in Table 3.1, was used. The standard production cement was delivered with approximately 3.5% inter-ground limestone, as determined by Thermogravimetric analysis (TGA).

### **3.2.2 Limestone Filler (LF)**

The limestone filler used was obtained from the Hanson Group. It conformed to the requirements of BS EN 197-1:2011, where the chemical composition is given in Table 3.1.

### **3.2.3 Ground Granulated Blast Furnace Slag (GGBS)**

The ground granulated blast-furnace slag (GGBS) was obtained from Hanson Heidelberg Cement Group, UK. It complied with BS EN 15167-1:2006 and the mineralogical composition determined using XRF is shown in Table 3.1.

### **3.2.4 Pulverized Fly Ash (PFA)**

Pulverised fly ash (PFA) conforming to BS EN 450-1:2005+A1:2007 obtained from Ash Solutions Ltd was used. Its chemical composition is shown in Table 3.1.

### **3.2.5 Aggregate**

Siliceous medium graded natural concrete sand (passing 5mm sieve) conforming to BS EN 12620:2002-A1 2008 was used. The chemical composition and physical properties of this sand are given in Table 3.2.

### **3.2.6 Water**

Standard portable tap water available at the laboratory was used to make all mortar mixes.

**Table 3.1.** Chemical and mineralogical composition of cement, LF, PFA and GGBS (XRF analyses performed at Leicester University).

| Oxide/Phases<br>(Mass, %)      | Material      |           |       |       |
|--------------------------------|---------------|-----------|-------|-------|
|                                | CEM I (52.5N) | Limestone | PFA   | GGBS  |
| SiO <sub>2</sub>               | 19.85         | 0.63      | 50.83 | 35.58 |
| CaO                            | 64.61         | 55.2      | 2.56  | 40.66 |
| Al <sub>2</sub> O <sub>3</sub> | 4.67          | 0.28      | 24.95 | 12.82 |
| Fe <sub>2</sub> O <sub>3</sub> | 2.74          | 0.15      | 9.78  | 0.45  |
| Na <sub>2</sub> O              | 0.23          | < 0.003   | 0.92  | 0.32  |
| K <sub>2</sub> O               | 0.45          | 0.054     | 3.54  | 0.63  |
| MgO                            | 1.09          | 0.47      | 1.72  | 7.52  |
| SO <sub>3</sub>                | 3.015         | < 0.002   | 0.44  | 2.38  |
| LOI                            | 2.52          | 42.89     |       |       |
| C <sub>3</sub> S               | 68.28         |           |       |       |
| C <sub>2</sub> S               | 5.4           |           |       |       |
| C <sub>3</sub> A               | 7.74          |           |       |       |
| C <sub>4</sub> AF              | 8.34          |           |       |       |

**Table 3.2** Chemical composition and physical properties of concrete sand, as provided by the supplier.

| Component                                   | (%)   | Property                           | Value |
|---|-------|------------------------------------|-------|
| Silica (SiO <sub>2</sub> )                  | 94.8  | Aggregate Abrasion Value           | 4.1   |
| Aluminium (Al <sub>2</sub> O <sub>3</sub> ) | 2.9   | Aggregate Crushing Value           | 12    |
| Calcium (CaO)                               | < 0.1 | Aggregate Impact Value             | 19    |
| Calcium carbonate (CaCO <sub>3</sub> )      | 0.1   | Magnesium sulfate Soundness        | 88    |
| Iron (Fe <sub>2</sub> O <sub>3</sub> )      | 0.8   | Relative density (Oven dry)<br>O.D | 2.82  |
| Magnesium (MgO)                             | 0.2   | Relative density S.S.D             | 2.63  |
| Magnesium carbonate (MgCO <sub>3</sub> )    | 0.4   | Water Absorption by weight<br>(%)  | 0.5   |
| Manganese (MnO)                             | < 0.1 |                                    |       |
| Potassium (K <sub>2</sub> O)                | 0.9   |                                    |       |
| Sodium (Na <sub>2</sub> O)                  | 0.1   |                                    |       |

### 3.3 Mixing and casting of mortars

A series of mortar cubes (50mm), prisms (40x40x160 mm), cylinders (100Øx50H), cylinders (50Øx100H) were cast according to mixes shown in Table 3.3, using a fixed water to binder ratio of 0.6, binder to sand ratio of 1:2.5. This high w/b ratio was selected to accelerate chemical diffusion and



interaction, thus allowing identification of any potential reactions within a shorter time frame.

The limestone, PFA and GGBS replacements were dry mixed with CEMI cement prior to the inclusion of the aggregate and which was further dry mixed prior to the addition of the water. The moulds were filled in two layers and where applicable, 10mm diameter mild steel reinforcement bars were installed. The samples were compacted on a vibrating table to remove any entrapped air after each layer was poured. The moulds were then covered with plastic sheets for the first 24 hours at room temperature ( $\sim 20^{\circ}\text{C}$ ), before they were transferred into curing water for 6 days at  $20^{\circ}\text{C}$ , followed by 21 days in air at room temperature ( $\sim 20^{\circ}\text{C}$ ). The specimens were then marked and placed in individual containers, with specific solutions, until required for testing. The 50 mm cube specimens were weighed before being placed in solutions.

The steel bars were degreased and coated with bitumen at the mortar-air interface and at their ends to prevent crevice corrosion. Table 3.4 shows the chemical composition of steel rebars used in this study.

In order to monitor the pH and chemical changes to the test solutions, a range of 20mm mortar cubes were also mixed and cast separately using similar materials and procedures to those mentioned above. These were kept in small plastic containers at 5 and  $20^{\circ}\text{C}$ .

**Table 3.3.** Mortar mixtures.

| Mix       | Binder       | Per weight of binder |     |     |      |       |      |
|-----------|--------------|----------------------|-----|-----|------|-------|------|
|           |              | CEMI                 | LF  | PFA | GGBS | Water | Sand |
| CEMI      | CEMI         | 1                    | 0   | 0   | 0    | 0.6   | 2.50 |
| CEMI-LF   | CEMI/10%LF   | 0.9                  | 0.1 | 0   | 0    | 0.6   | 2.50 |
| CEMI-PFA  | CEMI/50%PFA  | 0.5                  | 0   | 0.5 | 0    | 0.6   | 2.50 |
| CEMI-GGBS | CEMI/70%GGBS | 0.3                  | 0   | 0   | 0.7  | 0.6   | 2.50 |

**Table 3.4.** Chemical compositions of steel rebar (wt. %), as provided by the supplier.

| C    | Mn   | Si   | P     | S     | Cr   | Ni   | Cu   | Mo    | Al    | Sn    | V     | Ti    | N      | Ca     |
|------|------|------|-------|-------|------|------|------|-------|-------|-------|-------|-------|--------|--------|
| 0.17 | 0.18 | 0.28 | 0.016 | 0.029 | 0.05 | 0.03 | 0.12 | 0.002 | 0.038 | 0.009 | 0.004 | 0.002 | 0.0084 | 0.0016 |

### 3.4 Test solutions

As shown in Table 3.5, five solutions were made by dissolving sodium chloride (NaCl) and Epsom salt ( $\text{MgSO}_4 \cdot 7\text{H}_2\text{O}$ ) in deionised water as follows: sodium chloride only (2.0% Cl<sup>-</sup>), magnesium sulfate only (0.6%  $\text{SO}_4^{2-}$ ) and three combinations of chloride and sulfate (i) magnesium sulfate plus 0.5% chloride (ii) magnesium sulfate plus 1.0% chloride (iii) magnesium sulfate plus 2.0% chloride. The concentration of sulfate was equivalent to Design Sulfate Class DS4 according to BRE Special Digest 1:2005. The solutions were replenished every three months up to 12 months and then left until the end of the experiment. Since, all containers were covered, the solution did not evaporate.

**Table 3.5** Compositions of test solutions.

| Test solutions   | Salts in test solutions |                  |               |                    |                  |               |
|------------------|-------------------------|------------------|---------------|--------------------|------------------|---------------|
|                  | [g/l]                   |                  |               | [%]                |                  |               |
|                  | $\text{SO}_4^{2-}$      | $\text{Mg}^{2+}$ | $\text{Cl}^-$ | $\text{SO}_4^{2-}$ | $\text{Mg}^{2+}$ | $\text{Cl}^-$ |
| Water            | 0                       | 0                | 0             | 0                  | 0                | 0             |
| C20              | 0                       | 0                | 20            | 0                  | 0                | 2.0           |
| Sulfate only (S) | 6.0                     | 1.52             | 0             | 0.6                | 0.152            | 0             |
| SC5              | 6.0                     | 1.52             | 5             | 0.6                | 0.152            | 0.5           |
| SC10             | 6.0                     | 1.52             | 10            | 0.6                | 0.152            | 1.0           |
| SC20             | 6.0                     | 1.52             | 20            | 0.6                | 0.152            | 2.0           |

### 3.5 Curing regime

#### 3.5.1 Initial curing

After de-moulding, the specimens were placed in water at 20°C for 6 days and then they were air-cured for 21 days at laboratory temperature (~20°C). This procedure is considered to be close to the circumstances in field constructions (Kakali et al., 2003). Figure 3.2. Shows the specimens undergoing air curing before transferred to solutions.

#### 3.5.2 Long term exposure to sulfate/chloride solutions

Mortar cubes, prisms and cylinders were placed in different types of solutions in individual containers at two different temperatures, namely  $5 \pm 0.5$  and at  $20 \pm 1$ °C (room temperature) till the testing dates. Figure 3.3 and Figure 3.4 show the view of the containers in the controlled temperature tanks which were maintained at 5°C by circulating chilled water around the containers. Other containers were stored in the laboratory at about 20°C.



**Figure 3.2.** Mortar specimens in air curing (~20°C-room temperature).



**Figure 3.3** Containers in 5°C temperature tanks.



**Figure 3.4** Containers at 20°C in laboratory room.

### **3.6 Test method**

The performance of the samples was monitored using the following techniques/procedures:

#### **3.6.1 Visual observations assessment**

A visual assessment of the 50 mm cubes was made on a monthly basis by removing the cubes from the solutions and photographing them. Particular note was made of any changes in colour, spalling and precipitation of any materials.

#### **3.6.2 Mass measurement**

Mortar cubes of 50mm were taken regularly from their containers and the surface was dried and any loose parts were removed by hand before weighing.

#### **3.6.3 Length change**

40x40x160mm mortar prisms were used to monitor the length change. The specimens were taken from their containers at the end of experimental work and changes in length were measured according to BS 812-123:1999.

### 3.6.4 Sample preparation for X-ray diffraction (XRD) and infrared spectroscopy (IRS)

Samples were taken from surfaces of sound and attacked mortar cubes for XRD and IRS examination. They were air dried at room temperature to avoid any change in crystallization of deteriorated materials. The samples were then crushed using a porcelain mortar and pestle to pass a 150 micron sieve in order to remove quartz from the fine aggregate and reduce the size of quartz peak on the XRD trace. The passed materials were further ground to pass a 63 micron sieve. In order to avoid contamination from other samples, the sieve, the mortar and pestle were washed with acetone between each sample preparation. The powders were kept in air tight containers at about 5°C before tests. For corrosion specimens, selected mortar-steel interface samples were taken and treated as mentioned above for XRD analysis.

### 3.6.5 X-ray diffraction (XRD)

The XRD pattern can show obvious movement in peak position and this should be adjusted by direction on other peaks, such as quartz and calcite, or using an internal standard, before the final evaluation (Freyburg and Berninger, 2003). Because the primary peaks at about  $9^{\circ}2\theta$  are almost identical for thaumasite and ettringite, therefore the differences of secondary peaks must be used as distinction angles (Stark, 2003). The peak position of the general reaction products according to published literature by Stark (2003), Hill et al.(2003), Nobst and Stark (2003) are listed below:

|             |                            |              |                            |
|-------------|----------------------------|--------------|----------------------------|
| Calcite:    | 29.4°2 $\theta$            | Portlandite: | 18.0; 34.0°2 $\theta$      |
| Aragonite:  | 26.3°2 $\theta$            | Quartz:      | 26.5°2 $\theta$            |
| Gypsum:     | 11.6°2 $\theta$            | Brucite:     | 18.5; 38.0°2 $\theta$      |
| Ettringite: | 9.0; 15.8; 18.9°2 $\theta$ | Thaumasite:  | 9.2; 16.0; 19.4°2 $\theta$ |

XRD analyses were performed using a Philips PW 1830 X-ray generator using a copper electrode operating at 40 kV and 30 mA with a scanning speed of 2 $\theta$ /min with step size 0.02 over a 2 $\theta$  range of 5–55. The database of the Joint committee for Powder Diffraction Files (JCPDF) built into WinXPOW software was used to identify the different phases in the patterns.

### 3.6.6 Infrared spectroscopy (IRS)

As mentioned in Chapter 2, due to the similarity in crystal structure of ettringite and thaumasite, it is not easy to differentiate between these minerals

using XRD. However, octahedral coordinated silica in thaumasite can be distinguished from ettringite using this technique (Barnett et al., 2002). Thaumasite has a distinctive vibration waveband of  $500\text{ cm}^{-1}$ , in contrast to octahedral coordination of aluminate in ettringite, which is characterised by a waveband at  $855\text{ cm}^{-1}$ .

The infrared spectroscopy analysis was performed alongside XRD, using the same powder samples. The samples for IR spectroscopy were made using 2 mg of sample to 200 mg of potassium bromide (KBr) which were ground together until a fine homogeneous material was achieved. A 12 mm disc of the sample was then prepared and tested. The IR spectrum was determined using a Perkin-Elmer FT-IR 2000 spectrometer. The equipment was set to scan the samples in Mid infrared (MIR) range of  $4800\text{--}370\text{ cm}^{-1}$ . Before scanning the sample, the background was first scanned in order to eliminate atmospheric effects.

### **3.6.7 Scanning electron microscopy (SEM) and energy dispersive X-ray analysis (EDX)**

Changes in microstructure of mortars provide evidence about the nature of reactions and deterioration mechanisms and any changes in composition reflect the chemical interactions between the aggressive ions in solution with cement paste. The detection of materials using scanning electron microscopy (SEM) is becoming more popular in material science. Deterioration products, such as thaumasite have distinctive appearance, and can also be identified without problems using the included energy dispersive x-ray analysis (EDX) ((Pipilikaki et al., 2009), (Torres et al., 2003), (Brown et al., 2004)).

Mortar samples exposed to test solutions for 450 and 630 days were resin saturated under vacuum, cut and polished to be analyzed by means of backscattered electron imaging and energy dispersive X-ray analyzer. After 450 days, samples (1cm cube) were cut from the corner of prisms using a dry diamond cutting wheel to avoid any possible change to the structure of deteriorated surface and to prevent washing out any soluble compounds such as calcite and gypsum. Then the samples were dried in a desiccator, impregnated with epoxy resin and manually ground using in four grades of silicon carbide paper (400, 800, 1000 and 1200) and the surface polished using diamond discs of between  $0.25\mu$  and  $6\mu$ . The surface of sections was cleaned using isopropanol between each stage. Carbon coating was used to prevent the build up of surface electrical charges during scanning. After 630 days, similar

procedure was followed but on fracture samples collected from the surface of cubes. The specimens were analysed using an Inspect F scanning electron microscope (SEM) with an accelerating voltage of 20 Kv. Chemical analysis using an energy dispersive X-ray (EDX) system and the appropriate link software was employed to identify the phases present.

In order to identify the nature of the deteriorated products after 360 days of immersion, fractured samples from the surfaces of prisms were taken and dried in a desiccator and then fixed to a carbon tape on a metal disc, exposed for a few minutes to vacuum to remove any moisture and dust, and immediately placed in the Electron Microscope (Carl Zeiss Merlin Field Emission SEM).

### **3.6.8 Chemical analysis of test solutions**

Chromatography technique was used for this. Dionex DX-120 system was used to separate the ions; in a system comprising an AS40 automated sampler, analytical pump and conductivity detector. The system was interfaced with Dionex Chromeleon software (Version 6.11) which used to collect the data and control the auto-sampler.

The ions that could be quantitatively determined include anions like fluoride, acetate, chloride, nitrite, bromide, nitrate, phosphate and sulphate; as well as cations like sodium, ammonium, potassium, magnesium and calcium.

Special attention was paid to the concentration of sulfate, calcium, chloride and magnesium ions. Due to very high concentration of elements in the solutions, the samples were first diluted using dilute machine MICROLAB 500. Some duplicate samples were run to examine the accuracy of the test.

### **3.6.9 pH measurement of test solutions**

Chemical reactions depend on electric charges of various ions present in the system and these can be partly monitored by means of pH measurement.

The pH of solutions in the individual containers was measured regularly after the immersion of specimens using digital pH meter with an electrode (Type HI8424 HANNA). This was calibrated before taking the reading and it was also washed by deionised water between each measurement.

### **3.6.10 Calcite and gypsum solubility**

Because, calcite and gypsum have significant roles in thaumasite formation, the effect of chloride level on the solubility of calcite and gypsum was also

investigated. Calcite and gypsum were dissolved in prepared solutions in concentrations similar to those used in this study. The solutions were manually vibrated on daily basis. After a week, the solutions were filtered and samples were analysed using the ion chromatography technique. The amount of calcium ion in the solutions was used as indication for both calcite and gypsum solubility, since both are the only source of calcium.

### 3.6.11 Open porosity

The open porosity accessible by water was measured using the simple method of water displacement. Porosity measurement by saturated technique is not as accurate as that measured by other technique such as mercury intrusion porosimetry (MIP) techniques, but its simplicity enables it to be used to indicate and compare open porosity values in the samples. A 50 mm cube was vacuum saturated until constant weight was achieved and weighed in water and air. They were then dried in an oven at 105°C for 24 hours and weighed again, the porosity was then calculated.

### 3.6.12 Oxygen permeability

The oxygen permeability was measured using the CEMBUREAU-type gas permeameter (Verdier et al., 2002). At the end of experiment work and after performing corrosion measurement (900 days of exposure), 25 mm diameter and 10mm high cores were taken from the central sound part of the corrosion specimens and they were then dried in an oven at 105°C until constant weight obtained. They then tested for air permeability. The obtained results compared with initial values (after initial 28 days immersion in water), in which cylindrical specimens with 100mm diameter and 50mm height were used. The modified Darcy's equation was used to calculate intrinsic oxygen permeability (Verdier et al., 2002):

$$K = \frac{2\mu P_{out}QL}{A(P_{in}^2 - P_{out}^2)} \quad (3.1)$$

Where, K = intrinsic permeability (m<sup>2</sup>)

$\mu$  = viscosity of gas (for oxygen at 20°C = 2.02x10<sup>-5</sup> N.s/m<sup>2</sup>)

Q = flow rate (m<sup>3</sup>/s)

$P_{out}$  = outlet pressure (=1 bar at standard temperature and pressure)

$P_{in}$  = inlet pressure (=2 bars used)

A = cross sectional area of specimen (m<sup>2</sup>)

L = length of specimens (m)



A negative aspect of this test is the need for oven-drying the samples. Due to the sensitivity of pressure induced flow to micro-cracking that oven-drying at 105°C, could cause, the results may not be values of the absolute intrinsic permeability. Its use, however, is reasonable for comparative study.

### **3.6.13 Chloride content and diffusion**

- **Chloride content:**

Cylindrical mortar specimens ( $\text{Ø}100 \times \text{H}50 \text{mm}$ ) made with different binders were used to evaluate chloride concentration profiles and diffusion. All surfaces except top face of the specimens were sealed with bitumen coating so that immersion in test solutions would result in the chloride penetration occurring only in one-direction (See Figure 3.5). The test solutions respectively contained 2.0% chloride only and combined sulfate and 2.0% chloride. Water-soluble chloride contents were determined as they are assumed to be accountable for the corrosion process. The specimens were taken at the required ages from the axis so that 1 cm from edge was left at four different depth intervals; 0-5mm, 5-10mm, 10-15mm and 15-20mm using equipment shown in Figure 3.6. Powdered samples were obtained by slow-speed grinding using steel wheels. The powders so obtained were sieved through 150 micron in order to reduce the amount of aggregate, then kept in oven at 50°C for 24 hours, and then stored in sealed plastic bags until tested. Water extraction was carried out on collected powders as described by Zuquan et al., (2007) for free (water soluble) chloride content measurement. A 3 g of the powder was weighed to the nearest  $\pm 0.001$  g and dispersed in 100 ml of distilled water at room temperature, and stirred for approximately 1 minute. After this it was left to stand for 24 hours. The extract was filtered using a fast grade Whitman filter paper and made up to 100 ml with distilled water. Orion 4 Star pH/ISE bench top meter and combined chloride ion selective electrode was used in order to measure chloride concentration. Before the measurement, the electrode was calibrated using standard solutions.

- **Chloride diffusion:**

There are two different ways of determining diffusion: 1) the intrinsic diffusion coefficient which describes the movement of substance where the flux is calculated per unit cross sectional area of the pores and the concentration in

the free liquid and 2) the apparent diffusion coefficient which describes the movement of an ion where the flux is calculated per unit area of the porous material and the average concentration in the material (Lizarazo and Claisse, 2009). The apparent diffusion coefficient is calculated in this thesis because it is usually the one used to predict the service life of reinforced concrete structures.

The chloride binding capacity factor is defined as the ratio of total chloride ions per unit volume of solid to the free chloride ions per unit volume of liquid, as Lizarazo and Claisse (2009) explain.

In this work, the specimens were partly dry (21 days in air) before exposure to test solutions. This led to chloride penetration being partly due to absorption when the specimens were placed in the solution. The consequence of this would be rapid penetration of chloride as absorption is a relatively rapid transport mechanism. It should be mentioned that the effect of absorption on chloride diffusion was ignored.

The chloride concentration profiles for one dimensional migration into a semi-infinite medium would be expected to follow an error function solution to Fick's second law as in Equation 3.2 (Zuquan et al., 2007). The experimental results were exponentially fitted to this to calculate chloride diffusion coefficient.

$$C(x,t) = C_s \left[ 1 - \operatorname{erf} \left( \frac{x}{2\sqrt{Dt}} \right) \right] \dots \dots \dots (3.2)$$

where;  $D$  = apparent diffusion coefficient ( $\text{m}^2/\text{s}$ );  $t$  = time of exposure (s);  $C(x,t)$  = chloride concentration at depth  $x$  after time  $t$  (%/ww);  $C_s$  = surface chloride concentration (%/ww); and erf is the error function.

Surface chloride concentration ( $C_s$ ) values were estimated from the best fit (exponential fit) to experimental data and then  $D$  values were calculated by iteration to generate the best fit by least squares.

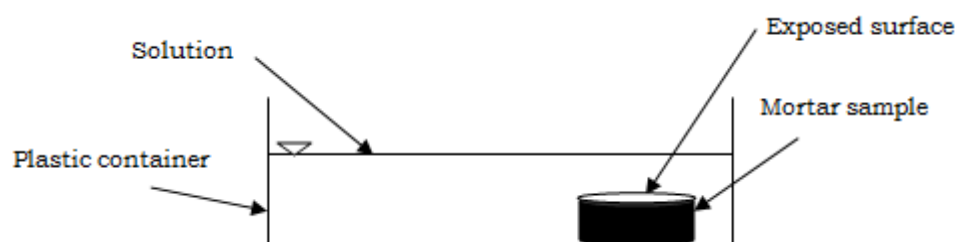


**Figure 3.5.** Schematic diagram for diffusion.

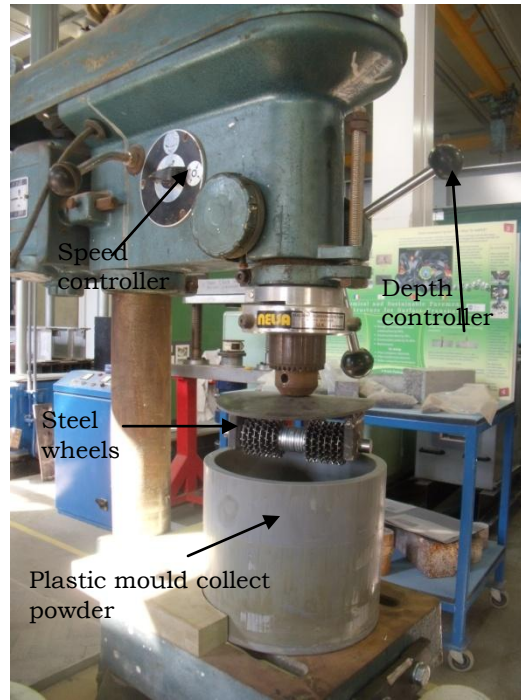


**Figure 3.6** Grinding equipment used to collect powders.

#### **3.6.14 Carbonation depth by phenolphthalein**

Corrosion specimens were used to investigate the carbonation depth of specimens made with different binders at the end of experimental programme. Chang and Chen,(2006) explain that the depth of carbonated layer in a concrete/mortar component can be evaluated by several different methods. In this study it was assessed by spraying a solution of phenolphthalein on freshly split mortars as described by Al-Amoudi et al.(1991). The indicator becomes pink in contact with alkaline concrete ( $\text{pH} > 9$ ) and colourless at lower pH values. At the end of experimental work, specimens stored in SC20 solution at  $5^{\circ}\text{C}$  were split in half and the carbonation depths were evaluated visually on the half specimens.

#### **3.6.15 Corrosion evaluation**

Evaluation of corrosion was made by means of linear polarisation resistance (LPR) and visual assessment of steel surface at the end of experimental work on reinforced mortar specimens made with different binders stored in composite sulfate and 0.5% chloride (SC5) and composite sulfate and 2.0% chloride(SC20) solutions at 5 and  $20^{\circ}\text{C}$ .

After 720 days of exposure, reinforced mortar specimens transferred from covered boxes to open large containers with similar solutions at room temperature (~20°C). Because the solutions were subject to evaporation, the levels in the containers were regularly checked and compensated. The first LPR measurements were then taken.

After 720 days, the corrosion was subjected to acceleration by applying a positive 100 mV DC voltage to the steel bar (anode) , where the negative terminal consisted of stainless steel mesh (cathode) immersed in the solution (electrolyte). This acceleration continued for 180 days and the LPR measurements were taken twice: after 720 days and after a further 180 days of acceleration (720 plus 180 days). After finishing all the LPR measurements, the specimens were broken open to facilitate visual examination of the state of steel surfaces.

To ensure a stable system, the 900 days LPR measurements were taken after 3 days of disconnecting the applied voltage (+100mV). Some samples were repetitively tested in order to examine the accuracy of the test. No significant variations were found between the repeated measurements.

#### **A. Linear polarisation technique**

Among several methods that exist to measure corrosion rates in concrete, the most frequently used is linear polarization resistance (LPR), a non-destructive technique that provides quantitative information regarding corrosion rate (Andrade and Alonso, 2001). It can be used in both field and laboratory investigations. However, (Claisse, 1988) pointed out that care should be taken when considering evaluation of corrosion using this technique and correction against uncompensated resistance errors should be made. The fundamental theory of the linear polarization technique to determine the corrosion rate of each steel bar embedded in mortar is to apply a slowly changing voltage close to the corrosion potential and to record polarization current. The polarization resistance ( $R_p$ ) of the reinforcing steel is defined as the slope of a potential-current density plot at the corrosion potential (Claisse, 1988) as:

$$R_p = \left( \frac{\Delta V}{\Delta I} \right) \quad (3.3)$$

where;

$\Delta V$  is applied potential and;

$\Delta I$  is current response.

The corrosion current density then can be calculated from the Stern-Geary equation (Broomfield, 1997):

$$I_{\text{corr}} = \frac{B}{R_p} \quad (3.4) \quad \text{and} \quad B = \beta_a \times \beta_b / 2.303 (\beta_a + \beta_b) \quad (3.5)$$

where; B is a constant that can be determined from Tafel slopes;  $\beta_a$  and  $\beta_b$  for the anodic and cathodic reactions, respectively.

The values of B are taken from the empirical values of 26 and 52 mV (Broomfield, 1997), for active and passive steel, respectively. In this study, B equal to 26 was used.

In this study, the electrochemical measurements was made using the equipment shown in Figure 3.7, which is a VersaSTAT 3F potentiostat model, manufactured by Princeton Applied Research. A carbon rod placed outside the specimen was used as a counter electrode, while a saturated calomel electrode used as the reference electrode. The polarization resistance ( $R_p$ ) determinations were performed at a scan rate of 0.167 mV/s over a range of  $\pm 10$  mV. A computer program, VersaStudio model, developed by EG&G Princeton Applied Research, was used for applying the potential scan, analysing the data, and calculating the polarization resistance ( $R_p$ ), corrosion current ( $I_{\text{corr}}$ ) Parameters. Figure 3.8 is a schematic diagram for these measurements. LPR measurements were repeated on selective specimens in order to examine the accuracy of the test. Since, the purpose of the tests in this study was to provide comparative data rather than absolute values of the parameters, no corrections were made to the results, which may result in overestimated values.



**Figure 3.7.** Corrosion equipment.

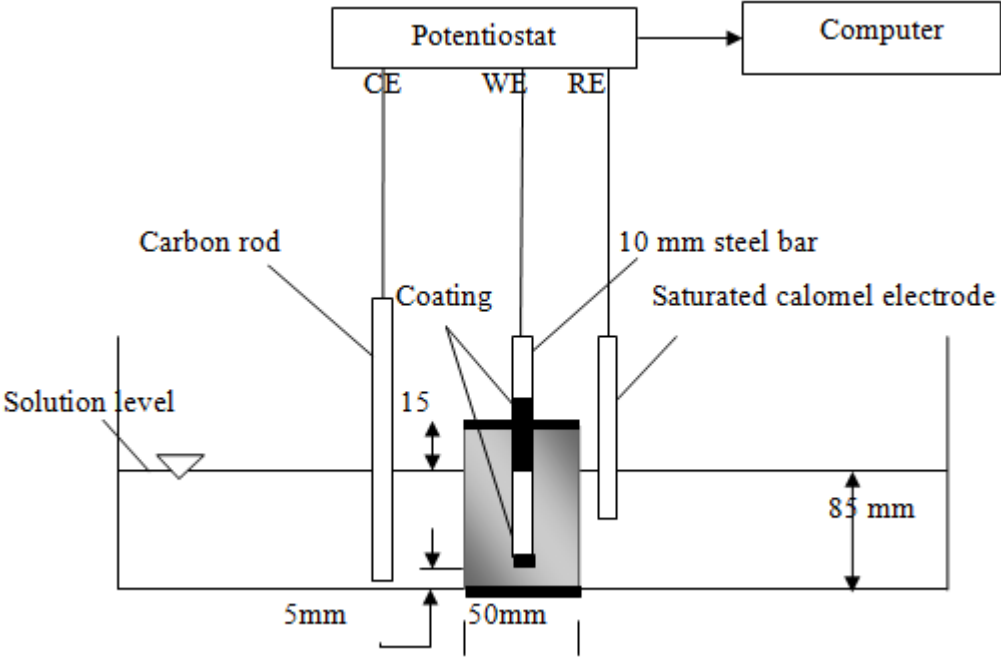


**Figure 3.8.** Set up of corrosion measurements by LPR.

**B. Visual assessment of steel surface area**

At the end of the experimental work and after all LPR measurements were carried out, the corrosion specimens were broken open and the steel rebars were removed, cleaned by acetone and photographed. The extent of corrosion was then visually examined.

## **4. Performance of cement mortars subjected to sulfate and chloride exposure at 5 and 20°C**

### **4.1 Introduction**

This chapter presents and discusses the results of the evaluation of performance of mortar specimens made with four types of binders exposed to combined action of sulfate (Class DS4 as magnesium sulfate) and chloride (0, 0.5, 1 and 2%Cl-) solutions at 5 and 20°C. The performance of CEMI, CEMI blended with 10% limestone filler (CEMI-LF), CEMI blended with 50% pulverised fly ash (CEMI-PFA) and CEMI blended with 70% ground granulated Blast-furnace (CEMI-GGBS) mortars stored in sulfate solution only were compared to those immersed in composite sulfate and chloride solutions in terms of the severity of thaumasite attack after 6, 9, 12, 15, 18 and 21 months exposure at 5, and 20°C.

The evaluation of the performance of the specimens was based on visual observations, mass change, expansion, chemical analysis of test solutions as well as X-ray diffraction, infra-red spectroscopy and scanning electron microscopy of deterioration products and powdered sample. In order to investigate the effect of chloride on leaching of cement mortar, the pH and the chemistry of the test solutions of different binders were monitored at early exposure periods (during the 180 days of immersion) using 20mm mortar cubes kept in small plastic containers at 5 and 20°C. The effect of chloride level on the solubility of calcite and gypsum was also investigated. Details about mix proportions, mortar casting, curing, preparation of test solutions and experimental details were given in Chapter 3.

### **4.2 Visual observation assessment**

The assessment by visual inspections was mainly made on 50mm cubes, however, since some 20mm cubes, particularly those made with GGBS and PFA, showed attack at 90 and 180 days of immersion they were also investigated. It should be mentioned that the main purpose for using 20mm

mortar cubes was to monitor the pH and chemical changes in the test solutions during the early exposure period. The assessment was made in terms of surface features e.g. cracking, change in colour, swelling and spalling, using a qualitative scale for damage, given in Table 4.1.

**Table 4.1.** Summary of visual assessment for 50mm mortar cubes.

| Sample Code<br>(Binder-Solution) | Temp.<br>(°C) | Exposure period in solution (days) |     |     |     |
|----------------------------------|---------------|------------------------------------|-----|-----|-----|
|                                  |               | 90                                 | 180 | 360 | 630 |
| CEMI- S                          | 5             | 0                                  | 2   | 3   | 4   |
| CEMI-SC5                         |               | 0                                  | 2   | 4   | 5   |
| CEMI-SC10                        |               | 0                                  | 2   | 2   | 2   |
| CEMI-SC20                        |               | 0                                  | 0   | 0   | 0   |
| CEMI-LF-S                        |               | 1                                  | 2   | 3   | 5   |
| CEMI-LF-SC5                      |               | 1                                  | 3   | 5   | 6   |
| CEMI-LF-SC10                     |               | 1                                  | 2   | 2   | 3   |
| CEMI-LF-SC20                     |               | 0                                  | 0   | 0   | 0   |
| CEMI- S                          | 20            | 0                                  | 0   | 0   | 0   |
| CEMI-SC5                         |               | 0                                  | 0   | 0   | 0   |
| CEMI-SC10                        |               | 0                                  | 0   | 0   | 0   |
| CEMI-SC20                        |               | 0                                  | 0   | 0   | 0   |
| CEMI-LF-S                        |               | 0                                  | 0   | 1   | 1   |
| CEMI-LF-SC5                      |               | 0                                  | 0   | 1   | 2   |
| CEMI-LF-SC10                     |               | 0                                  | 0   | 0   | 1   |
| CEMI-LF-SC20                     |               | 0                                  | 0   | 0   | 0   |

0= No visible damage, 1= minor cracking to corners and edges, 2= moderate damage at corners and edges, 3= severe attack at corners, 4= cracking and spalling, 5= swelling of surfaces, and 6=extensive cracking and swelling.

#### 4.2.1 Visual assessment after 90 days

##### **50mm cubes:**

This section presents the performance of the 50mm mortar cubes exposed to sulfate only and combined action of sulfate and chloride (0.5, 1 and 2% Cl<sup>-</sup>). The first signs of damage were detected within 100 days of immersion in sulfate only, SC5 and SC10 solutions at the corners and edges of the CEMI and CEMI-LF specimens at 5°C, and it was more evident in the CEMI-LF specimens. This damage characterised by formation of microcracks and deposition of white materials on corners and edges of mortar cubes.

##### **20mm cubes:**

As for 50mm cubes, and as Figure 4.1 illustrates, the 20 mm mortar cubes made with CEMI-LF immersed in SC5 solutions at 5°C showed the earliest signs of damage in contrast to the other mortars and solutions. This degradation which occurred after 74 days of exposure consisted of softening, microcracks and the deposition of white materials on corners and edges of the



cubes. The presence of 1% chloride in SC10 solution (Figure 4.2) caused a delay to 90 days of immersion in the instigation of damage.



**Figure 4.1.** 20mm mortar cubes of CEMI-LF mortar stored for 74 days in SC5 at 5°C.

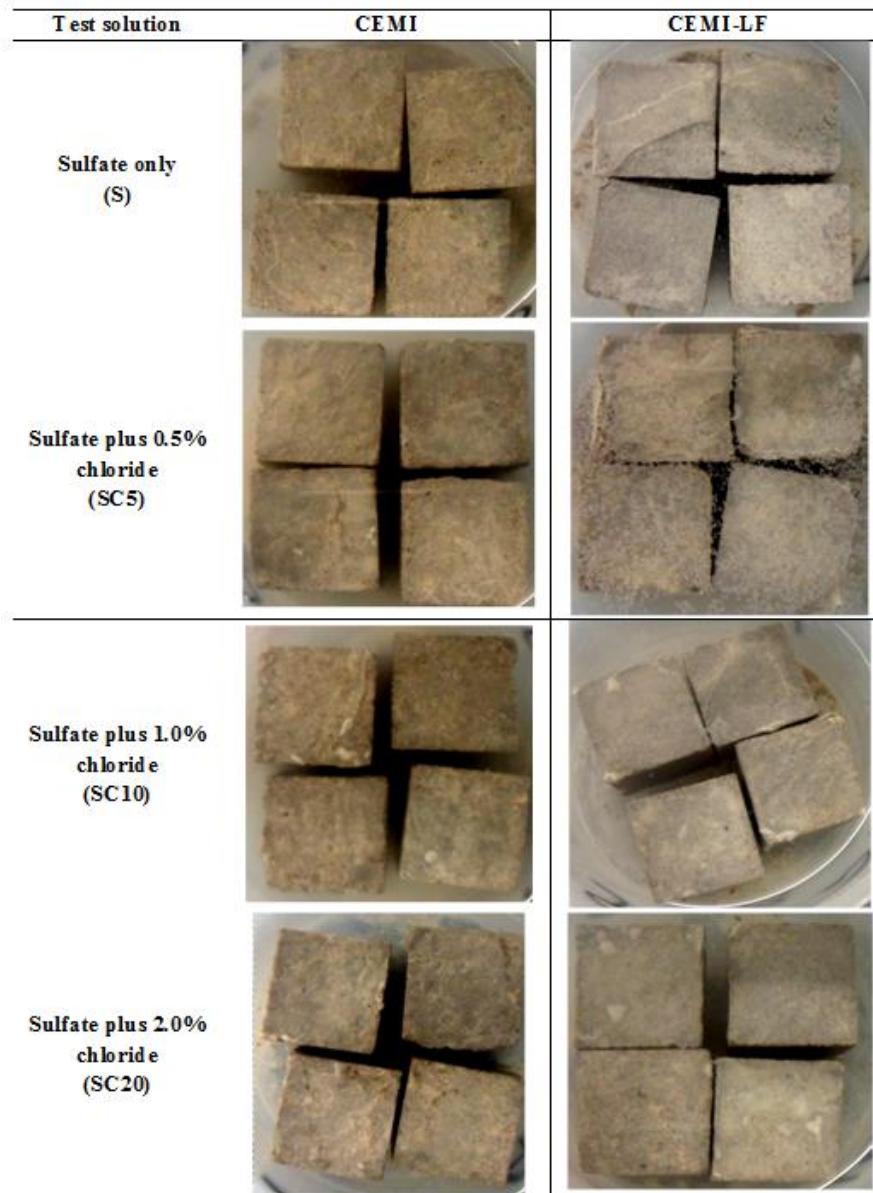


**Figure 4.2.** 20mm cubes of CEMI and CEMI-LF stored for 90 days at 5°C.

#### 4.2.2 Visual assessment after 180 days

##### **50mm cubes:**









The 50mm specimens stored for 180 days in test solutions at 5°C are shown in Figure 4.3. It can be noted that CEMI and CEMI-LF mortar samples exposed to S, SC5 and SC10 solutions at 5°C suffered further attack as time progressed.

Differences due to the chloride concentration and carbonate content were evident. The highest extent of damage was observed for CEMI-LF specimens exposed to SC5 solution at 5°C. At 20°C, all specimens remained intact with no visual damage, which was also the case for CEMI-PFA and CEMI-GGBS mortar specimens stored at both temperatures.

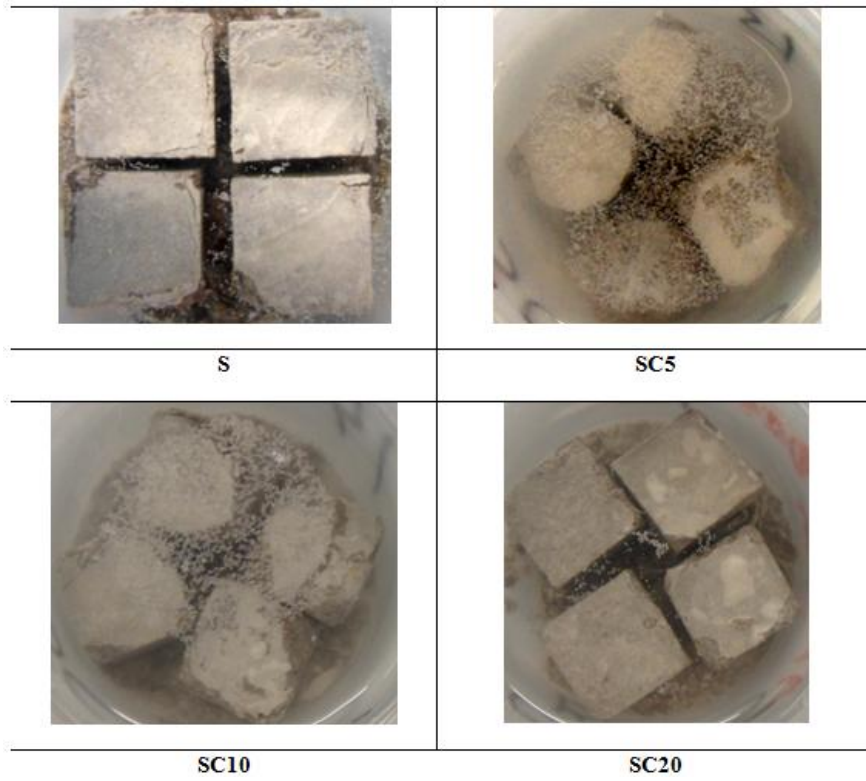
**20mm cubes:**

Figure 4.4 shows the appearance of the 20mm of CEMI-LF mortar specimens placed for 180 days in different solutions at 5°C. It can be seen that the results follow similar trends, but extent of attack was more advanced compared with the 50mm cubes. This was probably because of the higher interaction rate in smaller sample size. However, after replenishment of the solution at 90 days, mortars in SC20 solution showed clear evidence of attack.

The attack in 20mm mortar cubes containing PFA and GGBS showed different results, depending on temperature and test solution. At 5°C, one of CEMI-PFA (Figure 4.5) mortar samples stored in sulfate only (S) solutions suffered attack by cracking, whereas, combined sulfate and chlorides (0.5 and 2.0%) solutions showed no marks of damage at this stage of exposure. In contrast in mortars made with CEMI-GGBS shown in Figure 4.6, damage consisting of cracking along edges occurred for SC5 solution. All mortars stored at 20°C remained intact at this stage of immersion.

| Test Solution                          | 180 days   |   |
|--|--|---|
|  | CEMI   | CEMI-LF   |
| Only sulfate<br>(0.6%SO <sub>4</sub> ) |    |    |
| Sulfate plus 0.5%<br>chloride          |    |    |
| Sulfate plus 1.0%<br>chloride          |   |   |
| Sulfate plus 2.0%<br>chloride          |  |  |

**Figure 4.3.** CEMI and CEMI-LF mortar stored for 180 days at 5°C.



**Figure 4.4.** General view of 20mm of CEMI-LF specimens stored for 180 days at 5°C.



**Figure 4.5.** 20 mm CEMI-PFA mortar cubes stored for 180 days in S at 5°C.



**Figure 4.6.** 20mm CEMI-GGBS mortar cubes stored for 180 days in SC5 at 5°C.

#### **4.2.3 Visual assessment after 360 days**

Figure 4.7 shows the appearance of the specimens stored for 360 days. It can be noted that the effect of chloride on the sulfate attack became clearer as time passed. It was evidently chloride level and temperature dependent, as seen by both form and intensity of the damage at the different solutions at 5°C, where CEMI-LF samples showed the highest extent of attack. The intensity varied with the concentration of chlorides in solutions. The worst case occurred in specimens immersed in the combined solution of sulfate and 0.5% chloride, followed by those stored in sulfate only and then combined sulfate and 1.0% chloride solutions. No signs of deterioration of specimens placed in combined sulfate and 2.0% chloride (SC20) solution occurred at this age.

At 20°C and as time progressed, CEMI-LF specimens stored in sulfate (S) only and SC5 solutions showed small microcracks on mortar edges, whereas no damage was detected in any specimens stored in SC10 and SC20. No signs of attack at this stage were observed for mortar samples made with CEMI-PFA and CEMI-GGBS.

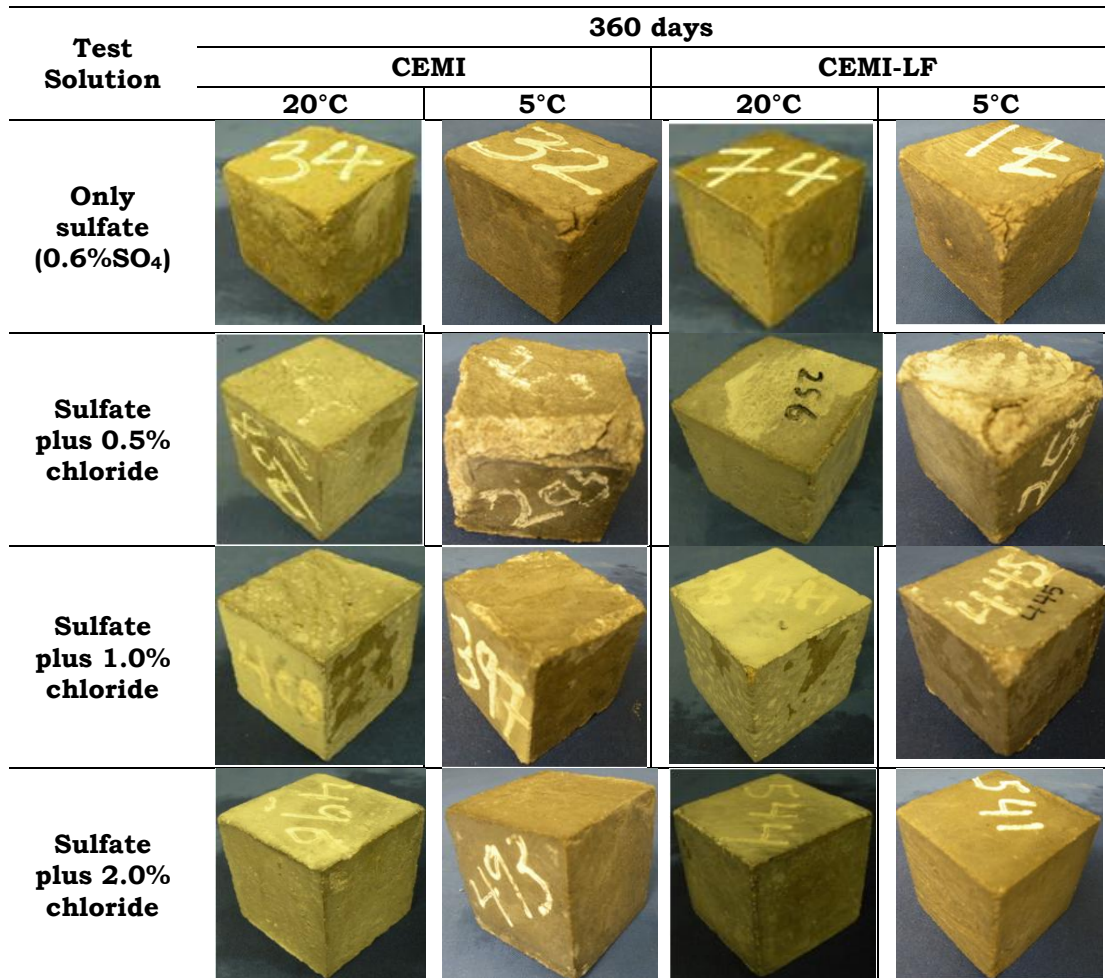


**Figure 4.7.** CEMI and CEMI-LF mortar specimens stored for 360 days at 5 and 20°C.

















#### 4.2.4 Visual assessment after 630 days

Figure 4.8 shows the CEMI and CEMI-LF specimens after 630 days storage at 5 and 20°C. As time progressed, the effect of chloride and temperature on the character and extent of sulfate attack became clearer. It was obvious that it was chloride and temperature dependent, as seen by both form and intensity of the damage at different solutions, more markedly at 5°C. CEMI-LF samples showed the highest degree of attack, where the intensity varied with the concentration of chlorides in solutions. The worst case occurred in specimens placed in SC5, followed by those stored in sulfate only (S) and (SC10) solutions; whereas, no signs of damage at this age was observed for specimens immersed in SC20.

At 20°C and as time progressed, the damage of specimens placed in SC5 became more evident, but with slower rate compared with those at 5°C. Mortar

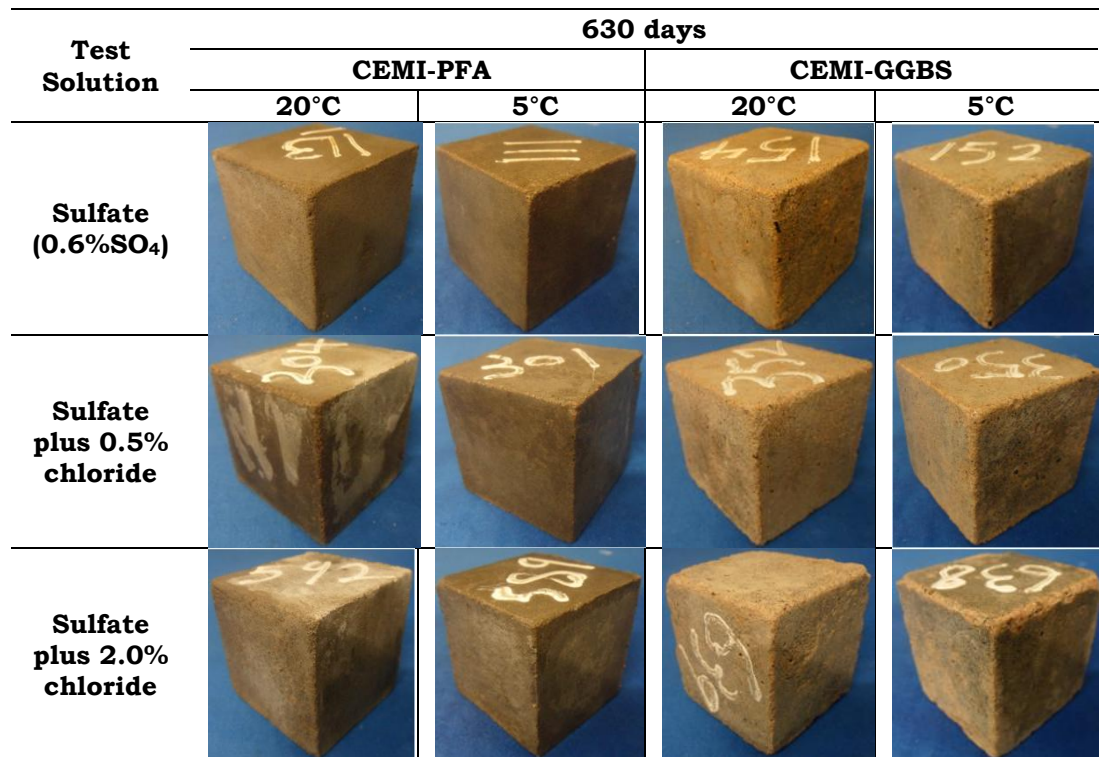
specimens made with CEMI and immersed in the same solutions showed less attack, as characterized by small microcracks on the edges. No damage was observed in any CEMI and CEMI-LF specimens stored in SC20 at 20°C, or in CEMI-PFA and CEMI-GGBS samples, as Figure 4.9 illustrates.

Figure 4.10 shows the general view of cubes and prisms after 630 days of immersion. It should be mention that prisms were used for length change measurement shown later in Section 4.4. It can be noted that cubes and prisms exhibited similar damage trend, in which severe attack, characterised by forming extensive mushy materials, were observed on surface layers of specimens in SC5 solution. As shown in Table 4.1, the sequence of the attack severity in CEMI and CEM-LF mortar stored in different solutions at 5°C was as follows, with relatively higher degradation degree in CEMI-LF mortars: Combined sulfate and 0.5% chloride (SC5) > Sulfate only (S) > Combined sulfate and 1.0% chloride (SC10) > Combined sulfate and 2.0% chloride (SC20).

| Test Solution                       | 630 days  |   |  |   |
|-------------------------------------|---|---|--|---|
|                                     | CEMI  |   | CEMI-LF  |   |
|                                     | At 20°C   | At 5°C  | At 20°C  | At 5°C  |
| <b>Sulfate (0.6%SO<sub>4</sub>)</b> |  |  |  |  |
| <b>Sulfate plus 0.5% chloride</b>   |  |  |  |  |
| <b>Sulfate plus 1.0% chloride</b>   |  |  |  |  |
| <b>Sulfate plus 2.0% chloride</b>   |  |  |  |  |

**Figure 4.8.**CEMI and CEM-LF mortar specimens stored for 630 days in solutions at 5 and 20°C.





**Figure 4.9.** PFA and GGBS mortar specimens stored for 630 days in solutions at 5 and 20°C.

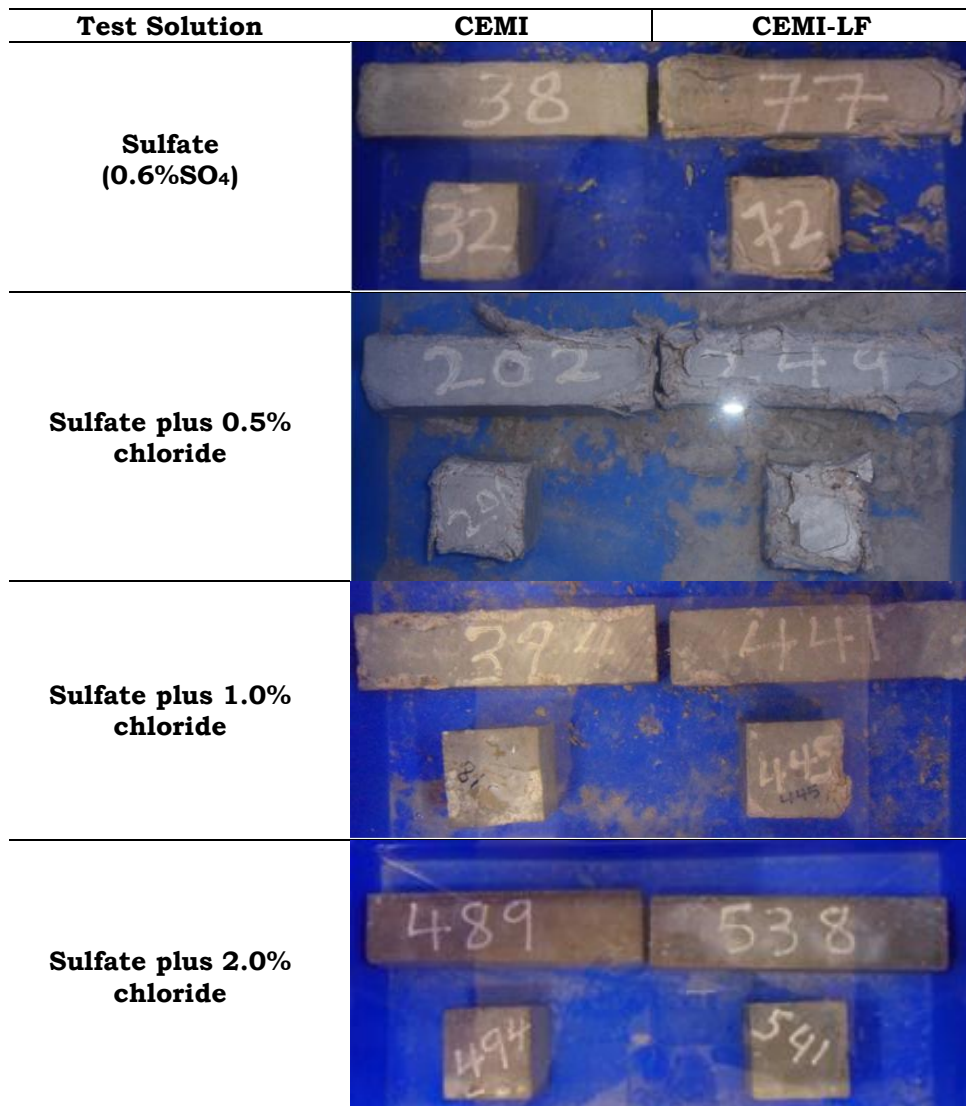


**Figure 4.10.** General view of CEMI and CEMI-LF mortar in containers stored for 630 days at 5°C.

### 4.3 Mass change up to 630 days

In this section the changes in mass of the 50mm mortar cubes are presented. Figure 4.11 and 4.12 respectively show the mass changes for CEMI and CEMI-LF mortar cubes stored for 630 days in test solutions at 5°C. All specimens initially showed weight gain in all test solutions. However, whereas this increase in weight continued for specimens stored in composite sulfate and 2.0% chloride (SC20) solution for the whole exposure period, specimens stored in combined sulfate and 0.5% chloride (SC5) solution showed first loss in mass

after 160 days, while those stored in sulfate only (S) solution began to lose mass after 270 days. Mass loss was greater for the CEMI-LF mortars than for CEMI mortars, at 360 days in composite sulfate and 0.5% chloride solution (SC5) amounting to 4.5 % and 1.4 % of the 28-day mass, respectively, and this increased to 9.4 % and 3.7 %, respectively after 630 days of immersion.

At 20°C and as shown in Figure 4.13 and 4.14, CEMI and CEMI-LF mortar cubes showed continuous gain in mass for the whole exposure period. Similarly, CEMI-GGBS and CEMI-PFA samples (Figure 4.15) stored in all test solutions at 5 and 20°C showed continuous gain in mass during the experiment. Visually, those specimens remained intact and no signs of damage were observed during the experiment.

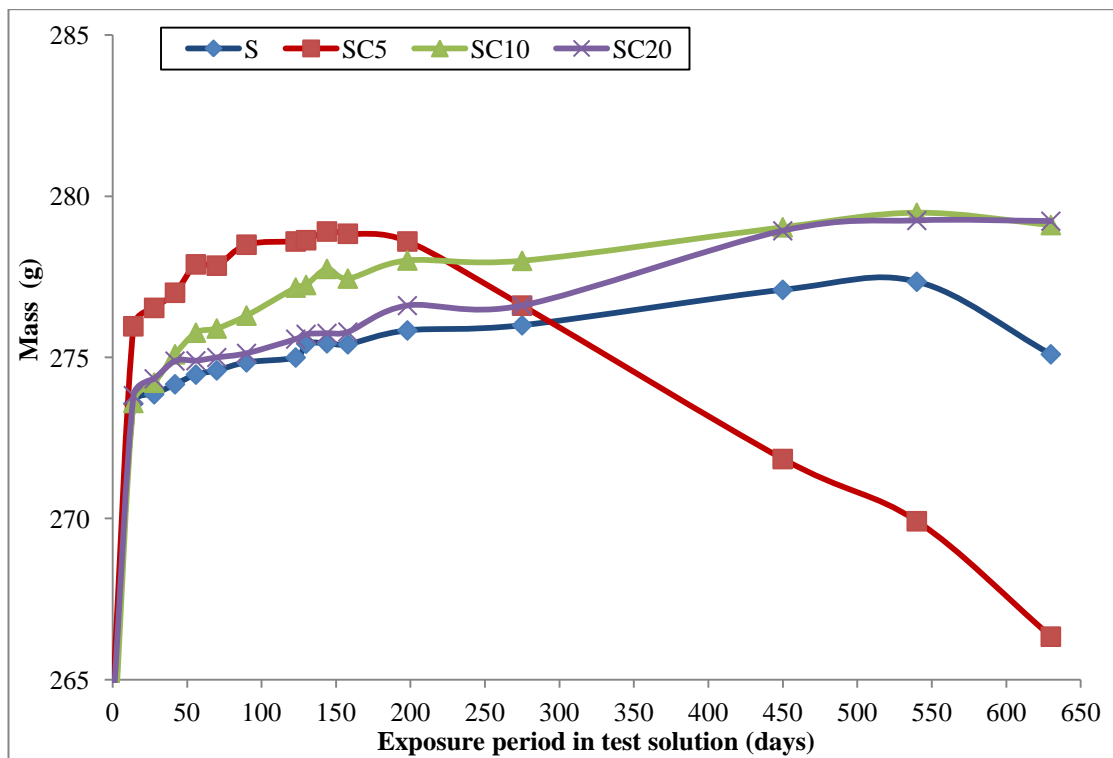


**Figure 4.11.** Mass changes for CEMI mortar cubes stored 630 days at 5°C.

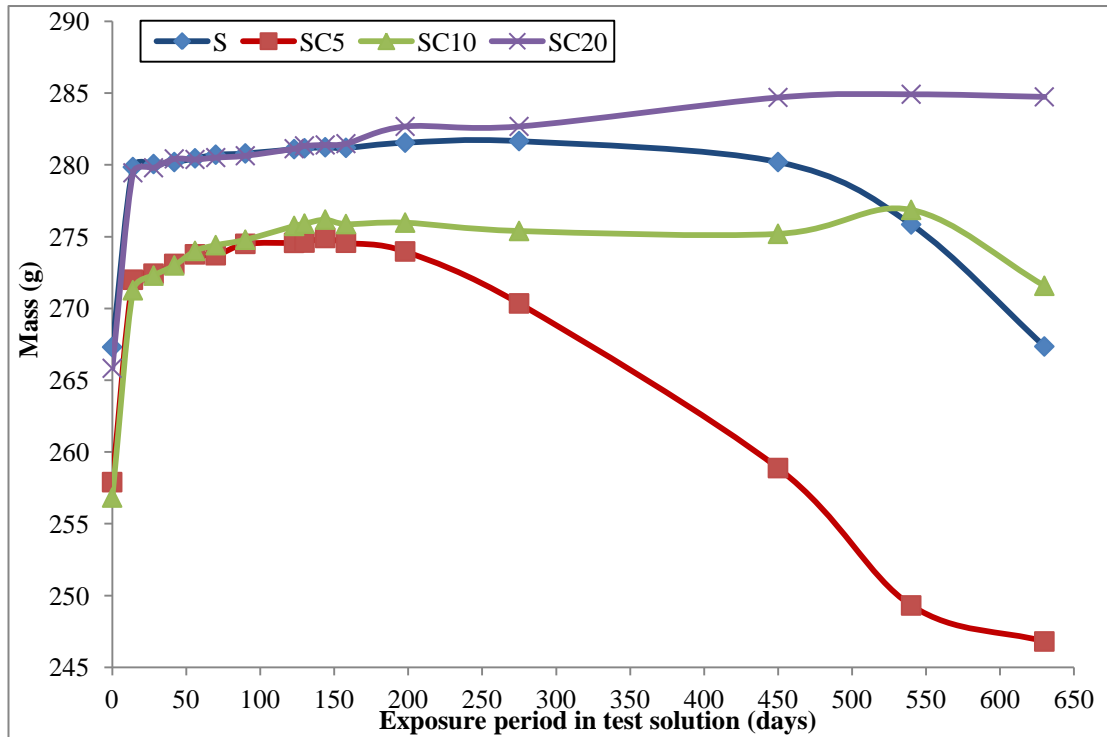


**Figure 4.12.** Mass changes for CEMI-LF mortar cubes stored 630 days at 5°C.

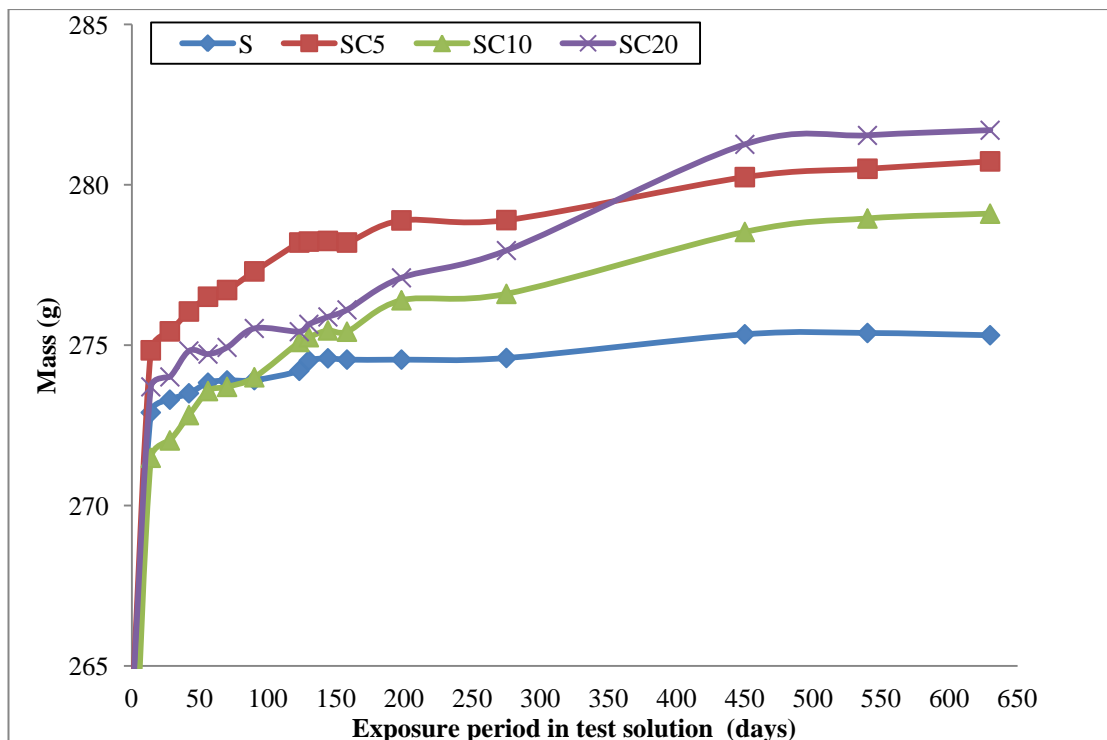


**Figure 4.13.** Mass changes for CEMI mortar cubes stored for 630 days at 20°C.

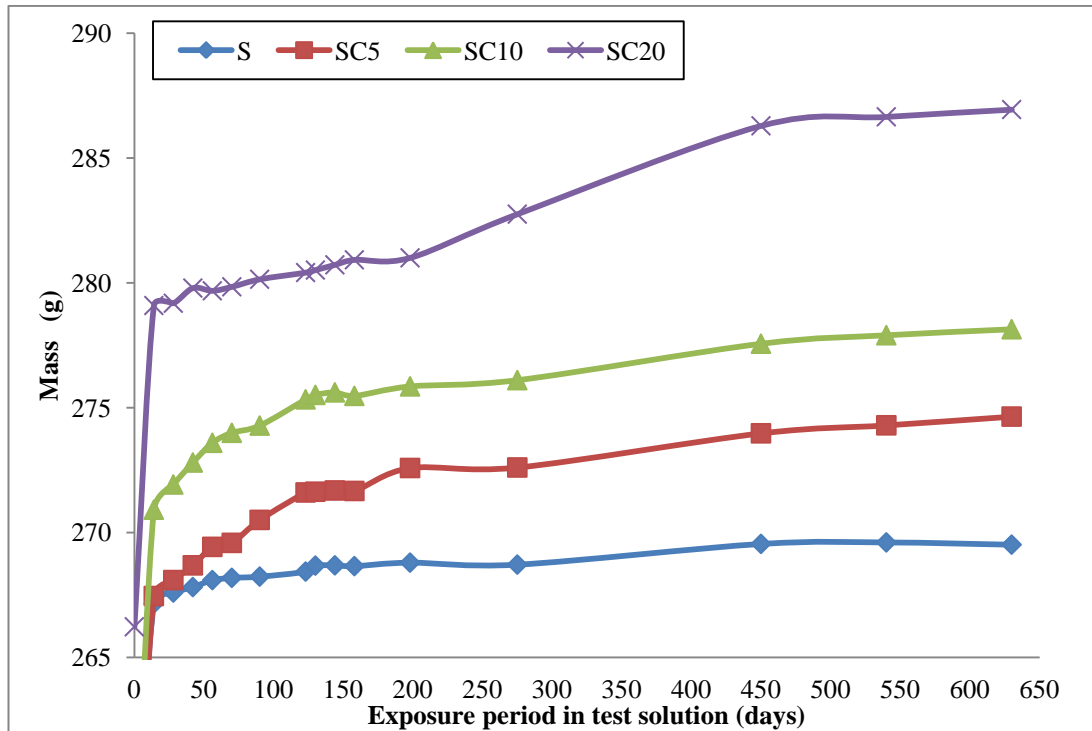


**Figure 4.14.** Mass changes for CEMI-LF mortar cubes stored 630 days at 20°C.

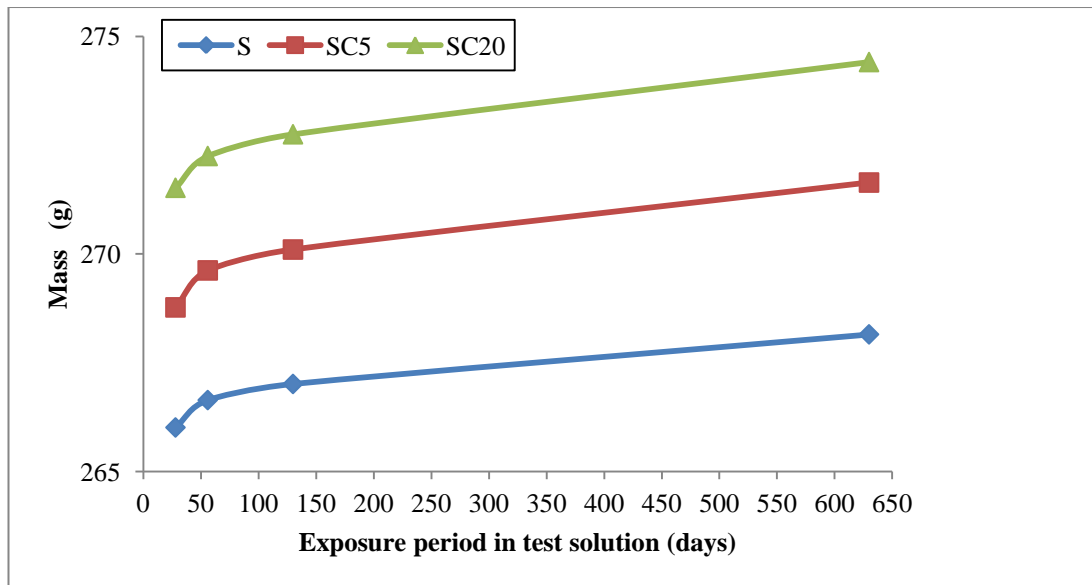


**Figure 4.15.** Mass changes for CEMI-PFA mortar cubes stored 630 days at 5°C.

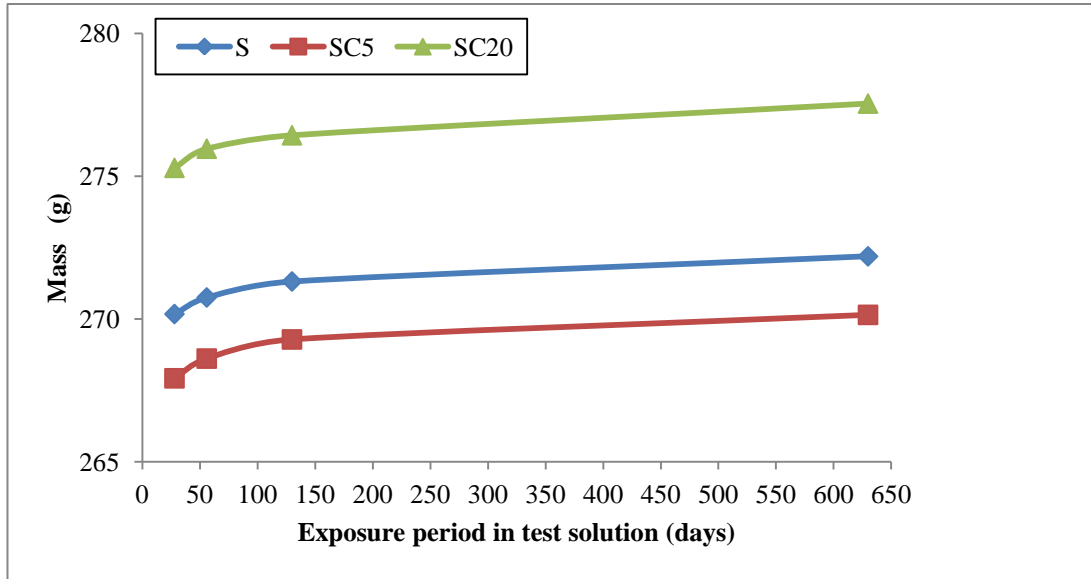


**Figure 4.16.** Mass changes for CEMI-PFA mortar cubes stored 630 days at 20°C.

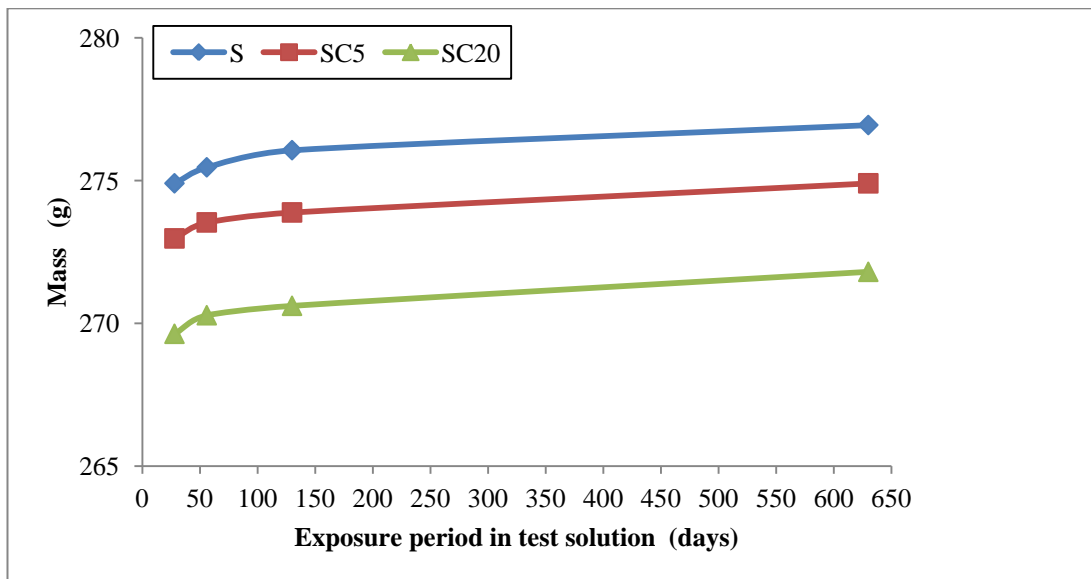


**Figure 4.17.** Mass changes for CEMI-GGBS mortar cubes stored 630 days at 5°C.

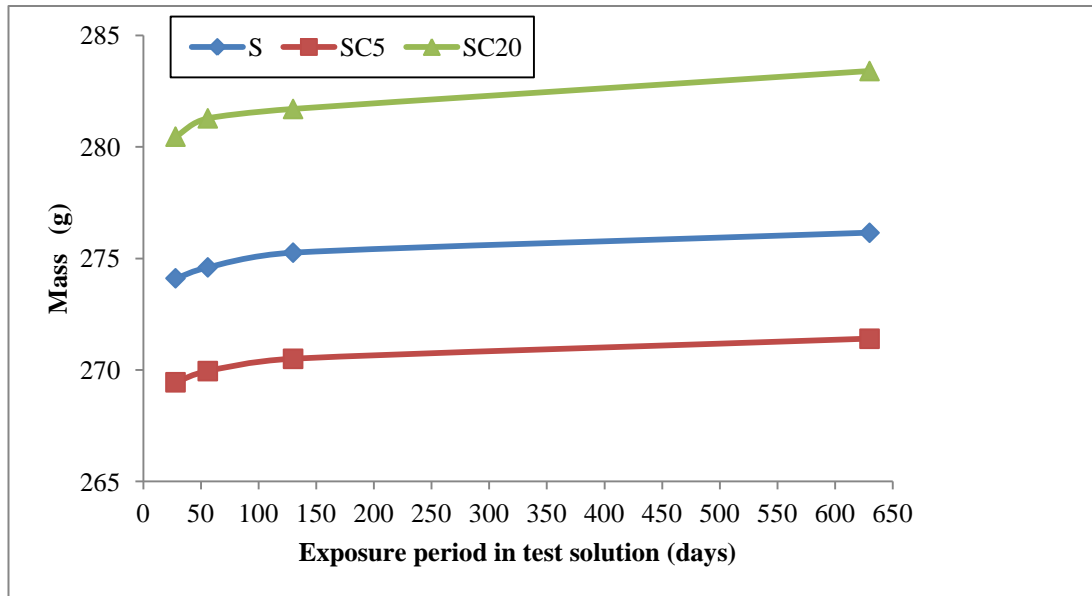


**Figure 4.18.** Mass changes for CEMI-GGBS mortar cubes stored 630 days at 20°C.

#### 4.4 Length change up to 630 days

This section presents the measurements of length changes during 630 days of immersion in sulfate only and composite solutions at 5 and 20°C of CEMI and CEMI-LF mortar. These measurements were carried out on prisms that had been cast and cured in the same manner as was used for the cubes, shown in Figure 4.10.

All CEMI and CEMI-LF mortar prisms stored for 630 days in test solutions showed slight increase (Expansion) in length, as given in Figure 4.19. It can be also seen that there was no significant variations in the expansion values among the samples. Although, SC10 samples at 5°C showed lower extent of surface attack compared with sulfate only and SC5 samples, they showed the highest expansion values of 0.081% and 0.095% for CEMI and CEMI-LF, respectively. Samples in SC5 solutions which showed the highest extent of surface degradation showed no remarkable change in length when compared with other samples.

The intensive sulfate attack (Figure 4.10) on surfaces of limestone cement mortars does not appear to have significantly affected the mortar expansion under investigated conditions.

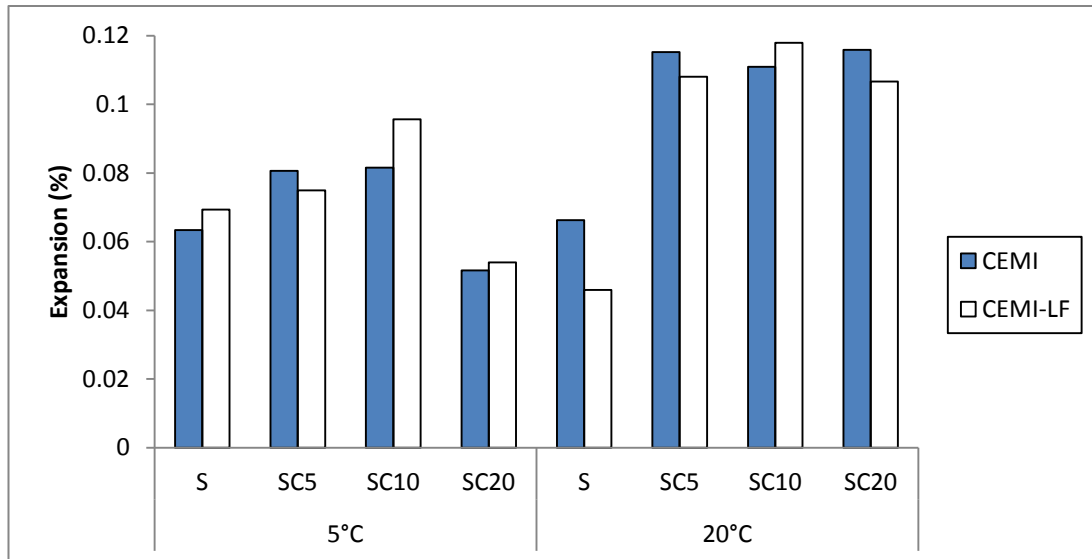


**Figure 4.19.** Length change variations for CEMI and CEMI-LF mortars stored for 630 days at 5 and 20°C.

## 4.5 Mineralogy of deteriorated materials

In order to clarify the findings reported in the previous sections, the mineralogy of deteriorated products was identified by means of X-ray diffraction (XRD) and infrared spectroscopy (IRS). In cases in which mortar specimens remained almost intact, the sound surfaces were also investigated.

### 4.5.1 X-ray diffraction (XRD)

Degraded materials collected from surfaces of mortar cubes which suffered visual attack after storage in different solutions at 5 and 20°C for 630 days were analyzed by means of X-ray diffraction (XRD) in order to identify their mineralogy. In cases in which cubes remained almost intact, the surface was scratched and the dry ground powder was analyzed. The results are presented and discussed in the following sections. Since CEMI-LF mortar at 5°C showed the highest extent of attack, the XRD of these degraded surface materials are also compared to samples of sound core material. Degraded surface samples from 20mm CEM-PFA and CEMI-GGBS mortar cubes which showed visible attack after 180 days of immersion, were also analyzed by XRD.

- **XRD analysis of CEMI and CEMI-LF mortars stored at 5 and 20°C**

Figure 4.20 and 4.21 show the XRD patterns of samples collected from the degraded surfaces of CEMI and CEMI-LF mortar specimens stored for 630 days



in S, SC5 and SC10 solutions compared with that taken from intact surface of SC20 at 5°C. It can be clearly seen that the presence and intensity of some phases depended strongly on test solutions chemistry. The peaks used for the identification of the various phases are shown in Table 4.2.

**Table 4.2.** Peaks for various phases.

| <b>Phase</b>       | <b>Peak on XRD trace (CuK<math>\alpha</math> radiation used) - 2<math>\theta</math> angles (degrees)</b> |
|--------------------|--|
| Calcite (C)        | 23.05, 29.4, 35.97, 39.40, 43.16, 47.5, 56.56, 57.40 and 58.08   |
| Thaumasite (T)     | 9.2, 16.0, 18.12, 19.4, 23.4, 26.01, 28, 32.83, 35.73 and 41.66  |
| Gypsum (G)         | 11.6, 20.72, 29.1, 31.1, 32.0, 33.3 and 34.5   |
| Brucite (B)        | 18.52 and 37.98  |
| Aragonite (A)      | 26.21, 27.22, 33.13, 36.18, 37.26, 37.88 and 45.85   |
| Portlandite (P)    | 18.01, 34.17, 28.72 and 47.25  |
| Friedel's salt (F) | 11.2 and 31.18   |
| Ettringite (E)     | 9.09, 15.8, 17.83, 18.9, 22.94, 25.61, 27.5, 32.26, 35.023, 40.87, and 41.97                             |
| Quartz (Q)         | 26.62, 20.85, 42.5, 47.12 and 50.1   |

Calcite was detected in both mixes and as expected, strong peaks were detected in CEMI-LF mortar samples. The presence of relatively strong peaks for thaumasite, gypsum, brucite, aragonite and the absence of portlandite were detected in both mixes samples and for sulfate only (S) and composite sulfate and 0.5% chloride (SC5) solutions. Instead, marked peaks for Friedel's salt; portlandite, ettringite and traces of thaumasite were detected in samples in composite sulfate and 2.0% chloride (SC20) solution.

The increase in the dissolution of portlandite at lower temperature would result in a rapid reaction with sulfate ions to form gypsum and brucite, both of which were identified in the degradation products of mortar immersed in sulfate only and combined sulfate and 0.5% chloride solutions. The very low solubility of brucite would cause a reduction in pH so that ultimately C-S-H would become more vulnerable to sulfate attack. This process appeared to occur more rapidly in mortar specimens immersed in combined sulfate and 0.5% chloride (SC5) solution, which showed higher degree of attack.

In addition, Friedel's salt becomes unstable in pH lower than 10 (Goñi and Guerrero, 2003), which is a value attained when insoluble brucite precipitates at the surface. It is also reported by Torres (2004) that Friedel's salt is not stable in the presence of thaumasite which may explain why it was not present in the degraded mortars stored in SC5. Due to the use of Philips aluminium sample holder, peaks at 38.47 and 44.7 2theta for aluminium were presented for all samples.

At 630 days, thaumasite was rarely detected in SC20 mortars, instead Friedel's salt which is a non-expansive product, was observed. It is possible that at high chloride concentration, the amount of Friedel's salt produced could present a physical barrier impeding ingress or chemical diffusion and it may also result in limiting the availability of aluminates phases free to engage in degrading sulfate bearing products. In addition, mortars in SC20 solution were distinguished by exhibiting clear peaks for portlandite with low peaks for ettringite and no peaks for gypsum.

Quartz were detected in all samples with strong peaks for those in SC10 and SC20 samples, which showed low or no attack. The siliceous aggregate used is the main source of quartz in all samples.

At 20°C, the XRD patterns of material samples collected from surfaces of CEMI and CEMI-LF mortar specimens stored for 630 days in different solutions are shown in Figure 4.22 and 4.23. All samples showed strong peaks for portlandite, with relatively more in CEMI samples. The reduction in portlandite intensity in CEMI-LF samples was expected due to the dilution effect of limestone filler. The decreased portlandite dissolution as temperature increased is one main reason why sulfate attack is slow at 20°C compared with 5°C.

In case of CEMI-LF mortars, the SC5 sample showed the lowest portlandite peak intensities. Traces of gypsum and brucite were detected in both sulfate only and SC5 of CEMI-LF samples, with relatively higher peak intensities in the SC5 sample. Portlandite most probably reacted with sulfate and magnesium ions to form gypsum and brucite, both found in the surface layer of SC5 mortar, but with smaller quantities compared with samples stored at 5°C. This indicated earlier reactions between portlandite and magnesium sulfate in both samples, more evidently in SC5. The higher solubility of gypsum at higher temperature might result in decreasing the chance of gypsum formation in samples stored at 20°C.

It can be clearly seen that the intensity of Friedel's salt increased in all samples as chloride level increased in solutions. CEMI samples showed higher peak intensities for Friedel's salt than CEMI-LF samples. This was also expected as it would be caused by the diluting effect of limestone filler which reduced the amount of C<sub>3</sub>A in the system.

Traces of thaumasite were detected in all samples, more evidently in CEMI-LF sample stored in SC5 solution. Thaumasite was also reported (Martinez-

Ramirez et al., 2011, Hartshorn et al., 2002, Irassar et al., 2005) to form at ambient temperature, however, it is generally accepted that extensive thaumasite formation is associated with low temperature conditions.

Aragonite, which is a metastable form of calcium carbonate compared with calcite, was also detected in all samples stored in all solutions at 20°C, but with higher amounts in composite solutions and lesser quantities than at 5°C. Gollop and Taylor (1995) reported that aragonite precipitation is kinetically favoured over calcite if magnesium sulfate is present.

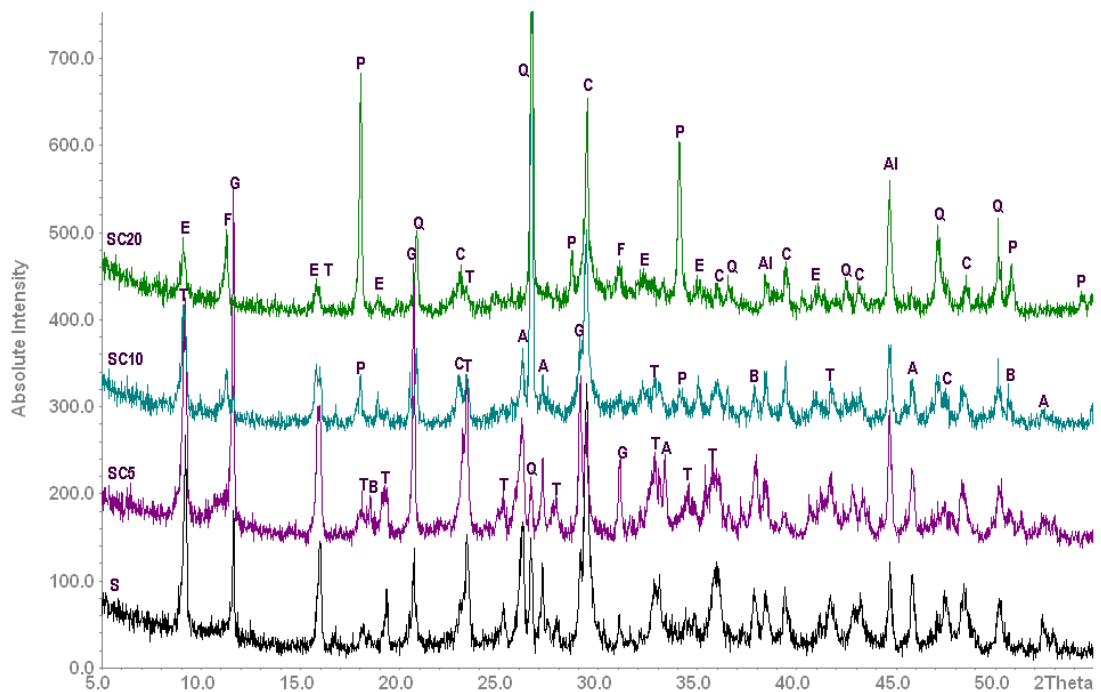


**Figure 4.20.** XRD patterns of CEMI samples stored for 630 days at 5°C.

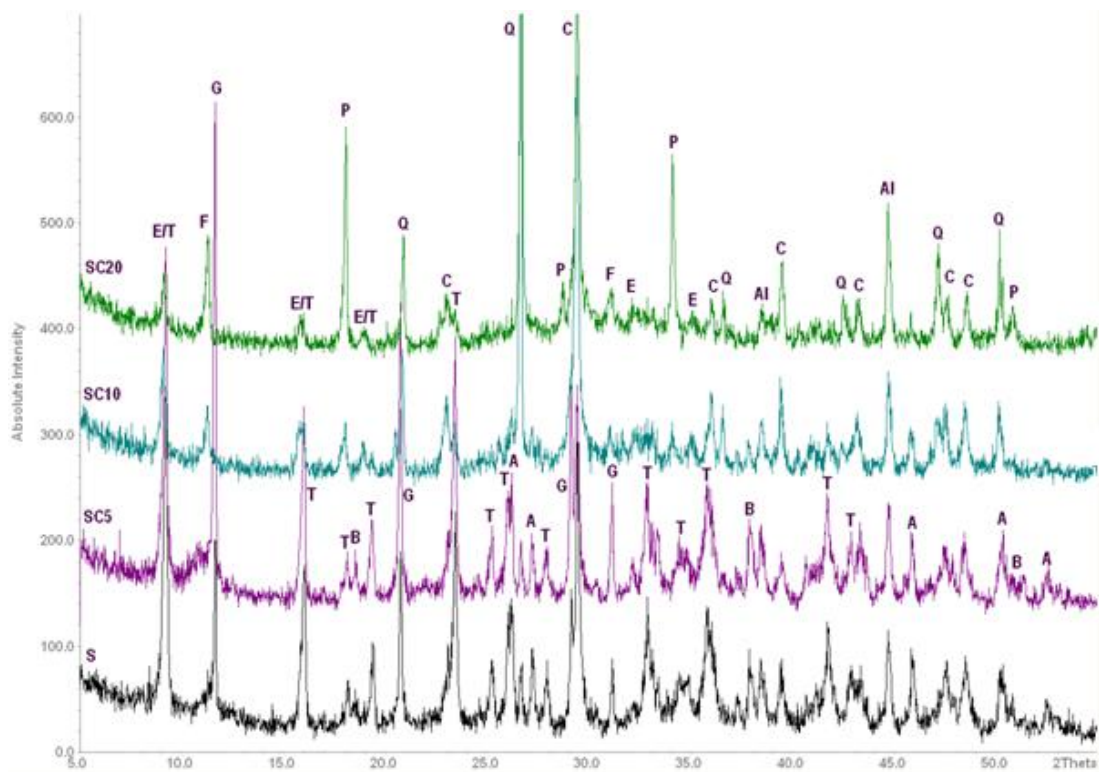


**Figure 4.21.** XRD patterns of CEMI-LF samples stored for 630 days at 5°C.

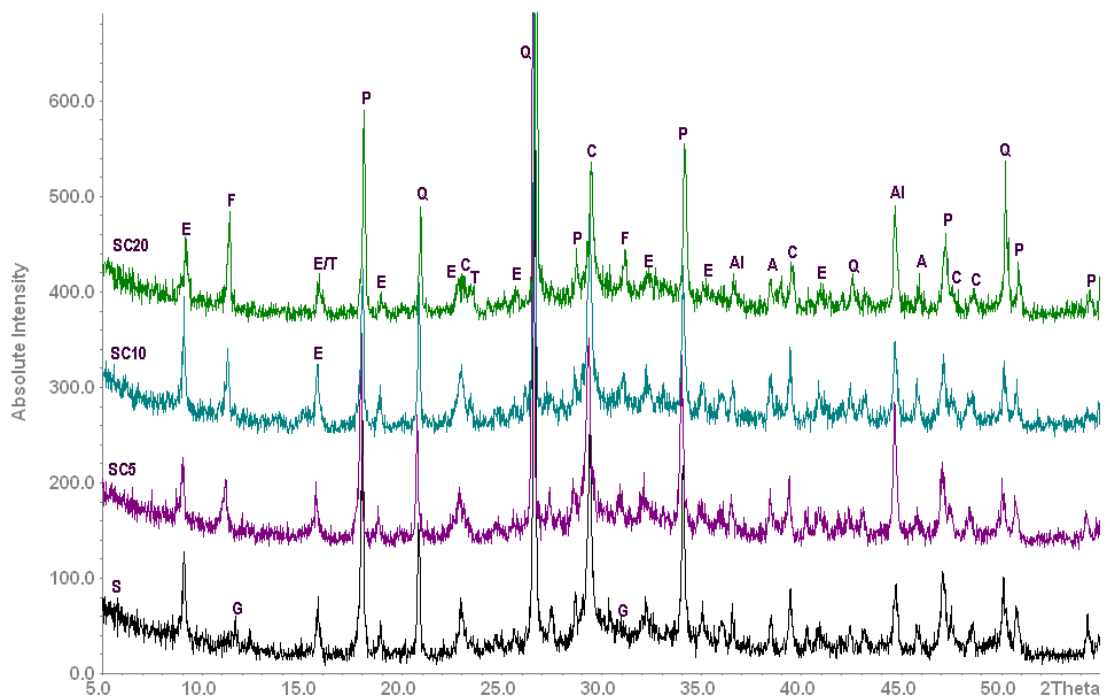


**Figure 4.22.** XRD patterns of CEMI samples stored for 630 days at 20°C.

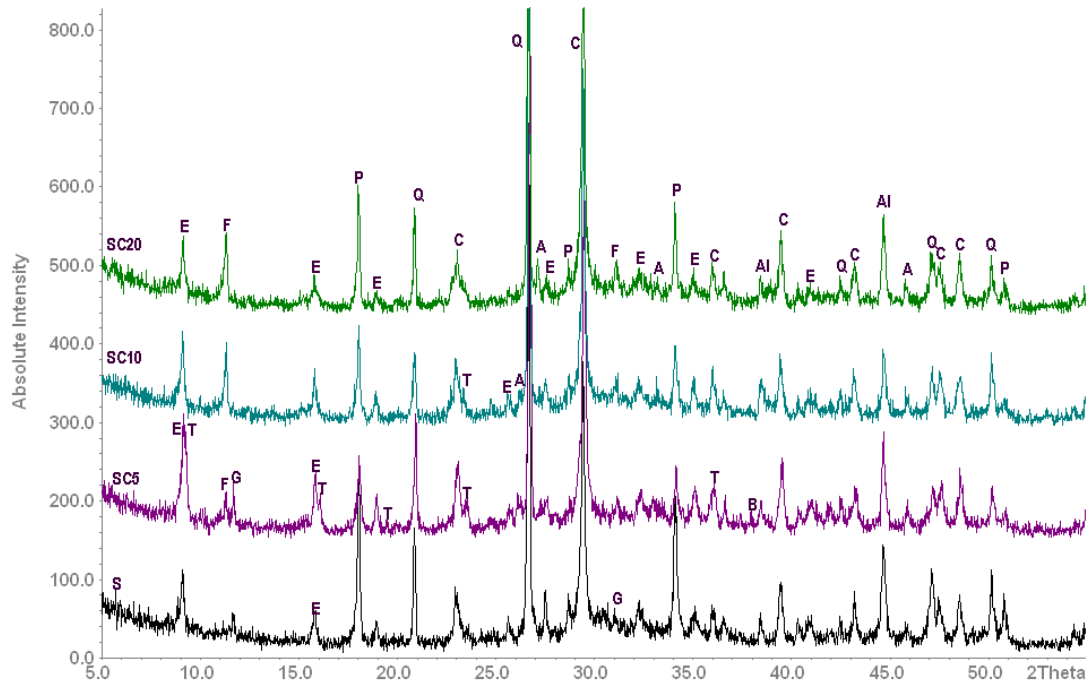
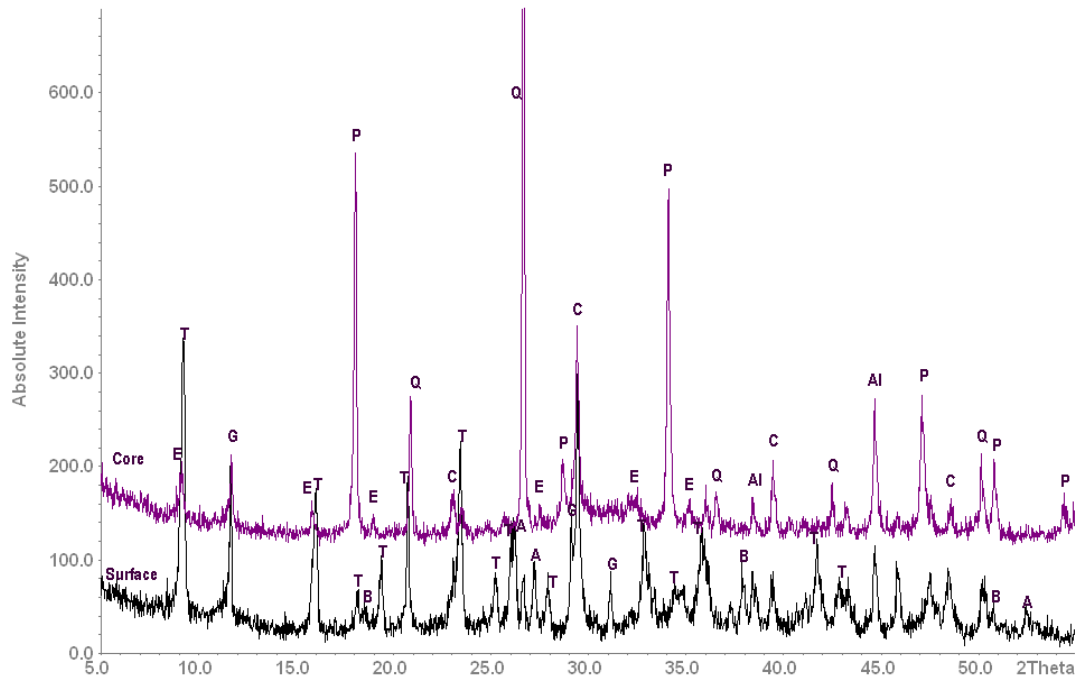


**Figure 4.23.** XRD patterns of CEMI-LF samples stored for 630 days at 20°C.

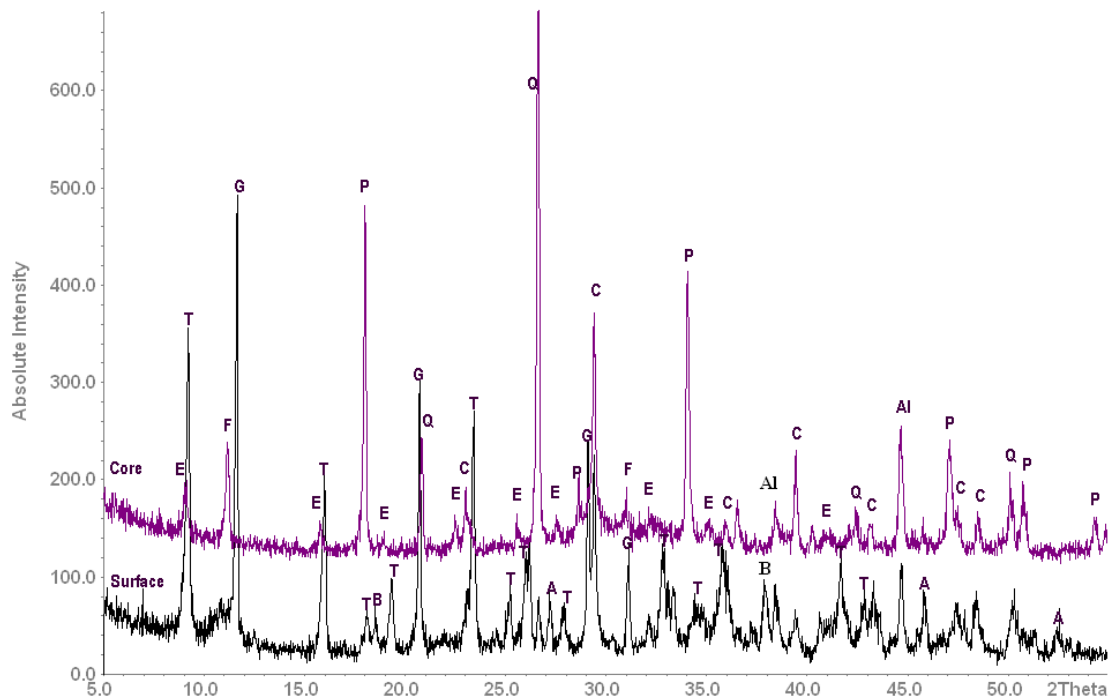
- ***XRD analysis of sound core materials for CEMI-LF mortars stored at 5 °C***

Figure 4.24 and 4.25 show the XRD patterns of degraded surface and sound core material samples for CEMI-LF mortar specimens stored for 630 days in S and SC5 solutions at 5°C. Since the degraded materials of surface mortar was presented and discussed above, this section will focus on the core of samples. It can be seen in Figure 4.24 that the main sulfate phases in the core sample of sulfate only solution were ettringite and gypsum, both in low intensities but no thaumasite peak was detected. The presence of strong peaks for portlandite indicates that no significant interaction with sulfate took place, as portlandite is not stable in presence of sulfate, as found in the surface sample.

In case of SC5 and SC20 (Figure 4.25 and 4.26) core samples, it can be seen that no gypsum and almost similar peak intensities for ettringite were detected and instead of gypsum, moderate peak intensities for Friedel's salt were present in SC5 and SC20 core samples. This indicates that penetration of chloride into the mortars was more rapid than for sulfate. All results indicate that the core of CEMI-LF mortars, which showed extensive surface degradation, remained intact within this period of exposure. This may explain why these mortars showed negligible expansion.



**Figure 4.24.** XRD patterns for degraded surface and sound core samples for CEMI-LF specimens stored 630 days in sulfate only solution at 5°C.



**Figure 4.25.** XRD patterns for degraded surface and sound core samples for CEMI-LF specimens stored 630 days in SC5 at 5°C.

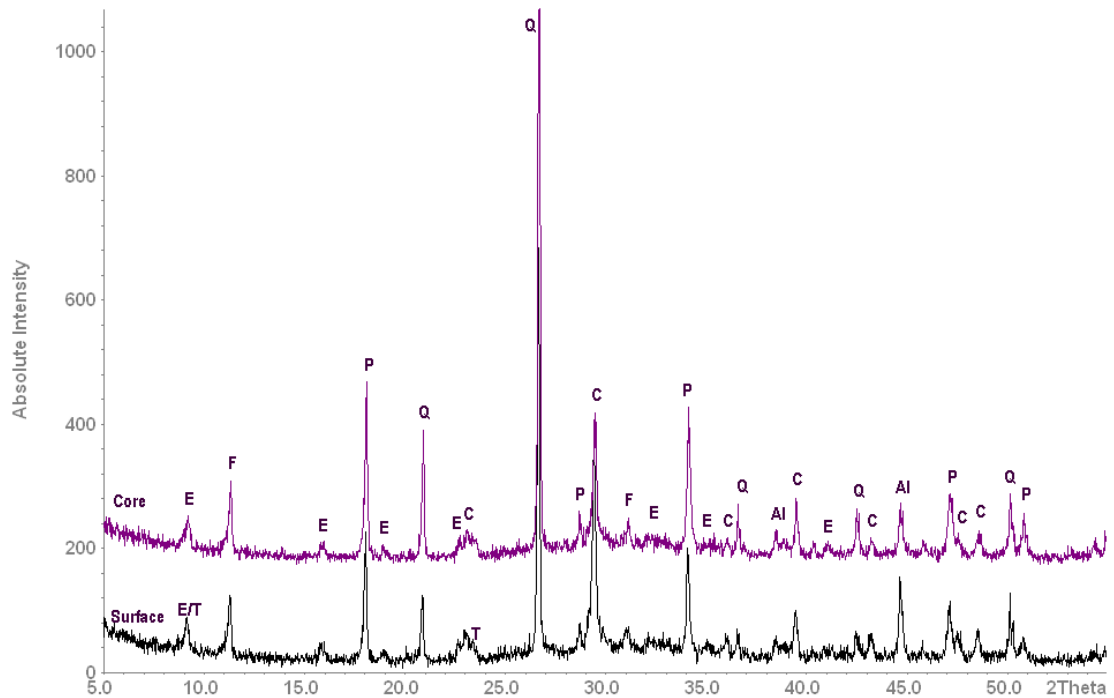


**Figure 4.26.** XRD patterns for sound surface and core samples for CEMI-LF specimens stored 630 days in SC20 at 5°C.

- ***XRD analysis of CEMI-PFA mortars at 5 and 20°C***

XRD patterns for CEMI-PFA samples stored in test solutions at 5 and 20°C are shown in Figure 4.27 and 4.28, where ettringite was observed to be a dominant sulfate phase in all samples. Traces of gypsum were found only in the S sample; while it was absent in the composite solution samples. This would indicate that S sample would be subjected to earlier sulfate attack compared with those stored in composite solutions, as was observed later in 20mm cubes. Instead, Friedel's salt was detected in all composite solution samples, with higher intensities at 20°C. The higher chloride level in solution, the greater the amount of Friedel's salt formed. The higher quantities of aluminates in the fly ash also resulted in relatively more Friedel's salt, compared to other cements.

Friedel's salt which is non-expansive product, would inhibit the transport of sulfate ions ingress through the sample, which in turn would reduce gypsum formation within the interior of the sample. The strong peaks for calcite in all surface samples could be mainly due to standard carbonation (See Chapter 5) of calcium hydroxide present in the cement matrix by dissolved atmospheric CO<sub>2</sub>. This is further confirmed by absence of portlandite in the surface layer. It was reported by Bellmann and Stark, (2008) that in the absence of calcium

hydroxide, the CSH has a much lower calcium/silicon ratio and a higher resistance against the formation of thaumasite.

At this stage of exposure, no clear peaks for thaumasite were detected by XRD in any CEMI-PFA samples. Moreover, the relatively low concrete/mortar matrix permeability (See Chapter 5) produced by incorporation of fly ash may have resulted in lower sulfate diffusion and inhibited its interaction with cement paste. The performance of CEMI-PFA mortars at both temperatures further improved in presence of chloride, as indicated by XRD analysis.

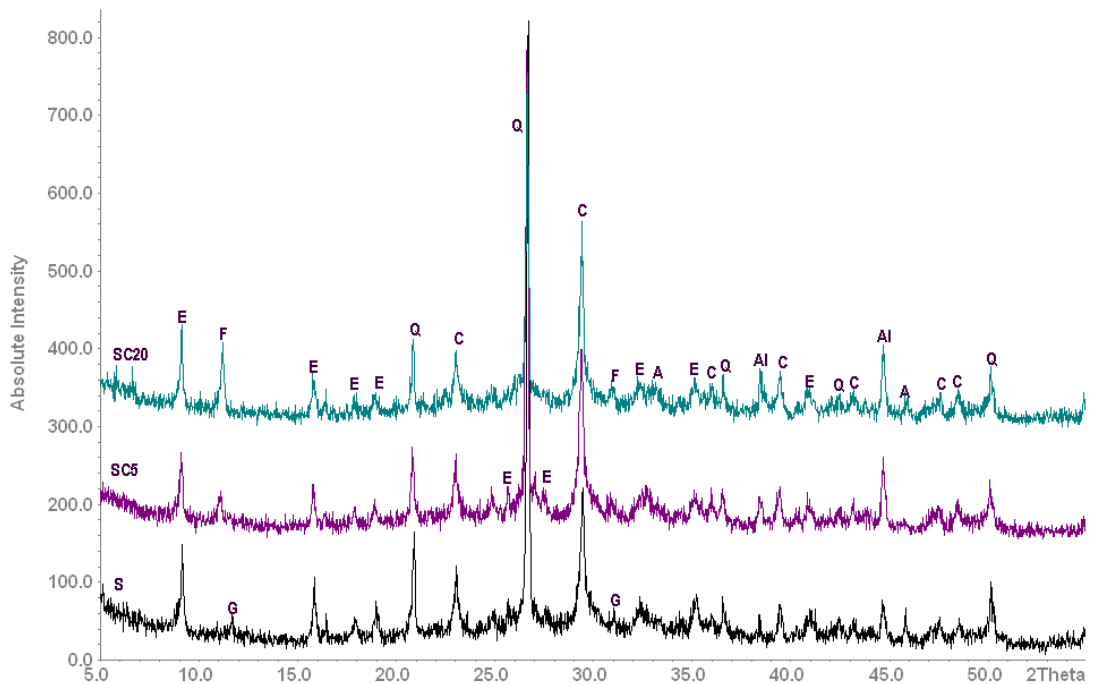


**Figure 4.27.** XRD patterns for CEMI-PFA samples stored for 630 days at 5°C.



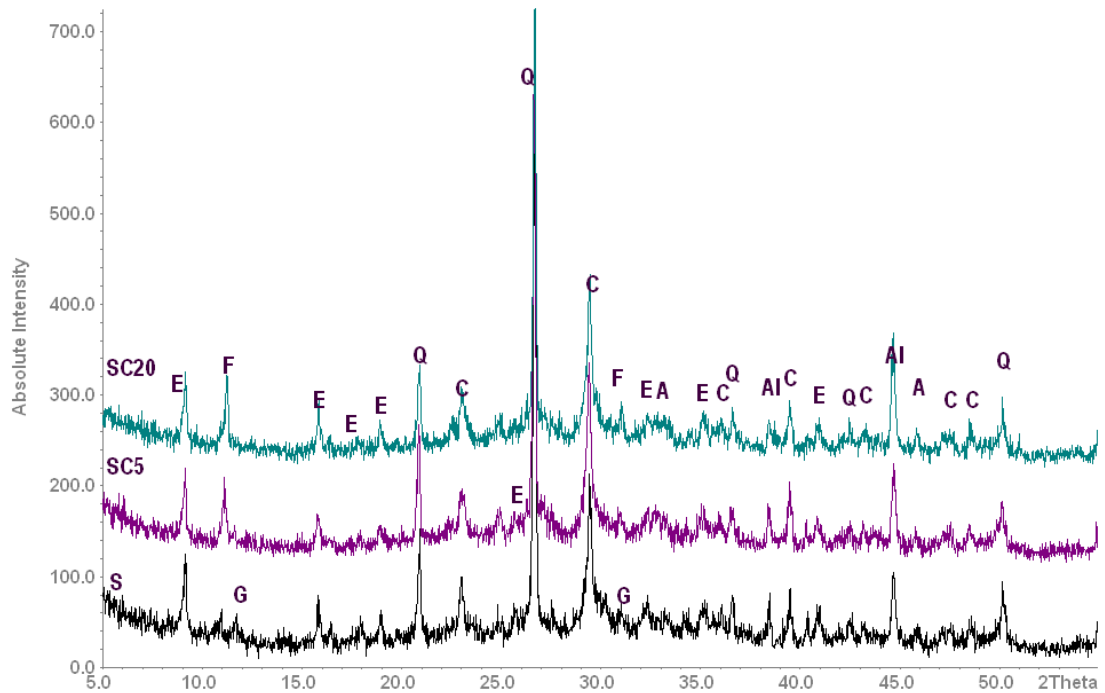


**Figure 4.28.** XRD patterns for CEMI-PFA samples stored for 630 days at 20°C.

- ***XRD analysis of CEMI-GGBS mortars at 5 and 20°C***

Figure 4.29 shows the XRD patterns for CEMI-GGBS samples stored in the different test solutions at 5°C. It can be seen that traces of gypsum were detected in S and SC5 samples, while, no gypsum and instead higher peaks for Friedel's salt were detected in the SC20 sample. This indicates that CEMI-GGBS specimens placed in S and SC5 solutions would be subjected to earlier attack, as confirmed later by the 20mm cubes. The formation of Friedel's salt, more evidently in SC20 samples, would inhibit ingress of sulfate ions into the sample, which consequently reduced gypsum formation within its interior. Moreover, this indicates that aluminates rapidly engaged in Friedel's salt formation which reduced the possibility of more ettringite formation. Lowering peak intensities for ettringite for composite solution samples show that this effect increases for higher chloride concentrations. The high slag replacement level would have produced C-S-H gel with lower calcium/ silica ratio which is capable of binding more alumina in its structure that would also result in a further reduction in ettringite.

The strong peaks for calcite in all samples could also be due either to the presence of limestone in CEMI or carbonation of CH present in cement matrix by dissolved atmospheric CO<sub>2</sub>, which would provide a source of carbonates for

thaumasite formation. Traces of thaumasite were detected only in S and SC5 samples.

The absence of portlandite peaks in all surface samples indicated that it was consumed either during the pozzolanic reaction or by carbonation to form calcite. It is frequently reported (Kandasamy and Shehata, 2014, Veiga and Gastaldini, 2012, Atahan and Dikme, 2011) that the consumption of portlandite in GGBS mortar/concrete is the key factor for the resistance GGBS cement possess against sulfate attack, as portlandite is not stable in presence of sulfate ions.

Samples stored in sulfate only and composite sulfate with 0.5% chloride solutions showed traces of gypsum, whereas, no gypsum and instead stronger peaks for Friedel's salt were detected in sample stored in composite sulfate with 2.0% chloride, probably due to the increase in gypsum solubility as chloride increases in solution (See Section 4.9).

The XRD patterns for CEMI-GGBS samples stored at 20°C are shown in Figure 4.30, from which it can be observed that portlandite was not present in any samples regardless of solution composition. This may be a result of carbonation or/and its consumption during pozzolanic reactions.

Ettringite and gypsum were observed as the main sulfate phases in S and SC5 samples, whereas thaumasite was detected in small traces. Since these samples did not show any visual signs of attack in this immersion period, it is expected they would be subjected to sulfate attack after a longer exposure time. It should be mentioned here that the relatively high permeability (water/binder ratio of 0.6) of the CEMI-GGBS mortars in this study might be the main reasons why these samples showed rapid sulfate interaction.

It was noted that the intensity of peaks for Friedel's salt increased and those for ettringite decreased as chloride in solution increased, in that SC20 sample showed the highest peak intensities for Friedel's salt and lowest peak intensities for ettringite. This may indicate the rapid engagement of aluminates in the formation of Friedel's salt resulted in lowering active aluminates available for ettringite formation.

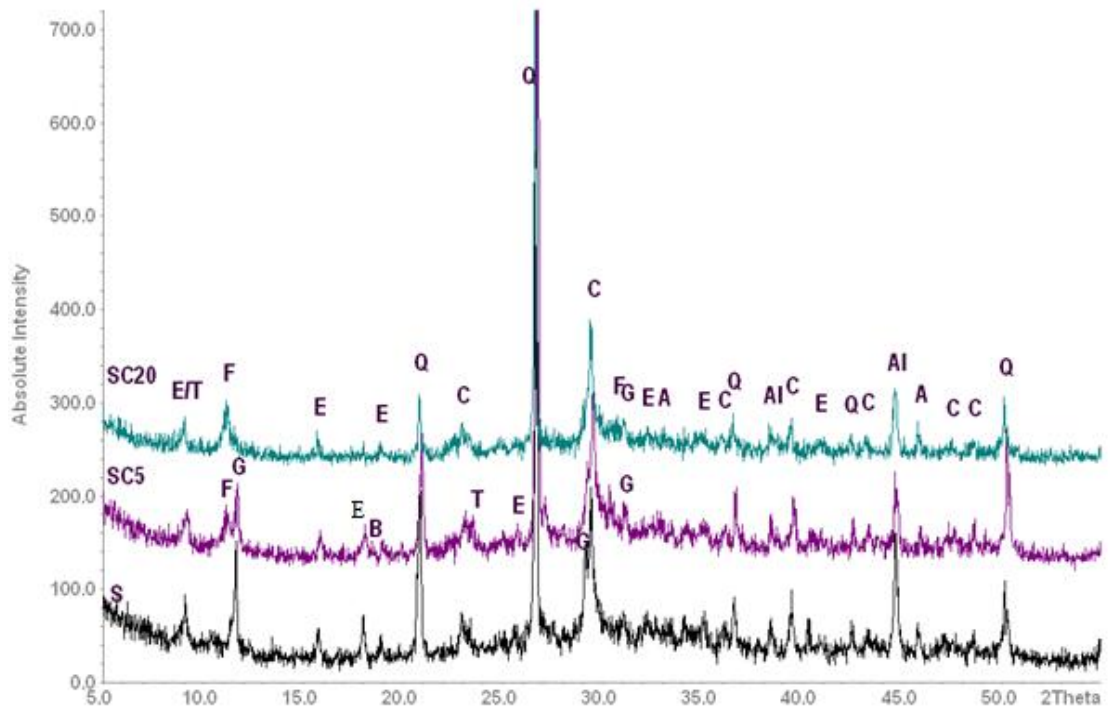


**Figure 4.29.** XRD patterns for CEMI-GGBS samples stored for 630 days at 5°C.

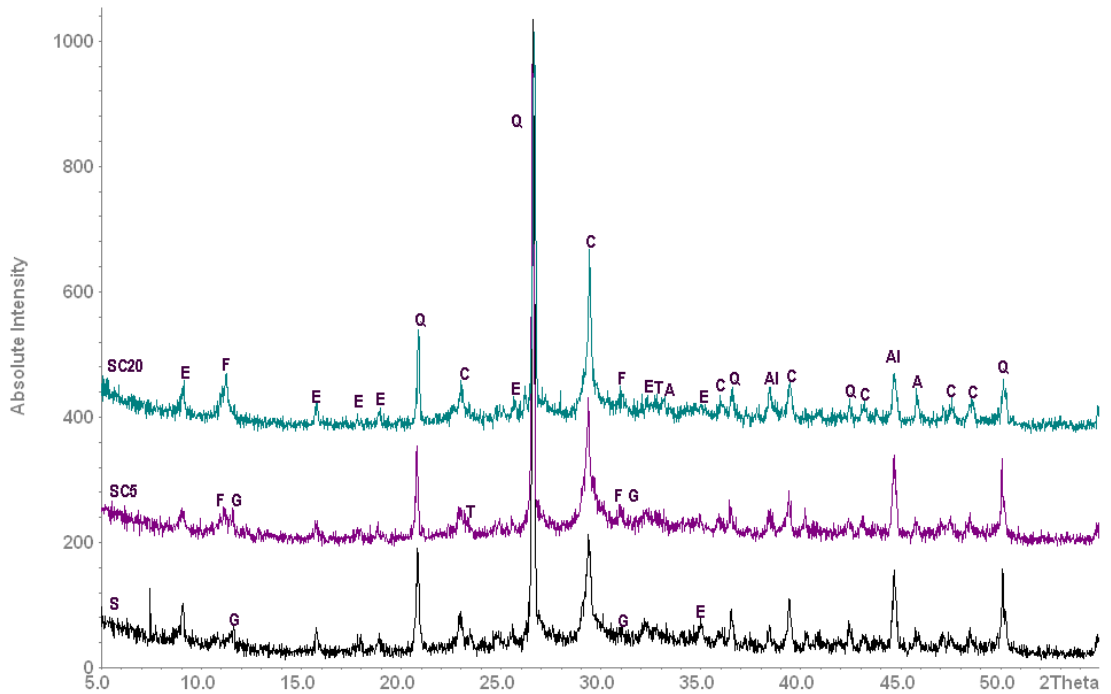


**Figure 4.30.** XRD patterns for CEMI-GGBS samples stored for 630 days at 20°C.

**XRD analysis of CEMI-PFA and CEMI-GGBS samples of 20mm cubes at 5°C:**

Figure 4.31 shows the XRD patterns for CEMI-PFA surface samples stored for 180 days in sulfate only and composite solutions at 5°C. It can be seen that ettringite was detected in all samples and with approximately similar peaks intensities, while, high intensity gypsum peaks were only detected in sulfate only solutions. Since mortar placed in this solution showed visual damage (Figure 4.5), it is most likely attributed to gypsum formation. Instead, peaks for Friedel's salt were detected in samples placed in composite solutions and its peak increased as the dissolved chloride level rose. No portlandite was detected in any sample, which could be a result either of pozzolanic reaction or carbonation by atmospheric CO<sub>2</sub>. However, traces of brucite were detected in all samples which indicate reactions between sulfate and portlandite also took place. In addition, small traces of thaumasite were also detected in all samples. At this early stage of exposure, the presence of chloride in solutions led to mitigation of sulfate attack, which most likely attributed to the formation of Friedel's salt, as discussed earlier.

In case of the CEMI-GGBS samples, the XRD patterns of surface samples after 180 days of storage in sulfate only and composite solutions at 5°C are presented in

Figure 4.32, which shows that ettringite was detected in all samples, but with lower peaks intensities in the SC20 sample. This observation may be due to the reduction in the amount of available C<sub>3</sub>A as it was mostly consumed during Friedel's salt formation. This most likely caused a reduction in sulfate interaction in the mortar sample stored in SC20 solution.

High intensity gypsum peaks were detected in S and SC5 samples, but not in SC20. The observed attack (Figure 4.6) in S and SC5 mortars, most likely related to gypsum precipitation. The decalcification of C-S-H gel due to the aggressiveness of magnesium sulfate solution can be the main source of calcium ions in pore solution for gypsum formation.

Calcite was detected as a main phase of carbonate in all samples, but with relatively higher peak intensity for the SC20 sample, which may be related to its solubility as chloride concentration decreased.

Traces of thaumasite were detected in samples placed in sulfate only and SC5 solutions, but not in SC20 solution. The reduction of calcite peaks in samples

placed in sulfate only and SC5 solutions may indicate its involvement in thaumasite formation, as they both showed traces of thaumasite peaks.

Relatively high peak intensities for ettringite were observed in CEMI-PFA samples compared with CEMI-GGBS samples. This was expected due to higher aluminates contents of CEMI-PFA cement compared with CEMI-GGBS cement. The results of the small cube sets indicate that CEMI-PFA and CEMI-GGBS mortars would also be subjected to sulfate attack, but after a longer time interval. In case of CEMI-PFA, the presence of chloride in solutions led to delayed sulfate attack, which was most likely due to the formation of Friedel's salt, as discussed earlier. However, the presence of chloride did not benefit CEMI-GGBS mortar against sulfate attack which may also be attributed to lower Friedel's salt formation.

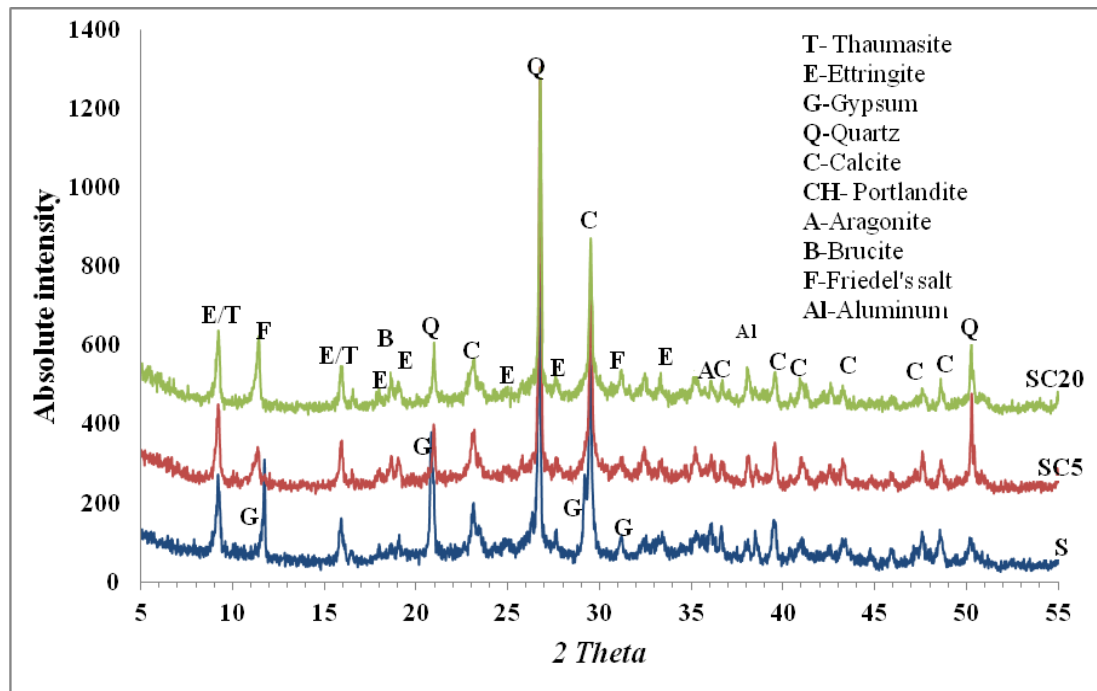


**Figure 4.31.** XRD patterns for CEMI-PFA samples stored for 180 days at 5°C.

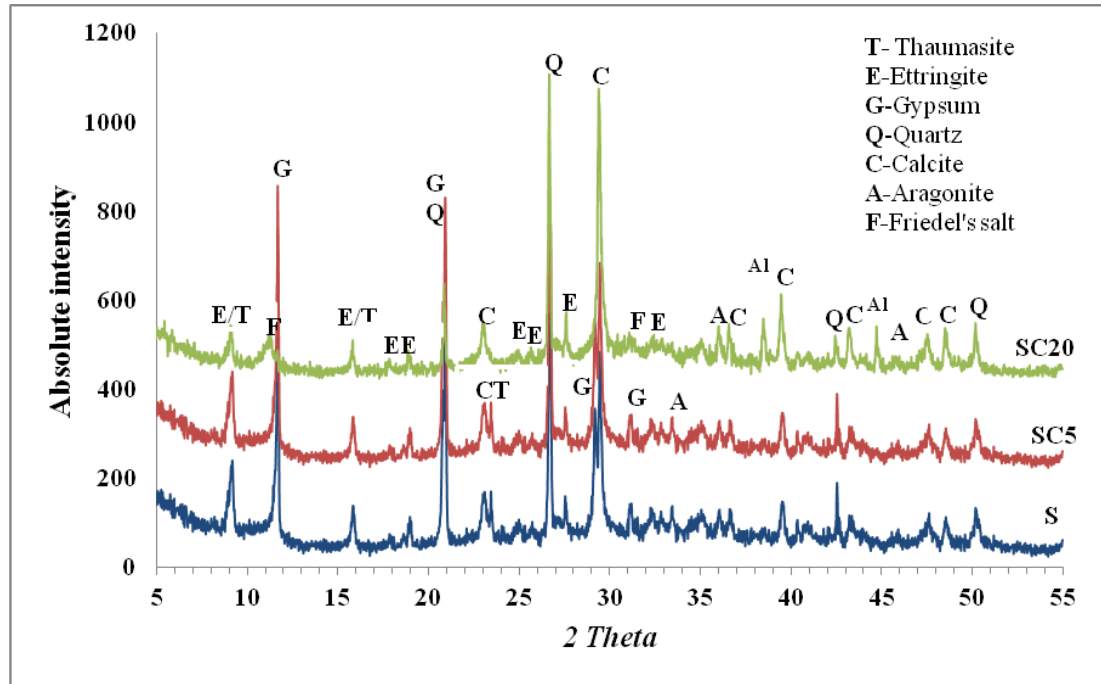


**Figure 4.32.** XRD patterns for CEMI-GGBS samples stored for 180 days at 5°C.

#### 4.5.2 Analysis by infrared spectroscopy

In order to obtain further evidence about the deterioration process and to confirm the XRD identifications of thaumasite, ettringite and other minerals, IR spectroscopy was used. This technique enables silicon in octahedral coordination, as in thaumasite, to be identified by a waveband at  $500\text{cm}^{-1}$ , in contrast to octahedral coordination of aluminate in ettringite, which is characterised by a waveband at  $855\text{cm}^{-1}$  (Zhou et al., 2006, Torres et al., 2004b, Bensted and Satya Prakash, 1976, Barnett et al., 2002).

The degraded materials affecting CEMI-PFA and CEMI-GGBS 20mm cubes stored for 180 days in test solutions at 5°C were also investigated by this technique.

#### **IR analysis of CEMI and CEMI-LF samples: 50mm cubes:**

At 5°C, the surface deterioration products of CEMI and CEMI-LF samples in sulfate only (S), composite sulfate and 0.5% chloride (SC5) and composite sulfate and 1.0% chloride (SC10) solutions were examined and compared with material from the sound surfaces of mortars stored in solution with sulfate and 2.0% chloride (SC20). The relevant infra-red spectra are shown in Figure 4.33 to 4.35. The spectra of degraded samples (Figure 4.33 and 4.34) show the presence of thaumasite and ettringite. This indicates that thaumasite was not

present as the end member of the solid solution series with ettringite as found by Torres et al. (2004). It can clearly be seen in spectra of the deteriorated surfaces of mortars stored in S, SC5 and SC10 solutions that peak belong to C-S-H was absent, while it was strongly present in SC20 samples (Figure 4.35), which did not show any visual deterioration after 630 days of immersion. In the deteriorated surfaces, it was most likely that the C-S-H is converted into thaumasite as confirmed later by SEM analysis. These results agree with the XRD findings in showing that thaumasite or thaumasite-ettringite solid solution resulted from the attack in all deteriorated materials.

At 20°C, the degraded sample of CEM-LF mortar surface stored in SC5 was examined and compared with material from the surfaces of mortars stored in sulfate only and SC20 solutions, shown in Figure 4.36. It can be clearly seen that the sulfate attack product of SC5 sample was thaumasite, while peaks for C-S-H in case of CEMI-LF mortar samples stored in sulfate only and SC5 solutions at 20°C indicate that less damage occurred compared with those stored at 5°C.

Peaks at around 600  $\text{cm}^{-1}$ , 670  $\text{cm}^{-1}$  and 1100  $\text{cm}^{-1}$  are indicative of  $\text{SO}_4^{2-}$  groups, which belong to sulfate phases such as thaumasite, ettringite and gypsum. Peaks around 712, 875 and 1400  $\text{cm}^{-1}$  relate to  $\text{CO}_3^{2-}$  groups that belong to thaumasite and calcite. The double peaks around 700  $\text{cm}^{-1}$  and around 1480  $\text{cm}^{-1}$  are assigned by Torres (2004) to aragonite. Peaks at around 815  $\text{cm}^{-1}$  and 966  $\text{cm}^{-1}$  are related to C-S-H (García Lodeiro et al., 2009).

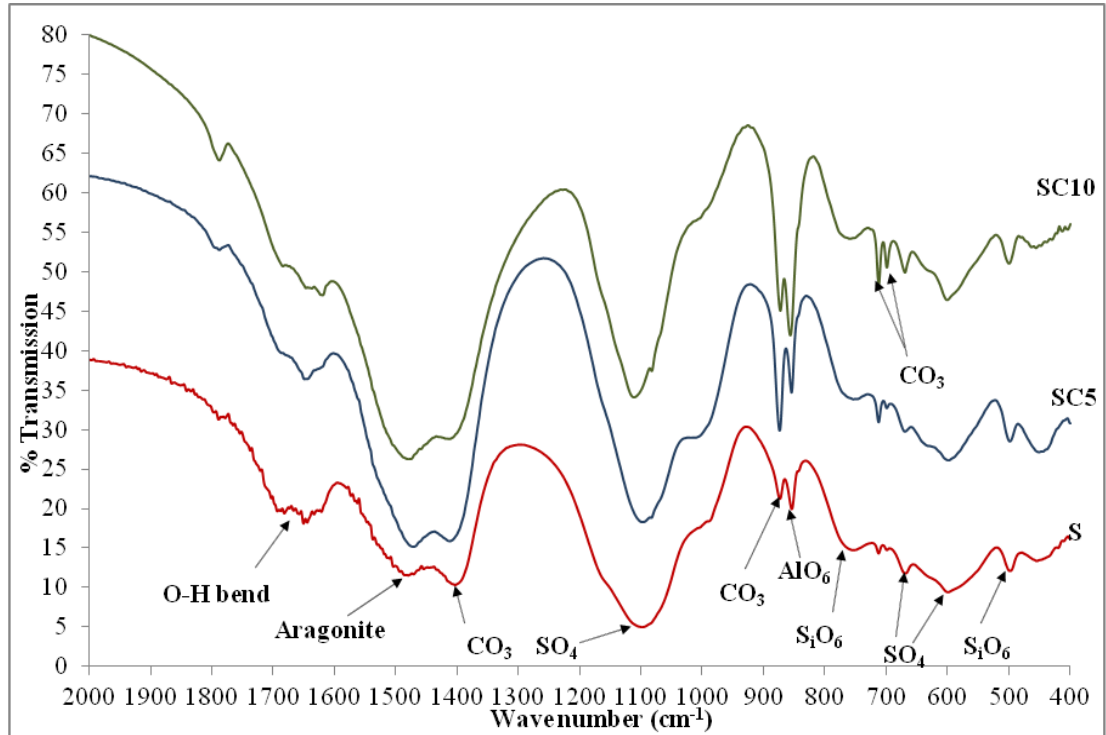


Figure 4.33. Infrared spectra for CEMI degraded samples at 5°C.

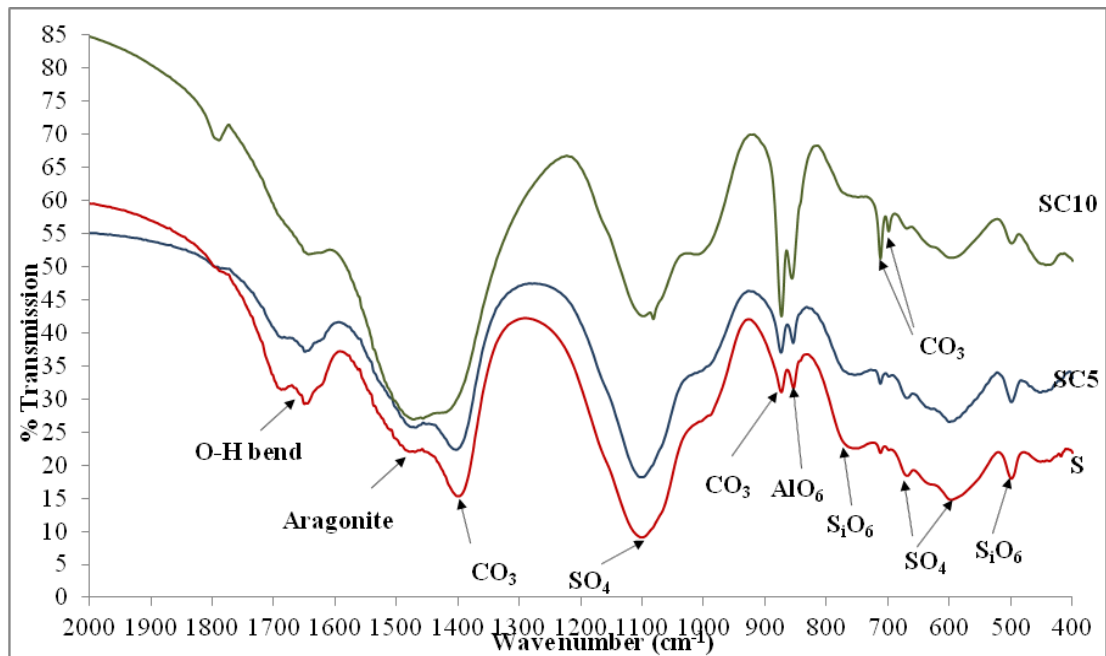
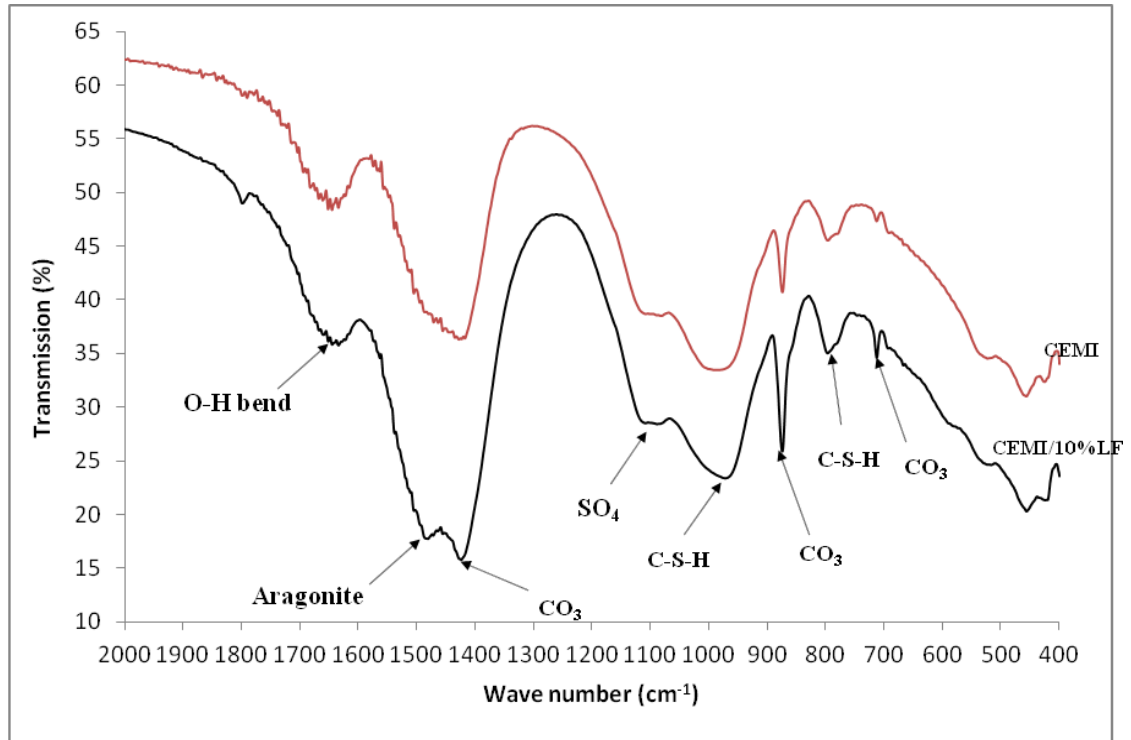
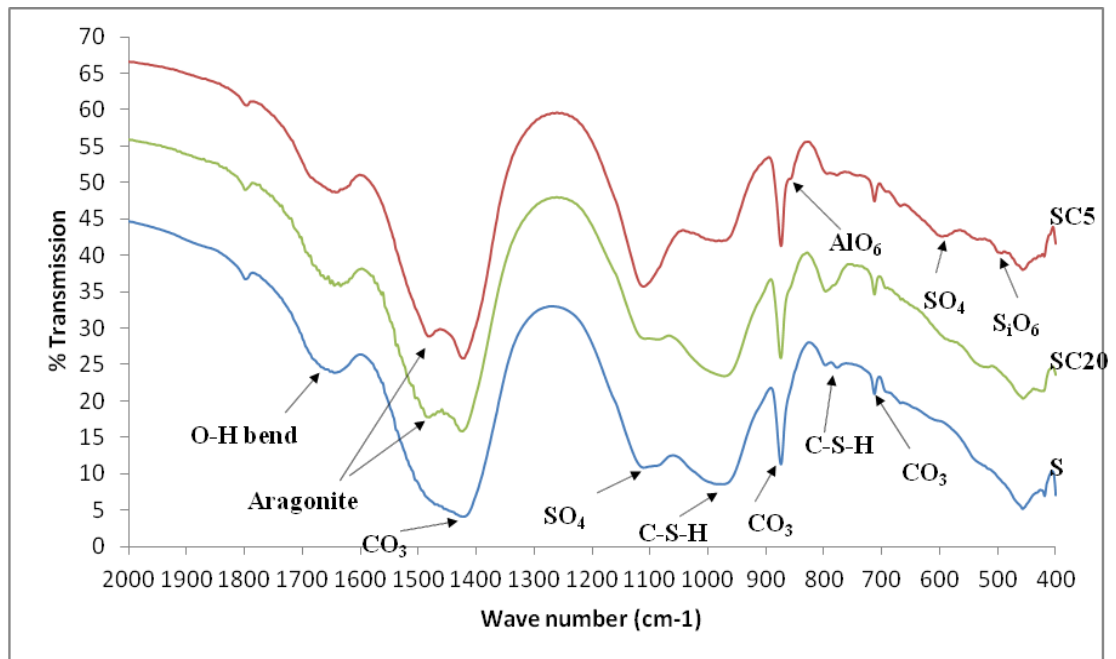


Figure 4.34. Infrared spectra for CEMI-LF degraded samples stored at 5°C.





**Figure 4.35.** Infrared spectra for CEMI and CEMI-LF surface samples stored in SC20 at 5°C.



**Figure 4.36.** Infrared spectra for surface samples of CEMI-LF stored at 20°C.

***IR analysis of CEMI-PFA and CEMI-GGBS samples of 20mm cubes at 5°C:***

Degraded products from some of the CEMI-PFA and CEMI-GGBS 20mm mortars cubes that showed earlier attack than the 50mm cubes were also examined by IR technique.

Figure 4.37 to 4.39 show IR spectra for degraded surfaces and sound core samples of CEMI-PFA and CEMI-GGBS mortars stored for 180 days in sulfate only and SC5 solutions at 5°C.

The presence of sulfate peaks at 600 and 670  $\text{cm}^{-1}$  which is attributed to gypsum and the absence of a 500  $\text{cm}^{-1}$  thaumasite peak in all degraded surface samples indicates that the attack of the surface was mostly related to gypsum formation, which confirmed the XRD finding. Peaks at 855  $\text{cm}^{-1}$  assigned to  $\text{AlO}_6$  group and  $\text{SO}_4$  associated peaks at 1100  $\text{cm}^{-1}$ , attributed to ettringite phase, and were clearly identified in degraded surface samples of CEMI-PFA mortar in sulfate only and SC5 solutions. However, the degraded surface of CEMI-GGBS in S and SC5 solutions showed very weak peaks at 855  $\text{cm}^{-1}$  and lower peaks at 1100  $\text{cm}^{-1}$ , which indicated more ettringite formed in the surface material of the CEMI-PFA sample, which was also found by XRD analysis. It should be mentioned that the fly ash contained higher aluminates which most probably reacted with sulfate to generate ettringite.

Peaks associated with C-O group in the form of calcite were identified at 713 and 875  $\text{cm}^{-1}$ , more evidence for this in the surface samples. These relatively higher peaks for calcite in surface samples may reflect the higher degree of carbonation in this layer on account of exposure to atmospheric  $\text{CO}_2$  before immersion.

The disappearance or the reduction of C-S-H peaks (peaks at 966  $\text{cm}^{-1}$  in IR spectra in the degraded surface samples compared with core samples indicated the decalcification of C-S-H due to magnesium ions attack. In the degraded surfaces, it is most likely that the C-S-H is converted into M-S-H as indicated later by SEM analysis.

The results discussed in this section confirm the XRD finding in which mortars made with either CEMI-PFA or CEMI-GGBS as cement replacement and exposed to magnesium sulfate solution can be deteriorated by gypsum formation but not thaumasite. This may be due to the absence of adequate internal amounts of carbonate required for thaumasite formation and instead

the availability of high concentration of calcium and sulfate ions in mortar pore solution, which promoted gypsum formation.

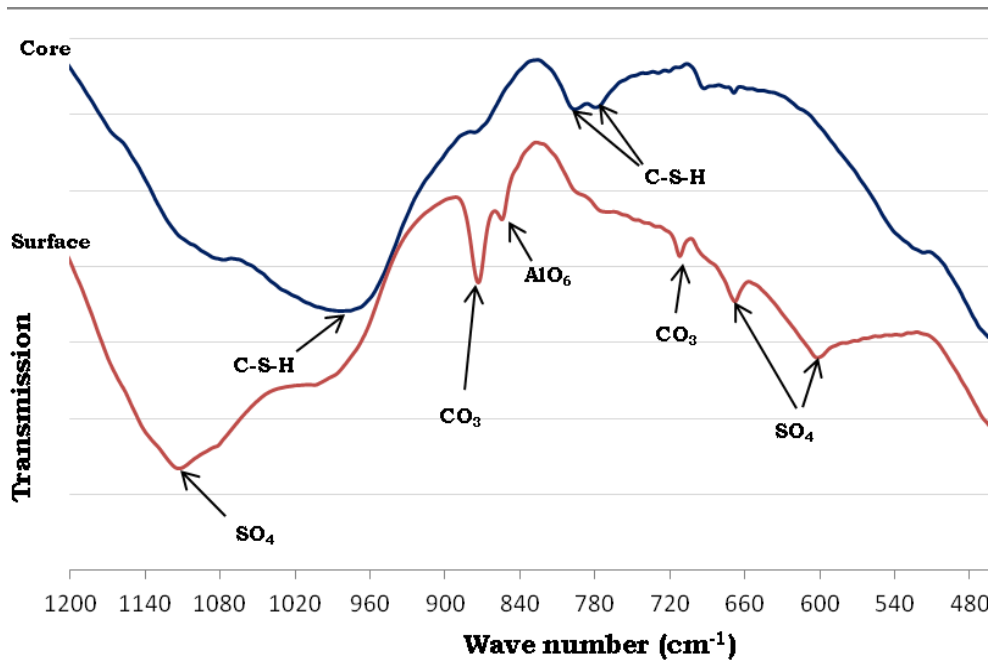


**Figure 4.37.** IR spectra for CEMI-PFA sample stored 180 days in sulfate only solution at 5°C.

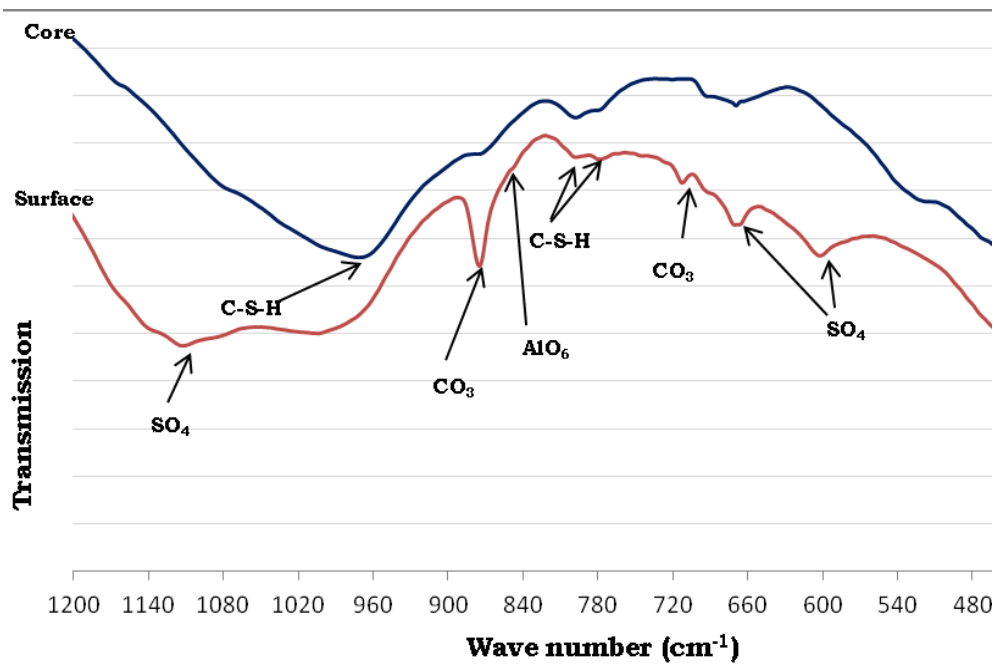


**Figure 4.38.** IR spectra for CEM-GGBS sample stored 180 days in sulfate only solution at 5°C.

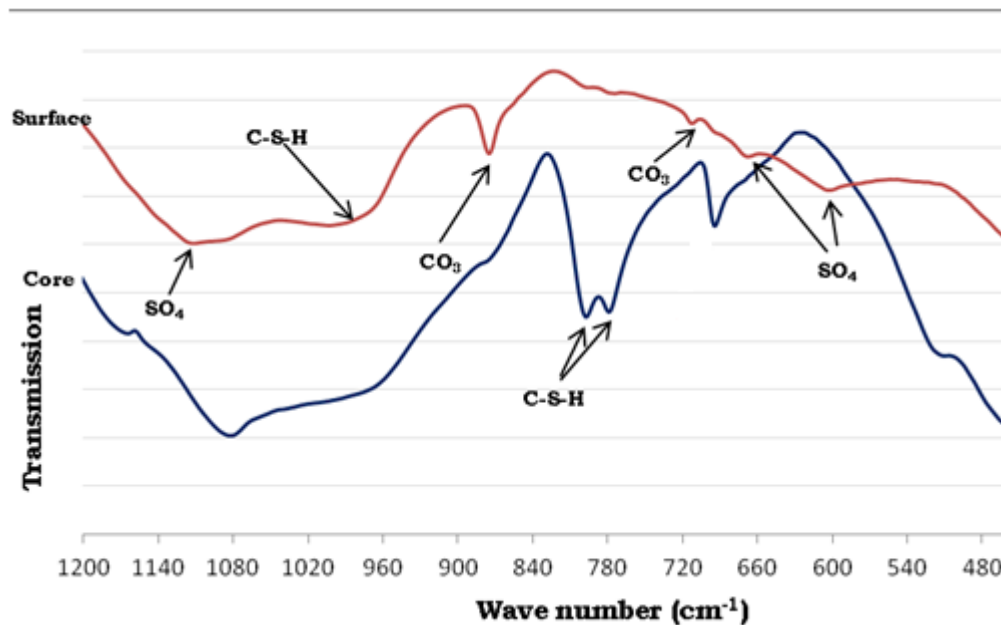


**Figure 4.39.** IR spectra for CEMI-GGBS sample stored 180 days in SC5 at 5°C.

## 4.6 Scanning electron microscopy (SEM) and energy dispersive X-ray (EDX) analysis

Scanning electron microscopy and energy dispersive X-ray system (SEM/EDX) were performed on fracture surfaces after 360, 450 and 630 days immersion to identify the deteriorated products. The 450 day samples consisted of 10 mm cubes cut from the corners of the prisms which were stored in the same containers as the cubes.

### **SEM/EDX of degraded materials after 360 days of exposure:**

Fracture samples collected from surfaces of CEMI-LF mortars stored for 360 days in S, SC5 and SC10 solutions at 5°C shown in Figure 4.40 to 4.42 show prismatic fine needle shaped crystals < 0.5 μm in thick and up to 10 μm long as the dominant product. EDX analysis shown in Figure 4.43, indicates that as these crystals consisted mainly of calcium, sulfur, oxygen, aluminium, silicon as well as a small amount of carbon, they are a thaumasite-ettringite solid solution series as reported by Torres et al. (2004).



**Figure 4.40.** Morphology of degraded surface of CEMI-LF mortar stored 360 days in sulfate only solution at 5°C.

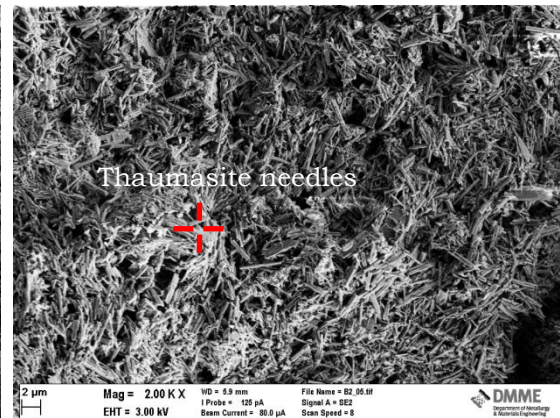


**Figure 4.41.** Morphology of degraded surface of CEMI-LF mortar stored 360 days in SC5 at 5°C.

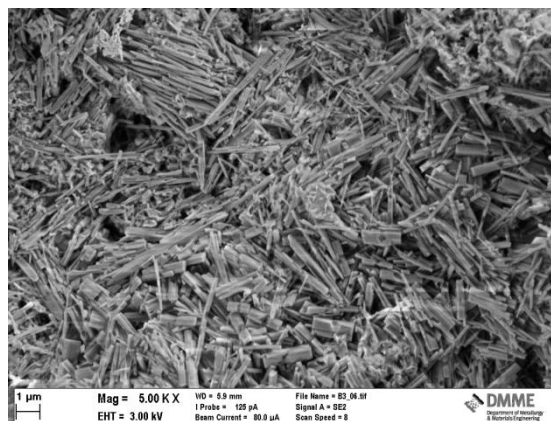


**Figure 4.42.** Morphology of degraded surface of CEMI-LF mortar stored 360 days in SC10 at 5°C.

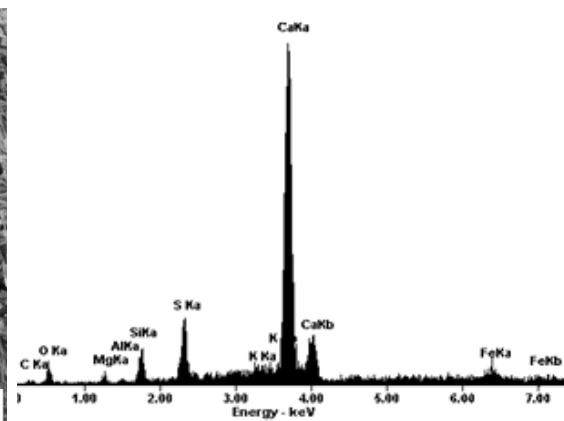


Figure 4.43. EDX of the needles (thaumasite-ettringite solid solution) in Figure 4.41.

**SEM/EDX of CEMI and CEMI-LF mortars stored 450 days at 5°C**

The microstructure images of CEMI and CEMI-LF mortar samples stored for 450 days in sulfate only and composite sulfate and chloride solutions at 5°C are given in this section.

Figure 4.44 and 4.48 show SEM images of CEMI and CEMI-LF degraded surface mortar samples that were stored in S. Both mortars showed strong alteration, as indicated by transformation of grey areas of cement to darker colour areas, and by the spreading of cracked areas. The EDX (Figure 4.46 and 4.49) analysis of dark grey area showed it contained mainly of Ca, Si, S and Al which is attributed to structure of thaumasite-ettringite solid solution series.

The cracked light grey area also consisted of Ca, S, Al and Si, but with Al to Si ratio more than one (Figure 4.45) so both these areas were thaumasite- ettringite solid solution but with different Al: Si ratios. This finding is consistent with thaumasite being formed from ettringite by replacement of Al by Si, as suggested by Bensted (2003b).

It was also observed in Figure 4.44 that both cracked and dark areas were surrounded by secondary gypsum as EDX analysis in Figure 4.47 indicates. Gypsum may have formed at an early stage and then acted as a major source of sulfate for thaumasite formation, as reported by Schmidt et al. (2008) and Hartshorn et al. (1999) who noted that thaumasite formation is often accompanied by formation of secondary gypsum when magnesium sulfate was present. Further discussion of this issue is presented in Chapter 6.

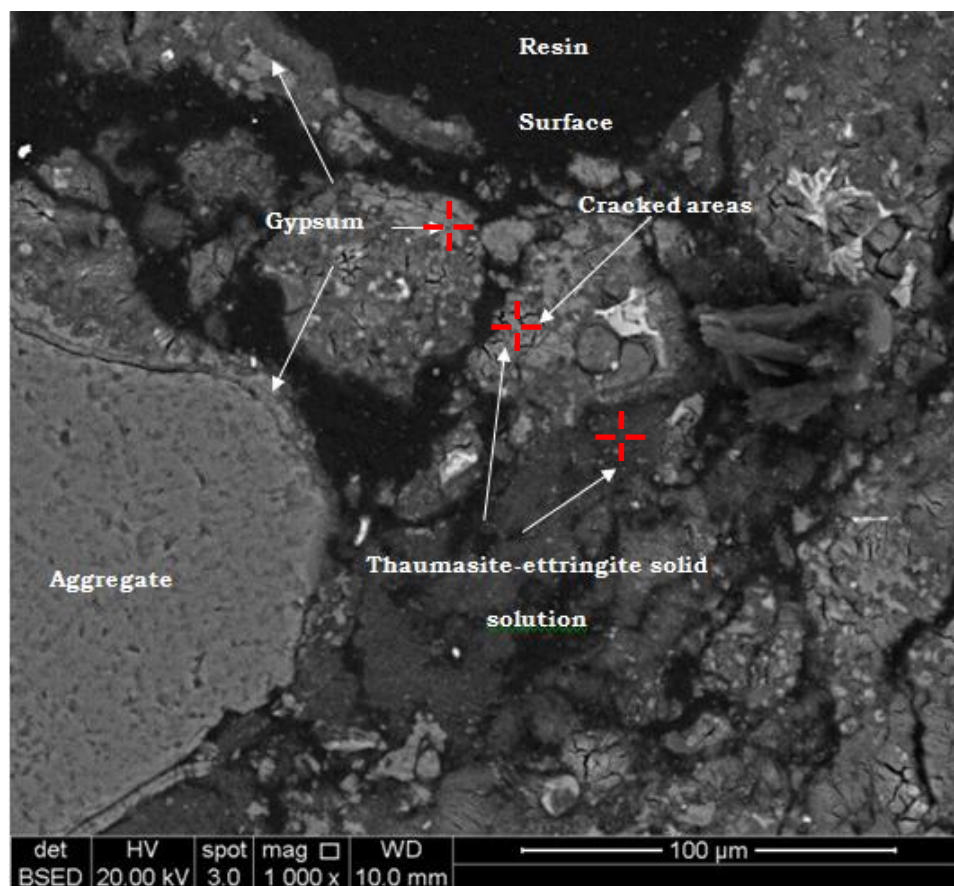


**Figure 4.44.** SEM image of CEMI sample stored 450 days in sulfate only solution.

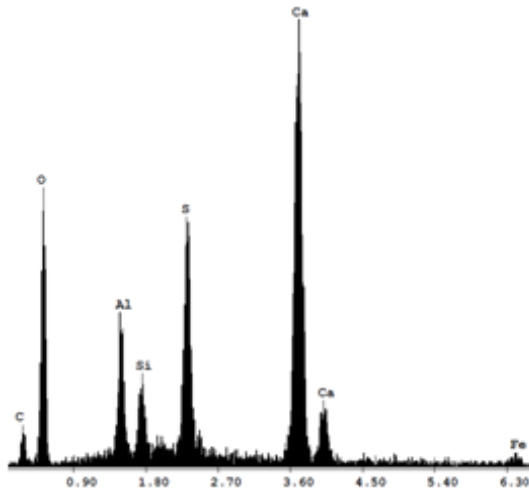


**Figure 4.45.** EDX of cracked light grey area (with Al:Si >1) in Figure 4.44.

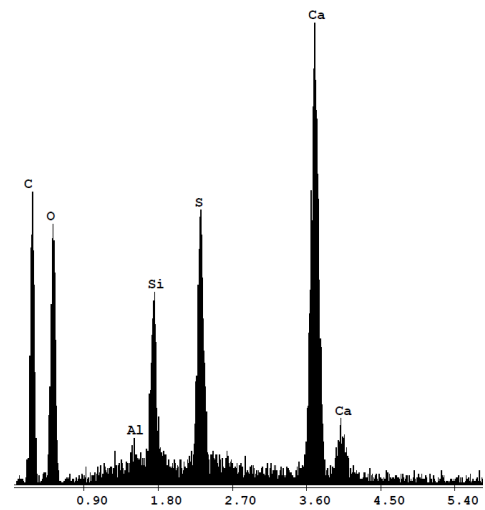


**Figure 4.46.** EDX of dark grey area (with Al: Si <1) in Figure 4.44.

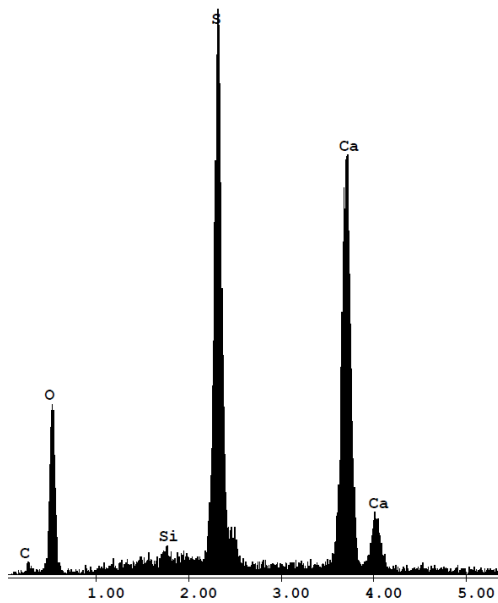


**Figure 4.47.** EDX of light grey area (gypsum) in Figure 4.44.

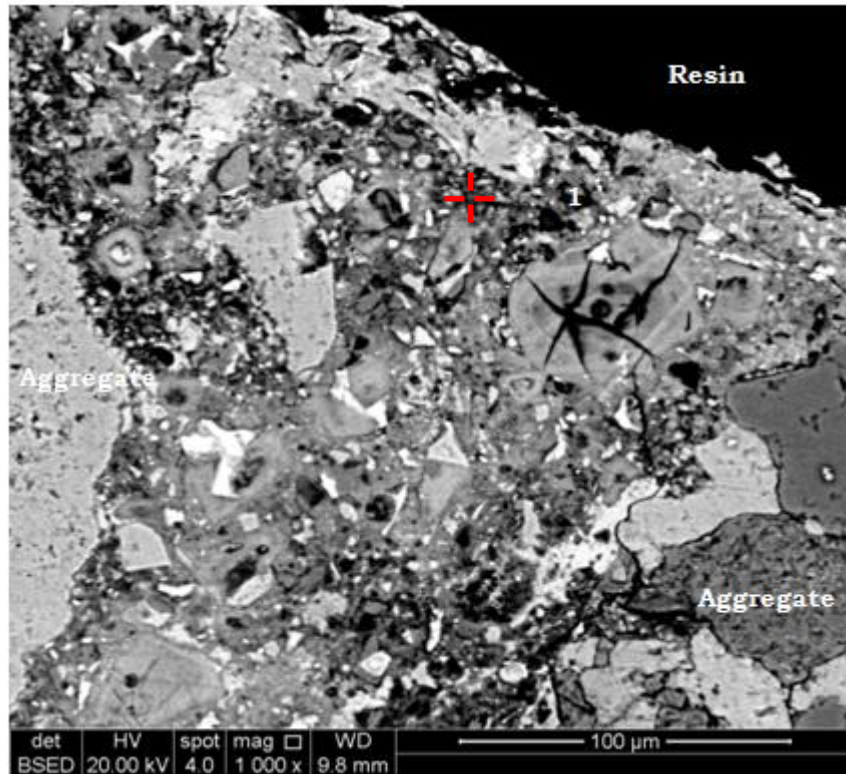


**Figure 4.48.** SEM image of CEMI-LF sample stored 450 days in sulfate only solution.

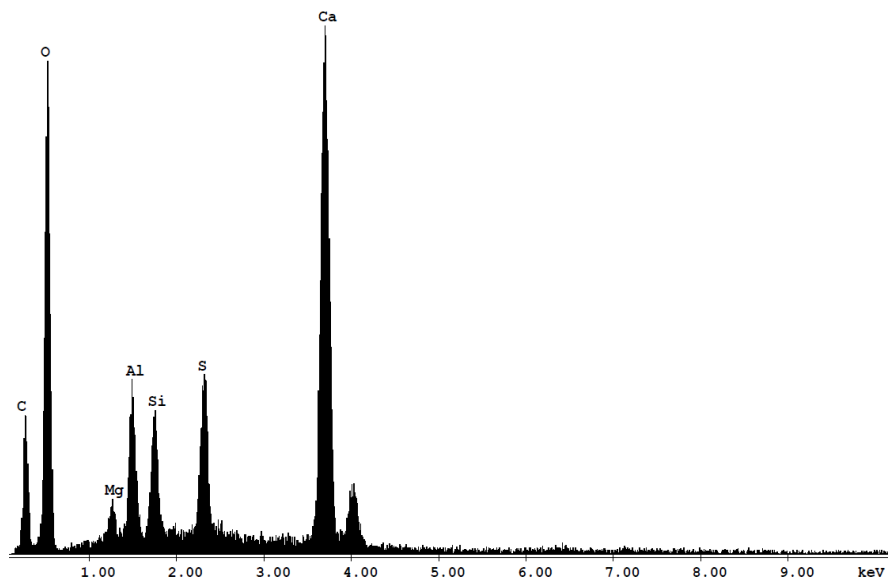


**Figure 4.49.** EDX of point shown in Figure 4.48



**Composite sulfate and 0.5% chloride (SC5) samples:** The SEM images in Figure 4.50 show the severe sulfate attack damage in CEMI-LF specimens after 450 days exposure to SC5 at 5°C. The massive intensity of the attack in CEMI-LF samples is very clear; the outer layer of the cement matrix has suffered conversion the dark grey area of thaumasite or thaumasite-ettringite solid solution (Figure 4.53) that dominates the attacked area.

In addition most of interfacial zones between the aggregate particles and the cement matrix have been removed, which explains the loss in the binding capacity of cement as it was converted to thaumasite. Closer investigation (Figure 4.51) showed obvious degradation of C-S-H occurred due to the deposition of thaumasite within the matrix. Detail 2 (Figure 4.52) shows the shape of thaumasite crystals developed within the matrix.

The EDX (Figure 4.53) analysis also indicates the absence of chloride in the dark grey area of samples stored in SC5 solution which is in agreement with the XRD analyses (Section 4.5.1), in that Friedel's salt was absent from the deteriorated material in this sample. Such an absence of chloride from the degraded materials may indicate low or reduced chloride binding capacity of thaumasite-affected area, as was suggested by Torres, (2004).

The cement matrix of CEMI sample (Figure 4.54 and 4.55) also suffered chemical degradation, but with lower severity than CEMI-LF, as indicated by the change in colour and the existence of microcracks. The EDX shown in Figure 4.56 indicates that these microcracks were related to thaumasite-ettringite solution.

The dark area (Figure 4.55) of the CEMI sample consists of high magnesium and low calcium, as indicated by EDX shown in Figure 4.57; which indicates that the C-S-H was decalcified.

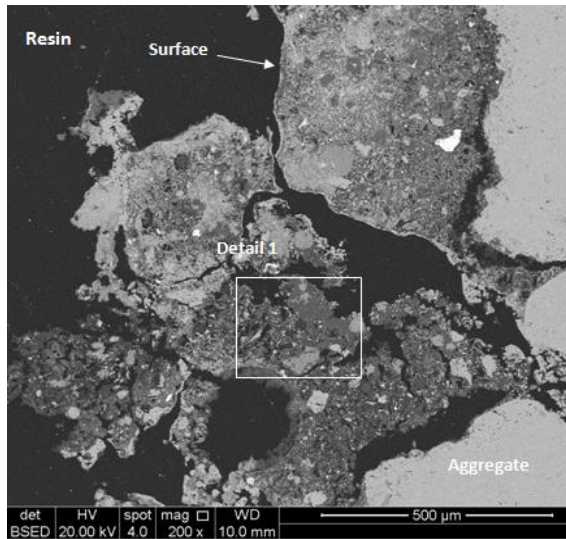


**Figure 4.50.** SEM image of CEMI-LF sample stored for 450 days in SC5.

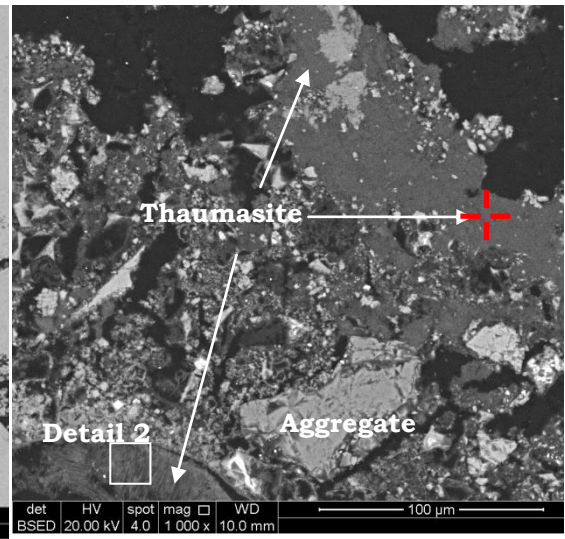


**Figure 4.51.** Detail 1 in Figure 4.50.

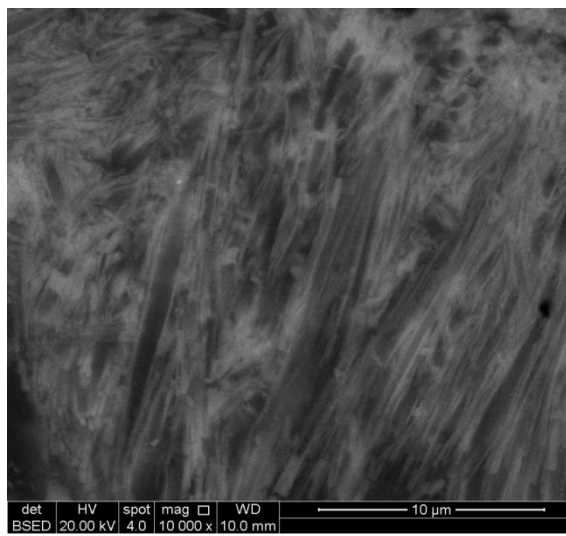


**Figure 4.52.** Details 2 (Thaumasite needles) in Figure 4.51.

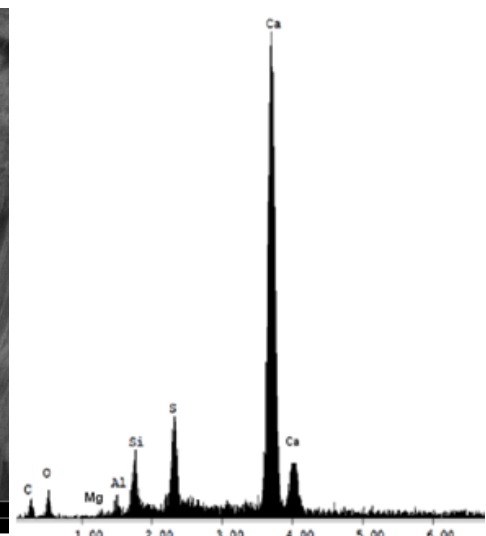


**Figure 4.53.**EDX of dark grey area in Figure 4.51

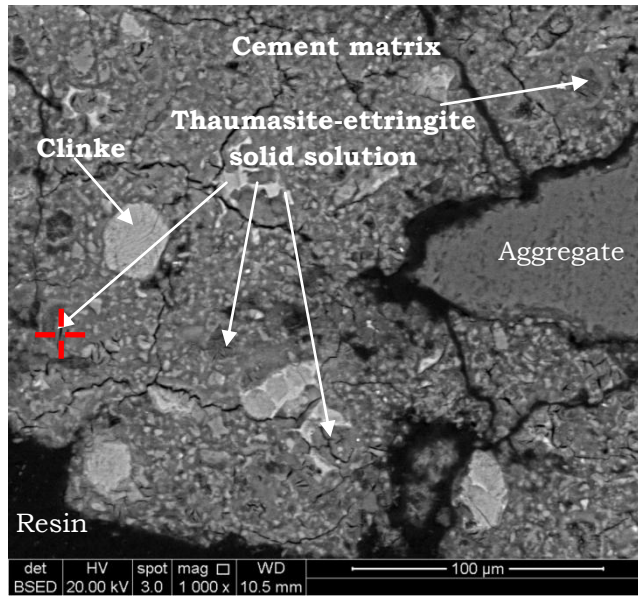


**Figure 4.54.** SEM image of CEMI sample stored 450 days in SC5.

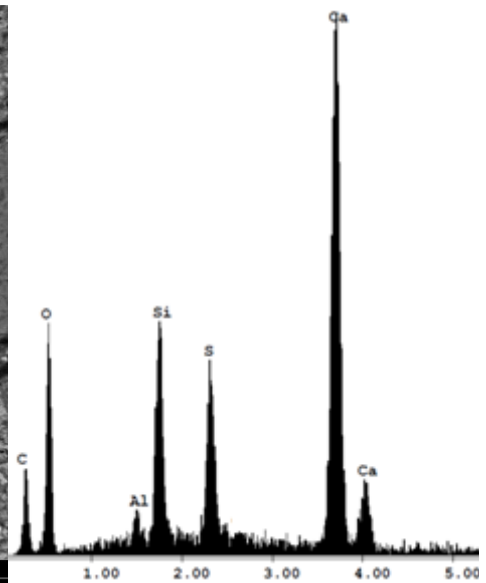


**Figure 4.56.** EDX of (Thaumasite-ettringite solid solution) in Figure 4.54

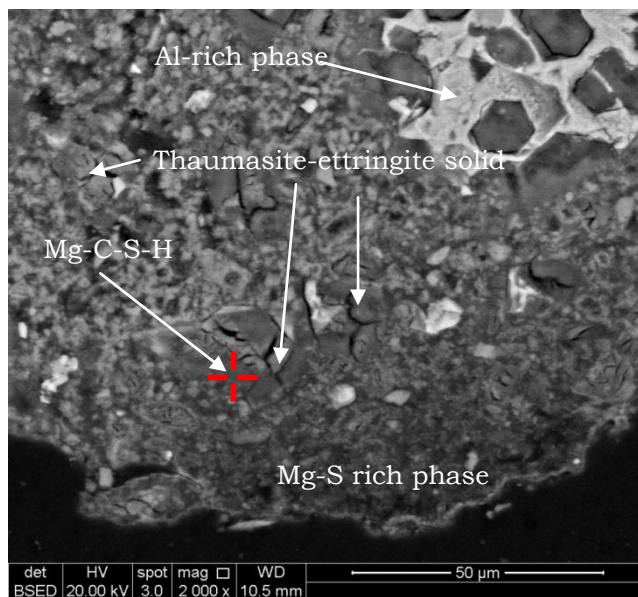


**Figure 4.55.** SEM image of CEMI sample stored for 450 days in SC5.

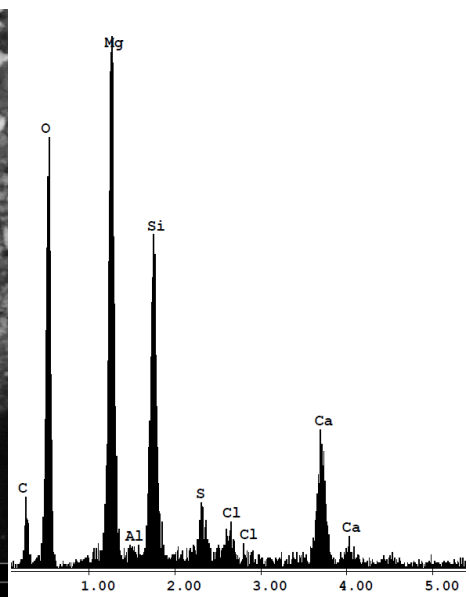


**Figure 4.57.** EDX of (Mg-C-S-H) in Figure 4.55.

**Composite sulfate and 1.0% chloride (SC10) samples:** Figure 4.58 and 4.58 show SEM images for CEMI and CEMI-LF mortar surfaces, respectively, stored for 450 days in SC10 solution at 5°C. It can be also noted these mortars suffered from microcracks formation, which were associated with thaumasite

and thaumasite-ettringite solid solution, as the EDX shown in Figure 4.59 and Figure 4.62 indicate.

The extent of damage was lower than for sulfate only and SC5 samples, as indicated by denser microstructure. The EDX analysis (Figure 4.60) showed clearly formation of Friedel's salt on mortar surface. The amount of Friedel's salt produced could present a physical barrier impeding ingress or chemical specie and it may also limit the availability of aluminates phases free to engage in degrading sulfate bearing products.

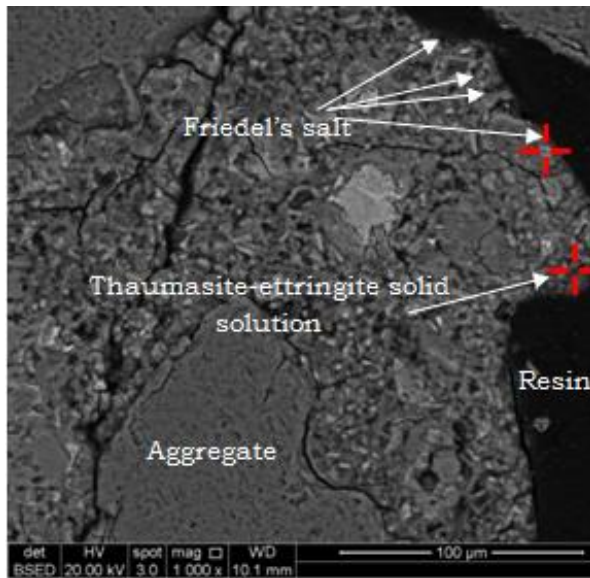


**Figure 4.58.** SEM image of CEMI sample stored 450 days in SC10.

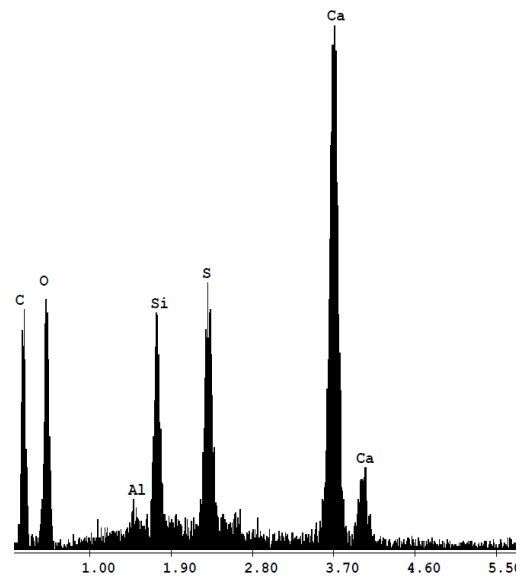


**Figure 4.59.** EDX of thaumasite - ettringite solid solution in Figure 4.58.

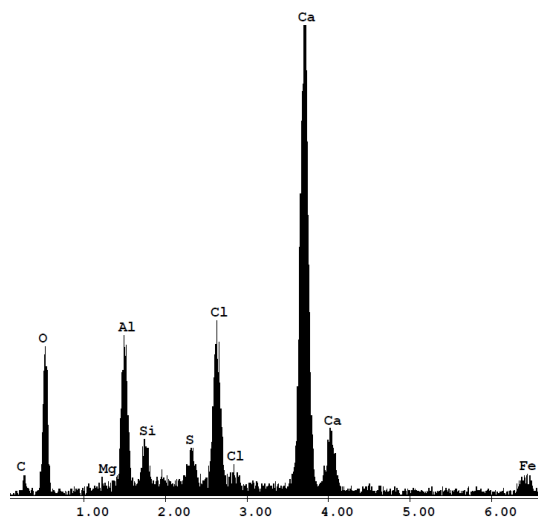


**Figure 4.60.** EDX of Friedel's salt in Figure 4.58.

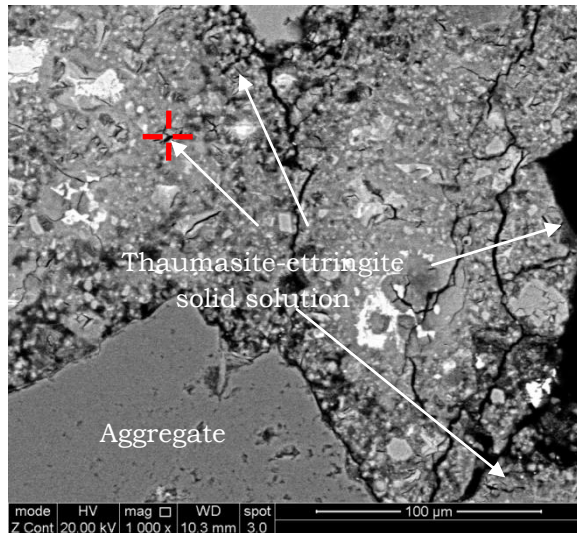


**Figure 4.61.** SEM image of CEMI-LF sample stored 450 days in SC10.

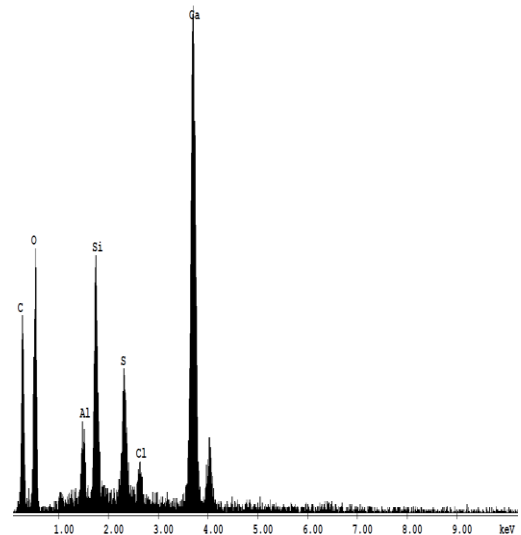


**Figure 4.62.** EDX for the point in Figure 4.61.

**Composite sulfate and 2.0% chloride (SC20) samples:** Figure 4.63 and 4.66 show SEM images for CEMI and CEM-LF samples stored in SC20 at 5°C. Although mortar specimens stored in SC20 solution showed no obvious damage, the EDX analysis (Figure 4.64 and 4.67) indicate that thaumasite was formed but without causing obvious deterioration to the specimens. Therefore, at this stage the samples could be said to have suffered thaumasite formation (TF) rather than TSA as would be expected, but the deterioration would be slower. Sotiriadis et al., (2012) attributed such a mitigation effect to the rapid penetration and interaction of chloride ions compared to sulfate.

Friedel's salt which is a non-expansive product, was determined by EDX shown in Figure 4.65 and 4.68. As mentioned above, it is possible that at high chloride concentration, the amount of Friedel's salt produced could present a physical barrier impeding ingress of chemical specie and it may also result in limiting the availability of aluminates phases free to engage in degrading sulfate bearing products. It was reported (Irassar et al., 2005) in a study conducted to investigate the effect of C<sub>3</sub>A content of cement on thaumasite formation, that cement with zero C<sub>3</sub>A, such as SRPC and containing limestone filler showed no thaumasite formation.

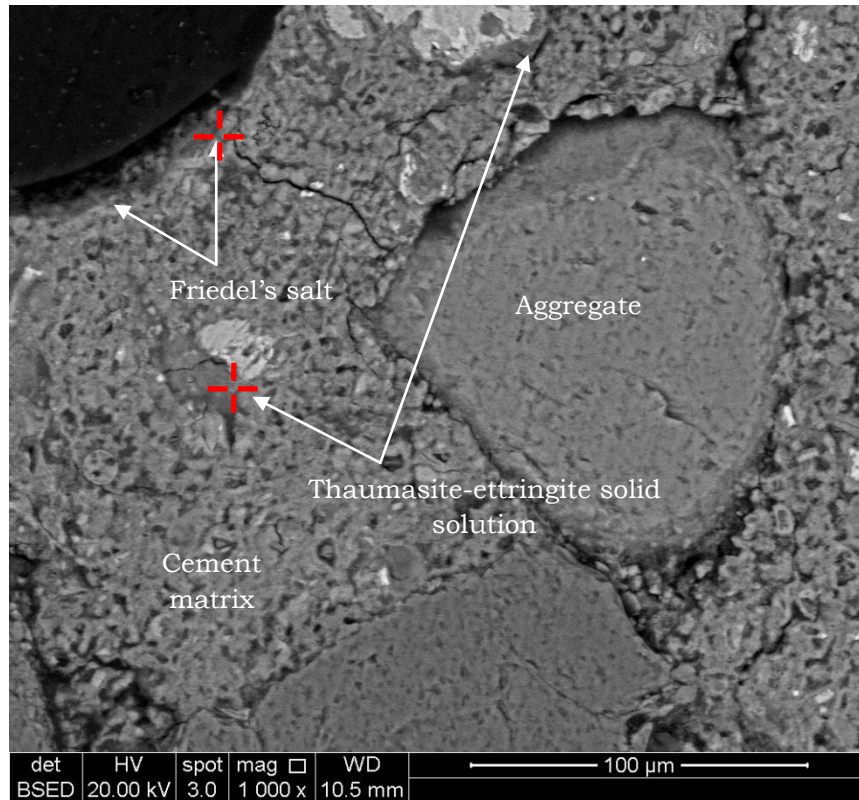


**Figure 4.63.** SEM image of CEMI sample stored 450 days in SC20.

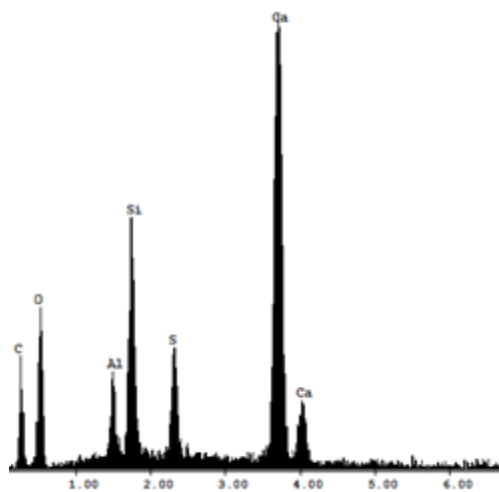


**Figure 4.64.** EDX for 2 in Figure 4.63.

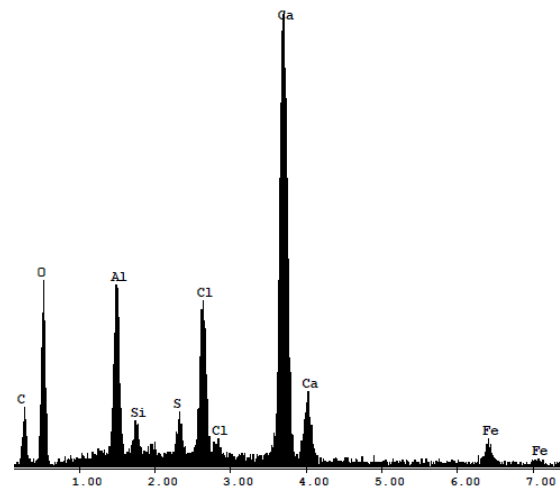


**Figure 4.65.** EDX Friedel's salt in Figure 4.63.

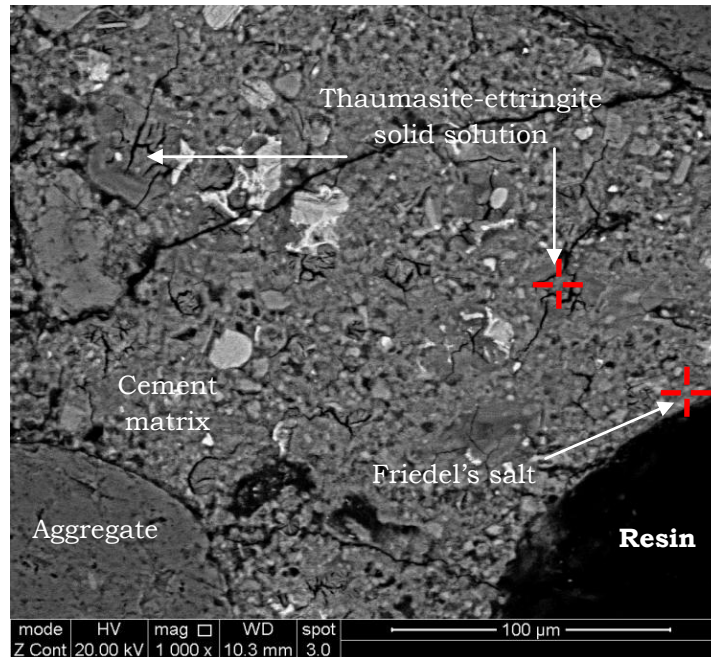


**Figure 4.66.** SEM image of CEMI-LF sample stored 450 days in SC20.

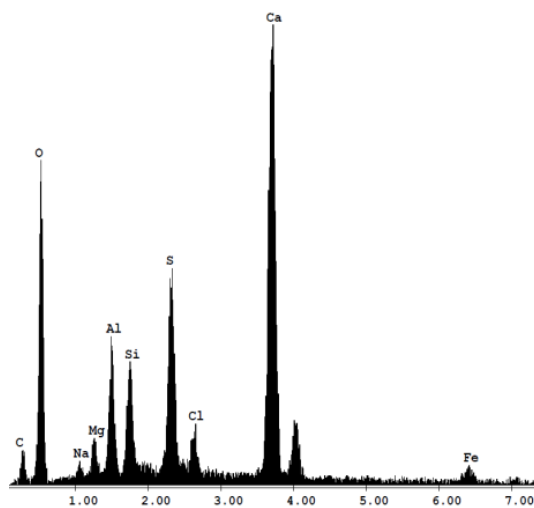


**Figure 4.67.** EDX of cracked material in Figure 4.66.

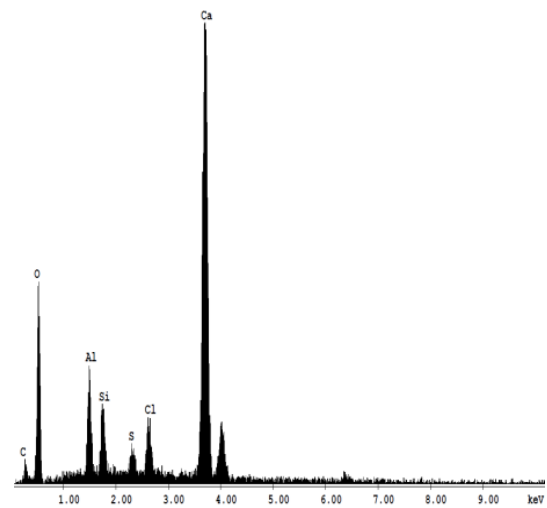


**Figure 4.68.** EDX of Friedel's salt in Figure 4.66.

**SEM/EDX of CEMI-LF mortar stored 630 days at 20°C**

The SEM images of samples taken from surface layer of mortar specimens stored in S, SC5 and SC20 solutions at 20°C are shown respectively in Figure 4.69, 4.72 and 4.75. Mortar sample stored in sulfate only solution showed evidence of thaumasite formation, as indicated by EDX shown in Figure 4.71 , which probably caused visually observed small micro-cracks on some parts of the mortar surface within this stage of exposure. The SEM images (Figure 4.72

and 4.73) of the SC5 sample showed deposition of thaumasite or thaumasite-ettringite solid solution (Figure 4.74) within the cement matrix and around the aggregate particles, whereas this sample showed clear damage on the surface edges after 630 days. However, SC20 sample showed denser microstructure (Figure 4.75) and no clear formation of thaumasite was detected. Instead, Friedel's salt was dominantly presented in the surface region of SC20 sample, as determined by EDX shown in Figure 4.76.

It was reported by Hartshorn et al.(2002) that thaumasite can also form at ambient temperature, but at slower rate than at 5°C. The presence of 0.5% chloride in solution also showed that mortar damage due to thaumasite formation seems to accelerate when samples are stored in SC5 solution at 20°C. However, the higher deposition of Friedel's salt may also play a role in mitigating sulfate attack in SC20 mortar, as reported by Zhang et al. (2013).

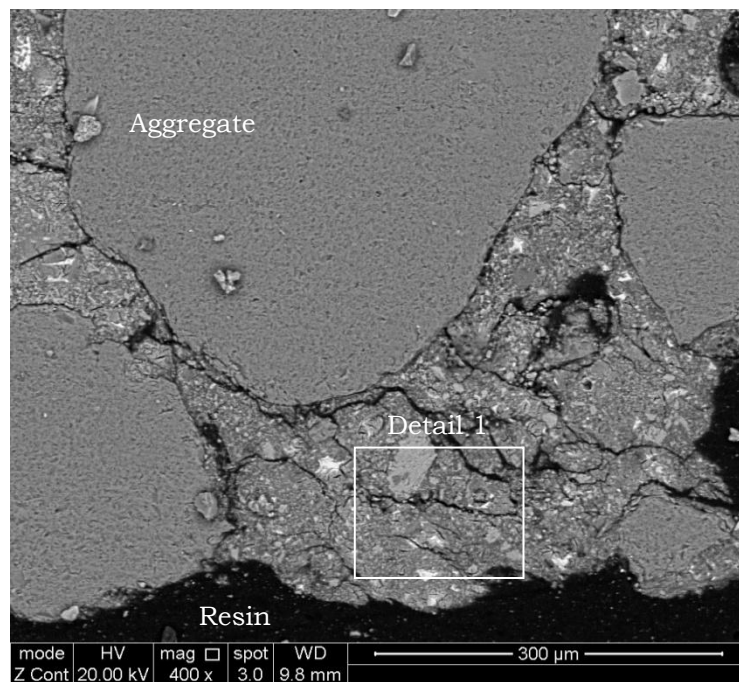


**Figure 4.69.** SEM image of CEMI-LF sample stored 630 days in sulfate only solution at 20°C.



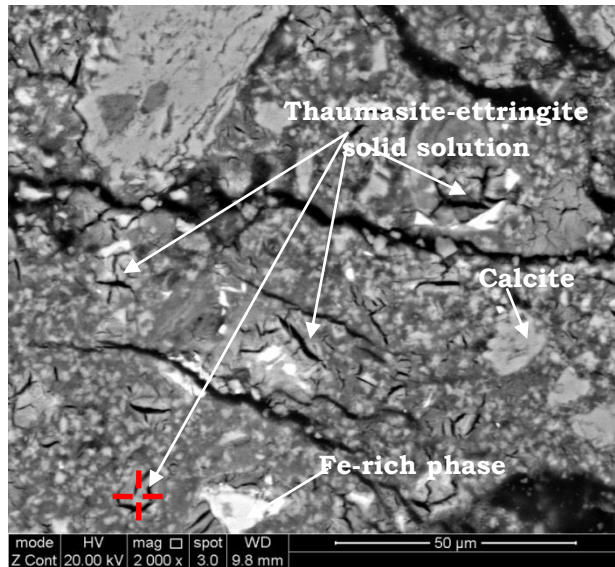


**Figure 4.70.** Detail 1 in Figure 4.69.

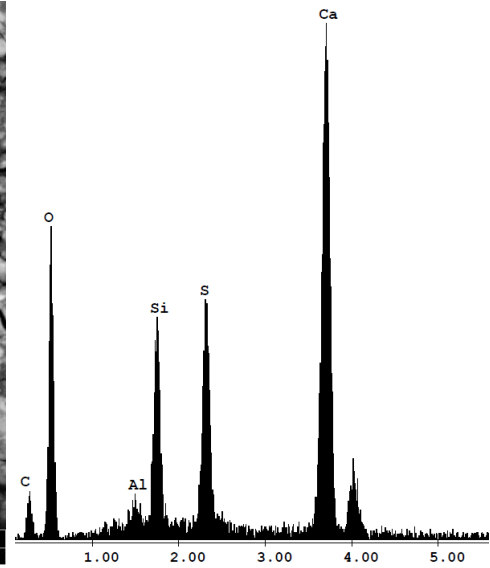


**Figure 4.71.** EDX of cracked material in Figure 4.70.

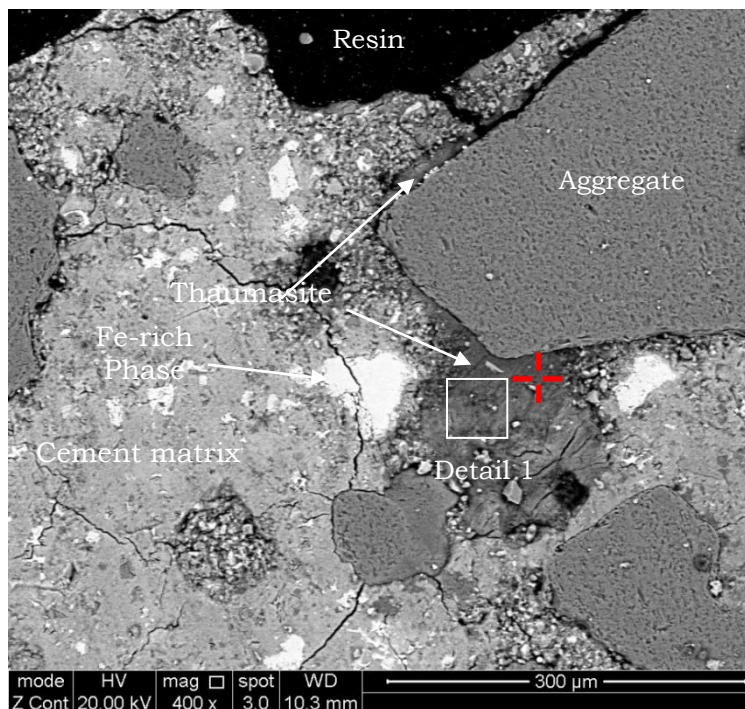


**Figure 4.72.** SEM image of degraded CEMI-LF sample stored in 630 days in SC5 at 20°C.

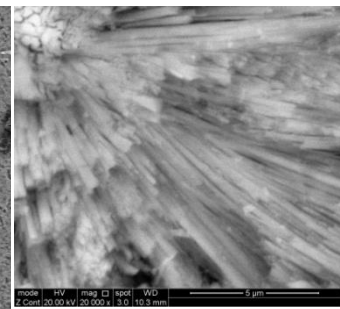


**Figure 4.73.** Detail 1 in Figure 4.72.

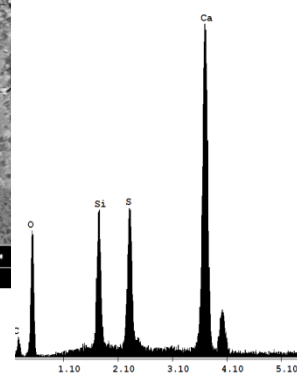


**Figure 4.74.** EDX of dark grey area in Figure 4.72

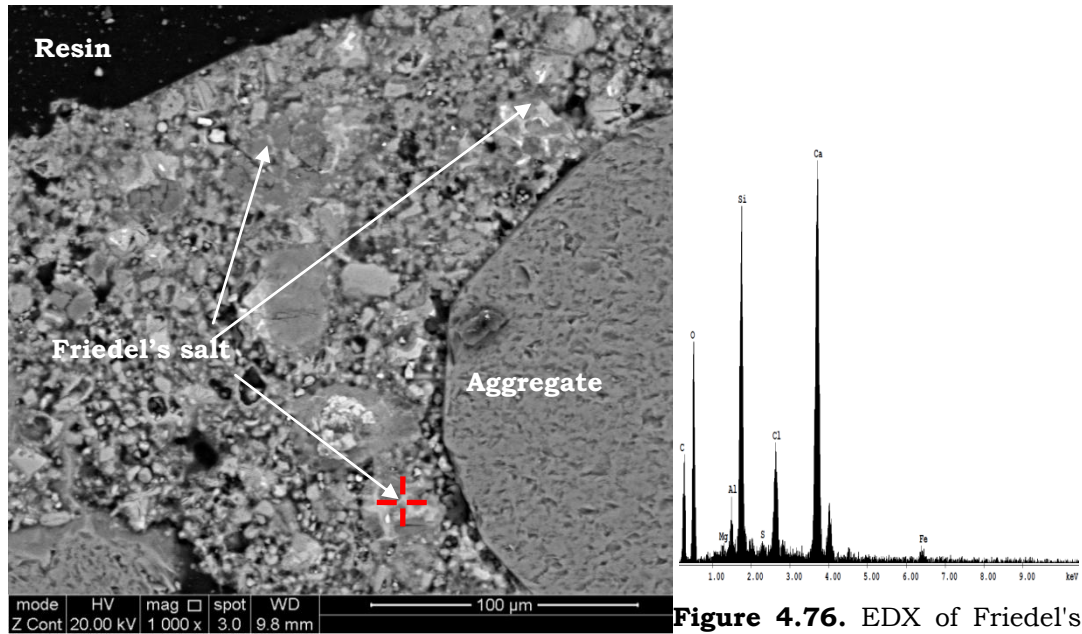


**Figure 4.75.** SEM image of CEMI-LF sample stored 630 days in SC20 at 20°C.

**Figure 4.76.** EDX of Friedel's salt in Figure 4.75.

**SEM/EDX of CEMI-PFA mortars stored 630 days at 5°C:**

The SEM images of samples taken from surfaces of CEMI-PFA mortar specimens stored for 630 days in sulfate only, SC5 and SC20 solutions at 5°C are shown respectively in Figure 4.77, 4.79 and 4.81. It should be mentioned that the PFA mortar specimens did not show any visual signs of damage and remained intact during the experiment. The SEM/EDX analysis indicated no thaumasite or thaumasite-ettringite solid solution was formed in any CEMI-PFA samples, except those stored in sulfate only solution which showed traces of thaumasite-ettringite solid solution (mixed dark gray and cracked areas in Figure 4.77) and, as indicated by the EDX analysis of Figure 4.78. The carbonated layer may provide carbonate ions for thaumasite formation, as reported by Torres et al. (2003).

Partly reacted particles of PFA distributed in the cement matrix indicate participation in the pozzolanic reactions and depletion of portlandite from the system. It should be noted that scattered formation of thaumasite-ettringite solid solution within the matrix of sample stored in sulfate only solution resulted in microcracks which could increase the diffusion of sulfate ions into the pore structure of the binder paste. This may indicate that after longer exposure period, this mortar may be subjected to TSA.

No clear formation of thaumasite occurred within this stage of exposure in mortars exposed to composite sulfate and chloride solutions (Figure 4.79 and 4.81). Instead, dark grey areas that are attributed to Mg-rich phases, as determined by EDX (Figure 4.80 and 4.82) were detected in both samples.

The production of sub silica gel as a result of pozzolanic reactions led to improve mortar compaction, and acted to delay the ingress of sulfate ions. This retardation may improve in presence of chloride, as the reactive aluminium phases in fly ash reacted with chloride, producing Friedel's salt, which would tend to block pores and result in a further reduction in sulfate ingress, as mentioned earlier. Hong and Glasser (2002) reported that fly ash and slag cement exhibit high chloride binding due to the high alumina content and the consequent formation of C-A-S-H which has ability to bind chloride, which would further reduce free chloride available in pore solution, and thus reduce the corrosion risk.

Blanco-Varela et al. (2006) found that thaumasite formation decreased as the content of  $C_3A$  decreased. This may suggest that the consumption of  $C_3A$  in the presence of chloride associated with the formation of Friedel's salt enhanced the performance of CEMI-PFA mortars placed in composite sulfate and chloride solutions.

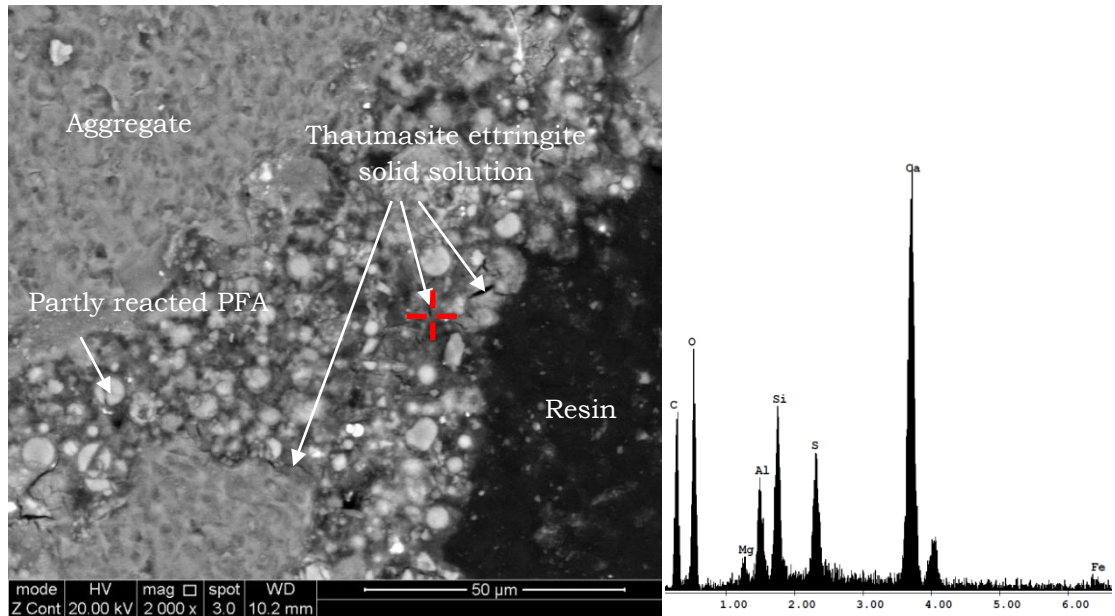


**Figure 4.77.** SEM image of CEMI-PFA sample stored 630 days in sulfate only solution at 5°C.

**Figure 4.78.** EDX of cracked material in Figure 4.77.

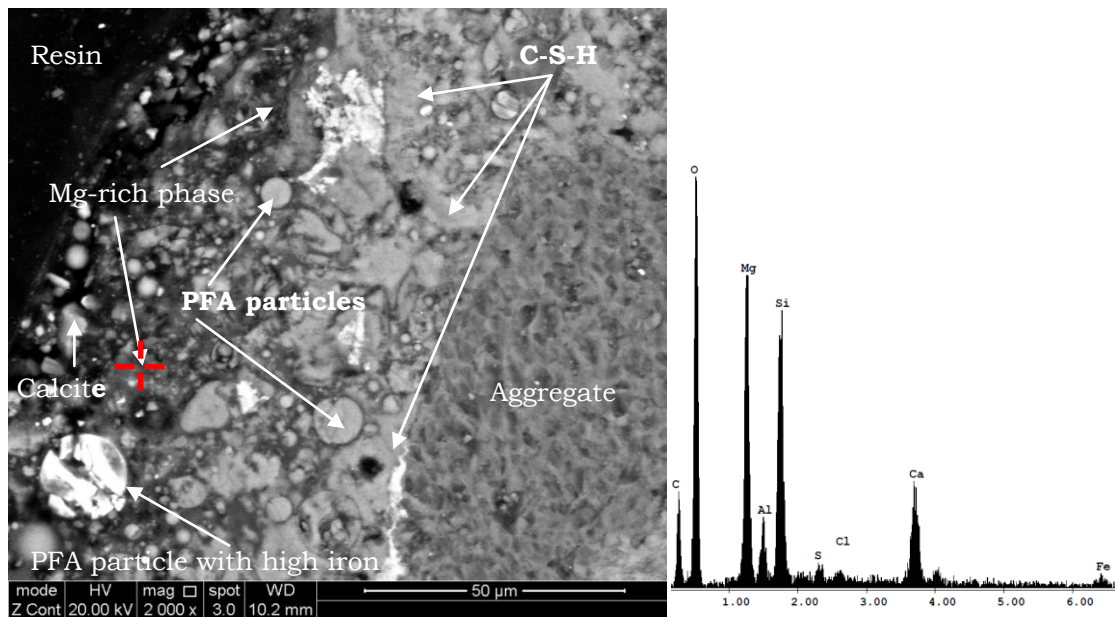


**Figure 4.79.** SEM image of CEMI-PFA sample stored 630 days in SC5 at 5°C.

**Figure 4.80.** EDX of dark area (Mg rich phase) in Figure 4.79.

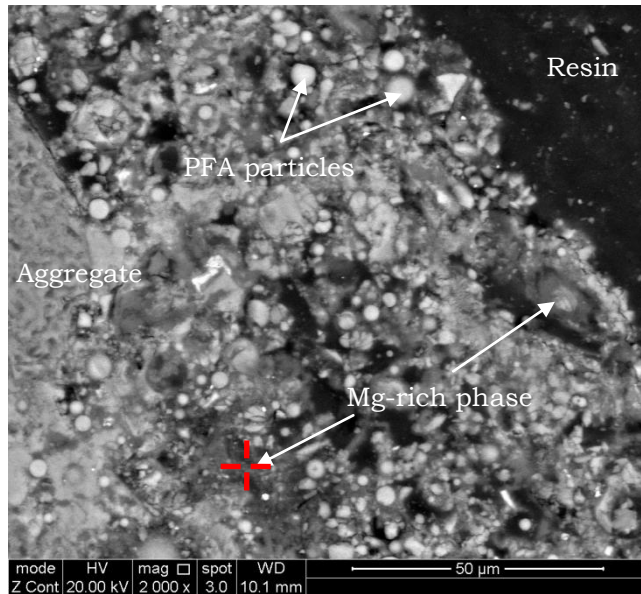


**Figure 4.81.** SEM image of CEMI-PFA sample stored 630 days in SC20 at 5°C.

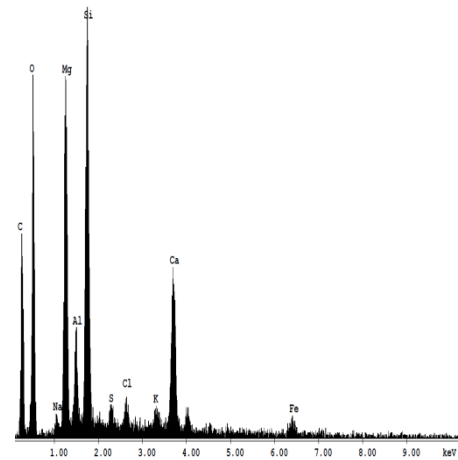


**Figure 4.82.** EDX of dark grey area (Mg rich phase) in Figure 4.81.

**SEM/EDX of CEMI-GGBS mortars stored 630 days at 5°C:**

Figure 4.83, 4.86 and 4.89 show SEM images of CEMI-GGBS samples stored for 630 days in sulfate only, and composite sulfate and chloride solutions at 5°C. According to visual inspection, no signs of damage were observed in any CEMI-GGBS mortar specimens within the experiment period. However, the investigations of the microstructure of mortar samples indicate that interactions between cement matrix and sulfate took place, as indicated by changing in colour of the sulfate only mortar sample (Figure 4.83) and spreading of microcracks in the SC5 and SC20 mortar samples (Figure 4.86 and 4.89).

The dark grey areas in the SEM image of sulfate only sample consisted (Figure 4.84) mainly of S, Si, Ca and Al with Ca/Si ratio of about 0.5 which may attribute to a phase similar to thaumasite- solid solution, as reported by Pouya (2007) who found that the incorporation of sulfate and aluminates in the structure of C-S-H gel being formed involved slight deterioration of the main cementitious matrix towards phases like thaumasite-ettringite solid solution. The high slag replacement level produced secondary C-S-H gel with lower calcium/ silica ratio which was capable of binding more alumina in its structure which resulted in reduced ettringite formation, as explained by Gollop and Taylor (1996).

The deposition of light area in the sulfate only sample surrounding the darker one was attributed to gypsum, as indicated by EDX (Figure 4.85) analysis. It was reported by Schmidt et al (2008) that gypsum deposition precedes thaumasite formation and then acts as a source of sulfate for its formation, which may explain why phases similar to thaumasite-ettringite solid solutions were extensively formed surrounding gypsum deposition.

In case of composite solutions, scattered microcracks in the SC5 and SC20 mortar samples was found to relate to thaumasite-ettringite solid solutions, as indicated by EDX analysis (Figure 4.87 and 4.91). The EDX for some areas surrounding the cracks in SC5 sample (Figure 4.88) indicated that secondary C-S-H gel incorporating sulfate, aluminates and magnesium in its structure was present. The EDX (Figure 4.90) analysis for secondary C-S-H gel of SC20 sample (Figure 4.89) further showed chloride bound in its structure.

The microstructure of CEMI-GGBS mortars indicated that after longer exposure period, all mortars, including those exposed to composite solutions, would be subject to sulfate attack, due to either gypsum or/and thaumasite formation. It should be mentioned that slag-cement /mortars can perform well if produced with low water to cement ratio, as well documented in the literature.

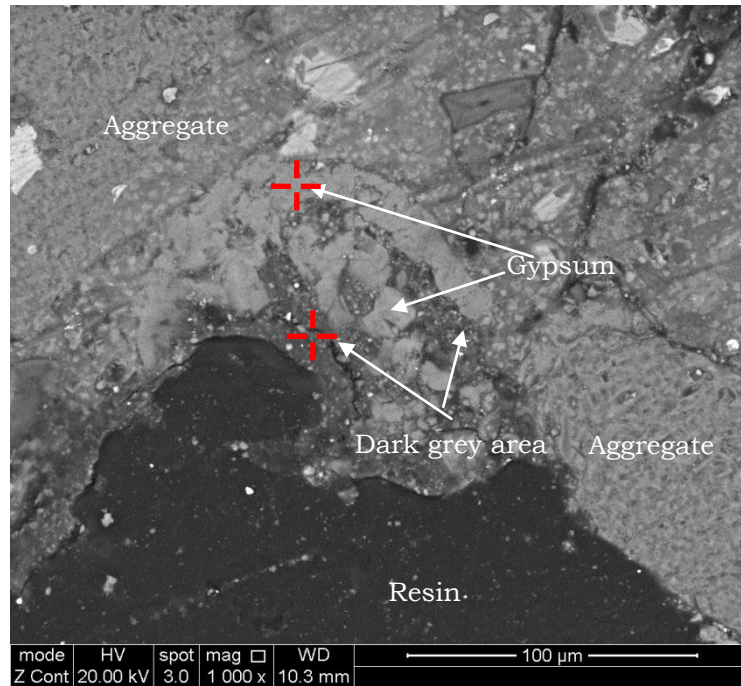


**Figure 4.83.** SEM image of CEMI-GGBS sample stored 630 days in sulfate only solution at 5°C.

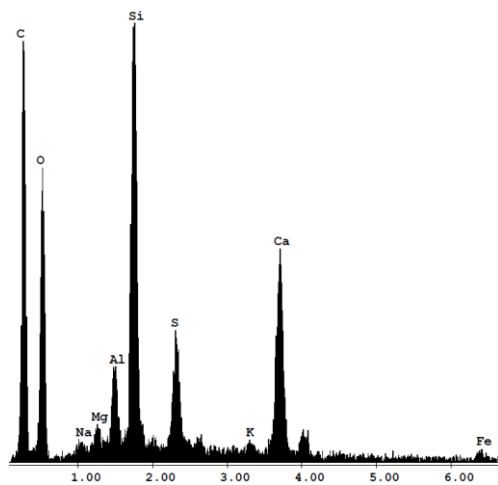


**Figure 4.84.** EDX of dark grey area in Figure 4.83.

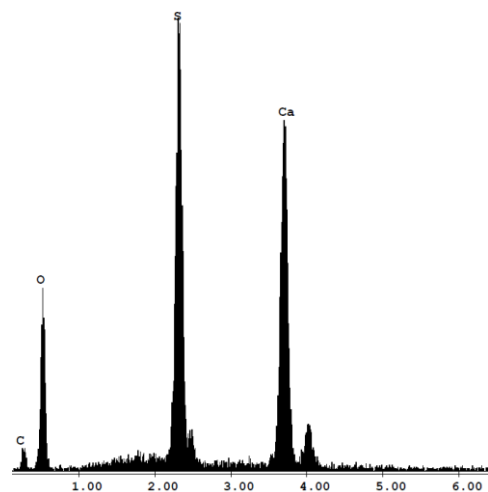


**Figure 4.85.** EDX of light grey area (gypsum) in Figure 4.83.

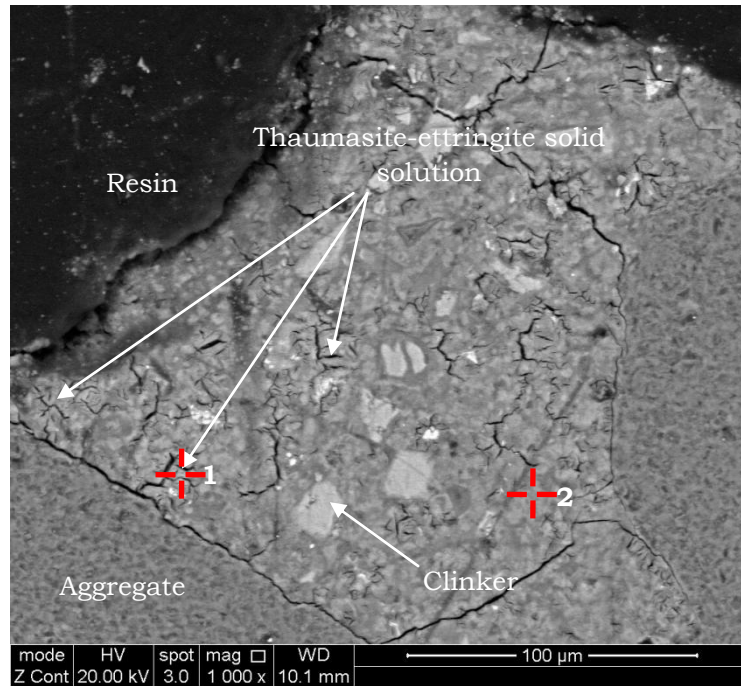


**Figure 4.86.** SEM image of CEMI-GGBS sample stored 630 days in SC5 at 5°C.

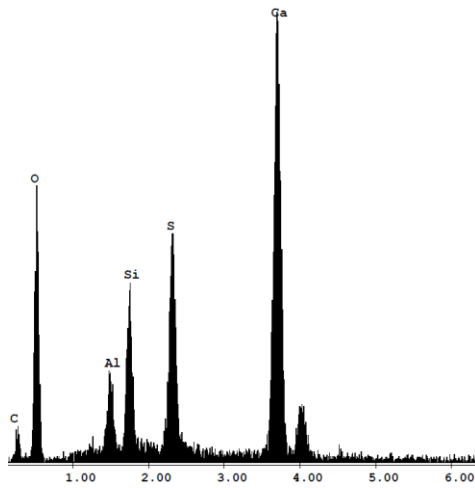


**Figure 4.87.** EDX of 1 (Cracked area) in Figure 4.86.

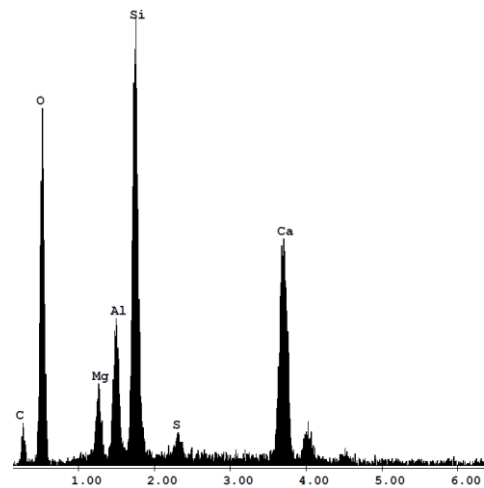


**Figure 4.88.** EDX of 2 (C-S-H) gel with Ca/Si = 0.5 in Figure 4.86.



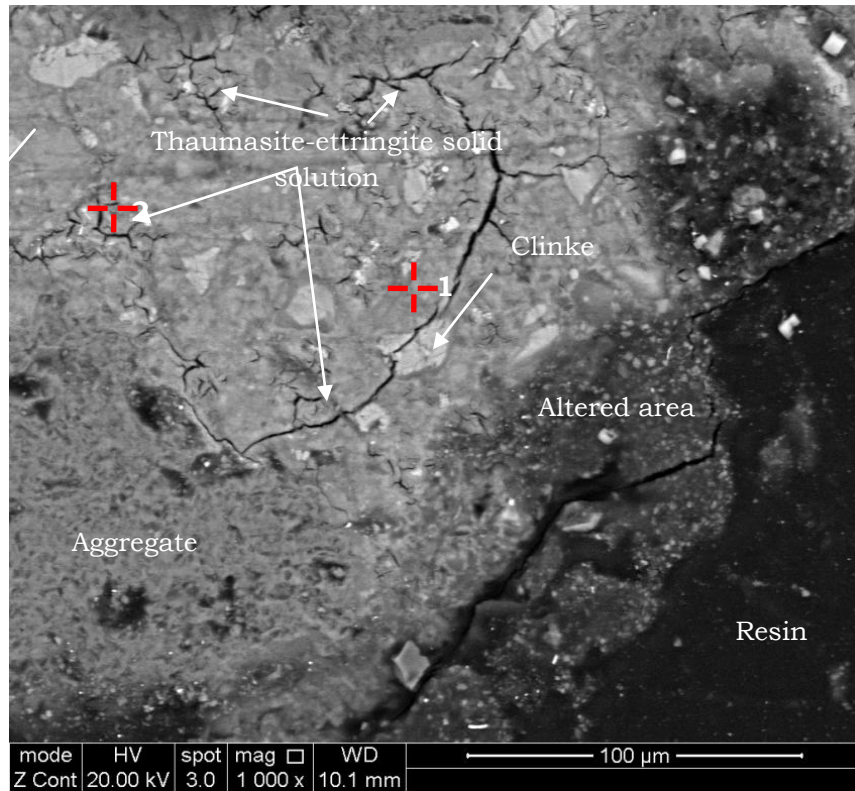


**Figure 4.89.** SEM image of CEMI-GGBS sample stored 630 days in SC20 at 5°C.

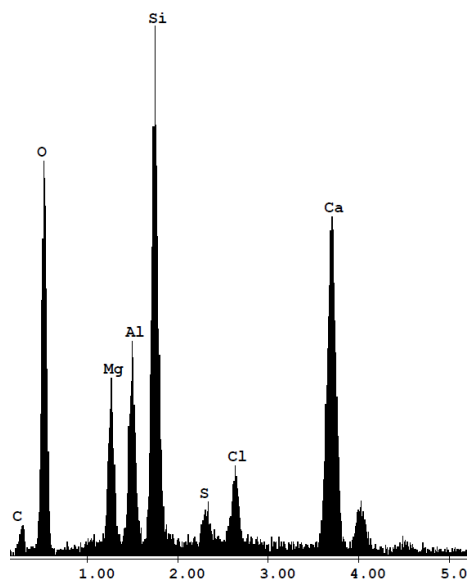


**Figure 4.90.** EDX of 1 in Figure 4.89.

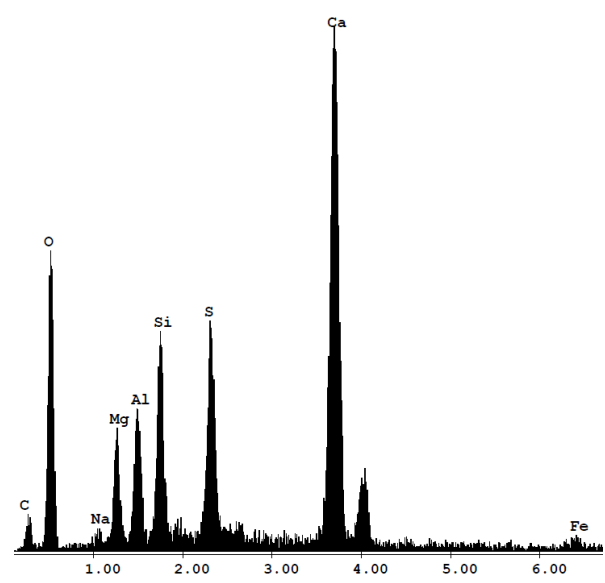


**Figure 4.91.** EDX of 2 in Figure 4.89.

**SEM/EDX analysis of CEMI-GGBS samples of 20mm cubes at 5°C:**

Figure 4.92 shows the SEM image of CEMI-GGBS sample stored 180 days at 5°C. Although no visual damage was observed, the EDX scan in Figure 4.94 indicates that thaumasite or thaumasite-ettringite solid solution was formed in this sample, which confirms the XRD finding. Although, no gypsum was detected in this part of sample by SEM/EDX analysis, its formation was confirmed by XRD analysis. It should mention that gypsum was also confirmed by both SEM/EDX and XRD analysis in 50mm mortar cubes placed in sulfate only solution, which indicates that with long-term storage to sulfate only solution, this mortar would be subjected to damage due to gypsum formation. An SEM image of a degraded SC5 samples appears in Figure 4.95 in which intensive attack by the formation of prismatic crystals particularly around the aggregate. EDX analysis shown in Figure 4.96, confirmed the presence of gypsum. It was indicated by Figure 4.97 that the C-S-H in regions close to this gypsum was decalcified, which is the most probable source of the calcium required. This process appears to have occurred more rapidly in SC5 mortars, which showed early deterioration due to gypsum deposition and as visually observed.

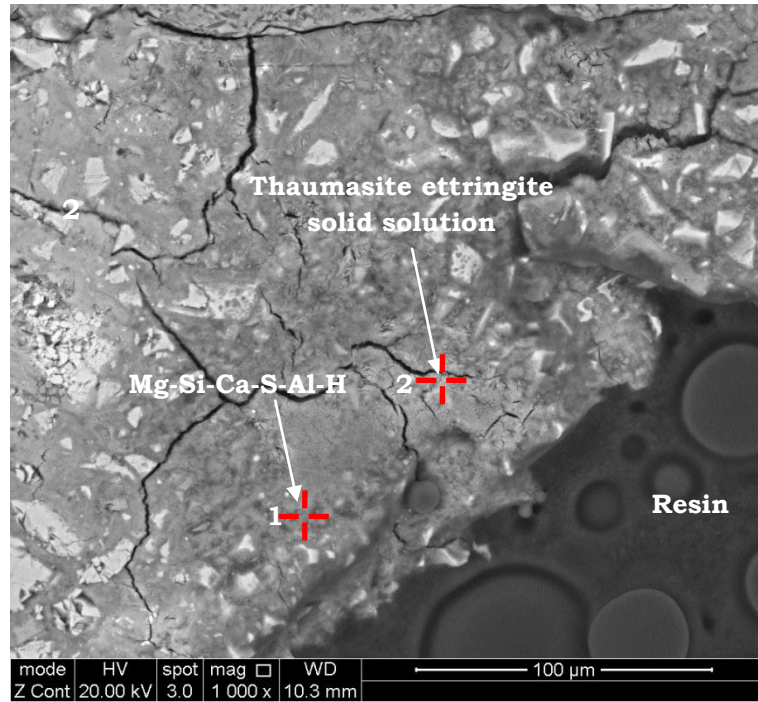


Figure 4.92. SEM of CEMI-GGBS sample stored 180 days in sulfate only at 5°C.

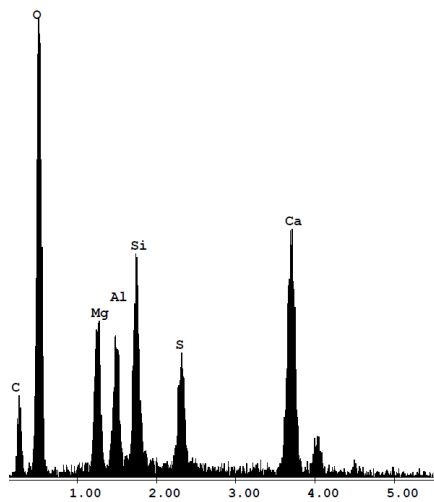


Figure 4.93. EDX of 1 in Figure 4.92.

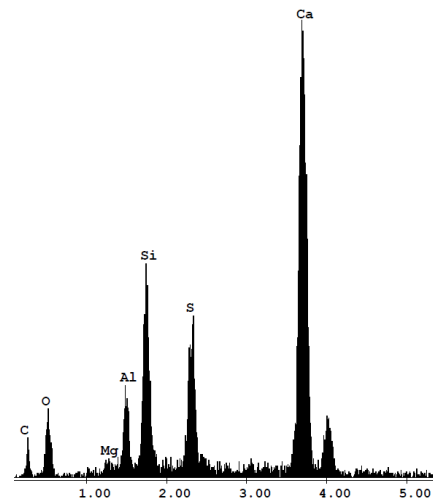
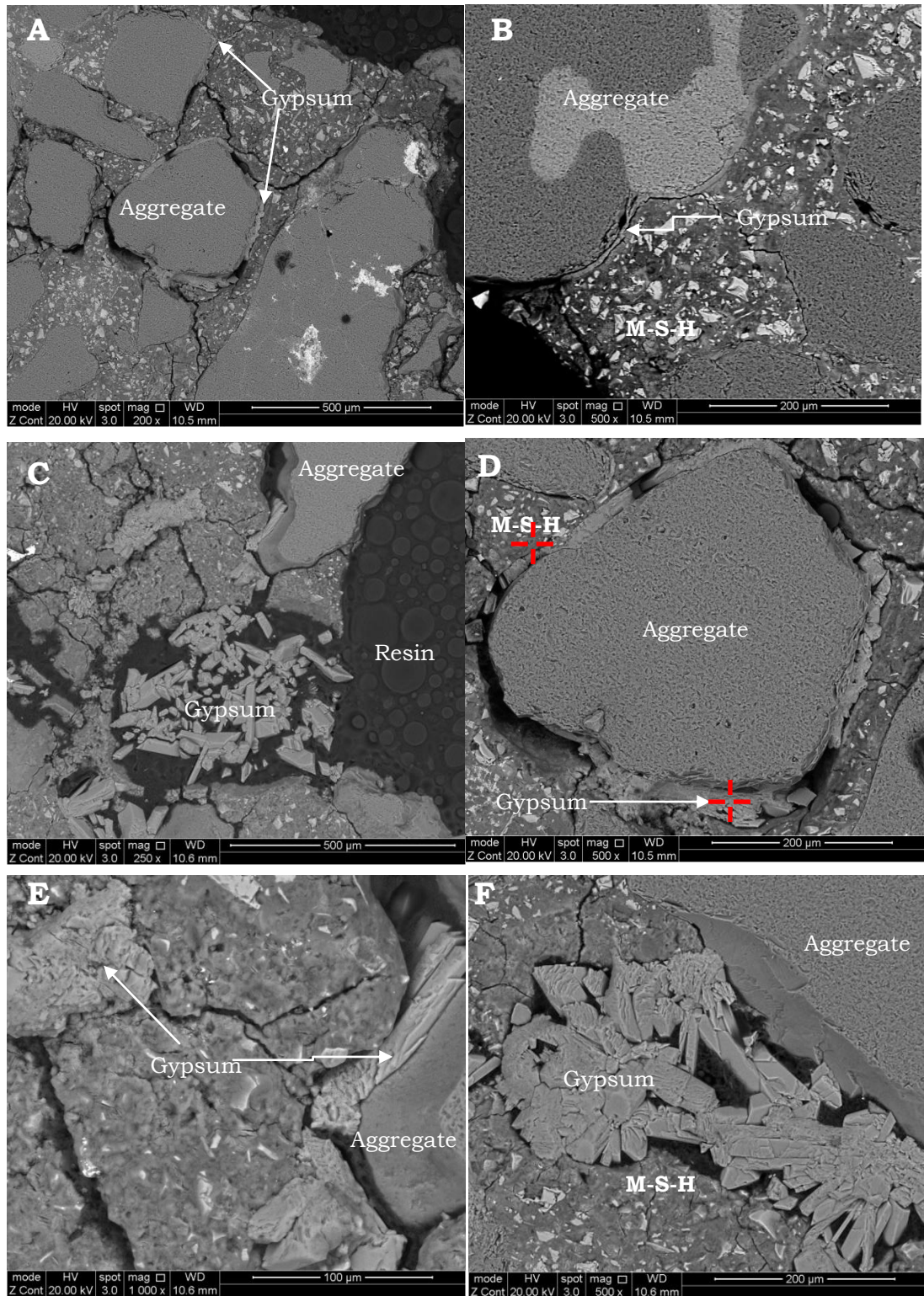
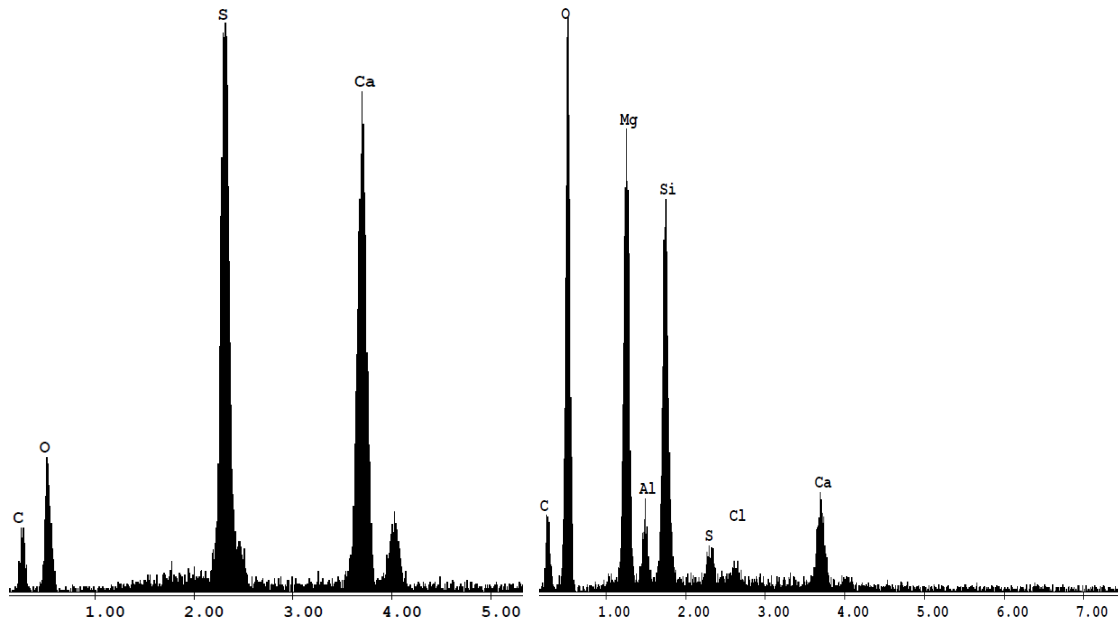


Figure 4.94. EDX of 2 in Figure 4.92.



**Figure 4.95.** SEM images of CEMI-GGBS samples stored 180 days in SC5 at 5°C.



**Figure 4.96.** EDX of prismatic crystals and light grey area around aggregate particles in Figure 4.95-D. **Figure 4.97.** EDX of dark area (M-S-H) in Figure 4.95-D.

## 4.7 Chemical analysis of test solutions

In order to monitor the changes of chemical compounds of test solutions of combined mortar specimens made with CEMI and CEMI blended with 10% limestone filler over the experimental period, the concentration of sulfate, calcium, chloride and magnesium were measured using the ion chromatography technique after different durations of exposure of 50mm mortar cubes and prisms to test solutions at 5 and 20°C. In order to monitor the change of the chemistry of test solutions within the early exposure period, for each cement binder, a 20mm mortar cubes were also cast. Due to very high concentration of ions in the test solutions, diluted sample of solutions were tested to avoid any potential problems with the measurements.

- **Chemical analysis of test solutions of CEMI and CEMI-LF mortar specimens:**

Table A. 1 and A.2 (See Appendix) summarise the results of chemical analysis of test solutions at 3, 6, 9, 12 and 18 months after the samples were placed in the test solutions. It should be mentioned that the solutions were renewed every 3 months up to 12 months, after which the replenishment ceased.

Variations in ion concentration against time and temperature are presented and discussed in the following sections.

**At 5°C:**

Variations of sulfate, calcium, magnesium, and chloride ions in test solutions of combination of mortar samples made with CEMI and CEMI-LF at 5°C are shown in Figure 4.98 to 4.101, where as can be seen in Figure 4.98 in sulfate only solution, the concentration of sulfate ions decreased with time. This reduction may be related to the penetration of sulfate ions through deteriorated mortar, as noted in visual observations, and a raised extent of deterioration as time progressed. In addition, the formation of thaumasite and gypsum would result in sulfates being bound in insoluble compounds.

Clearly the lowest drop in sulfate ion value was found for SC5 solution for most of exposure periods. The reduction, which was about 46% at 630 days of exposure compared with 41% for sulfate only solution, while SC10 and SC20 showed only a reduction of around 16%. The large drop in sulfate in S and SC5 solutions may be attributed to higher formation of sulfate products in forms of thaumasite and gypsum, as indicated by XRD analysis, remembering that stronger intensity peaks for these minerals were found in SC5 samples compared to other solutions. This impact could be a consequence of higher penetration of sulfate ions through the deteriorated mortar. These results are also in agreement with the mass changes noted in Section 4.3, in which mortar samples stored in composite sulfate and 0.5% chloride solution showed the highest extent of deterioration.

In the case of SC20, however, the variation in sulfate concentration was approximately zero which indicated lower sulfate ingress and denser structure as samples immersed in this test solution did not show any evidence for damage. No gypsum was precipitated and only traces of thaumasite that were detected by XRD analysis for samples taken from outer part of mortar immersed in SC20.

The variation of calcium is shown in Figure 4.99, where the highest value was found in both sulfate only and combined sulfate and 0.5% chloride (SC5) solutions, and more pronounced in SC5 solution, which at 630 days of exposure, showed about 3.6 times higher release in calcium relative to that of sulfate only solution. As shown in Figure 4.100 both solutions exhibited the lowest reduction in magnesium concentration, with a greater reduction for SC5

solution. After 630 days of exposure, the SC5 solution showed the highest drop of magnesium concentration of about 77%, while in sulfate only solution, the fall was about 41%. Magnesium ions are most likely to be consumed during the reaction with portlandite and CSH to form both brucite and non-binding Mg-S-H, as indicated by XRD and SEM/EDX results shown in Sections 4.5.1 and 4.6, respectively.

The variation of chloride concentration in test solutions is shown in Figure 4.101, from which it can be seen that the highest chloride consumption was found in SC20 mortars. This may be attributed to high chloride binding and lower sulfate interaction of cement mortars placed in SC20 solution, as indicated by XRD and SEM/EDX analyses. After 9 months of storage, chloride consumption decreased in SC5 mortars, which might be related to the attack of Friedel's salt by sulfate, which would release free chloride to solution. This may also indicate the increase in the amount of free chloride in the pore solutions of the SC5 mortars. In turn, this would increase the corrosion risk for steel reinforcement in concrete/mortar in such conditions, as will be investigated in Chapter 5, Sections 5.8 and 5.9. Similar observations of lower damage were found in case of SC10 solution, but after 12 months of exposure. However, in the SC20 solution the samples showed a continuous increase in chloride consumption, probably due to higher chloride binding.

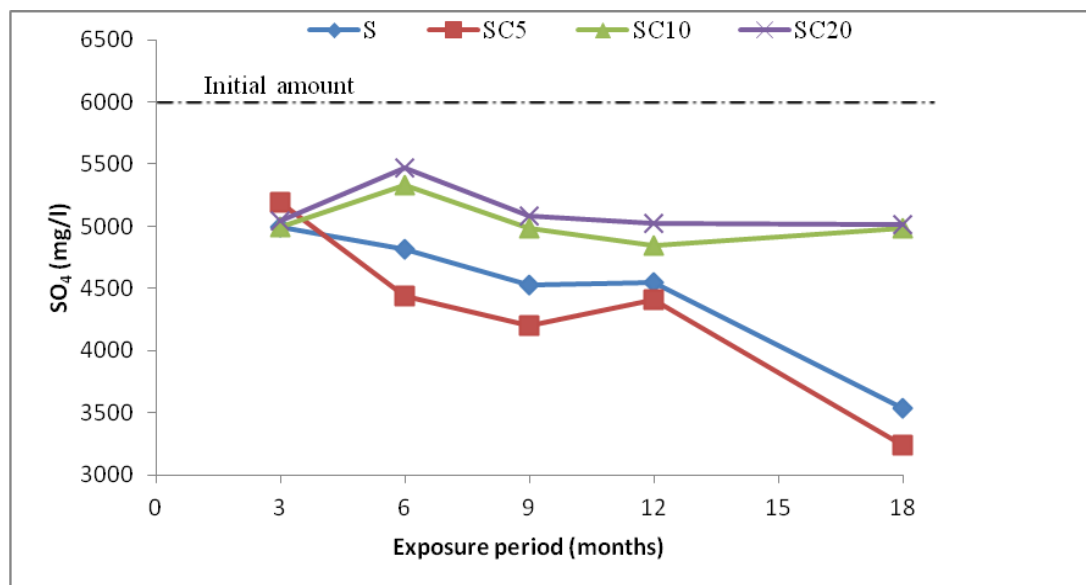


**Figure 4.98.** Variation of sulfate ion in test solutions at 5°C.

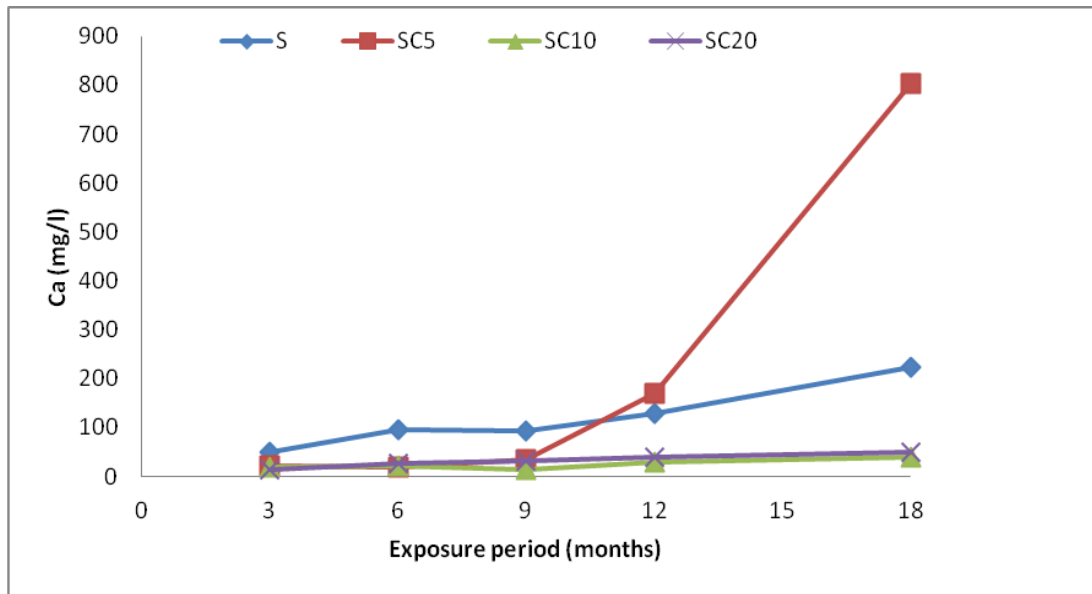


Figure 4.99. Variation of calcium ion in test solution at 5°C.

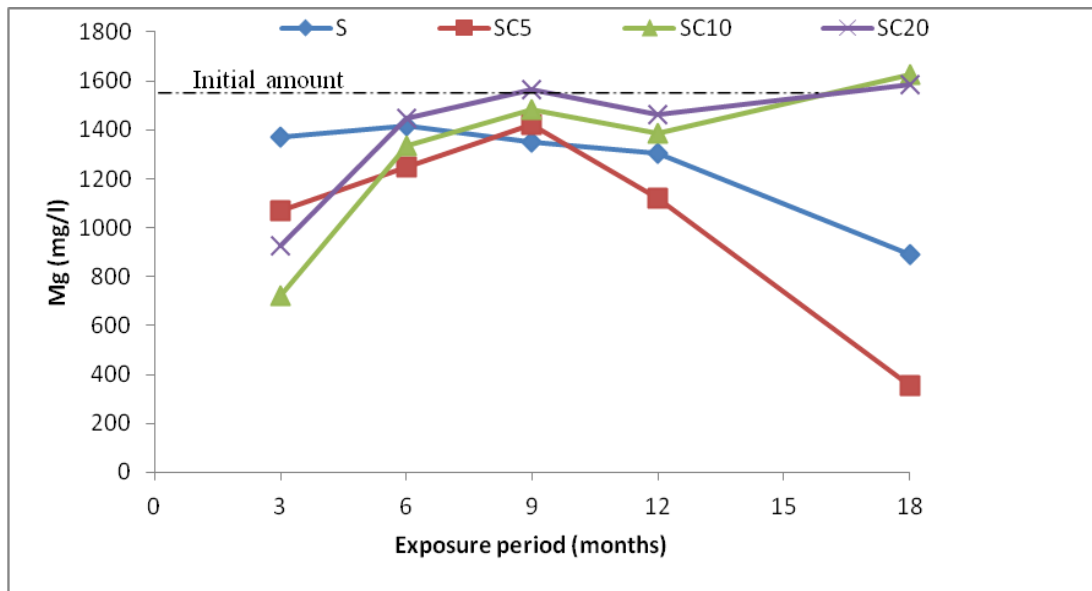
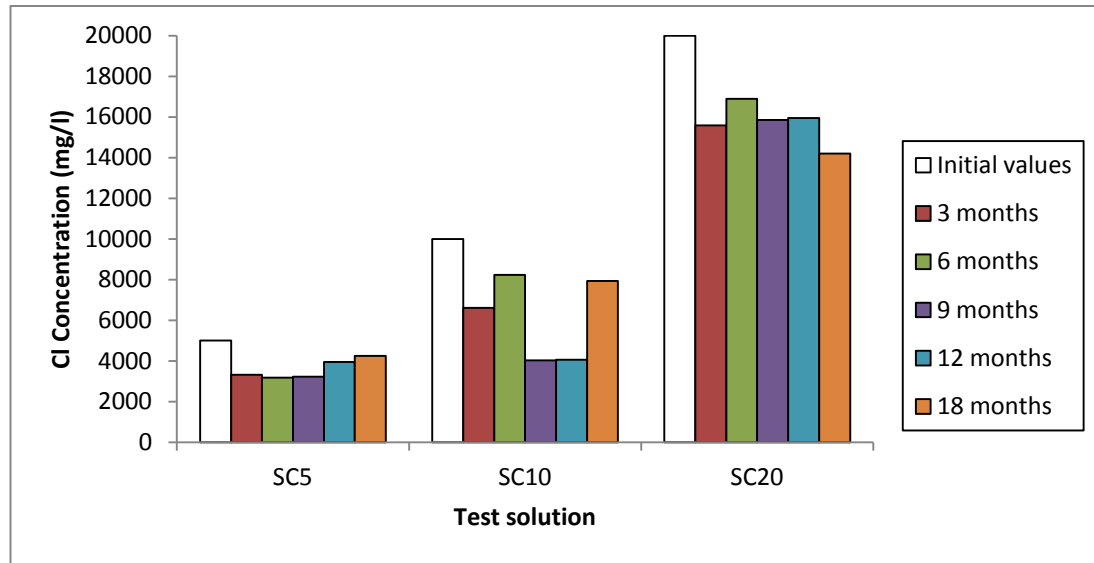


Figure 4.100. Variation of magnesium ion in test solution at 5°C.





**Figure 4.101.** Variation of chloride concentration in composite solutions at 5°C.

### **At 20°C**

The 12 months results for chemical analysis of test solutions at 20°C are shown in Figure 4.102 to 4.105; indicate that no significant activities occurred in test solutions at 20°C, which contrasted with those at 5°C. The negligible change in ion concentrations with time in all test solutions, which was in line with the visual observations, XRD and SEM data. After 12 months of exposure, as shown in Figure 4.102, both sulfate only and SC5 solutions showed a slight drop in sulfate concentrations. This may be attributed to the formation of thaumasite and gypsum, as confirmed later by XRD analysis, although no remarkable reduction in sulfate level was observed for the rest of the solutions.

Data in Figure 4.103 for calcium shows that sulfate only solution showed the highest Ca concentration, and furthermore its value increased from about 40 mg/l at 3 months to about 120 mg/l after 9 months. This increase in calcium ions in the sulfate only solution may be attributed to CH leaching, which would compensate the low pH of sulfate solution.

It can be also seen in Figure 4.104 that all solutions at 20°C showed no significant change in magnesium ion within 12 months of exposure, except for a slight drop at 12 months in sulfate only and SC5 solutions. This reflects the negligible interactions between magnesium ion with cement past in systems at 20°C, as was also confirmed by XRD.

In the early exposure period amount to the first 9 months, sulfate only solution specimens showed highest calcium and lowest sulfate concentrations. These changes were mainly related to relatively higher initial dissolution of CH and rapid ingress of sulfate in mortar samples placed in sulfate only solution compared with composite solution, in which the presence of chloride in sulfate solution at 20°C influenced sulfate ingress and as follows: 1) In the early exposure period, the higher chloride diffusion compared with sulfate resulted in the formation of Friedel's salt in mortar samples exposed to composite sulfate and chloride solutions. The formation of non-expansive product, Friedel's salt, would tend to block the pores and consequently reduce the amount of sulfate ingress. 2) At the latter stages, the presence of chloride in solution would result in elevating the pH of mortar pore solution which, in turn, would decrease the dissolution of portlandite.

Chloride concentration in composite solutions at 20°C are shown in Figure 4.105, from which it can be seen that the higher the chloride in sulfate solution, the higher its consumption by mortar specimens. This may reflect the higher chloride binding and lower sulfate interaction of cement mortars as chloride level increases in solution, as also indicated by XRD analyses described in Section 4.5.1.

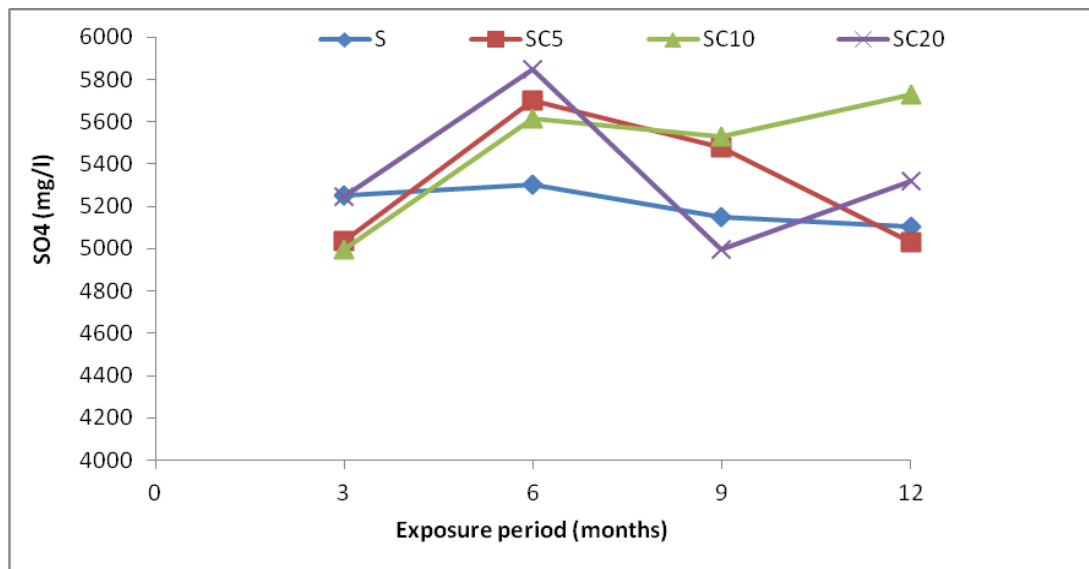


**Figure 4.102.** Variation of sulfate ion in test solutions at 20°C.

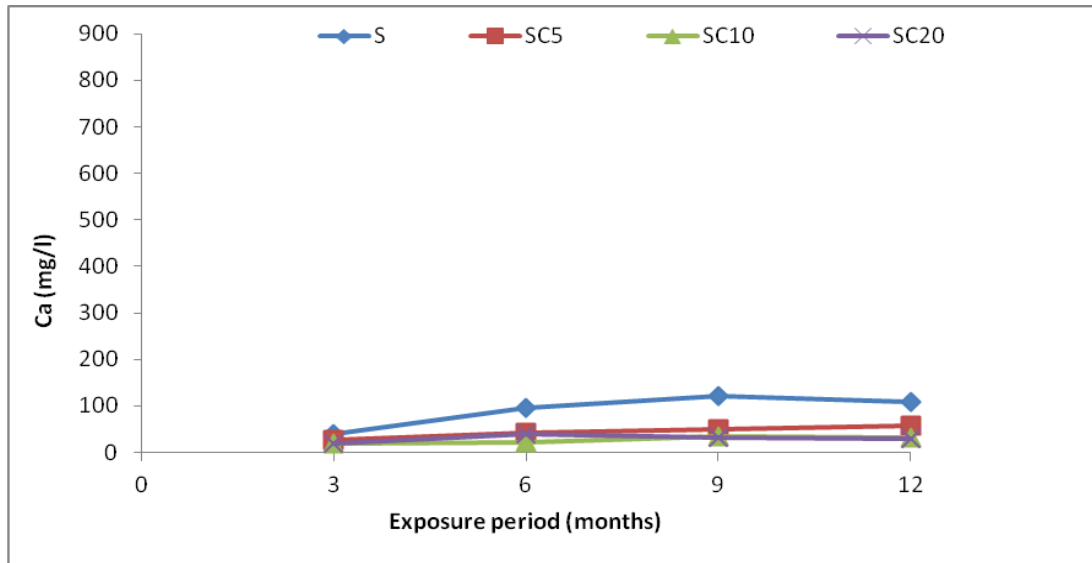


**Figure 4.103.** Variation of calcium ion in test solutions at 20°C.

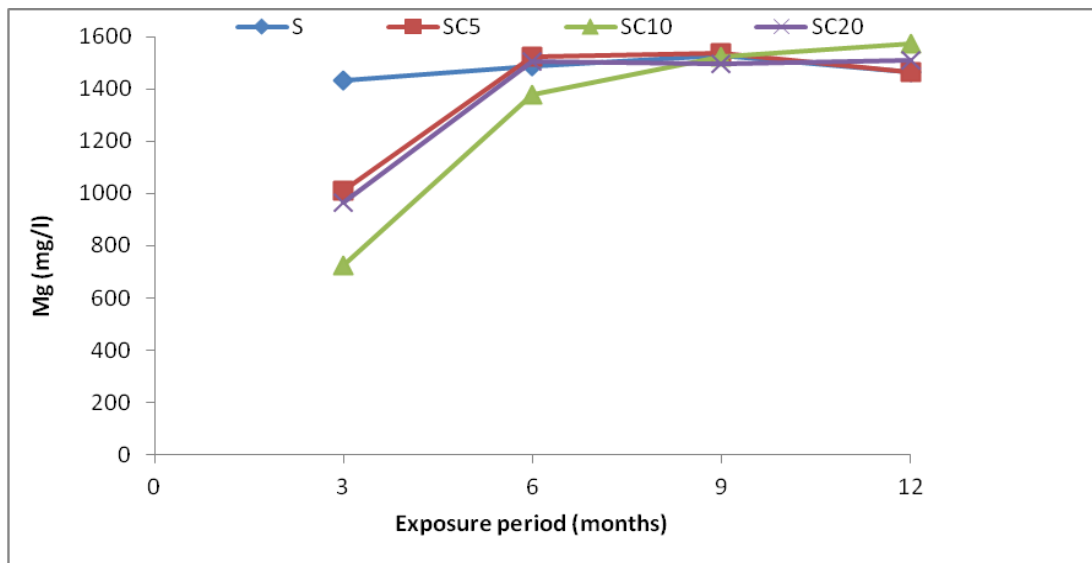


**Figure 4.104.** Variation in magnesium ion in test solutions at 20°C.

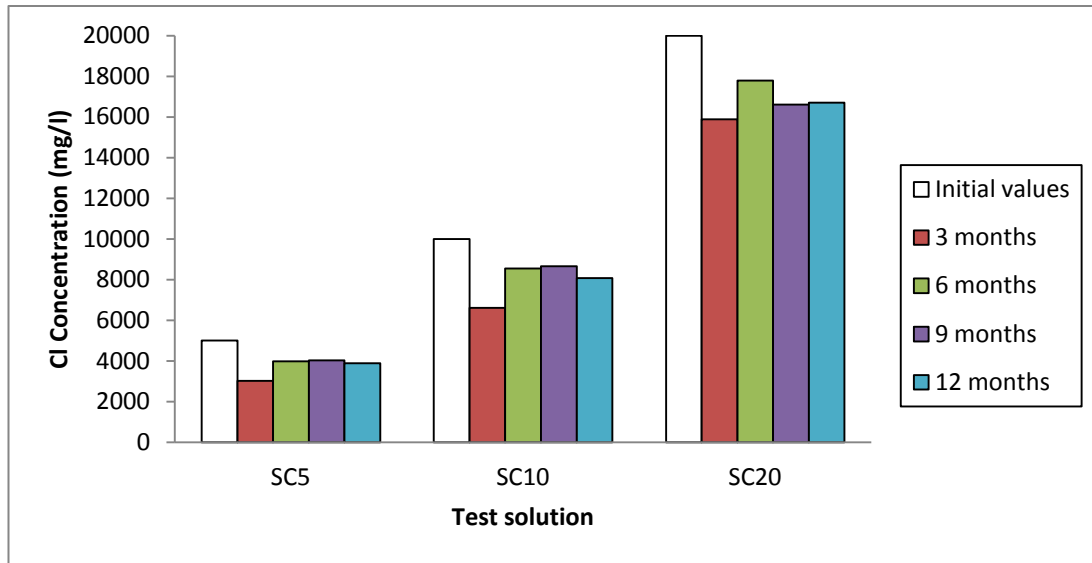


**Figure 4.105.** Variation of chloride concentration in test solutions at 20°C.

• **Chemical analysis of test solutions of 20mm mortar cubes:**

Table A. 3 and A.4 (See Appendix) summarise the ion levels in sulfate, chloride, magnesium and calcium of test solutions of 20mm mortar cubes made with different binders stored for 180 days at 5 and 20°C.

Since, as visually observed, CEMI-LF mortars stored at 5°C showed highest extent of damage, the chemical change with time was investigated in more details for test solutions containing CEMI-LF mortar samples.

**Test solutions for CEMI mortar at 5 and 20°C:**

Figure 4.106 shows concentrations of sulfate, calcium and magnesium ions in test solutions for CEMI mortar samples stored for 180 days at 5 and 20°C. At 5°C, all solutions showed significant drops in sulfate ions and increase in calcium ions. The drop in sulfate was most probably attributed to the formation of higher amounts of thaumasite and gypsum in these samples and also due to higher penetration of sulfate ions through deteriorated mortar, as visually observed.

At 20°C, Figure 4.106 records that the highest sulfate reduction, from 6000 to 4200 mg/l, was found in sulfate only solution, with no significant changes in magnesium and calcium in the 20°C test solution. The reduction in the amount of sulfate indicates higher sulfate interactions in these samples linked to the

formation of sulfate products. This also indicates that these mortars would be subjected to sulfate attack earlier than others.

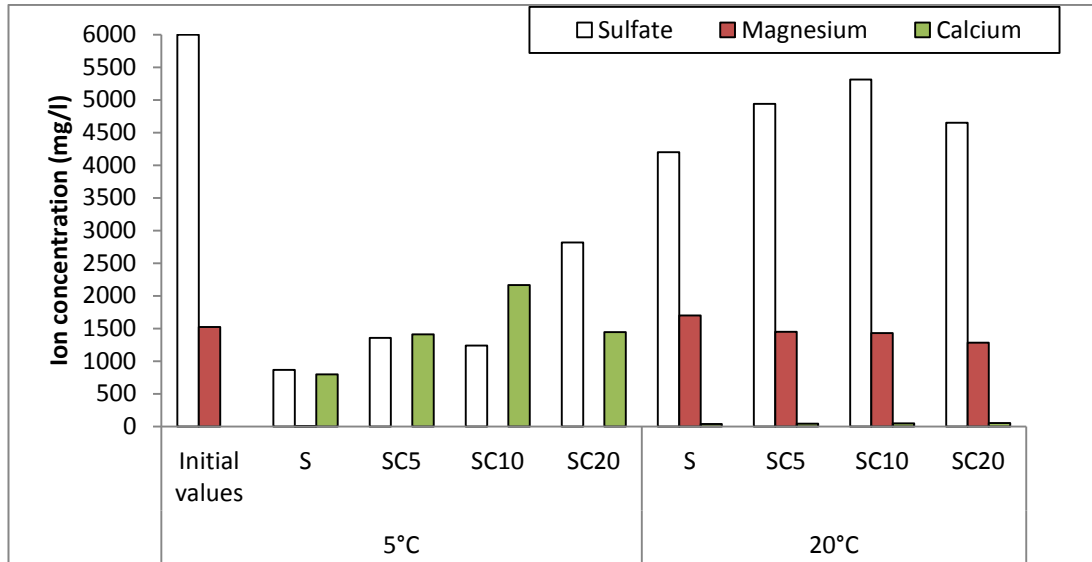


**Figure 4.106.** Concentration of sulfate, magnesium and calcium in CEMI solutions after 180 days at 5 and 20°C.

***Test solutions for CEMI-LF mortar at 5 and 20°C:***

Variations of sulfate, calcium and magnesium ions in test solutions for CEMI-LF mortar samples stored for 180 days at 5 and 20°C are shown in Figure 4.108 to 4.110.

At 5°C and as can be seen in Figure 4.107, that during the first 28 days of exposure, the higher the chloride level present in sulfate solution, the higher the calcium release. On the other hand SC20 solution showed the highest value of around 400 mg/l at 28 days exposure. This release in calcium was mainly associated with initial dissolution of portlandite, which in turn led to increase the initial pH (Section 4.8) of test solutions. At 56 days, all solutions showed reduction in calcium which could be related to its reaction with dissolved carbon dioxide derived from the atmosphere. As time passed and before solution replenishment, S and SC5 solutions showed higher calcium release compared with SC10 and SC20 solutions but this may be due to rapid propagation of microcracks in these mortars such that more lime was exposed to the solution.

After replenishment, all solutions showed significant increase in calcium concentration which indicates that more lime exposed to test solutions due to higher amount of propagated cracks, as visually observed. After 180 days of storage, a significant drop in sulfate and magnesium as Figure 4.108 and 4.109 reveal, followed by release of calcium was found in all test solutions stored at 5°C. The lowest drop in sulfate was found in SC20 solutions, indicating lower sulfate where bound in an insoluble compounds.

At 20°C, however, no remarkable release in calcium and reduction in sulfate and magnesium concentrations were found in all solutions (Figure 4.110). The concentration amounts were approximately equal in all test solutions at 20°C. It can be also noted that the higher the chloride in solution, the lower the reduction in sulfate. Mortar samples stored in all solutions at 20°C remained intact at this age of exposure. However, mortars stored at 20°C could be subjected to sulfate attack after a longer exposure period, as cement hydration products are not stable in the presence of sulfate and magnesium ions.

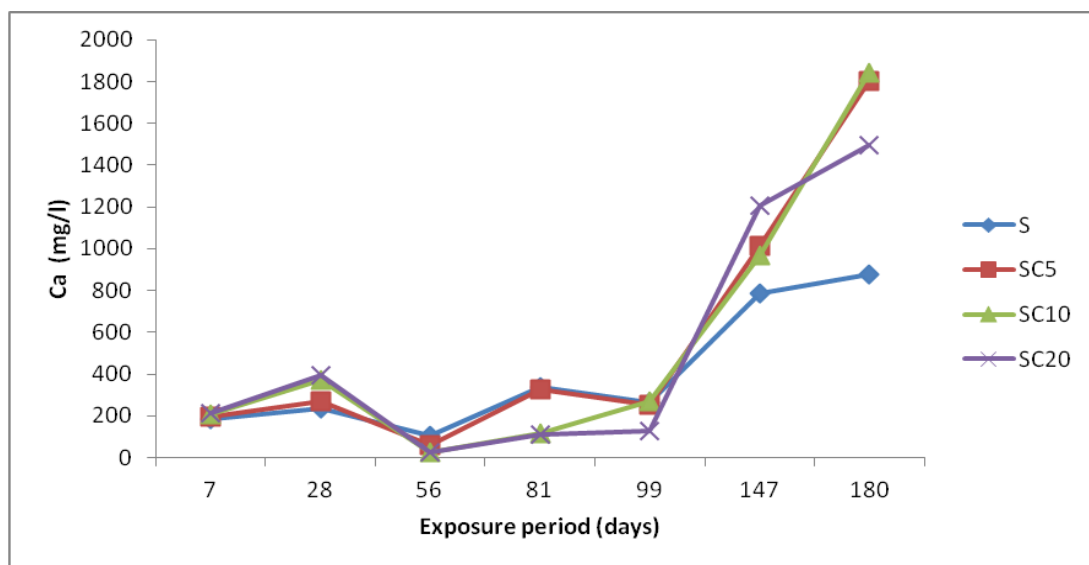


**Figure 4.107.** Variation of calcium level in CEMI-LF solutions stored 180 days at 5°C.

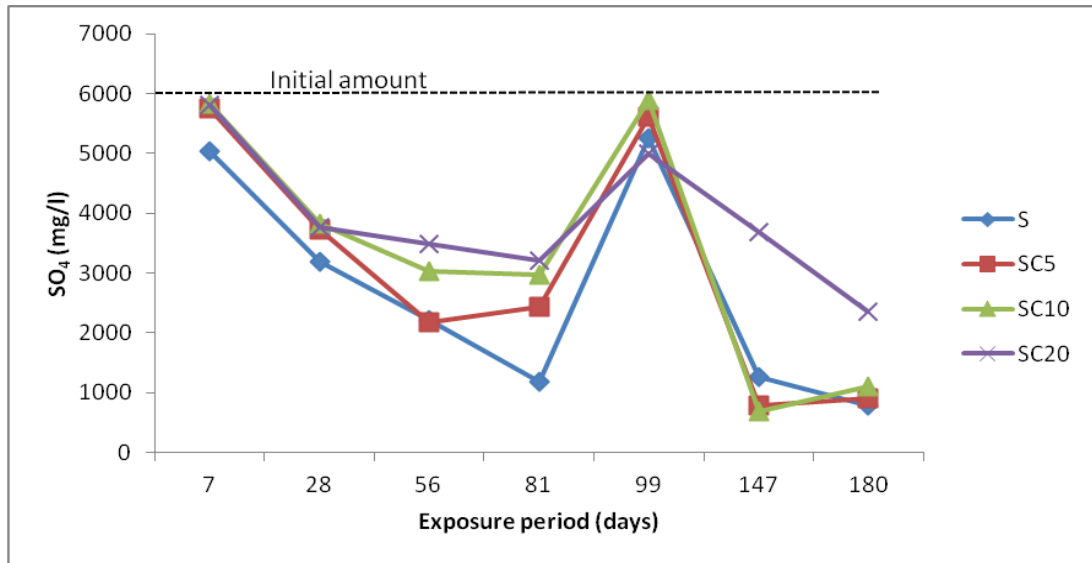


**Figure 4.108.** Variation of sulfate level in CEMI-LF solutions stored for 180 days at 5°C.

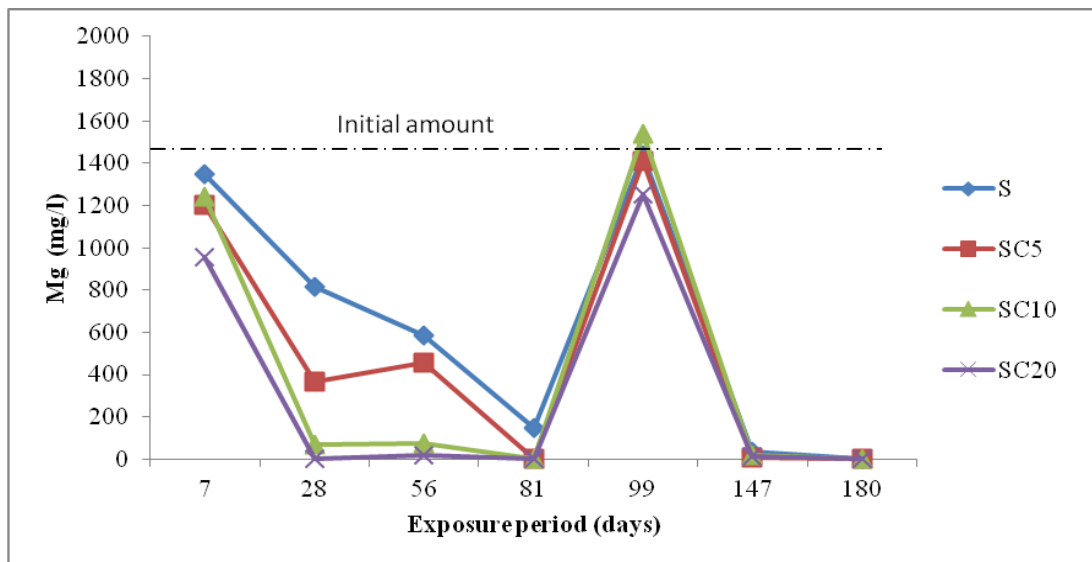


**Figure 4.109.** Variation of magnesium level of CEMI-LF solutions stored 180 days at 5°C.

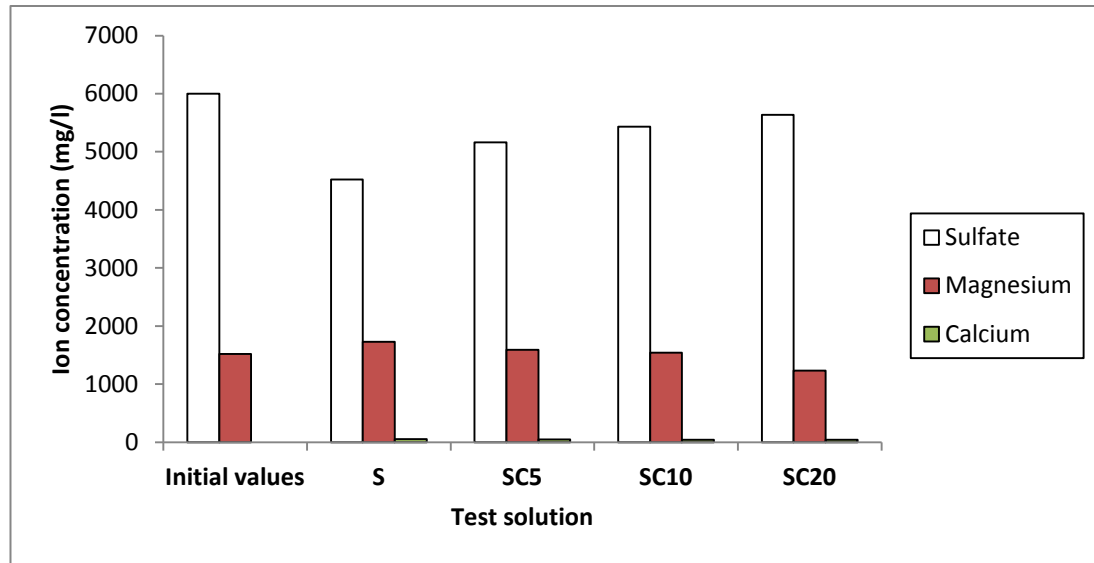


**Figure 4.110.** Concentration of sulfate, magnesium and calcium ions in CEMI-LF solutions stored 180 days at 20°C.

**Test solutions for CEMI-GGBS mortar at 5 and 20°C:**

The variation of ion concentrations for sulfate, magnesium and calcium of test solutions for CEMI-GGBS mortar samples stored for 180 days at 5 and 20°C are shown in Figure 4.111 and 4.112, respectively. It can be seen that sulfates remained at an almost constant level in SC20 solution at both temperatures after 180 days. However, sulfate only and SC5 solutions showed the lowest sulfate level at 5°C. This indicated that higher sulfate products formed or higher sulfate ingress in these mortars. Both surface samples showed significant amount of gypsum deposition, as indicated by the XRD and SEM/EDX results in Sections 4.5.1 and 5.6.

Sulfate only and SC5 solutions showed also high reduction in concentration of magnesium compared with SC20 at 5°C. This was expected due to higher interaction and ingress as these mortars showed damage at this stage of exposure.

As found by SEM/EDX in Section 4.6, magnesium can replace calcium in C-S-H gel to form solid solutions of M-C-S-H, increasing the amount of calcium ions and silica gel in the pore solution. The availability of high concentrations of calcium and sulfate ion would promote the formation of gypsum. At 20°C, a noticeable reduction in magnesium and an increase in calcium concentration were also observed, as shown in Figure 4.112. This may indicate a similar scenario occurred for mortars stored at 20°C, in which the replacement



between Mg and Ca ions occurred due to the attack of C-S-H by magnesium. Since gypsum solubility is higher at higher temperature, the damage due to gypsum formation of mortar stored at 20°C would be expected to take a longer time. Higher concentration of calcium, occurred for composite sulfate and chloride solutions, compared with sulfate only solutions at both temperatures.

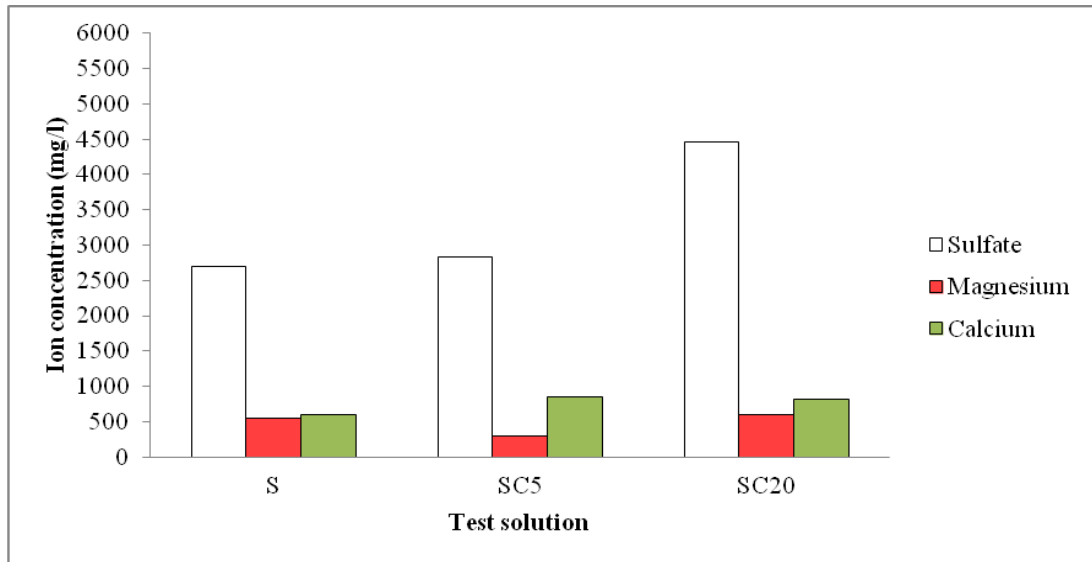


**Figure 4.111.** Variation of sulfate, magnesium and calcium ions in CEMI-GGBS solutions after 180 days at 5°C.

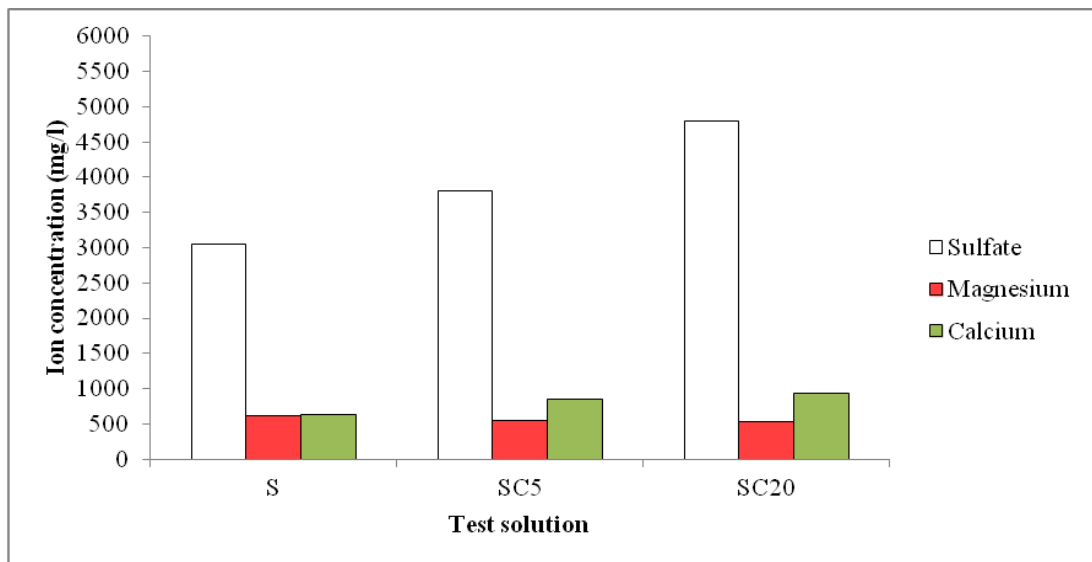


**Figure 4.112.** Variation of sulfate, magnesium and calcium ions in CEMI-GGBS solutions after 180 days at 20°C.

**Test solutions for CEMI-PFA mortar at 5 and 20°C:**

Figure 4.113 and 4.114 show the variation of ion concentrations of sulfate, magnesium and calcium of test solutions for CEMI-PFA mortar samples stored for 180 days at 5 and 20°C, respectively. Sulfate only solution at 5°C showed a clear reduction in the amount of sulfate and magnesium followed by increase in calcium level compared with composite solutions, which showed no significant change in the level of sulfate, magnesium ions and no noticeable release in calcium. This implied higher sulfate and magnesium interactions of mortar samples stored in sulfate only solution, which confirmed visually determined (Section 4.2, Figure 4.5) and XRD analysis results (Section 4.5.1).

As mentioned earlier, the replacement of calcium in C-S-H gel by magnesium would result in increasing the concentration of calcium ions in the pore solution, and with of high amount of sulfate ions in solution would promote gypsum formation. However, at 20°C, no significant variations in ion concentrations were found after 180 days of exposure to all solutions, as shown in Figure 4.114.

According to the results obtained, it is clear that the availability of chlorides in sulfate solution benefited CEMI-PFA mortar samples resistance against sulfate attack at this stage of immersion, particularly at 5°C. This could be related to the higher diffusion rate of chloride ions compared with sulfate ions that would result in rapid interaction with aluminates phases and consequently reduce sulfate interaction, as discussed previously.

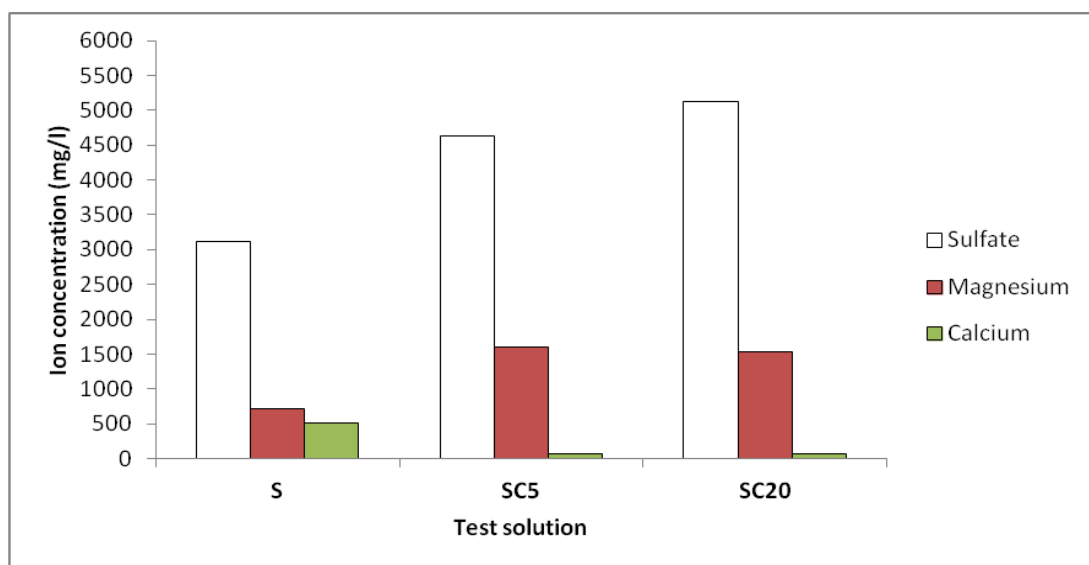


**Figure 4.113.** Variation of sulfate, magnesium and calcium ions in CEMI-PFA solutions after 180 days at 5°C.

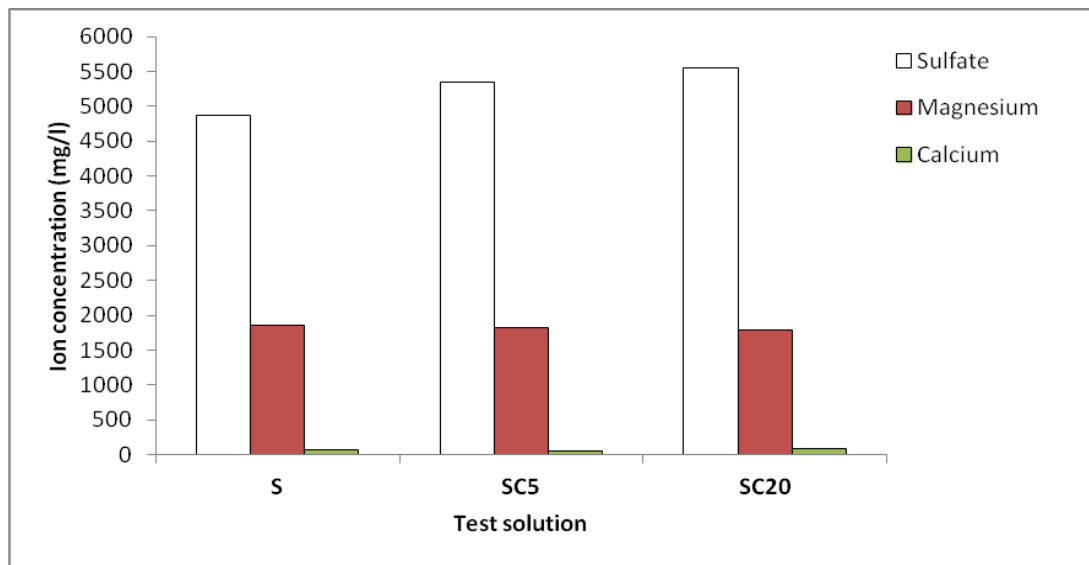


**Figure 4.114.** Variations of sulfate, magnesium and calcium ions in CEMI-PFA solutions after 180 days at 20°C.

#### 4.8 pH measurement of test solutions:

In this section, the pH of test solutions for the 20 mm mortar cubes made with different binders stored for 180 days at 5 and 20°C are presented and discussed.

##### ***pH of CEMI-LF samples at 5 and 20°C:***

Figure 4.115 and 4.116 show the pH variation in CEMI-LF samples placed in water and test solutions at 5 and 20°C, respectively. After immersion, it can be seen that all solutions showed sharp increases in the pH, which was associated to leaching of alkalis from outer parts of cement mortars.

The pH value of samples placed in water rapidly reached its maximum, of about 12.3, and gradually decreased towards 8.5 through the time of the experiment at both temperatures. Because the pH became almost stable at around 9.0, it is most likely that initial dissolution of calcium hydroxide was followed by the precipitation of calcium carbonate.

The pH of test solution showed a significant dependency on temperature and chloride level in solution. It can be noticed that the pH of all test solutions stored at 5°C were mostly higher than 10.5. At later ages, all test solutions were alkaline with pH higher than 11.0. However, at 20°C and after replenishment, all solutions showed a pH value lower than 10.0.

In case of sulfate only solution and before replenishment, it can be seen that the pH value almost stabilized at around 10.5. After replenishment, the pH increased sharply from a value of around 7.0 to reach 10.0 at 7 days and then it slightly increased to 10.5 at 137 days. Sulfate only solution showed continued increase in the pH and reached highest value of 11.5 at 180 days of immersion. It is postulated that the increased value in the pH was due to more lime being leached into the solution as a result of higher extent of deterioration as time progressed, as visually observed in Section 4.2. The chemical analysis shown in Section 4.7 of this test solution showed an increase in the amount of calcium ions, mainly attributed to leaching of calcium hydroxide.

When 0.5% chloride was present in the sulfate solution (SC5), the solution maintained a pH value around 10.6 during the 49 days of immersion and then showed sudden increase to reach a highest value of 12.1 at 88 days of immersion. This sudden increase in the pH value may suggest incidence of more damage and more lime leached into the solution. It should be mentioned that SC5 mortar samples showed the earliest and the highest extent of attack, as visually observed (Section 4.2) and as indicated by chemical analysis (Section 4.7). After replenishment, again SC5 solution showed an increase in the pH value, and reached a maximum of 12.5 at 147 days of immersion. Such an increase in the pH value could be related to further degradation at the surface of the samples either by propagation of more cracks or surface deterioration, or both. This was observed at low temperature but not at 20°C at this age.

The composite sulfate and 1.0% chloride (SC10) solution also showed an increase in pH value, which reached 12.2 at 35 days exposure. The pH fell to 11.0 at 56 days, and then rose to reach 12.1 at 88 days. The pH value remained above 10.5 during the early exposure period. After replenishment, also SC10 solution showed an increase in the pH value as time passed, to reach a value of 12.1 at 180 days of immersion. This increase in pH value also indicated increase in the extent of damage with time.

In case of SC20, the solution showed slight increase in the pH value from 10.5 at 7 days to 10.8 at 21 days followed by a sharp rise in the pH value from 10.8 at 21 days to 12.2 at 35 days. After that the pH remained almost stable at about 12.2 until the solution was replenished at 90 days. Such a rapid increase in the pH could be associated with a higher rate of initial dissolution of portlandite into SC20 solution, as will be discussed in Chapter 6. During this immersion

period, SC20 mortars did not show any signs of visual damage. After replenishment, again this solution showed sharp increase in the pH to about 10.3 between 99 to 137 days of immersion and reached a high value of 11.8 at 180 days. Again, such an increase in the pH value could be related to damage that occurred at the surface of the samples which resulted in more lime becoming exposed to test solution, as visually observed.

At 20°C, all solutions showed an increase in pH, but generally with lower values than at 5°C, which was probably due to decreased portlandite dissolution. However, no significant changes in pH were observed in any 20°C test solutions after replenishment and they mainly remained in the range of between 9 and 10. This indicates a lack of significant interactions between cement paste and the test solution. As mentioned in Section 4.2, visually, none of the mortar specimens stored at 20°C showed damage during the 180 days exposure period.

With respect to the formation of thaumasite, Gaze and Crammond (2000) reported that thaumasite forms only in an alkaline environment with pH above 10.5, and the results of the current study appear to agree with this. Further dissection is given in Chapter 6, regarding the role of the pH of composite sulfate and chloride solutions on thaumasite formation.

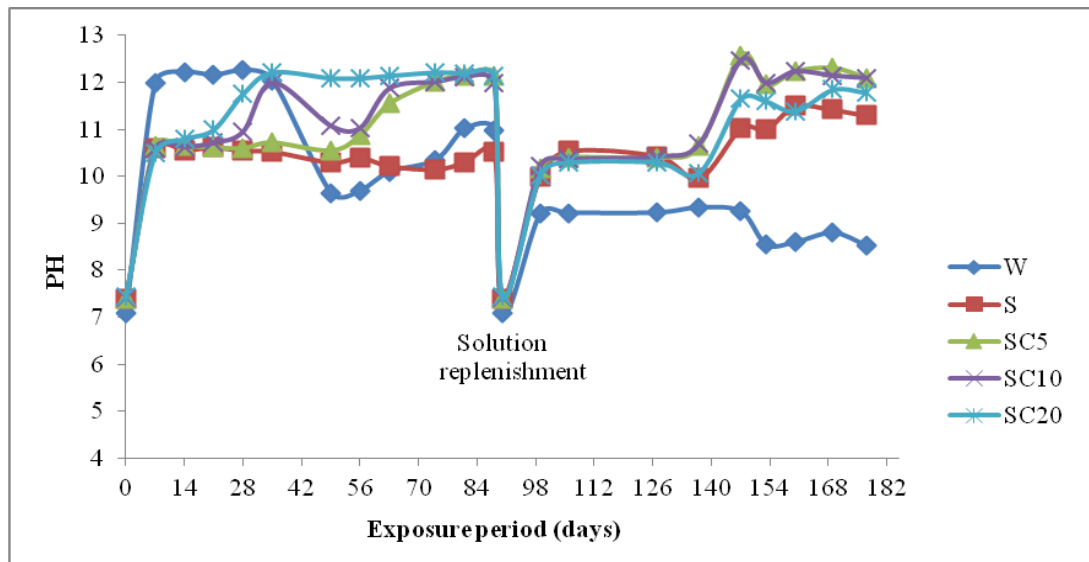


**Figure 4.115.** pH change in CEMI-LF stored for 180 days at 5°C.

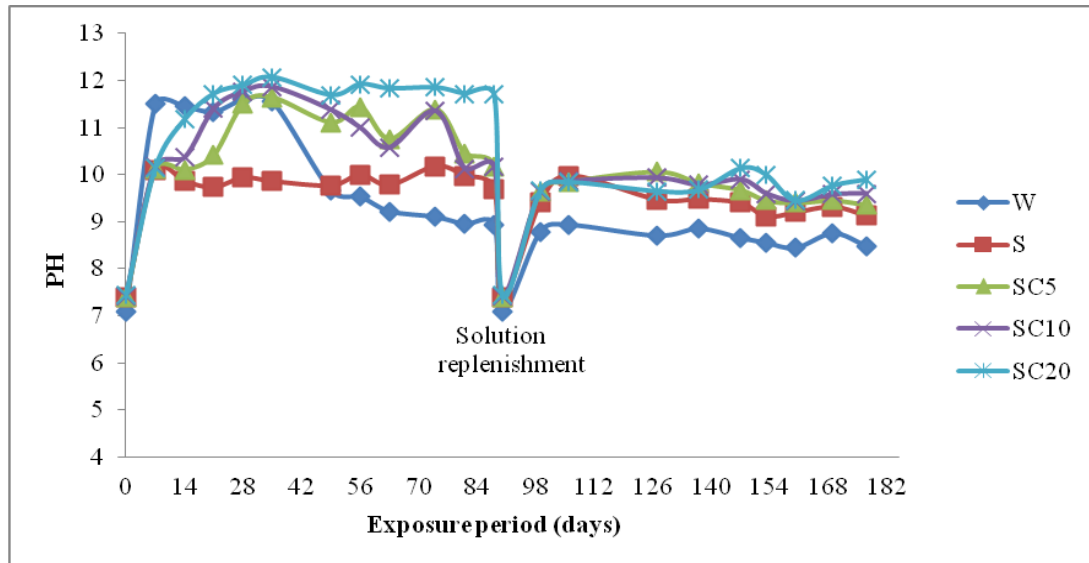


**Figure 4.116.** pH change in CEMI-LF stored for 180 days at 20°C.

**pH of CEMI-GGBS samples at 5 and 20°C:**

The pH profiles of CEMI-GGBS solutions at 5 and 20°C are given in Figure 4.117 and 4.118, respectively. The consumption of calcium hydroxide during surface carbonation and pozzolanic reactions resulted in maintaining a low pH value in all CEMI-GGBS solutions. This was more obvious after solution replenishment as this was after most of the alkalis in the outer layer of mortar specimens had been leached into the solutions.

It can be observed that the pH of test solutions depended on chloride concentrations and temperature. At 5°C and before the solutions were replenished, the sulfate only and SC5 solutions showed a gradual increase in the pH, where the former solution increased least, from a value of 10.0 at 7 days to about 10.8 at 74 days, while the maximum for SC5 solution was 11.6 at 74 days. The gradual increase in pH of these solutions may be related to increase in released alkalis into solutions as more sulfate diffused into the inner parts of the samples in contrast to SC20 solution in which a sharp rise in the pH from around 10.0 at 21 days to 11.5 at 35 days of immersion occurred. This was followed by a slight decrease in value. This decrease up to 35 days of immersion may be attributed to rapid interactions of chloride with cement paste in which Friedel's salt initially formed and blocked the pores which reduced sulfate and chloride penetration into the mortar. The greater pH increase in the composite solution also related to the interaction of sodium chloride, as mentioned above.

At 20°C, the initial immersion period resulted in increases in pH of all solutions up to 35 days of exposure, with higher values for composite solutions. After that there was a noticeable drop, which was not the case for the 5°C tests. This reduction in pH at higher temperature may be related to the decrease in the dissolution of lime.

After replenishment, the pH of test solutions for both temperatures dropped below the threshold pH value (10.5) for thaumasite formation, with lower values for the systems at 20°C, however, the pH remained low enough for the decalcification of C-S-H and the promotion of gypsum and as a result of most alkalis washed out into the solution.

The slight increase of pH at 5°C with time may indicate that the inner part of the mortar samples was becoming exposed to the solution. Within this stage of immersion, as recorded in Section 4.2, visual damage was only observed in SC5 samples. However, at 20°C and after replenishment, the pH of all solutions remained almost constantly at a value lower than 9.0 which would favour the stability of calcium carbonate. Mortars stored in all solutions remained intact and no marks of damage were observed.

It should be mentioned that the open microstructure, due to the high water to cement ratio used, prompted rapid interactions between sulfate, magnesium and chloride ions and the cement matrix. The use of high water to binder ratio would have produced a mortar of relatively high permeability and because compared to standard cement, CEMI blended with GGBS would undergo slow initial hydration, it was expected that pH would increase during the first 90 days of exposure of CEMI-GGBS mortars.

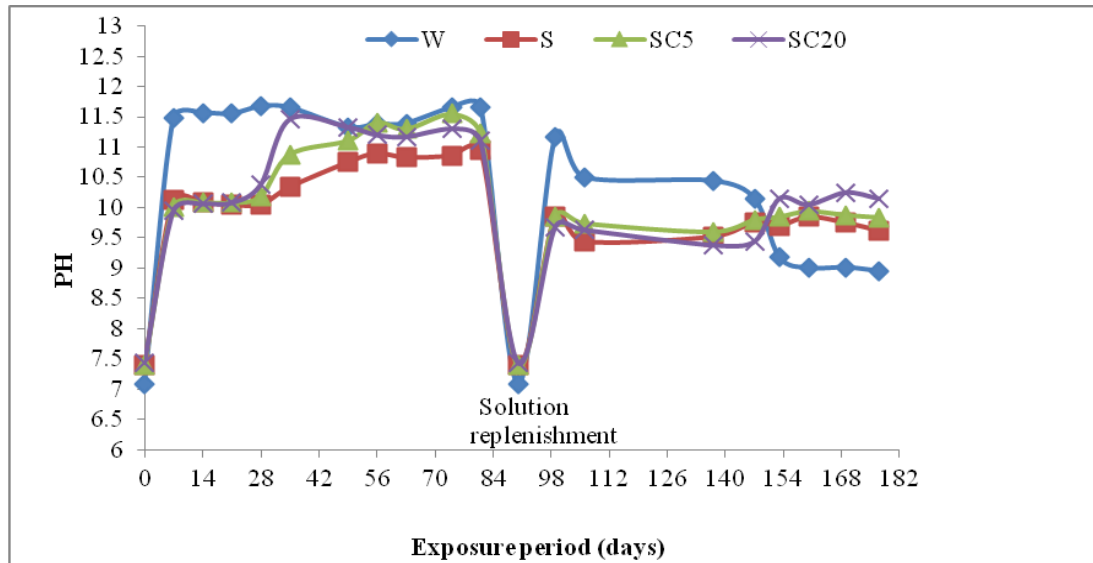


**Figure 4.117.** pH change in CEMI-GGBS solutions stored for 180 days at 5°C.

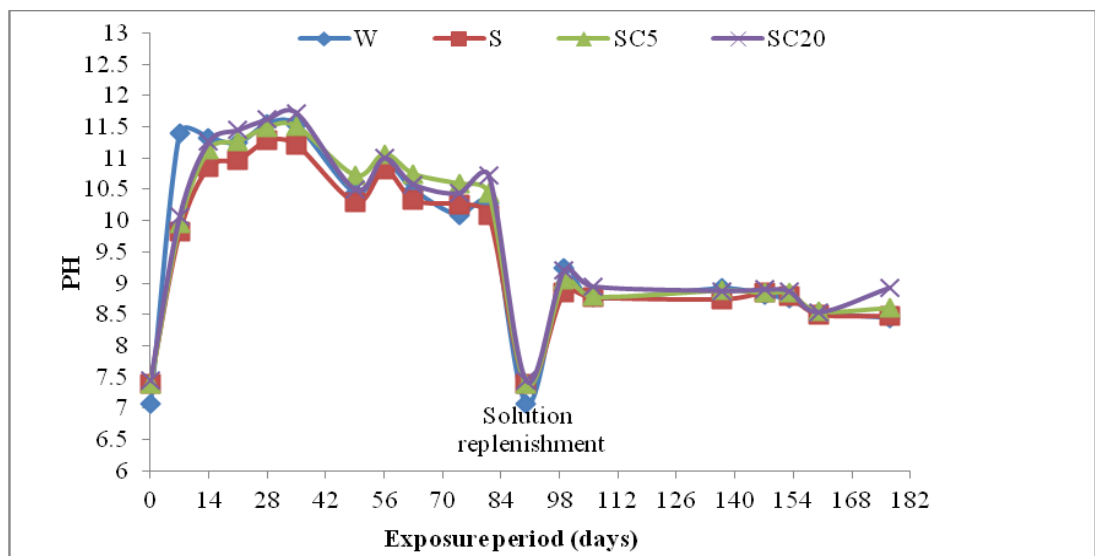


**Figure 4.118.** pH change of CEMI-GGBS solutions stored for 180 days at 20°C.

**pH of CEMI-PFA samples at 5 and 20°C:**

The pH variations of CEMI-PFA solutions at 5 and 20°C are shown in Figure 4.119 and 4.120, where in Section 4.2 damage was reported to these specimens stored for 180 days in sulfate only solution. On the other hand, samples placed in composite sulfate and chloride solutions remained intact and no such damage was observed within this period of immersion.

The pH of test solutions showed dependency on chloride level and storage temperature, in that the composite solutions showed higher pH values than



sulfate only solutions. SC20 showed the highest increase of pH value to 11.9 at 56 days of immersion, where as in SC5 the value was 11.6 at 74 days and in sulfate only solution there was no such increase in pH, but instead it remained at around 10.3 during the 90 days of immersion. This was probably due to formation of magnesium hydroxide which consumed part of the hydroxyl ions.

As the pozzolanic reaction between PFA and portlandite during cement hydration would result in less calcium hydroxide being available in the system, it would take longer to compensate the reduction of pH at early stage of exposure.

After replenishment when most of available alkalis on mortar surfaces had already leached into the solutions, the pH of all solutions fell in value. In the 20°C systems it attained an almost constant value at around 9.5, while at 5°C, the value was around 10.0. At such low pH values, the C-S-H would be subjected to decalcification which would promote gypsum formation in presence of high level of sulfate.

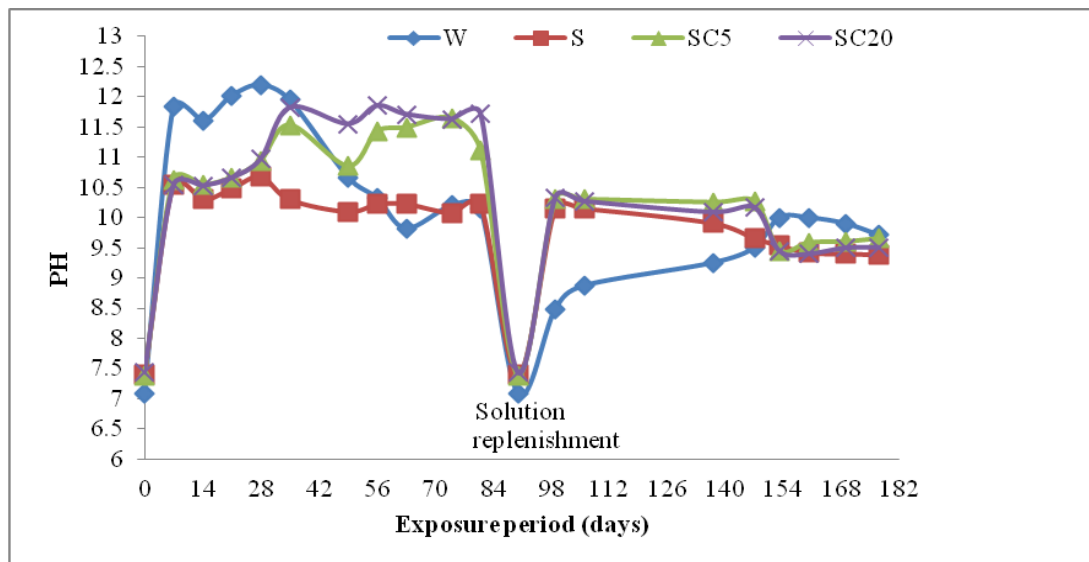
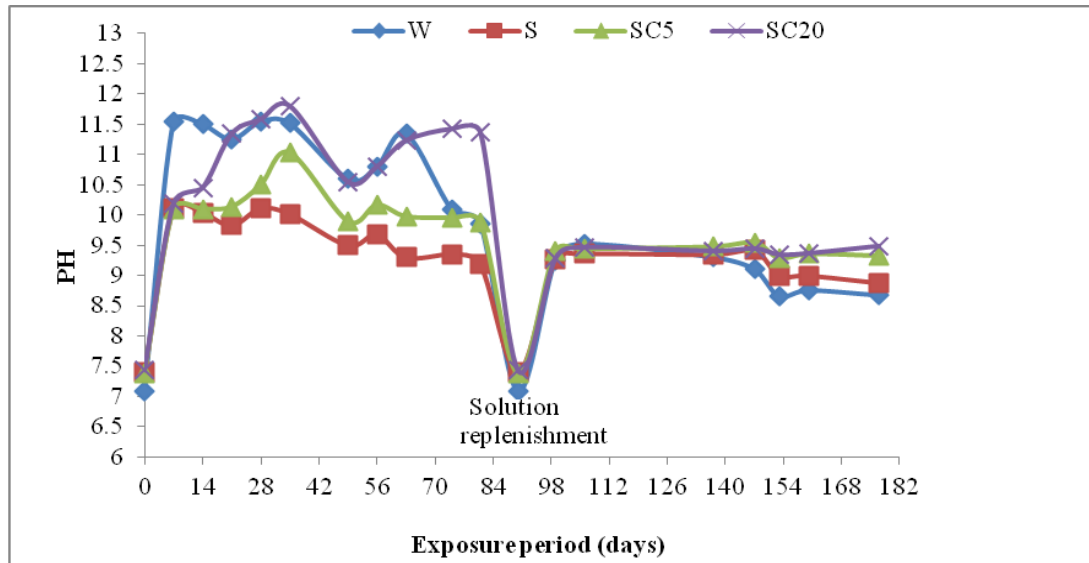


Figure 4.119. pH change in CEMI-PFA solutions stored for 180 days at 5°C.



**Figure 4.120.** pH change of CEMI-PFA solutions stored for 180 days at 20°C.

#### 4.9 The effect of chloride concentration on solubility of calcite and gypsum

The results of solubility of calcite and gypsum are presented in this section. Figure 4.121 shows the saturation level of calcium ions of  $\text{CaCO}_3\text{-NaCl-MgSO}_4\text{-H}_2\text{O-CO}_2$  and  $\text{CaSO}_4\text{-NaCl-MgSO}_4\text{-H}_2\text{O-CO}_2$  schemes at 5°C from which the affects of chloride concentration on the solubility of both calcite and gypsum are very clear. Furthermore, the solubility of calcite decreased as chloride concentration increased in that 0.5% chloride resulted in higher calcite solubility than 2.0% chloride did. In the tests calcium concentration reached 204 mg/l for SC5 compared with 32 mg/l for SC20.

The solubility of gypsum increased as chloride concentration increased where the solution made with 2.0% chloride showed higher gypsum solubility, in which the calcium concentration reached 283 mg/l compared with 127 mg/l for SC5.

Higher carbonate availability would raise the potential for thaumasite formation Irassar (2009a). An investigation by Duan and Li (2008) demonstrated that calcite solubility increased as chloride concentration increased up to certain amount and then decreased. In this study, in which sulfate was also present, Figure 4.121 indicates that calcite has higher solubility in combined sulfate and 0.5% chloride solution than solution containing combined sulfate and 2.0% chloride.

Visual assessment (Section 4.2) and mass loss (Section 4.3) showed that the extent of attack due to thaumasite formation depended on chloride concentration in solution, in which limestone mortar stored in SC5 showed greatest damage compared to those stored in SC10 and SC20 chloride. This behaviour corresponds with the calcite solubility tests, in which a higher calcium and carbonate release occurred for a low chloride concentration (SC5), compared to that of SC20. It seems that this is a significant factor affecting thaumasite formation, which is enhanced by the presence of calcium and carbonate ions in the pore solution.

Moreover, it can be also seen (Figure 4.121) that as the chloride level increases in sulfate solutions, the solubility of gypsum increases. This is also in agreement with the findings of XRD (Section 4.5.1), in which the intensity of gypsum decreased as the chloride increases in solution. Thaumasite formation considered to be a slow process compared to gypsum and ettringite formation and is the last phase formed in sulfate attack, and it may require gypsum or ettringite to initially be formed, as previously reported by Ramezani pour and Hooton,(2013).

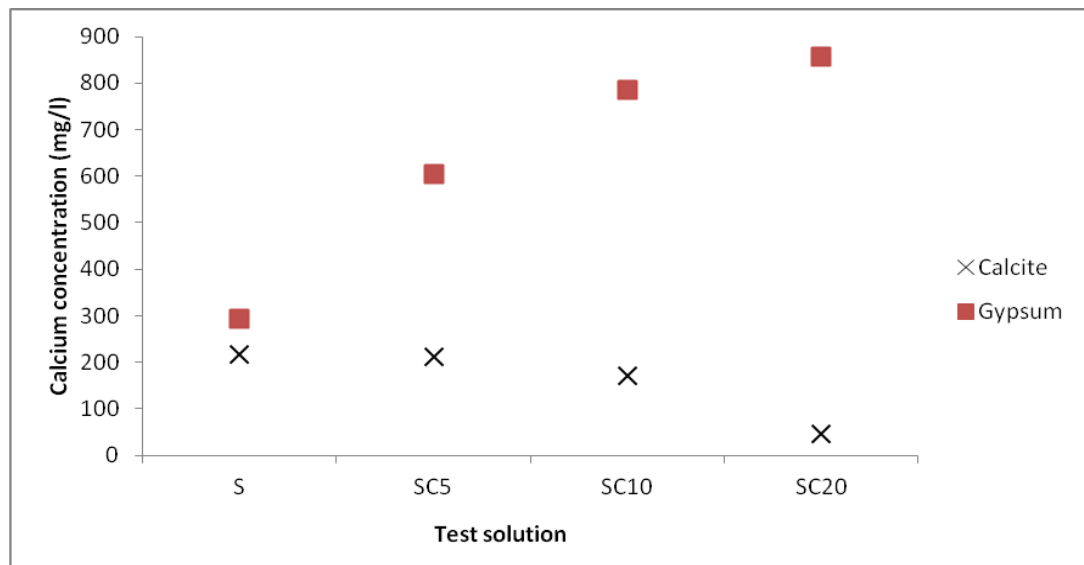


**Figure 4.121.** Calcium ion levels of  $\text{CaCO}_3\text{-NaCl-MgSO}_4\text{-H}_2\text{O-CO}_2$  and  $\text{CaSO}_4\text{-NaCl-MgSO}_4\text{-H}_2\text{O-CO}_2$  schemes at 5°C.

## 4.10 Summary

The main findings of these investigations into the performance of CEMI, CEMI blended with 10%LF, CEMI blended with 50%PFA and CEMI blended with 70%GGBS mortar specimens subjected to combined action of sulfate and chloride in terms of thaumasite form of sulfate attack at 5 and 20°C are presented in this section.

Most available research reported in the literature concerns the investigation of the effect of chloride on sulfate attack at 20°C, in which ettringite would be the main deterioration product. Furthermore, an extensive literature search identified very few available studies into the effect of chloride on sulfate attack at low temperatures and under conditions conducive to thaumasite formation. Even then the results were conflicting, with some studies indicating mitigation of attack and others enhancement of attack. This is probably due to the complexity of the chemical interactions at various concentrations.

In addition, the use of mineral admixtures such as PFA and GGBS are reportedly effective in preventing TSA at 5°C; however, the presence of chloride alongside sulfate at low temperature was found to have a negative effect on the performance of concrete made with these components. Accordingly, the performance of mortar specimens made with different binders subjected to sulfate and chloride at 5 and 20°C was evaluated in terms of visual observation, mass change, length change, monitoring of pH and chemistry of test solutions and mineralogy of deteriorated materials.

The experimental results obtained from this study indicate that the presence of chloride and its concentration have a significant impact on the performance of mortar in sulfate exposure in such conditions. The following findings can be drawn from the results:

- Early evidence of damage due to TSA were observed in CEMI and CEMI blended with 10%LF mortar samples exposed to DS4, composite DS4 and 0.5% chloride and composite DS4 and 1.0% chloride solutions stored at 5°C. Deterioration in the form of cracking and deposition of white materials appeared only after 100 days of storage in these solutions where CEMI blended with 10%LF experienced three times greater deterioration than CEMI mortar, as determined by mass loss shown in Figure 4.11 and 4.12.

- After 360 days exposure, both CEMI and CEMI blended with 10%LF mortar specimens exposed to sulfate only (S), composite sulfate and 0.5% chloride (SC5) and composite sulfate and 1.0% chloride (SC10) solutions at 5°C showed clear evidence of thaumasite attack, whereas no sign of deterioration occurred in specimens exposed to composite sulfate and 2.0 chloride (SC20) solutions. Samples exposed to combined sulfate and 0.5% chloride (SC5) solution stored at 5°C showed the largest deposit of thaumasite on the outer layer of the specimens (Figure 4.7).
- At 630 days of exposure CEMI blended with 10%LF mortar samples suffered from extensive thaumasite attack at 5°C with greater damage to samples in combined sulfate and 0.5% chloride (SC5) compared to sulfate only solution. It is probable that the effect of chloride on extent of attack became more evident as temperature decreased because of enhanced TSA at 5°C. As shown in Figure 4.10, extensive deterioration was accompanied by loss of edges and corners with large amounts of mushy materials around the samples and in the bottom of containers.
- XRD (Figure 4.21), IRS (Figure 4.34) and SEM/EDX (Figure 4.51) confirm that the deterioration observed in CEMI and CEMI blended with 10%LF specimens stored at 5°C, with or without chloride presence, was due to thaumasite or thaumasite-ettringite solid solution formation.
- At 20°C and after 630 days of exposure, SEM/EDX assessment (Figure 4.70 and Figure 4.72) of CEMI blended with 10%LF mortars in sulfate only and combined sulfate and 0.5% chloride (SC5) solutions showed the attack was due to thaumasite formation.
- Assessment by mass loss indicated that CEMI and CEMI blended with 10%LF mortar specimens stored in composite sulfate and 0.5% chloride (SC5) at 5°C had the greatest deterioration degree due to thaumasite and secondary gypsum formation. This depends on carbonate content and chloride level in sulfate solution. The sequence of degradation degree of both CEMI and CEMI blended with 10%LF mortar stored in different solutions at 5°C was as following with relatively higher deterioration degree in case of CEMI blended with 10%LF mortars (Figure 4.11 and 4.12): Combined sulfate and 0.5% chloride (SC5) > Sulfate only (S) > Combined sulfate and 1.0% chloride (SC10) > Combined sulfate and 2.0% chloride (SC20). At 20°C, although, CEMI blended with 10%LF mortars stored in SC5 showed cracks

on mortar surface, no mass loss was found in case of mortars stored in any solutions at 20°C.

- Evaluation by length change at 5°C (Figure 4.19) indicates that the extensive formation of thaumasite in the outer layers of CEMI and CEMI blended with 10%LF mortar stored in composite sulfate and 0.5% chloride does not contribute to any significant length change of mortar bars.
- At 5°C, the pH (Figure 4.115) measurement of CEMI blended with 10%LF samples showed that pH generally remained above the threshold required for stability of thaumasite (pH=10.5) and before any mark of attack was observed. For samples stored in composite sulfate and 0.5% chloride solution, pH increased gradually after 56 days of immersion corresponding to rapid attack on these samples which then resulted in greater damage and more of the inner parts of samples being exposed to sulfate solution. However, the high pH of solution made with 2.0% chloride due to higher initial CH dissolution may have protected the samples from sulfate attack.
- The absence or low chloride peaks in thaumasite structure (Figure 4.53) indicate its catalytic role on thaumasite formation.
- Chloride binding capacity of the cement matrix is reduced within the degraded materials where thaumasite was the dominate sulfate phase (Figure 4.51). The consequence of the reduction in chloride binding capacity of limestone cement mortars due to thaumasite formation will be subjected to further discussion in Chapter 5.
- The chemical analysis of test solutions (Figure 4.98 to 4.100) further confirmed the highest extent of damage to the outer layers of CEMI and CEMI blended with 10%LF specimens stored in composite sulfate and 0.5% chloride (SC5) at 5°C. This solution showed the largest release in calcium and highest reduction in sulfate and magnesium concentrations.
- Superior performance against sulfate attack was found where cement mortars incorporated 50%PFA in that no visual damage was observed in any samples after 630 days in any test solutions at both temperatures (Figure 4.9). However, the SEM/EDX analysis (Figure 4.77) showed small traces of thaumasite were formed in PFA mortars at 5°C, which suggests that with time TSA will occur.

- The presence of 0.5% or 2.0% chloride in DS4 sulfate solution led to a further improvement in the performance of PFA mortar samples against sulfate attack (Figure 4.31). This may be attributed to the high aluminates contents in its composition. This resulted in high chloride binding in form of Friedel's salt that blocked the pores and reduced the opportunity for interaction between aluminates and sulfate ions. This seemed not to be the case when chloride was present in GGBS mortars, placed in DS4 solution as indicated by XRD (Figure 4.32) and SEM/EDX (Figure 4.95).
- CEMI blended with 70% GGBS mortar samples showed also good performance against sulfate attack, as they did not show any visual damage within 630 days of exposure to any test solutions at both temperatures (Figure 4.9). However, the XRD and SEM/EDX analysis of mortar samples placed in sulfate only and composite sulfate and 0.5% chloride at 5°C showed clear deposition of gypsum. This indicates that GGBS mortars stored in these solutions could be subjected to sulfate attack involving gypsum formation, as confirmed in 20mm samples (Figure 4.95).
- At 20°C, the presence of chloride seemed to mitigate sulfate attack, with the only exception being CEMI blended with 10%LF specimens stored in composite sulfate and 0.5% chloride, where after 630 days of exposure cracks at edges was observed (Figure 4.8). The damage was related to thaumasite formation, as indicated by XRD (Figure 4.23), IR (Figure 4.36) and SEM (Figure 4.72) results.
- As indicating by SEM/EDX (Figure 4.77) analysis, mortars made with 50% PFA replacement exposed to sulfate only solutions could be subjected to TSA but with longer exposure time. However, the presence of chloride in solutions mitigates sulfate attack in PFA mortars. Pulverised fuel ash (PFA) mortars stored in combined sulfate and chloride solutions have the highest chloride binding capacity, as indicated by XRD results. This may be related to the higher aluminates content in the composition of PFA compared with the other cements used in this study.
- Also, it is indicated by SEM/EDX analysis that incorporation of 70%GGBS of cement mortars exposed to sulfate only (Figure 4.83) and combined sulfate and 0.5% chloride solution (Figure 4.95) would be subjected to sulfate attack due to gypsum precipitation. Evidence of thaumasite formation was also detected in all GGBS mortars (Figure 4.86). The high water to binder ratio

used in this study should be considered when considering about the performance of GGBS and PFA cements.

- Mortars made with 50%PFA as cement replacement showed the most effective performance against sulfate attack at low temperature.
- A 0.5% chloride concentration combined in a DS4 (BRE Ground aggressivity Class) sulfate solution (Figure 4.10) accelerated thaumasite formation in mortar specimens of CEMI and CEMI blended with 10%LF leading to early onset of specimen deterioration in comparison with sulfate only solution or solutions with higher chloride concentrations. At the higher chloride concentrations studied, thaumasite formation was delayed leading to mitigation at 2.0% chloride during the period of study.
- The study demonstrates that the underlying cause of the effect chloride has on the resistance to TSA is the control it exerts over the solubility of calcite and gypsum, and this effect is concentration sensitive (Figure 4.121). Calcite solubility is increased at 0.5% chloride concentration leading to greater availability of  $\text{CO}_3$  in the pore solution which enhances thaumasite formation and mortar/concrete deterioration. At higher chloride concentration, calcite solubility is reduced, favouring the formation of Friedel's salt which it is believed reduces chemical ingress/interaction through a physical barrier effect.
- The low pH values of pore solution of PFA and GGBS mortar specimens may play a role on promoting gypsum formation.



## **5. Corrosion behaviour of steel rebars embedded in cement mortars subjected to sulfate and chloride exposure**

### **5.1 Introduction**

This chapter presents the evaluation of corrosion of steel rebars embedded in cement mortars made with CEMI and CEMI blended with 10%LF, 50%PFA and 70% GGBS exposed for 900 days to solutions of composite sulfate (0.6%  $\text{SO}_4^{2-}$  as magnesium sulfate) and chlorides (0.5 and 2.0%  $\text{Cl}^-$ ) at 5 and 20°C. Evaluation was made by means of linear polarisation resistance (LPR), visual inspection of state of rebar surfaces and chloride diffusion and carbonation depth measurements at the end of the experiment. The oxygen permeability and porosity of mortars made with the different binders were also examined. X-ray diffraction (XRD) was carried out on dry materials collected from steel-mortar interfaces, together with scanning electron microscopy (SEM) and energy dispersive X-ray (EDX) analysis which were performed on steel-mortar interfaces of selected sound and degraded mortar specimens at 5°C.

Details about mix proportions, mortar casting, curing, preparation of test solutions and all experimental details are given in Chapter 3.

### **5.2 Visual assessment of mortars after 900 days of exposure**

Figure 5.1 to 5.4 show the corrosion suffered by specimens (50mm  $\varnothing$  x 100mm H) stored for 900 days in composite sulfate and 0.5% chloride (SC5) and composite sulfate and 2.0% chloride (SC20) solutions at 5 and 20°C. As explained in Section 4.2, the extent of deterioration depends upon chloride level, binder type and temperature.

At 5°C, CEMI and CEMI-LF mortars stored in SC5 exhibited deterioration, more serious in the latter, at the bases of the samples. It can also be observed in Figure 5.5 that the damage occurred few millimetres underneath a carbonated

layer. No signs of damage were observed for any specimens placed in SC20 solution at 5°C.

At 20°C, all mortar specimens remained intact with no visible damage in all solutions. Moreover, mortar specimens made with CEMI-GGBS and CEMI-PFA placed in solutions at 5 and 20°C performed well against sulfate attack.



**Figure 5.1.** Mortar specimens stored for 900 days in SC5 at 5°C.



**Figure 5.2.** Mortar specimens stored 900 days in SC5 at 20°C.

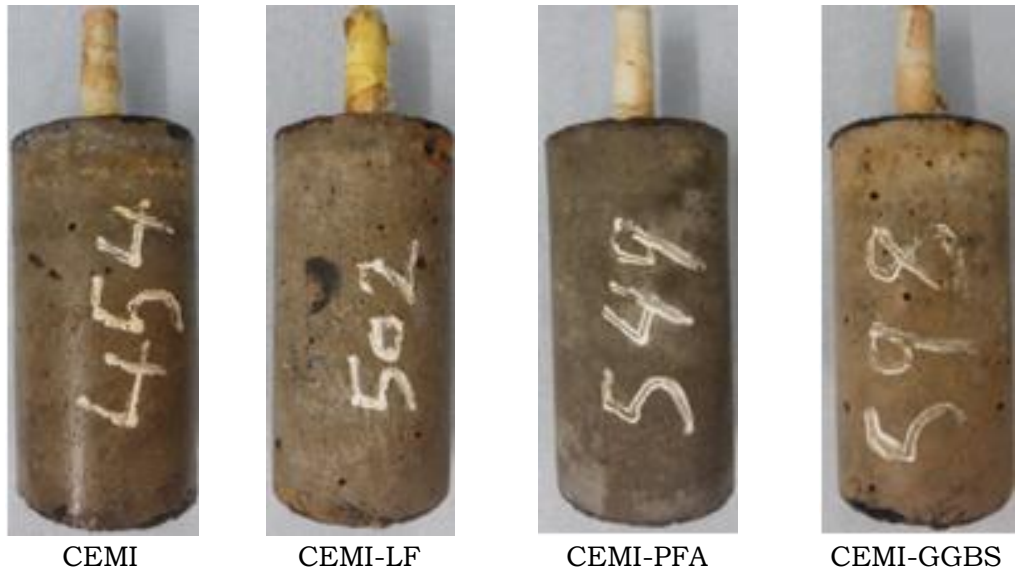


**Figure 5.3.** Mortar specimens stored for 900 days in SC20 at 5°C.

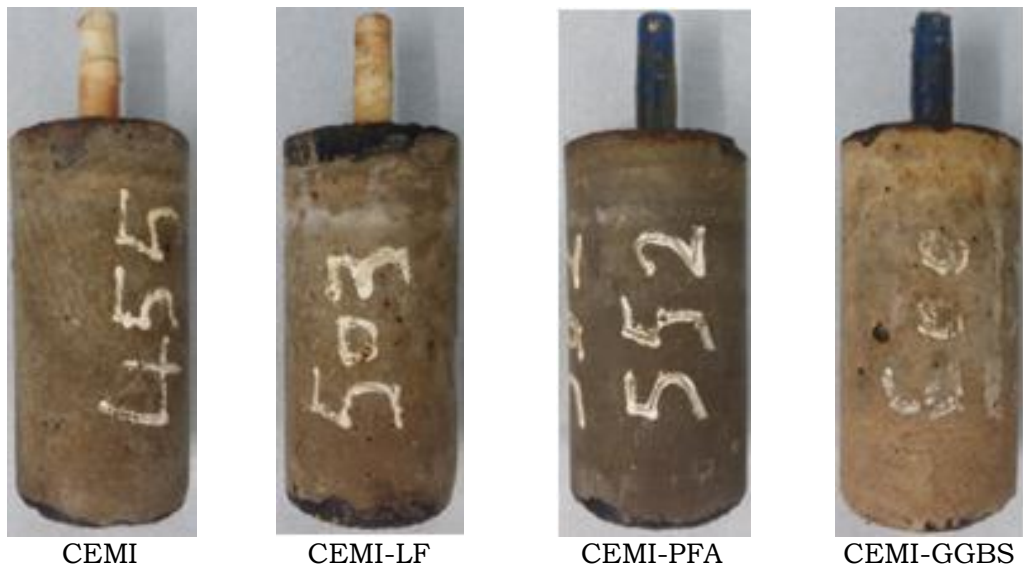


**Figure 5.4.** Mortar specimens stored for 900 days in SC20 at 20°C.

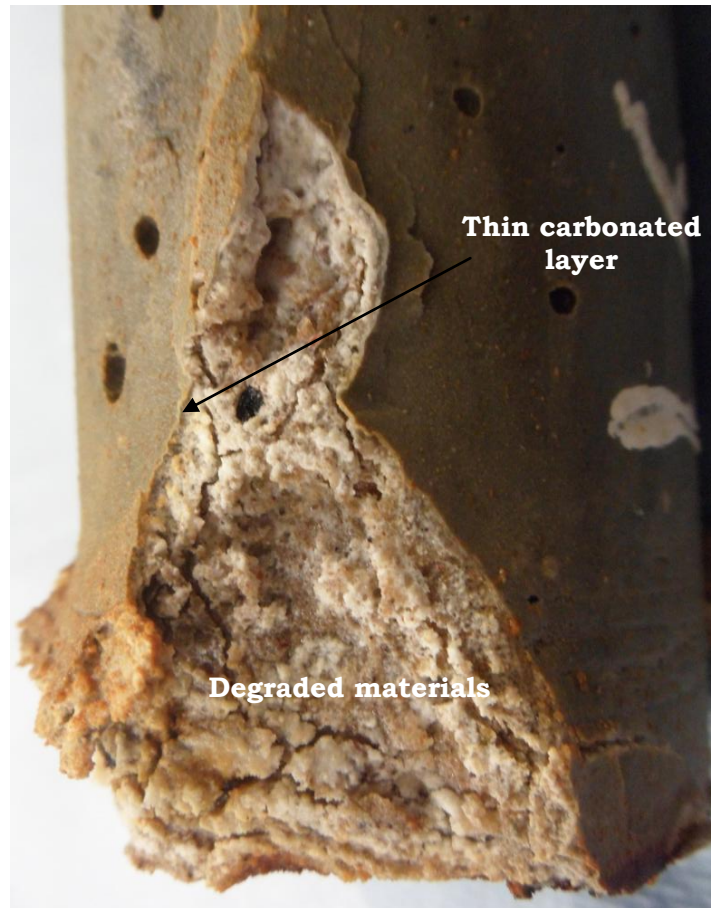


**Figure 5.5.** Degraded part of CEMI mortar at 5°C shown in **Figure 5.1**.

### **5.3 Open porosity and Oxygen permeability measurements**

In this section, the change in porosity and permeability of mortar specimens made with different binders in SC5 at 5°C are evaluated. Porosity was measured using 50mm mortar cubes after 28, 180 and 270 days.

After 900 days, oxygen permeability of core samples (Figure 5.6) collected from sound parts of mortar specimens were also evaluated and compared with the initial permeability (after 28 days immersion in water). The results are summarised in Table 5.1.

**Table 5.1.** Summary of air permeability and open porosity measurements.

| Mix       | Oxygen permeability $\times 10^{-15}$<br>( $m^2$ ) |                | Open porosity (%) |      |      |
|-----------|--|----------------|-------------------|------|------|
|           |  |                | Days              |      |      |
|           | 28 day in water                                    | 900 day in SC5 | 28                | 180  | 270  |
| CEMI      | 5.17   | 1.57           | 20.1              | 18.8 | 17.3 |
| CEMI-LF   | 9.04   | 1.79           | 20.9              | 19.2 | 18.0 |
| CEMI-PFA  | 8.15   | 0.90           | 23.3              | 15.9 | 14.0 |
| CEMI-GGBS | 6.43   | 0.89           | 23.8              | 14.0 | 13.1 |

As Figure 5.7 demonstrates after 28 days of immersion replacement of CEMI by 10% limestone filler increased permeability by approximately 75% equivalent to standard cement (CEMI). This may be due to the dilution effect of limestone filler which reduced cement hydration products and consequently increased the porosity. This probably led to rapid ingress of sulfate and interaction in this mortar and it would also provide a more open system for chloride penetration compared to other mortars.

CEMI-PFA and CEMI-GGBS mortar samples exhibited increase in initial permeability by about 57 and 24%, respectively, compared with standard cement, which may be attributed to the slow pozzolanic reactions of the cements. As time passed, and after 900 days of exposure, however, CEMI-PFA and CEMI-GGBS samples showed great reduction in permeability by about 42 and 43%, respectively, giving values much lower to those of standard cement. The reduction in permeability and porosity values were observed for all mortars but were more evident in those containing PFA and GGBS.

CEMI-GGBS and CEMI-PFA samples also displayed great decreases in open porosity with time (Figure 5.8) compared with those for CEMI and CEMI-LF. After 270 days of exposure, CEMI-GGBS and CEMI-PFA specimens showed reduction in open porosity by about 45 and 40%, respectively, compared with approximately 14% for CEMI and CEMI-LF (Values corresponds to those at 28 days immersion in water). This may be attributed to pore size refinement of cement past as a result of pozzolanic reactions of mortars made with GGBS and PFA, as reported by Leng et al., (2000). As expected and as Figure 5.9 explains the lower the porosity of mortars, the lower permeability.



**Figure 5.6.** Drilled core for permeability test after 900 days of exposure.

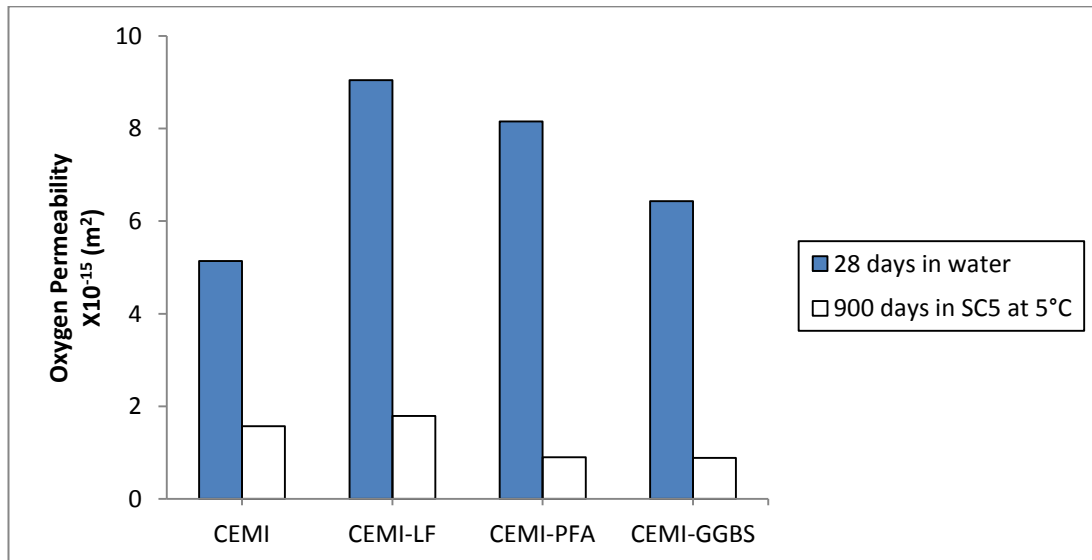


**Figure 5.7.** Variation in oxygen permeability for mortar samples made with different binders.

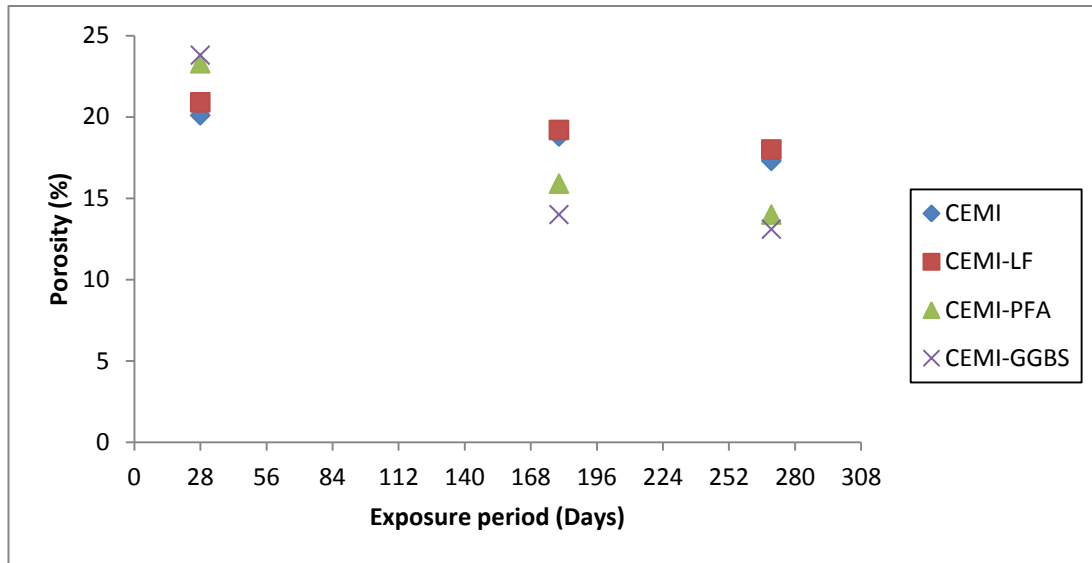


**Figure 5.8.** Changes of open porosity for mortars stored in SC5 at 5°C.

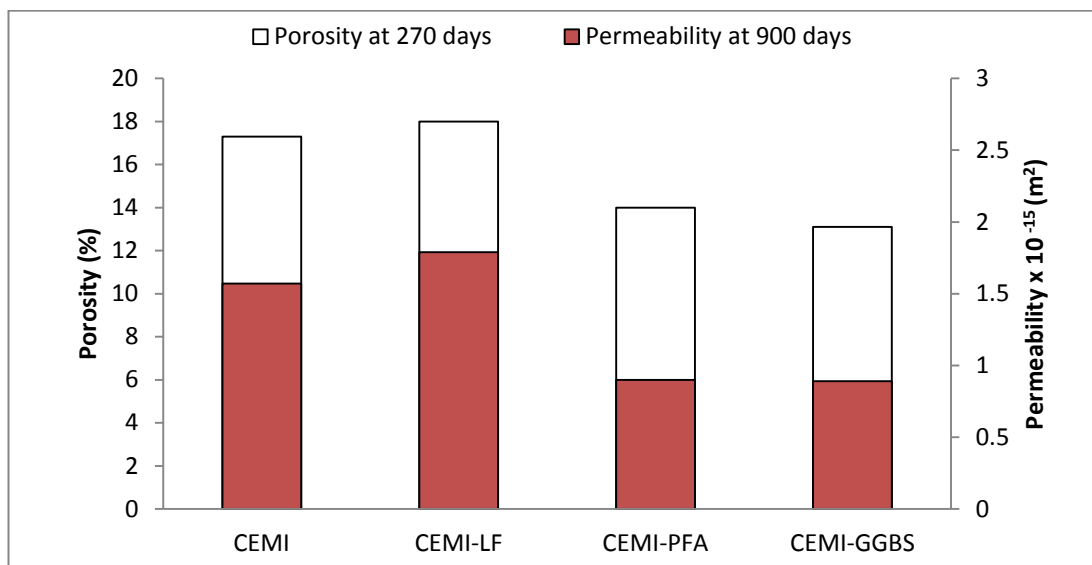


**Figure 5.9.** Open porosity vs. oxygen permeability for mortars with different binders.

## 5.4 Determination of carbonation depth

Carbonation depth of cement mortars made with different binders is examined and discussed in this section. The carbonation reaction in concrete/mortar is characterized by the conversion of calcium hydroxide into calcium carbonate by

atmospheric carbon dioxide. Since, calcium hydroxide is not stable in presence of sulfate, it can be expected that mortar with higher carbonation depth would stand longer against sulfate attack.

Pictures showing all the phenolphthalein treated mortars are given in Appendix. A typical treated mortar is shown in Figure 5.10. In the non-carbonated part of the specimen, where the mortar was still highly alkaline, a purple-red colour was obtained after spraying with phenolphthalein, whereas in the carbonated part of the specimen where the alkalinity of mortar was reduced, no coloration occurred. Generally, low carbonation depth values were observed for all mortars and this was expected due to the short period of exposure to air (21 days). However, CEMI-GGBS and CEMI-PFA had higher carbonation depths compared with CEMI and CEMI-LF mortars.

The higher permeability of CEMI-GGBS and CEMI-PFA mortars at early stage (during initial curing) would allow the access of carbon dioxide into these specimens, leading to greater carbonation depths. It was also reported by Kinoshita et al. (2014) that blended cement systems with fly ash or slag showed a larger CO<sub>2</sub> gain than that of standard OPC cement, which may also explain why CEMI-PFA and CEMI-GGBS mortars showed higher carbonation depths.

No clear difference was observed in carbonation depths for mortars made with CEMI and CEMI-LF. However, the difference was more obvious for CEMI-PFA and CEMI-GGBS specimens. Mortars made with CEMI-PFA showed the highest carbonation depths, indicating its higher permeability and porosity during initial curing, as explained in Section 5.3.

With sulfate exposure mortar/concrete with higher depth of carbonation may resist sulfate attack due to the consumption of portlandite in the carbonated zone, which otherwise is highly unstable in presence of sulfate.

The increase in the carbonation depths for mortars made with fly ash and slag as cement replacement may also cause a rise in electrical resistivity which is considered (Morris et al., 2002) to be a good indicator for evaluating corrosion risk.

The relationship between the resistivity measurement and the carbonation depth by phenolphthalein measurement was also investigated by Claisse (1988) who found that a resistivity increases by a factor of up to about 10 for silica fume concrete. Morris et al.(2002) based their assessment of the value of



electrical resistivity to evaluate corrosion risk on research in which steel rebars appeared to behave passive state when concrete resistivity was higher than 30 k $\Omega$ .cm and active state when the resistivity dropped to 10 k $\Omega$ .cm.

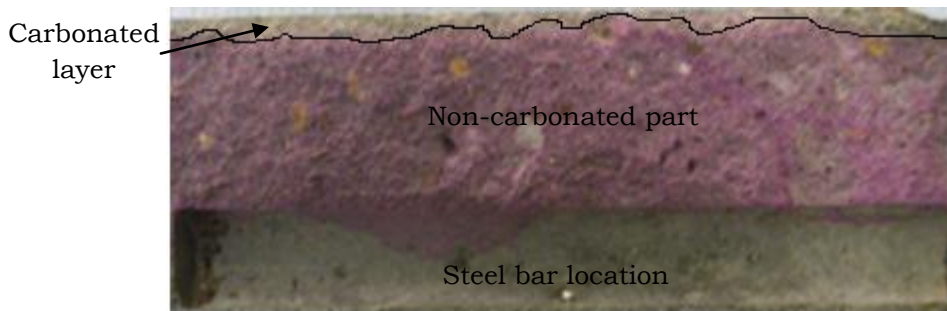


**Figure 5.10.** Typical treated mortar by phenolphthalein solution.

## **5.5 Chloride diffusion into mortars subjected to sulfate and chloride exposure**

### **5.5.1 Chloride content:**

The results of chloride contents at different depths for mortars made with different binders stored for 270 days in 2.0% chloride only (C20) and composite sulfate and 2.0% chloride (SC20) solutions at 5 and 20°C are given in Table 5.2.

**Table 5.2.** Summary of chloride contents at different depths.

| Mix       | Solution | Depth (mm) | Chloride content (% mass of mortar) |          |          |         |          |          |
|-----------|----------|------------|-------------------------------------|----------|----------|---------|----------|----------|
|           |          |            | 5°C                                 |          |          | 20°C    |          |          |
|           |          |            | 90 days                             | 180 days | 270 days | 90 days | 180 days | 270 days |
| CEMI      | C20      | 0-5        | 0.20                                | -        | 0.62     | 0.30    | -        | 0.54     |
|           |          | 5-10       | 0.17                                | -        | 0.55     | 0.27    | -        | 0.48     |
|           |          | 10-15      | 0.07                                | -        | 0.40     | 0.17    | -        | 0.40     |
|           |          | 15-20      | 0.02                                | -        | 0.27     | 0.07    | -        | 0.26     |
|           | SC20     | 0-5        | 0.33                                | -        | 0.81     | 0.20    | -        | 0.83     |
|           |          | 5-10       | 0.20                                | -        | 0.63     | 0.17    | -        | 0.73     |
|           |          | 10-15      | 0.10                                | -        | 0.45     | 0.10    | -        | 0.55     |
|           |          | 15-20      | 0.07                                | -        | 0.24     | 0.03    | -        | 0.36     |
| CEMI-LF   | C20      | 0-5        | 0.24                                | -        | 0.93     | 0.23    | -        | 0.79     |
|           |          | 5-10       | 0.17                                | -        | 0.77     | 0.20    | -        | 0.65     |
|           |          | 10-15      | 0.13                                | -        | 0.72     | 0.13    | -        | 0.56     |
|           |          | 15-20      | 0.11                                | -        | 0.47     | 0.10    | -        | 0.43     |
|           | SC20     | 0-5        | 0.20                                | -        | 0.90     | 0.23    | -        | 0.62     |
|           |          | 5-10       | 0.17                                | -        | 0.71     | 0.17    | -        | 0.55     |
|           |          | 10-15      | 0.13                                | -        | 0.63     | 0.13    | -        | 0.40     |
|           |          | 15-20      | 0.07                                | -        | 0.47     | 0.10    | -        | 0.27     |
| CEMI-PFA  | C20      | 0-5        | 0.20                                | 0.56     | -        | 0.23    | 0.53     | -        |
|           |          | 5-10       | 0.22                                | 0.52     | -        | 0.16    | 0.43     | -        |
|           |          | 10-15      | 0.11                                | 0.37     | -        | 0.13    | 0.37     | -        |
|           |          | 15-20      | 0.07                                | 0.29     | -        | 0.1     | 0.23     | -        |
|           | SC20     | 0-5        | 0.20                                | 0.47     | -        | 0.20    | 0.46     | -        |
|           |          | 5-10       | 0.18                                | 0.35     | -        | 0.19    | 0.35     | -        |
|           |          | 10-15      | 0.12                                | 0.28     | -        | 0.10    | 0.24     | -        |
|           |          | 15-20      | 0.06                                | 0.25     | -        | 0.07    | 0.23     | -        |
| CEMI-GGBS | C20      | 0-5        | 0.33                                | 1.44     | -        | 0.33    | 1.41     | -        |
|           |          | 5-10       | 0.12                                | 0.92     | -        | 0.15    | 0.75     | -        |
|           |          | 10-15      | 0.09                                | 0.46     | -        | 0.08    | 0.46     | -        |
|           |          | 15-20      | 0.01                                | 0.41     | -        | 0.02    | 0.35     | -        |
|           | SC20     | 0-5        | 0.30                                | 1.35     | -        | 0.33    | 1.32     | -        |
|           |          | 5-10       | 0.14                                | 0.77     | -        | 0.10    | 0.65     | -        |
|           |          | 10-15      | 0.07                                | 0.42     | -        | 0.06    | 0.36     | -        |
|           |          | 15-20      | 0.02                                | 0.32     | -        | 0.02    | 0.36     | -        |

As expected, the chloride content decreased with depth, and the highest chloride concentration occurred in the 0-5 mm surface layer where the mortar was in direct contact with the test solutions. Expected increases in chloride content as time passed were observed for all samples.

The chloride contents at different depths showed dependency on exposure period, binder type and presence of sulfate in composite solution, as Figure 5.11 to 5.18 demonstrate.

At 5°C (Figure 5.11) the presence of sulfate in composite solution for 90 days increased chloride content for CEMI mortars, which may indicate propagation of microcracks in SC20 mortars. At 20°C (Figure 5.12) lower chloride contents

were observed in mortars placed in composite solution than those in C20. This may be due to blocked mortar pores by sulfate products.

After 270 days of exposure, the presence of sulfate in composite solution stored at both temperatures led to increase chloride concentrations at different depths, probably due to the propagation of new microcracks.

In case of CEMI-LF mortars (Figure 5.13 and 5.14) after 90 days of immersion the mortars showed slight reduction in chloride content where this was greater for SC5 than SC20. After 270 days the presence of sulfate in SC20 solution reduced chloride ingress, which may be attributed to the formation of sulfate products which filled the open pores.

Incorporation of 50% PFA had no positive effect against chloride ingress after 90 and 180 days of exposure, as Figure 5.15 and 5.16 illustrates. Higher chloride contents were observed for most depths compared to CEMI. This may be due to the low pozzolanic activity of PFA, as indicated by permeability and porosity results shown in Section 5.3. Fly ash has a relatively low surface area and pozzolanic activity, thus at normal temperatures the pozzolanic reaction is very slow (Mehta and Gjrrv, 1982).

However, with time and due to pore refinement of fly ash mortars, as indicated by permeability results after 900 days of immersion and as also reported by Thomas et al. (1999), lower paths would be available for chloride ingress. In addition, the high aluminate content of PFA cement would chemically bound chloride (Section 4.5.1 in Chapter 4), resulting in reduction in the amount of free chloride in the pore solution.

It can be seen in Figure 5.17 and 5.18 that, replacement by 70% slag caused the greatest reduction in chloride content at deeper depths. The presence of sulfate in composite solutions at both temperatures also led to decreased chloride ingress.

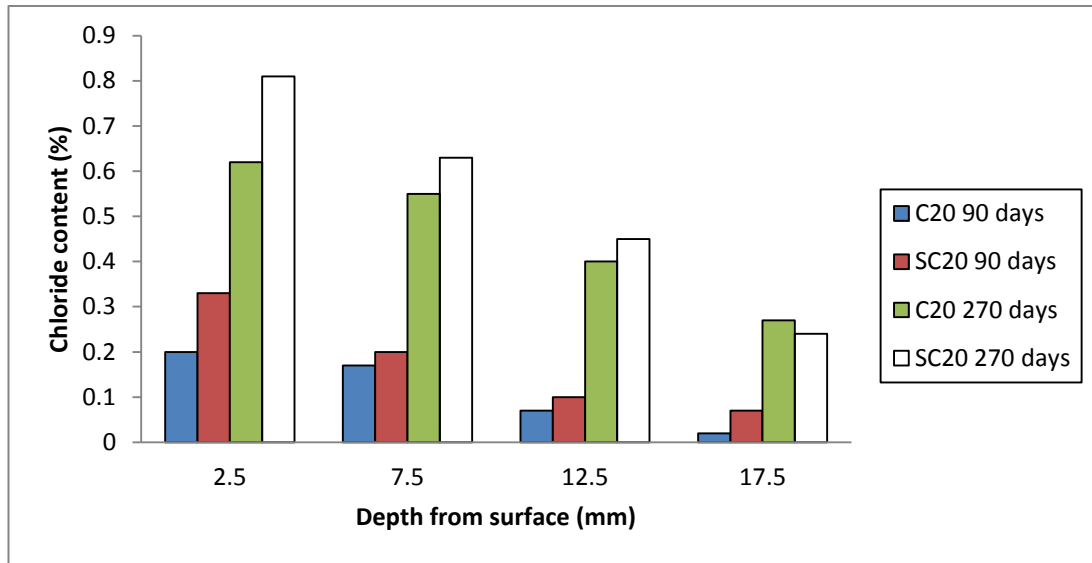


**Figure 5.11.** Chloride contents for CEMI mortars stored 90 and 270 days at 5°C.

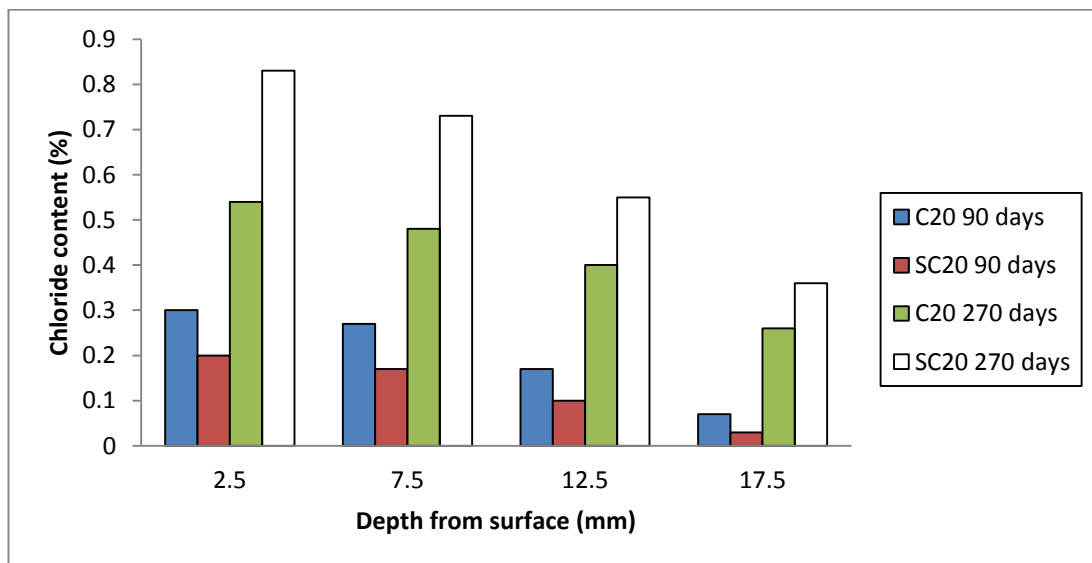


**Figure 5.12.** Chloride contents for CEMI mortars stored 90 and 270 days at 20°C.

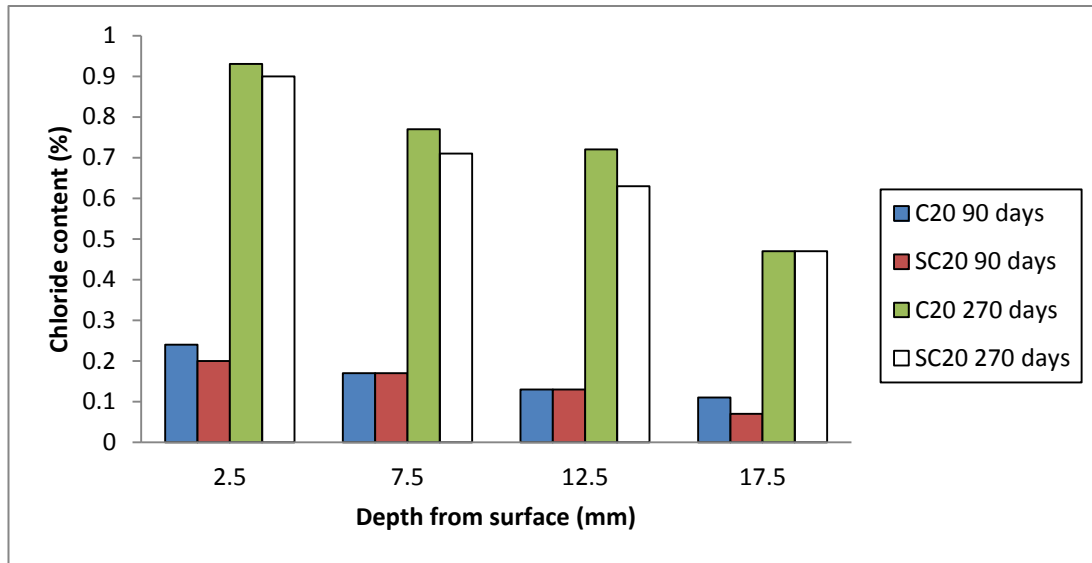


**Figure 5.13.** Chloride contents for CEMI-LF mortars stored 90 and 270 days at 5°C.

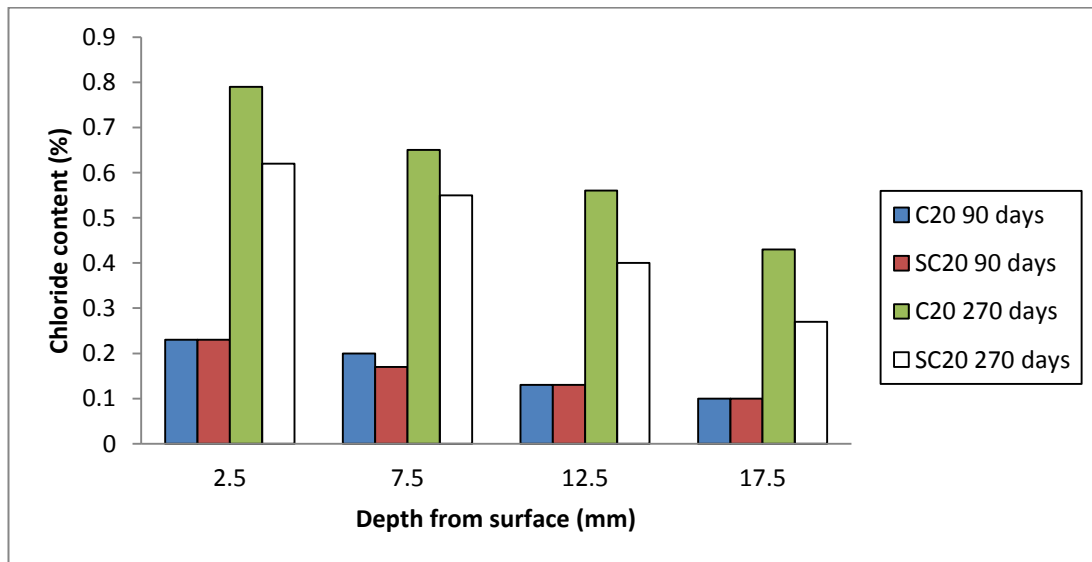


**Figure 5.14.** Chloride contents for CEMI-LF mortars stored 90 and 270 days at 20°C.

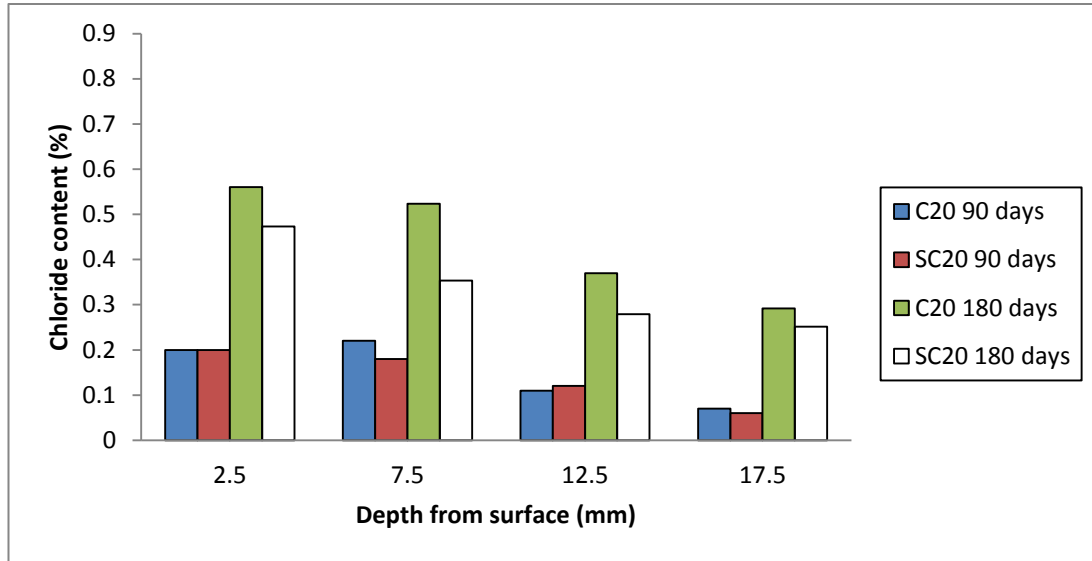


**Figure 5.15.** Chloride contents for CEMI-PFA mortars stored 90 and 180 days at 5°C.

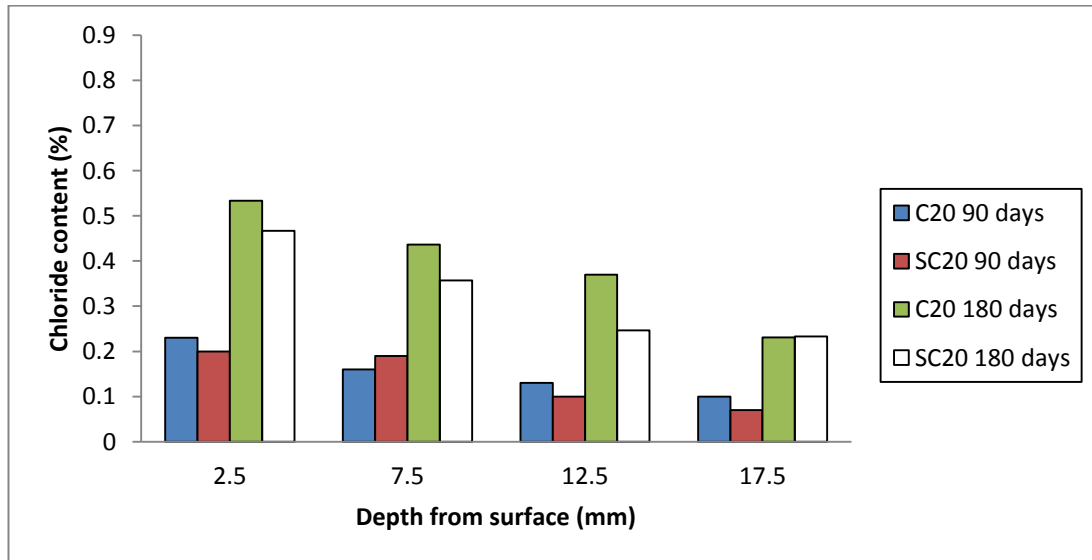


**Figure 5.16.** Chloride contents for CEMI-PFA mortars stored 90 and 180 days at 20°C.

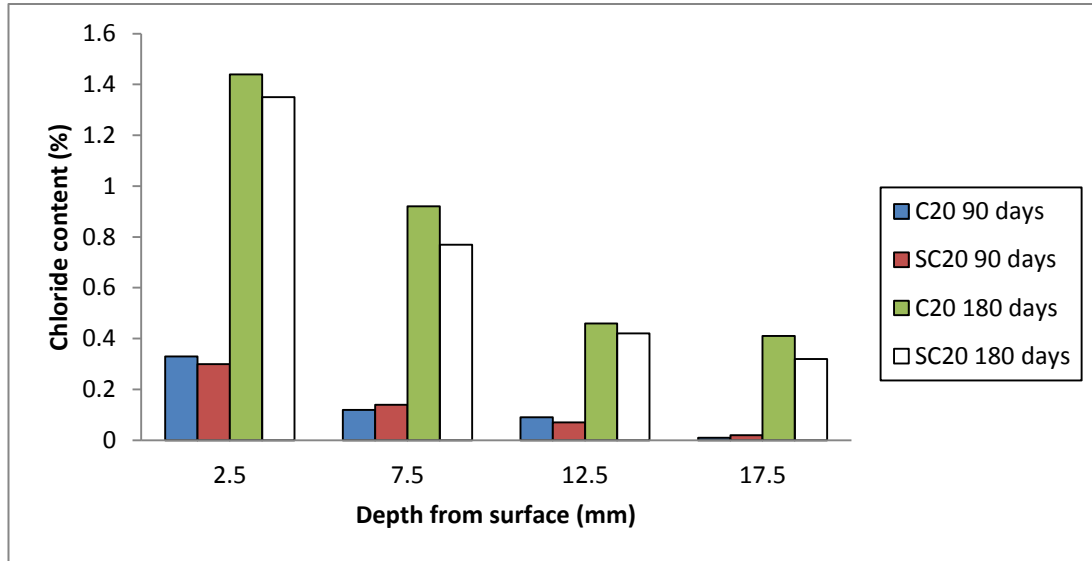


**Figure 5.17.** Chloride contents for CEMI-GGBS mortars stored 90 and 180 days at 5°C.

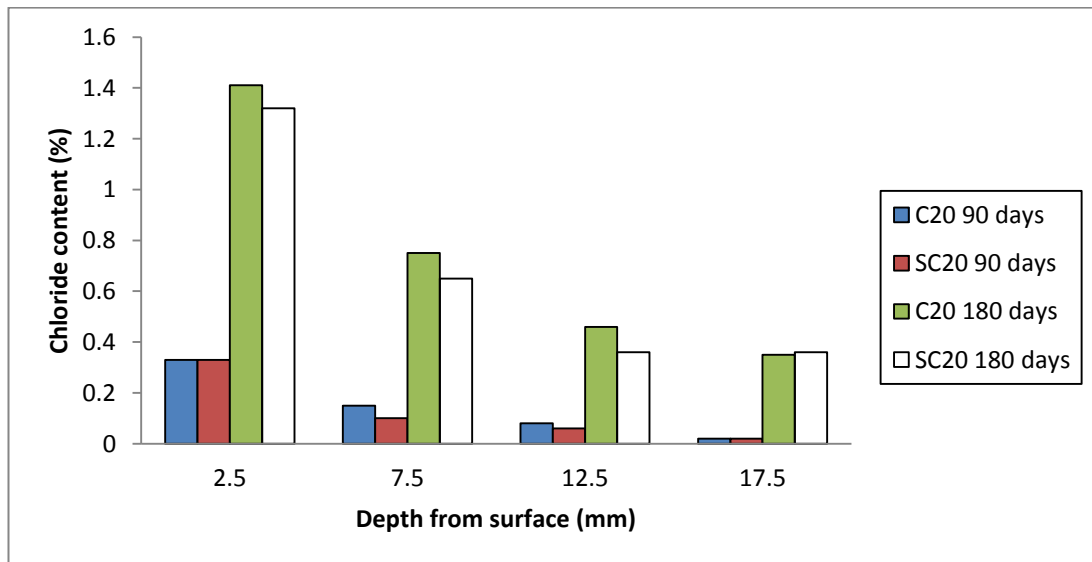


**Figure 5.18.** Chloride contents for CEMI-GGBS mortars stored 90 and 180 days at 20°C.

### 5.5.2 Chloride diffusion:

In this section, the apparent chloride diffusion coefficient for cement mortars made with different binders stored in chloride only (2.0%) and composite sulfate and 2.0% chloride solutions at 5 and 20°C were evaluated and the results for different chloride profiles are presented in Table 5.3 and Figure 5.20.

The error function solution to the Fick's second law (Section 3.6.13 in Chapter 3) was fitted to the exponential fit, which showed good correlation with the experimental chloride profiles, to calculate the apparent chloride diffusion coefficient. Surface chloride concentration ( $C_s$ ) values were estimated from the best fit (exponential fit) to experimental data (Section 5.5.1) and then diffusion coefficient (D) values were calculated by iteration to generate the best fit by least squares.

Figure 5.19 shows an example for the exponential fit of the chloride profile for CEMI mortars stored 90 days in SC20 at 5°C. It should be mentioned that the solutions were replenished every 90 days.

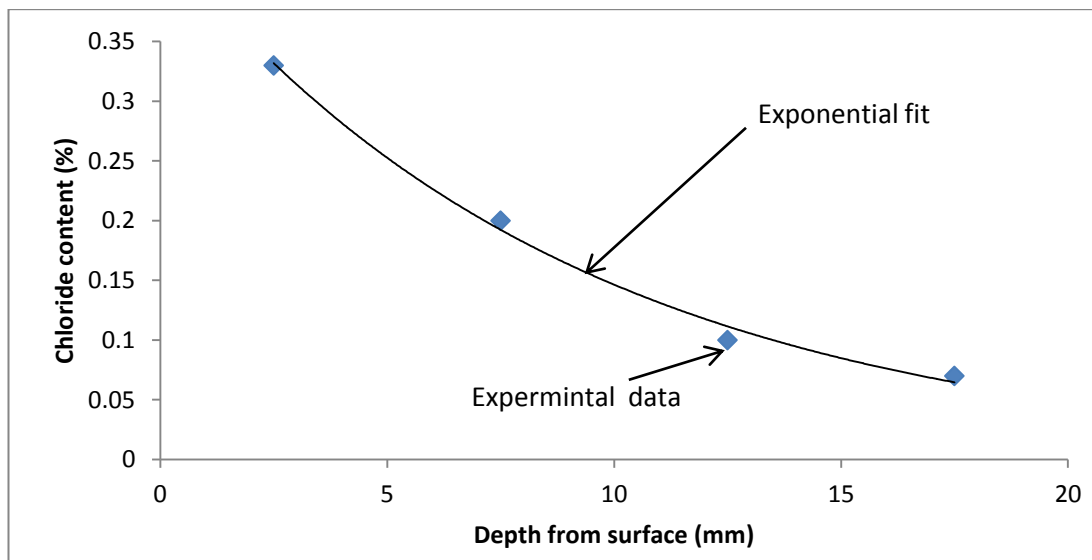


**Figure 5.19.** Chloride profile for CEMI mortars stored 90 days in SC20 at 5°C.



**Table 5.3.** Chloride diffusion coefficient and surface concentrations (least squares best fit).

| Mix       | Age (days) | Solution | Best fit values                          |      |                           |      |
|-----------|------------|----------|--|------|---------------------------|------|
|           |            |          | D ( $\times 10^{-12}$ m <sup>2</sup> /s) |      | C <sub>s</sub> (% mortar) |      |
|           |            |          | 5°C                                      | 20°C | 5°C                       | 20°C |
| CEMI      | 90         | C20      | 8.5                                      | 14.9 | 0.27                      | 0.38 |
|           |            | SC20     | 7.0                                      | 11.6 | 0.44                      | 0.26 |
|           | 270        | C20      | 9.0                                      | 11.9 | 0.73                      | 0.62 |
|           |            | SC20     | 5.4                                      | 8.9  | 0.98                      | 0.98 |
| CEMI-LF   | 90         | C20      | 22.6                                     | 24.3 | 0.27                      | 0.27 |
|           |            | SC20     | 21.2                                     | 23.3 | 0.24                      | 0.26 |
|           | 270        | C20      | 13.9                                     | 13.7 | 1.04                      | 0.88 |
|           |            | SC20     | 12.8                                     | 9.1  | 0.99                      | 0.73 |
| CEMI-PFA  | 90         | C20      | 19.6                                     | 22.1 | 0.26                      | 0.26 |
|           |            | SC20     | 18.1                                     | 17.6 | 0.25                      | 0.25 |
|           | 180        | C20      | 17.5                                     | 14.4 | 0.65                      | 0.61 |
|           |            | SC20     | 15.4                                     | 12.3 | 0.52                      | 0.53 |
| CEMI-GGBS | 90         | C20      | 2.7                                      | 3.7  | 0.50                      | 0.48 |
|           |            | SC20     | 3.5                                      | 2.0  | 0.45                      | 0.55 |
|           | 180        | C20      | 4.5                                      | 3.8  | 1.82                      | 1.80 |
|           |            | SC20     | 3.7                                      | 3.3  | 1.75                      | 1.71 |

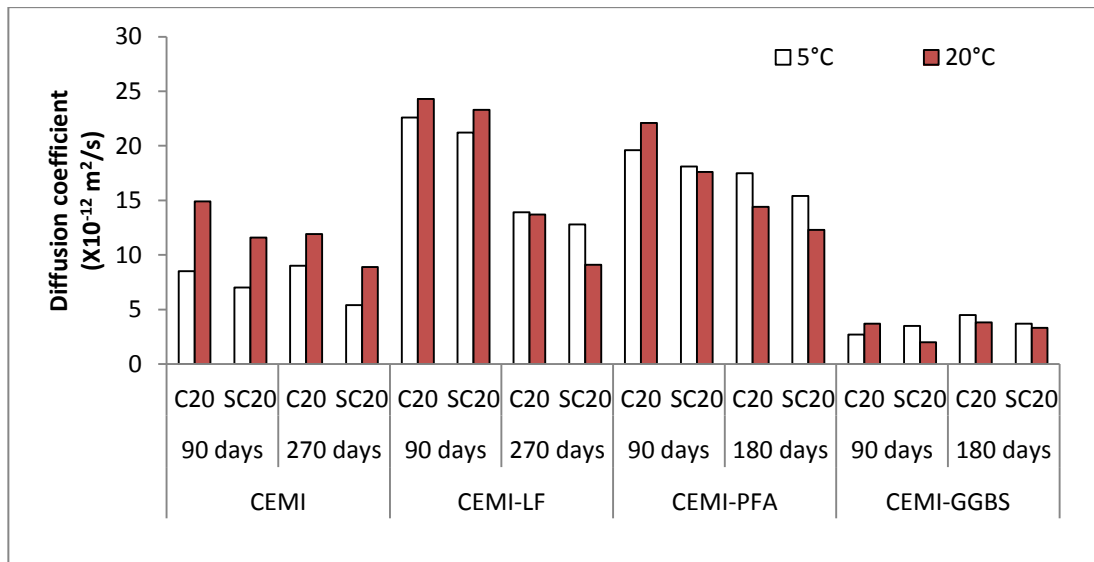


**Figure 5.20.** Chloride diffusion coefficients for mortars with different binder.

- **CEMI and CEMI-LF mortars:**

The chloride diffusion coefficients for CEMI and CEMI-LF mortar specimens stored in composite sulfate and 2.0% chloride solutions at 5 and 20°C are given in Figure 5.21.

The diffusion coefficient after 90 days of exposure ranged between 7 and  $24.3 \times 10^{-12} \text{ m}^2/\text{s}$ , which indicates high diffusivity characteristic of CEMI and CEMI-LF mortars. This is expected because of the high water to binder ratio used in this study (W/B=0.6). CEMI-LF mortars showed higher diffusion values than CEMI. An increase in diffusion coefficient by up to 3 times was observed for CEMI-LF compared to CEMI. This may be attributed to the lower availability of clinker which in turn increased the water to cement ratio compared to that without replacement. Increase in the volume of macro-pores in mortar made with limestone filler was reported by Moukwa, (1989).

As time progressed, diffusion values declined in all mortars, probably due to increase in cement hydration products which resulted in compacted microstructures.

It can also be observed that the diffusion coefficient for mortars stored for 90 and 270 days in composite sulfate and 2.0% chloride solution were lower than those stored in 2.0% chloride only solutions. This may be related to the formation of sulfate products which filled pores at this stage of immersion, as also suggested by Zuquan et al. (2007). However, at a longer exposure period sulfate attack would result in more rapid ingress of chloride. The generation of excessive expansive thaumasite crystals (Section 4.6 in Chapter 4) in pores and around aggregate particles would give rise to the rapid ingress of chloride into mortars, as suggested by Slater et al. (2003). Thus, higher chloride diffusion is expected in case of mortars exposed to SC5, which showed visual damage, than those in SC20, as confirmed later by corrosion measurement shown in Section 5.8 and 5.9.

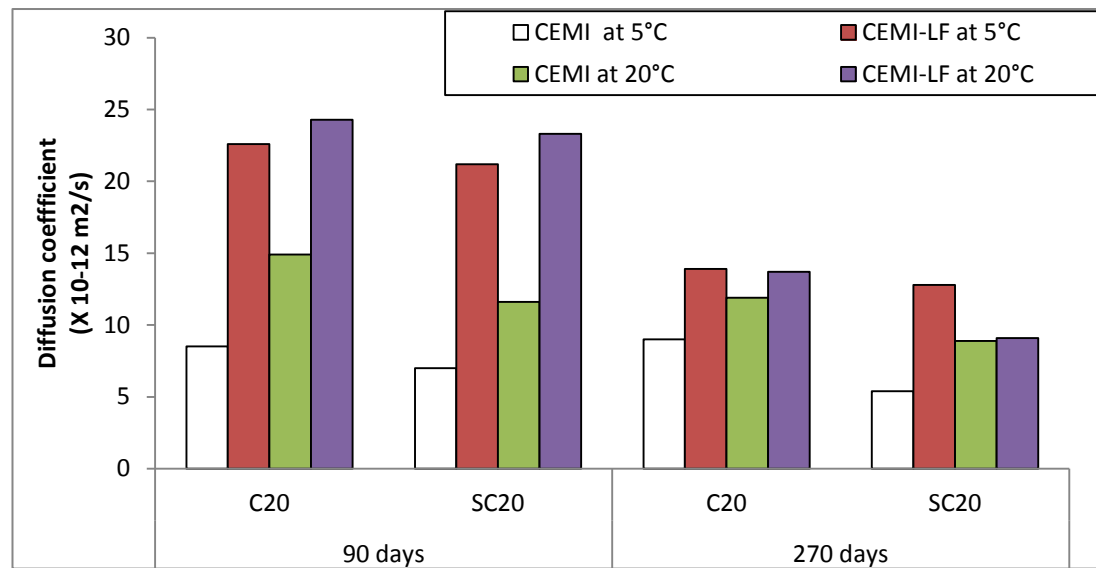


**Figure 5.21.** Chloride diffusion coefficient for CEMI and CEMI-LF mortars stored 90 and 270 days in chloride only (C20) and composite sulfate and 2.0% chloride (SC20) solutions at 5 and 20°C.

- **CEMI-PFA and CEMI-GGBS mortars:**

The apparent chloride diffusion coefficient for CEMI-PFA and CEMI-GGBS mortars placed in SC20 at 5 and 20°C are given in Figure 5.22 and 5.23. At 90 days of immersion, replacement by 50% PFA led to an increase by about double in chloride diffusion compared to standard cement. As time passed and after 180 days, a slight decrease was noted. The slow pozzolanic activity of fly ash would explain this (Mehta and Gjrv, 1982).

The improvement in resistance of chloride ingress resistance as time passes was reported by Zuquan et al. (2007), who stated that fly ash increases the ingress of chloride into concrete in the early exposure period, but can reduce it in the longer term. In the current study, the permeability and porosity results (Section 5.3) indicated potential reduction in chloride diffusion of PFA mortars as time passes.

The presence of sulfate in composite solutions reduced chloride ingress, in which chloride diffusion of mortars exposed to composite solution showed lower values compared with those in chloride only solutions.

70 % replacement by GGBS resulted in decreasing chloride diffusion compared with standard cement, as Figure 5.23 illustrates. After 90 days of immersion,

the diffusion was half that of standard cement. It was reported by Leng et al. (2000) that replacement by fly ash or slag can improve resistance to chloride penetration which they attributed to the following factors:

1. In PFA and GGBS concretes more calcium silicate hydration products are present in the concrete matrix and may therefore adsorb more chloride ions and block diffusion paths.
2. The pore size and pore shape are improved due to the replacement with fly ash and slag.
3. PFA and GGBS have more  $C_3A$  which can adsorb more chlorides to form Friedel's salt.

It was reported by Claisse (1988) that the initial electrical current flows through a concrete sample depends mainly on the mobility of hydroxyl ions in the pore solution. Claisse (1988) attributed the increase in resistivity that occurs in silica fume concrete to the consumption of calcium hydroxide by the pozzolan. Since hydroxyl ions are consumed in pozzolanic reactions that occur with PFA and GGBS, concretes and mortars containing these binders are also expected to have high electrical resistivity, where the increase would depend on the amount of pozzolan present.

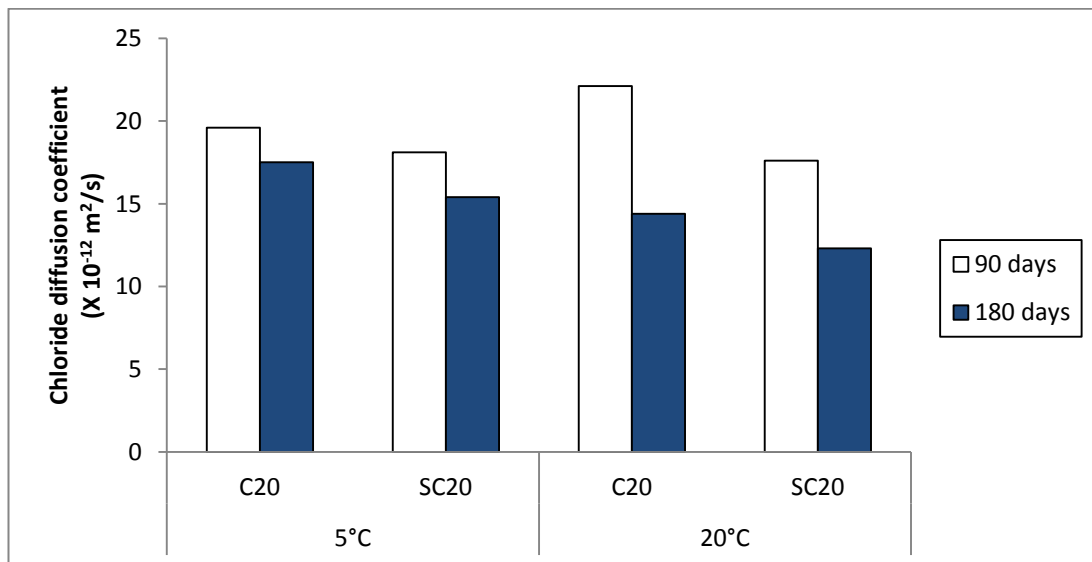


**Figure 5.22.** Chloride diffusion coefficient for CEMI-PFA mortars stored for 90 and 180 days in chloride only (C20) and composite sulfate and 2.0% chloride (SC20) solutions at 5 and 20°C.

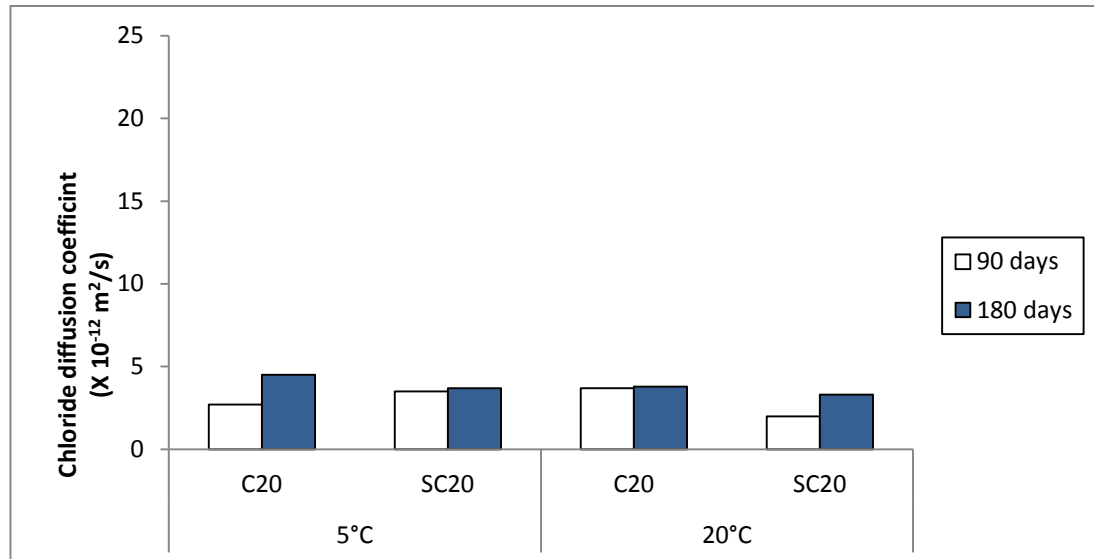


**Figure 5.23.** Chloride diffusion coefficient for CEMI-GGBS mortars stored in chloride only (C20) and composite sulfate and 2.0% chloride (SC20) solutions at 5 and 20°C.

## 5.6 X-ray diffraction of steel-mortar interface samples

Materials collected from steel-mortar interfaces of mortar specimens made with different binders stored 900 days in composite sulfate and 0.5% chloride (SC5) solutions at 5 and 20°C were analysed by means of X-ray diffraction (XRD). The results are presented in this section. Details of the sample preparation and analysis methodology are given in Chapter 3, Sections 3.6.4 and 3.6.5.

- **CEMI-LF samples in SC5 at 5 and 20°C:**

The XRD patterns for steel-mortar interfaces powders are shown in Figure 5.24. At 5°C, the sample showed strong peaks for gypsum and weak peaks for Friedel's salt and portlandite; while no gypsum and strong peaks for portlandite and Friedel's salt were detected in the 20°C sample. This may indicate the rapid ingress of sulfate ions in CEMI-LF mortar stored at 5°C, due to the damage described in Section 5.2 of the outer layer. Portlandite was most probably consumed in gypsum formation, which was strongly detected by XRD analysis. The absence of Friedel's salt in the 5°C sample may indicate its instability in such low pH (<11) and sulfate rich conditions. This would release of bound chloride to form free chloride in pore solution, giving an increasing risk of corrosion (This is further discussed in Chapter 6).

Thaumasite was also detected in the 5°C sample. Instead, relatively strong peaks for portlandite and moderate peaks for Friedel's salt were detected in 20°C sample, indicating the existence of a protective layer with high pH value surrounding the steel bar.

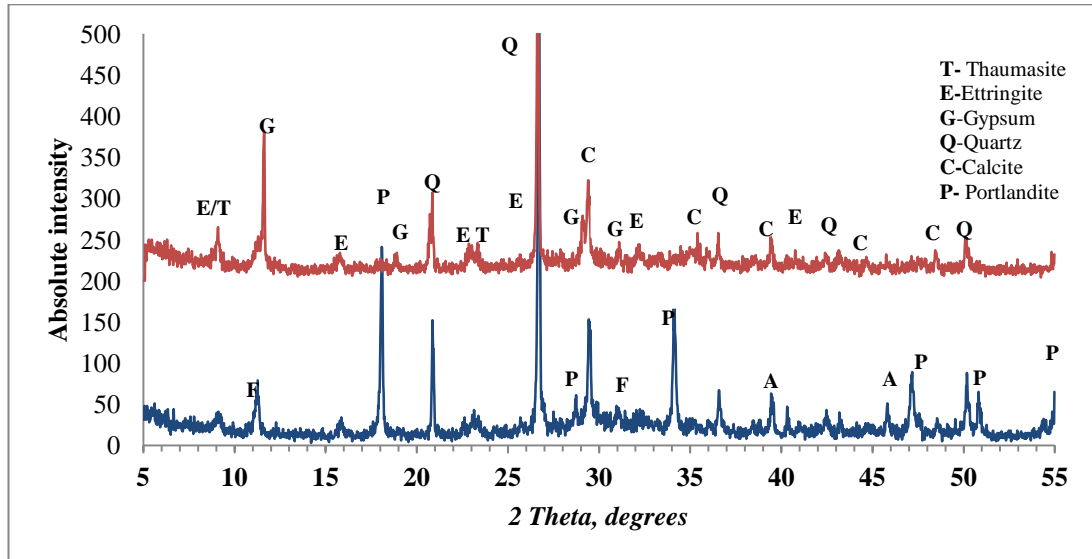


**Figure 5.24.** XRD pattern for CEMI-LF interface samples stored in SC5 at 5°C (Top, red) and 20°C (Bottom, blue).

- **CEMI-PFA samples in SC5 at 5 and 20°C:**

The XRD patterns in Figure 5.25 indicate that ettringite was present in relatively small amounts. The quantities of portlandite in CEMI-PFA samples were also low, as indicated by its relatively small peak intensities. This was due to both the dilution of standard cement and the pozzolanic reaction of PFA which would result in less CH and higher C-S-H gel production in the matrix. However, the reduction does not necessarily mean that the corrosion risk of steel bars in concrete/mortar also increases as factors such as the permeability and diffusion also control the rate of corrosion.

Instead, Friedel's salt was detected as relatively strong peaks in both samples, with higher peak intensities at 20°C, reflecting the high chloride binding capacity feature of fly ash cement and the increase in this as temperature increases. Because Friedel's salt is unstable when the pH value of pore solution is lower than 10, its presence with relatively moderate peak intensity in

interface samples, would indicate a pore solution with high pH value, maintaining a sufficient value to protect steel rebars from corrosion.

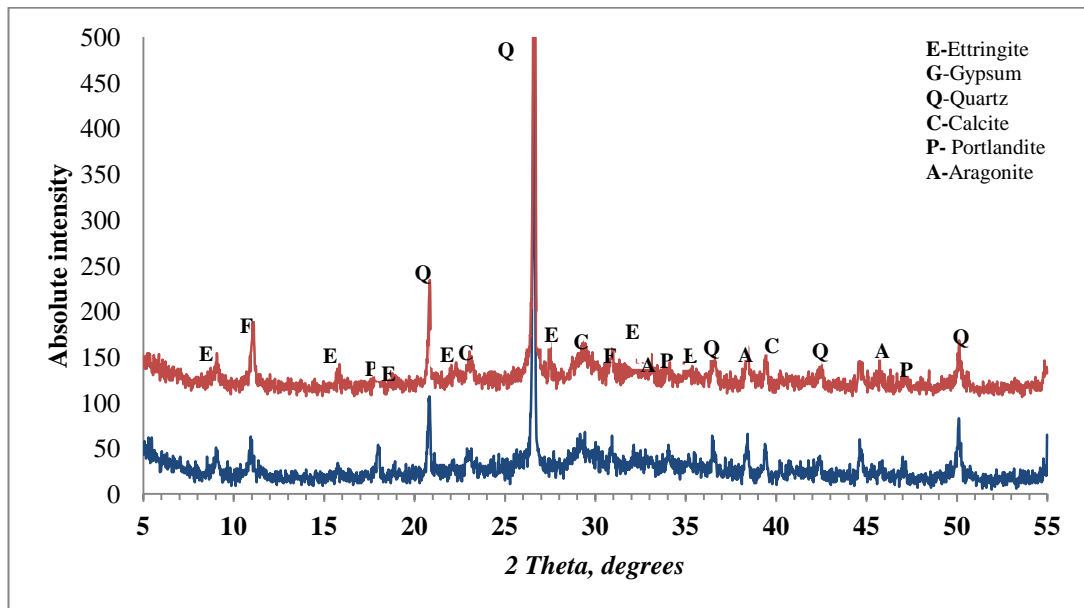


**Figure 5.25.** XRD pattern for CEMI-PFA interface samples stored in SC5 at 5 °C (Top) and 20°C (Bottom).

- **CEMI-GGBS samples in SC5 at 5 and 20°C:**

The XRD patterns for interface samples of CEMI-GGBS mortar are shown in Figure 5.26. Generally, both patterns were of similar peak intensities. Small amounts of both ettringite and portlandite were detected in both samples. This may be due to the dilution of cement and to the pozzolanic reaction, but its presence indicate that further C-S-H gel could be produced. This would further contribute to improving the mortar microstructure, particularly near steel bars. Consequently, the transport properties of mortar against chloride and sulfate ingress would have improved and resulted in enhancing the corrosion resistance of steel bar.

The presence of portlandite peaks indicates high pH of the pore solution, which would avoid the depassivation of steel bars.

Weak peak intensities were observed for calcite, which would be accounted for the limestone filler present. Low peak intensities for Friedel's salt were detected in GGBS samples compared with those for PFA, probably due to compacted microstructure of GGBS mortars, as demonstrates by diffusion measurements described in Section 5.5.2.

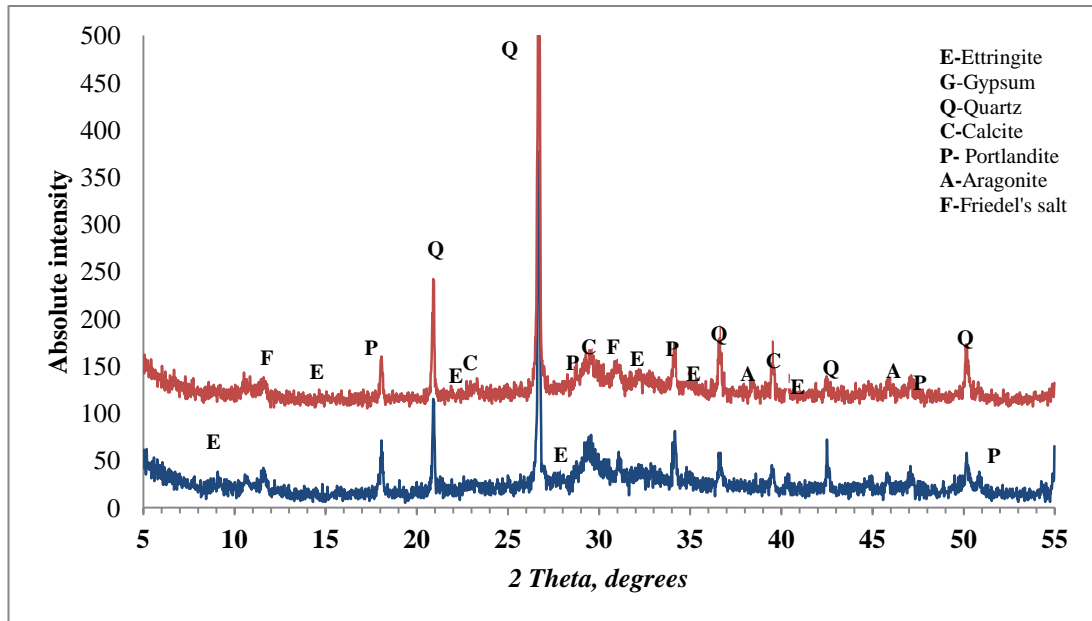


**Figure 5.26.** XRD patterns for CEMI-GGBS interface samples stored in SC5 at 5 °C (Top) and 20 °C (Bottom).

## 5.7 SEM/EDX of steel-mortar interface samples

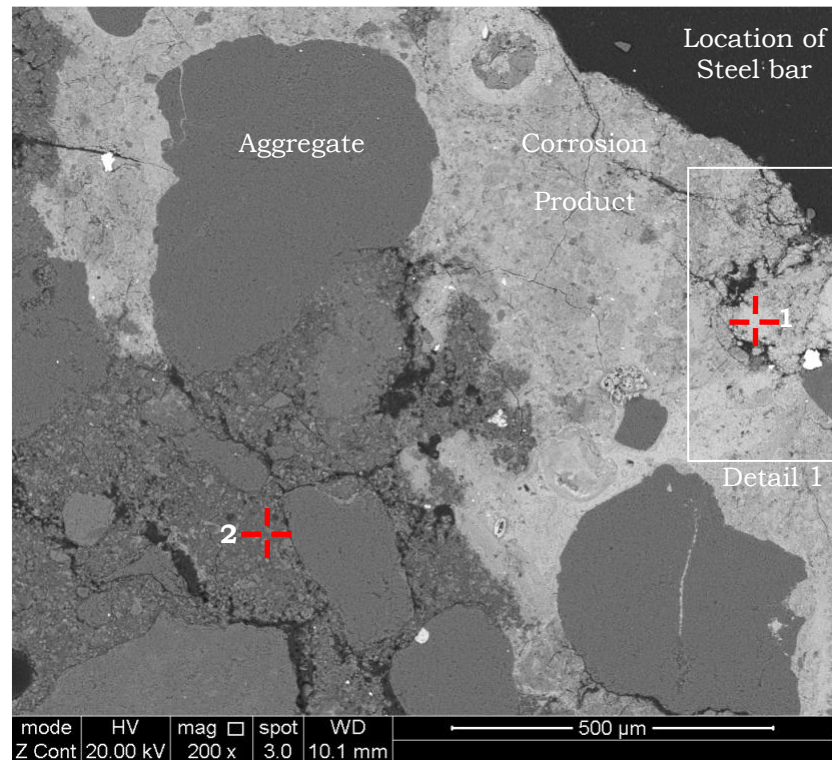
Interface samples for CEMI-LF mortars stored in composite sulfate and 0.5% chloride solutions (SC5) at 5 and 20 °C were selected and examined by scanning electron microscopy and Energy Dispersive X-ray analysis (SEM/EDX).

Figure 5.27 and 5.28 show the SEM image for an interface sample at 5 °C, in which changes to the mortar microstructure are indicated by the colour differences between dark grey and the light grey region close to the rebar. The EDX analysis in Figure 5.30 of the dark grey areas indicated the presence mainly of calcium, silicate, aluminate, sulfur which implies that the C-S-H had suffered transformation towards thaumasite, whereas, the light grey areas surrounding the steel bars consisted mainly of Fe and less Ca and Cl (Figure 5.29), which is interpreted as expanded steel corrosion products on the bar surface, as discussed later in Section 5.9.

The degradation of the outer surface layer of CEMI-LF mortars placed in SC5 at 5 °C, probably led to rapid chloride ingress and consequently an increased corrosion risk, as indicated by the presence of iron oxide in this region. The low binding capacity of deteriorated materials would also provide extra free chloride available in pore solution, which would increase the corrosion risk. Closer investigation (Figure 5.28) showed also formation of extensive microcracks, which probably attributed to expansive corrosion products.



No changes in colour, and therefore no microstructural changes, were observed for SC5 mortar interface sample that had been stored for 900 days at 20°C, as SEM (Figure 5.31) image indicates.



**Figure 5.27.** SEM image for SC5 steel-mortar interface sample stored 900 days at 5°C.

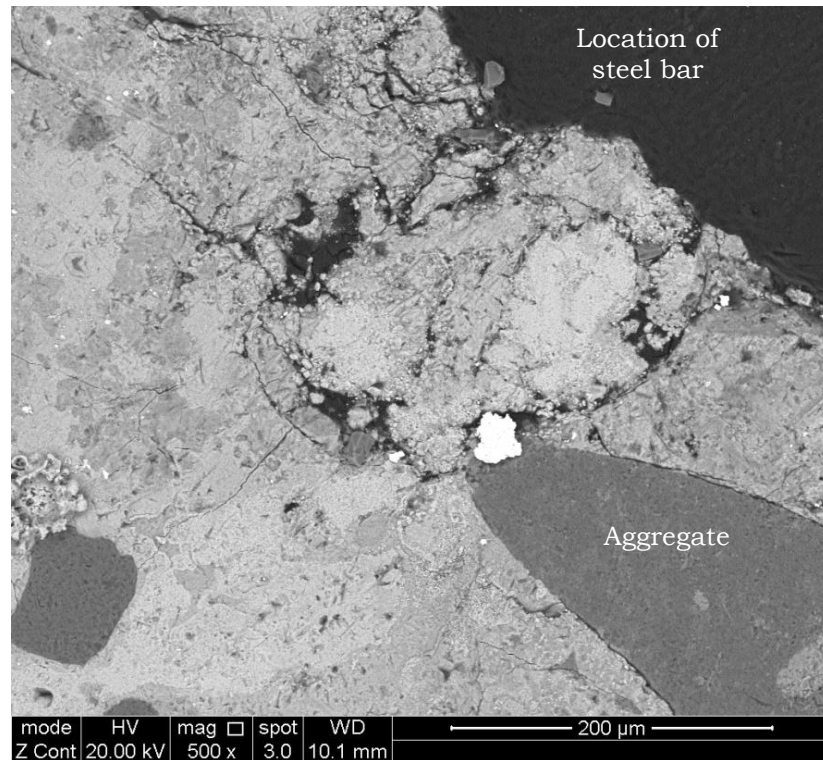


**Figure 5.28.** Detail 1 in Figure 5.27.

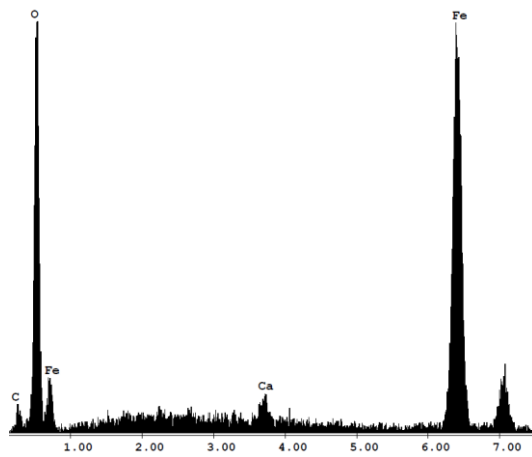


**Figure 5.29.** EDX for 1 (Iron oxide) in Figure 5.27.

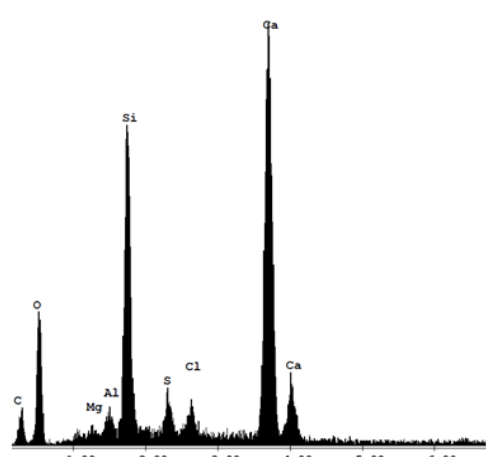


**Figure 5.30.** EDX for 2 in Figure 5.27.

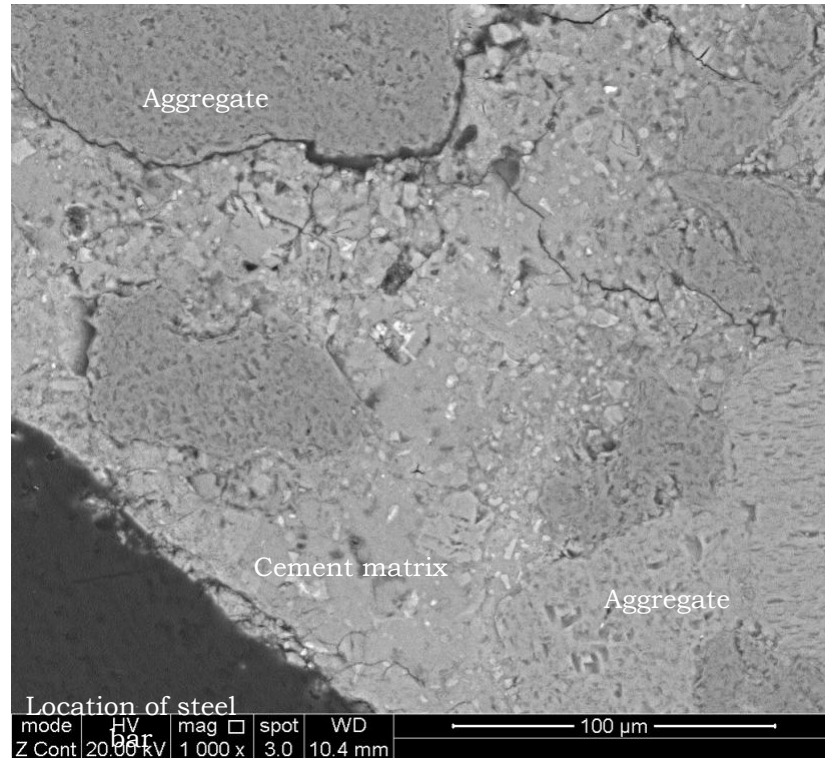


**Figure 5.31.** SEM image for SC5 interface sample after 900 days at 20°C.

## 5.8 Linear Polarization Resistance (LPR)

This section presents and discusses an evaluation of corrosion of steel rebars embedded in mortar specimens made with different binders stored in composite sulfate and 0.5% chloride (SC5) and composite sulfate and 2.0% chloride (SC20) solutions at 5 and 20°C by linear polarization resistance (LPR).

The extent of corrosion was evaluated at the end of 180 days of continuous acceleration (Acceleration procedure given Section 3.6.15 in Chapter 3) and compared with the situation before acceleration (720 days). Table 5.4 presents the corrosion results obtained after 24 and 30 months of exposure. All polarisation curves obtained by LPR measurements are given in the Appendix.

**Table 5.4.** Variations in corrosion measurements.

| Mix       | Sample no. | Temp. (°C) | Chloride level | Corrosion current density ( $\mu\text{A}/\text{cm}^2$ ) |                                 |
|-----------|------------|------------|----------------|---|---------------------------------|
|           |            |            |                | *Before acceleration (720 days)                         | **After acceleration (900 days) |
| CEMI      | 1          | 5          | 0.5%           | 0.60  | 6.13                            |
| CEMI      | 2          |            |                | 0.53  | 2.02                            |
| CEMI-LF   | 1          |            |                | 0.92  | 3.40                            |
| CEMI-LF   | 2          |            |                | 0.75  | 6.07                            |
| CEMI-PFA  | 1          |            |                | 0.23  | 0.13                            |
| CEMI-PFA  | 2          |            |                | 0.24  | 0.15                            |
| CEMI-GGBS | 1          |            |                | 0.28  | 0.30                            |
| CEMI-GGBS | 2          |            |                | 0.17  | 0.21                            |
| CEMI      | 1          | 20         |                | 0.49  | 1.93                            |
| CEMI      | 2          |            |                | 0.60  | 1.15                            |
| CEMI-LF   | 1          |            |                | 1.03  | 2.66                            |
| CEMI-LF   | 2          |            |                | 0.80  | 2.28                            |
| CEMI-PFA  | 1          |            |                | 0.12  | 0.13                            |
| CEMI-PFA  | 2          |            |                | 0.10  | 0.22                            |
| CEMI-GGBS | 1          |            |                | 0.27  | 0.28                            |
| CEMI-GGBS | 2          |            |                | 0.26  | 0.12                            |
| CEMI      | 1          | 5          | 2.0%           | 0.82  | 1.89                            |
| CEMI      | 2          |            |                | 0.54  | 3.72                            |
| CEMI-LF   | 1          |            |                | 0.59  | 5.10                            |
| CEMI-LF   | 2          |            |                | 0.69  | 3.90                            |
| CEMI-PFA  | 1          |            |                | 0.19  | 0.20                            |
| CEMI-PFA  | 2          |            |                | 0.23  | 0.10                            |
| CEMI-GGBS | 1          |            |                | 0.21  | 0.32                            |
| CEMI-GGBS | 2          |            |                | 0.15  | 0.17                            |
| CEMI      | 1          | 20         |                | 0.61  | 2.43                            |
| CEMI      | 2          |            |                | 0.54  | 3.76                            |
| CEMI-LF   | 1          |            |                | 0.85  | 3.03                            |
| CEMI-LF   | 2          |            |                | 0.33  | 5.20                            |
| CEMI-PFA  | 1          |            |                | 0.28  | 0.32                            |
| CEMI-PFA  | 2          |            |                | 0.28  | 0.16                            |
| CEMI-GGBS | 1          |            |                | 0.27  | 0.22                            |
| CEMI-GGBS | 2          |            |                | 0.20  | 0.13                            |

\*Before acceleration: After 24 months of storage in solutions with no applied voltage.

\*\*After acceleration: After applying +100mV continuously for 6 months (See Section 3.6.15).

- **CEMI and CEMI-LF specimens at 5 and 20°C**

The corrosion current densities ( $I_{\text{corr}}$ ) of steel rebars in CEMI and CEMI-LF specimens stored for 720 and 900 (24 normal submersion plus 6 months under

acceleration) days in test solutions at 5 and 20°C is presented in Figure 5.32. The  $I_{\text{corr}}$  values presented here are the average measurements of two samples.

After 720 days of exposure and before acceleration, the corrosion current densities ( $I_{\text{corr}}$ ) values ranged between 0.539 and 0.915  $\mu\text{A}/\text{cm}^2$ , suggesting that all steel rebars embedded in CEMI and CEMI-LF mortar specimens were in an active state (0.5-1  $\mu\text{A}/\text{cm}^2$ ), corresponding to moderate corrosion (Andrade and Alonso, 2001)

CEMI-LF samples showed higher corrosion values than CEMI which may be due to the dilution effect of limestone filler and the higher water to cement ratio. These factors would result in a relatively open pore systems thus allowing chloride penetration in CEMI-LF mortars compared with standard cement, as indicated by diffusion results shown in Section 5.5.2 and as shown in Figure 5.33.

In addition, CEMI-LF samples in SC5 solutions exhibited higher corrosion values compared with those in SC20, probably due to lower chloride binding capacity in case of SC5 mortars compared with those in SC20 (Section 4.5.1 in Chapter 4).

After 180 days of continuous application of +100mV, all samples showed great increase in  $I_{\text{corr}}$  values, as Figure 5.32 illustrates. For mortars stored in SC5 at 5°C, the  $I_{\text{corr}}$  increased from 0.565 and 0.835  $\mu\text{A}/\text{cm}^2$  before acceleration to 4.075 and 4.735  $\mu\text{A}/\text{cm}^2$  after acceleration, which indicated high corrosion rate (Andrade and Alonso, 2001) for CEMI and CEMI-LF. This indicates a reduction by a factor of up to 7 in the corrosion resistance of steel rebar after acceleration.

CEMI and CEMI-LF mortars exposed to SC5 at 5°C showed damage (Section 4.2) due to thaumasite formation (Section 4.5) and this most probably provided open paths for rapid chloride ingress (Slater et al., 2003). The damage also caused a reduction in mortar cover to the steel (Figure 5.5), which probably reduced time for corrosion initiation. Applying +100mV continuously for 180 days accelerated chloride penetration, which rapidly reached the steel surface, as indicated by corrosion measurements. This appears to occur more rapidly in samples that also displayed visual damage (Figure 5.1).

The rate of  $I_{\text{corr}}$  increase after 180 days of acceleration (900 days) depended on whether the specimens were intact or deteriorated. Whereas specimens placed

in SC5 at 5°C which exhibited damage (Figure 5.1) due to thaumasite formation, presented a greatly increase rate in  $I_{corr}$  values than those stored in SC5 at 20°C, which remained intact (Figure 5.2). This increase was approximately 7.2 and 5.7 times (corresponding to values after 720 days) for CEMI and CEMI-LF, respectively, compared with about 2.8 times for those at 20°C.

This damage probably occurred in mortar cover due to thaumasite formation involving open cracks and flaws, contributed in accelerating corrosion risk, as reported by Slater et al., (2003); and also due to more free chloride available in pore solutions due to low chloride binding capacity of deteriorated materials (Section 4.5.1 in Chapter 4), as also suggested by (Glass and Buenfeld, 2000, Glass et al., 2000).

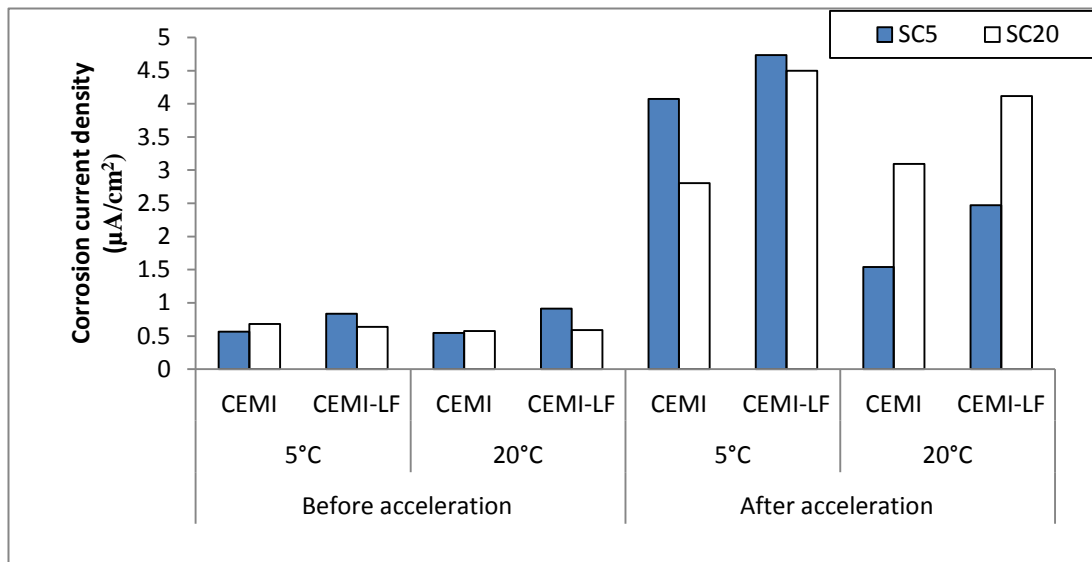


**Figure 5.32.** Variations in corrosion current densities for steel rebars in CEMI and CEMI-LF mortars stored in SC5 and SC20 at 5 and 20°C.

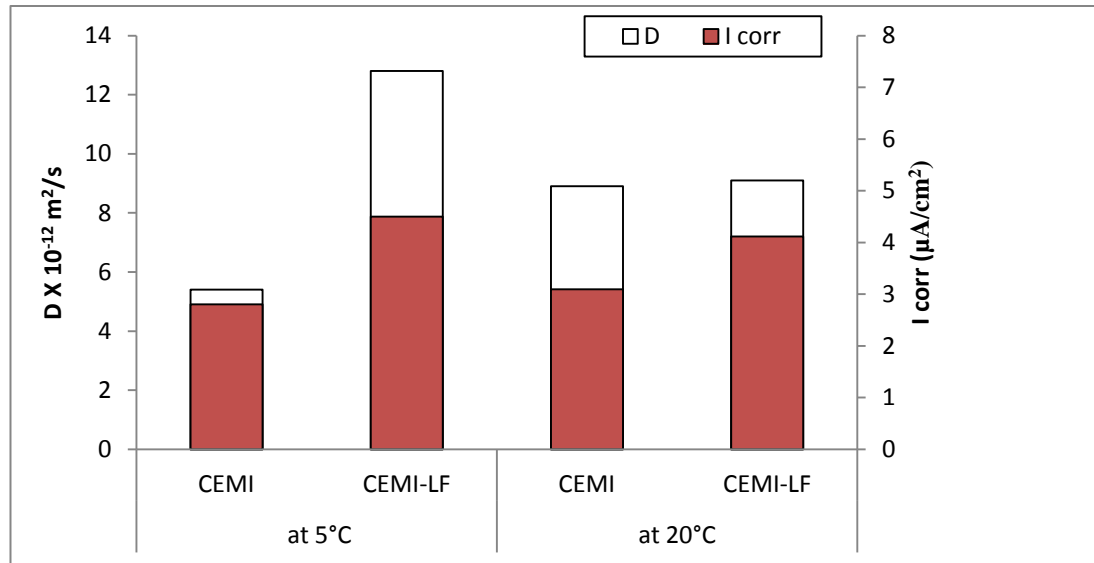


**Figure 5.33.** Corrosion current density ( $I_{corr}$ ) vs. diffusion coefficient (D) for CEMI and CEMI-LF specimens stored in SC20 at 5 and 20°C (Diffusion was calculated after 270 days of exposure, whereas corrosion was measured after 900 days).

- **CEMI-PFA and CEMI-GGBS specimens at 5 and 20°C**

The corrosion measurements of steel rebars embedded in CEMI-GGBS and CEMI-PFA mortars revealed (Figure 5.34 and 5.35) no significant changes in  $I_{corr}$  values before or after acceleration, indicating low activities on the surfaces of steel rebars.  $I_{corr}$  for all samples exhibited values lower than  $0.5 \mu A/cm^2$ , corresponding to low corrosion (Andrade and Alonso, 2001).

Figure 5.34 and 5.35 illustrate that the corrosion resistance of steel bars in CEMI-GGBS and CEMI-PFA mortars showed no change before and after acceleration, indicating no significant amount of chloride reached the steel surfaces. After acceleration, CEMI-PFA and CEMI-GGBS samples stored in SC20 at 20°C exhibited  $I_{corr}$  values of  $0.24$  and  $0.175 \mu A/cm^2$ , respectively, compared with about  $3.1 \mu A/cm^2$  for CEMI sample, indicating 12 to 17 times increase in corrosion resistance of steel rebar in mortars made with PFA and GGBS compared to standard cement (CEMI) mortar.

This high corrosion resistance of steel bars in PFA and GGBS mortars may be related to the depletion of calcium hydroxide and production of extra C-S-H gel, which would cause reduction in open porosity and formation of a more compacted microstructure with passage of time. This would accord with the

porosity, permeability and diffusion measurements described in Sections 5.3 and 5.5.

Based on an extensive experimental work, Claisse (1988) found that concrete with silica fume showed improvement in corrosion resistance and this was primarily attributed to the consumption of calcium hydroxide which was caused by the pozzolanic activity of the silica fume.

Mindess et al. (2003) stated that the reaction of slag and fly ash with calcium hydroxide to form extra calcium silicate hydrate (C-S-H) gel would result in a more homogenous mortar microstructure, with a finer pore size and lower overall porosity. The low corrosion activity of PFA and GGBS samples may also be related to the greater resistivity of concrete/mortar compared with cement replacement materials as reported by Mangat and Molloy (1991).

The beneficial effect of PFA and GGBS replacement on both chloride penetration and reinforcement corrosion was also reported by Page et al. (1986) and Thomas and Matthews (2004). Xu et al. (2013) reported that the partial replacements of cement by PFA and GGBS increase chloride binding and reduced the release of bound chloride when subjected to sulfate attack, decreasing the amount of aggressively free chloride in pore solution.

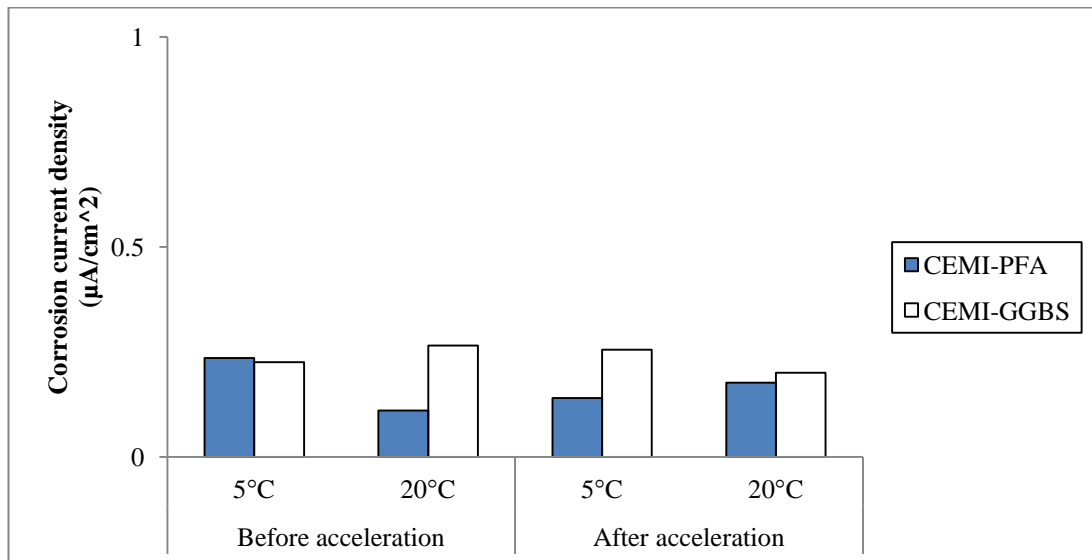


**Figure 5.34.** Variations of corrosion current densities for steel rebars in CEMI-PFA and CEMI-GGBS mortars stored in SC5 at 5 and 20°C.



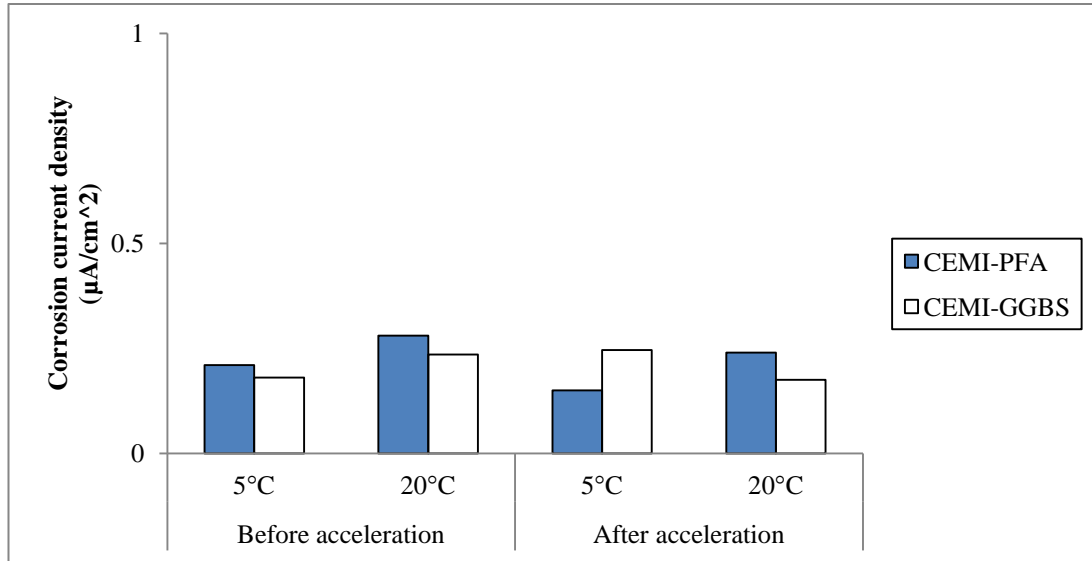


**Figure 5.35.** Variations of corrosion current densities for steel rebars in CEMI-PFA and CEMI-GGBS mortars stored in SC20 at 5 and 20°C.

## 5.9 Visual assessment of steel rebar

At the end of the corrosion experiments and the LPR measurements, the specimens were broken open and the state of the reinforcing rods were visually examined. Figure 5.36 to 5.39 show the appearance of these bars for mortars made with different binders and stored for 900 days in test solutions at 5 and 20°C.

The largest corroded areas were observed on steel rebars embedded in CEMI and CEMI-LF mortars at 5°C, which showed damage due to thaumasite formation (Section 5.2). Steel rebar in CEMI-LF suffered from highest corrosion extent, as indicated by large corroded areas and red rust products appeared on its surfaces.

It can be also observed that the corrosion products were mainly concentrated on the bottom parts of steel rebars in CEMI and CEMI-LF mortars stored in SC5 at 5°C, whereas, pitting corrosion products were distributed in the middle and top parts of the rebar surfaces of SC20 mortars. This indicates that rapid chloride ingress had occurred through the deteriorated materials (Figure 5.5 in Section 5.2).

No steel rebars in any CEMI-PFA and CEMI-GGBS mortars showed visible changes to their surfaces. The dense microstructure produced in case of CEMI-PFA and CEMI-GGBS mortars, probably delayed the ingress of chloride, as

indicated by porosity, permeability and diffusion measurements (Sections 5.3 and 5.5).

Good agreement was found between the measurements obtained by LPR (Section 5.8) and visual assessment of steel rebars, in which the higher corrosion measured, the more corroded areas observed on the surface of steel rebars.

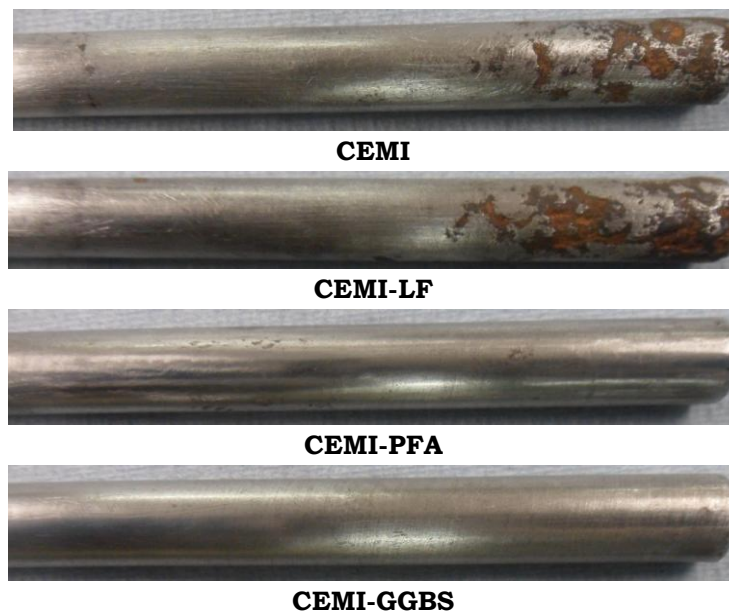


**Figure 5.36.** Surface of steel bars in mortar specimens stored 900 days in SC5 at 5°C.

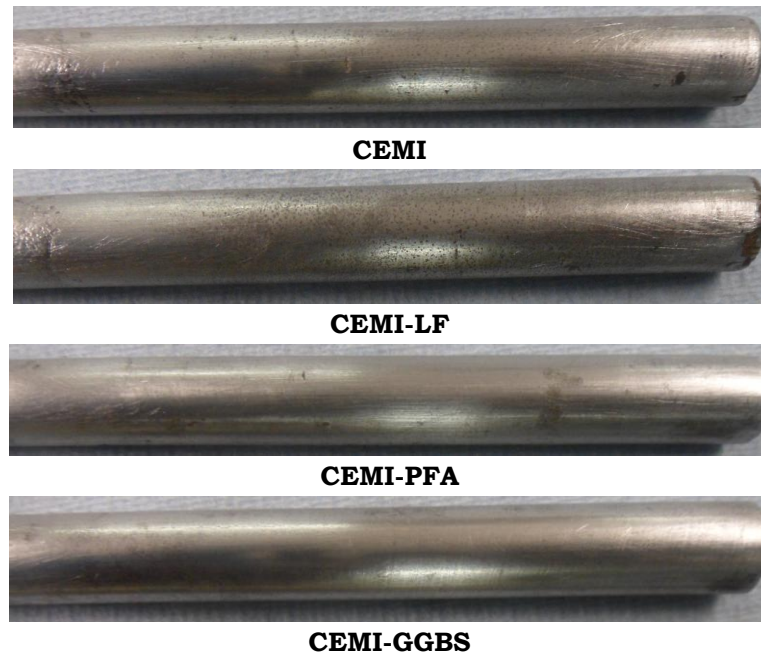


**Figure 5.37.** Surface of steel bars in mortar specimens stored 900 days in SC5 at 20°C.

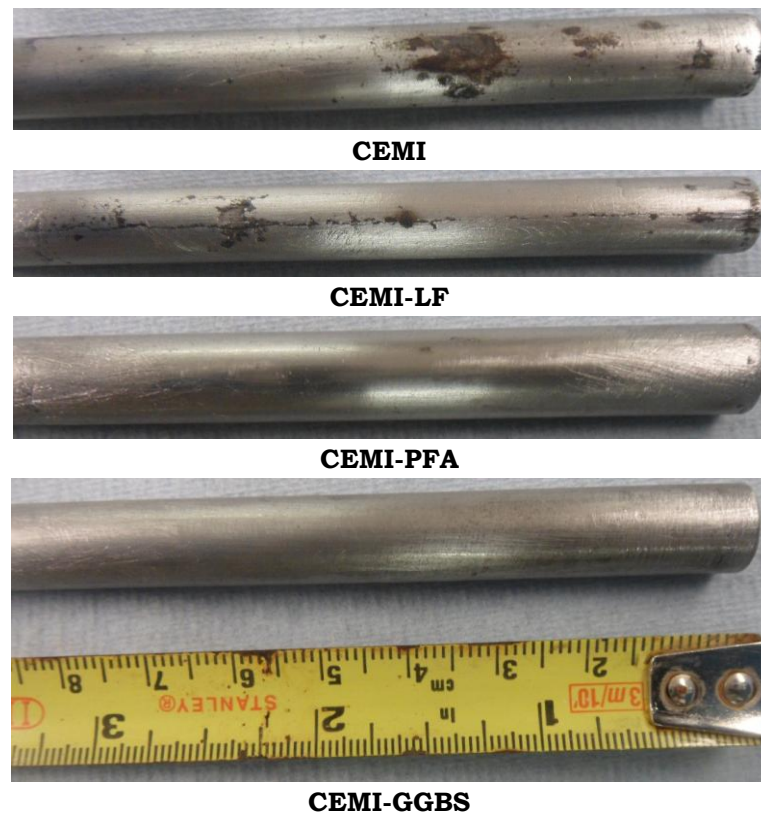


**Figure 5.38.** Surface of steel bars in mortar specimens stored 900 days in SC20 at 5°C

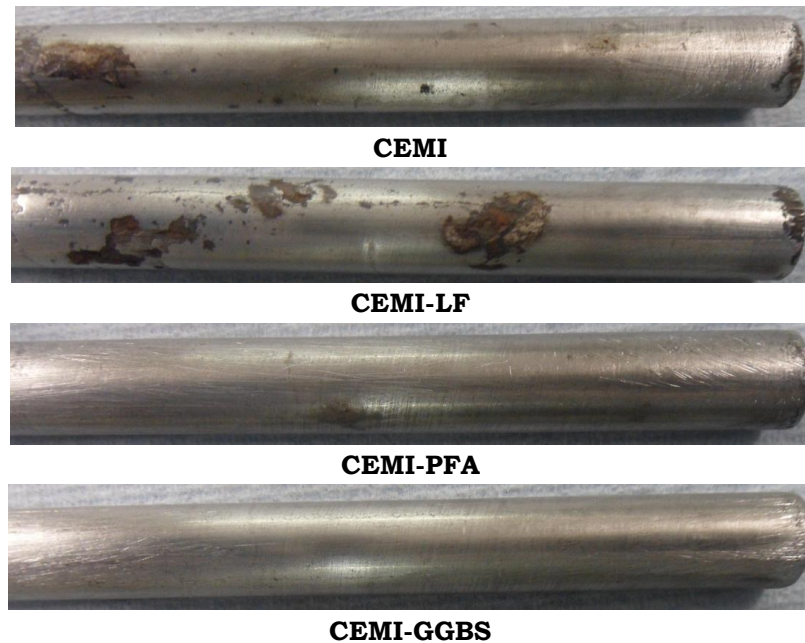


**Figure 5.39.** Surface of steel bars in mortar specimens stored 900 days in SC20 at 20°C

## 5.10 Summary

The main findings of these investigations into chloride induced corrosion risk of steel rebars embedded in cement mortars made with CEMI, CEMI blended with 10%LF, CEMI blended with 50%PFA and CEMI blended with 70%GGBS mortar specimens subjected to combined action of sulfate and chloride in terms of thaumasite form of sulfate attack at 5 and 20°C are presented in this section.

Most of existing research reported in the literature is on the investigation of corrosion risk of steel reinforcement in concrete/mortar exposed to chloride and sulfate exposure at temperature where ettringite and gypsum are the main deterioration sulfate products. Field investigations revealed an increase in corrosion risk of steel reinforcement in concrete suffered from thaumasite sulfate attack. In most of these areas, de-icing salt is considered to be the main source of chloride. Due to the runoff and the subsequent potential variations in chloride concentrations, it was of great interest to investigate the effect of chloride level and the potential sulfate attack on corrosion risk of steel reinforcement in media conducive to thaumasite sulfate attack.

In addition, the use of mineral admixtures such as PFA and GGBS are reportedly effective in preventing TSA at 5°C; however, the presence of chloride

alongside sulfate at low temperature was found to have a negative effect on performance of concrete made with these components. Accordingly, the change in corrosion activity of steel rebars embedded in mortar specimens made with different binders subjected to sulfate and chloride at 5 and 20°C was evaluated by means of linear polarization (LPR) and visual assessment of steel bars. Carbonation depth, permeability, porosity, chloride diffusion and microstructure investigations were also carried out.

The experimental results obtained from this study indicate that the presence of low chloride concentration contaminated with magnesium sulfate solutions and the consequence thaumasite sulfate attack have a negative impact on corrosion resistance of steel reinforcement in mortar. The following findings can be drawn from the results:

- Corrosion specimens showed similar visual observations to those of 50mm cubes (Chapter 4), in which performance of limestone cement mortars stored in combined sulfate and chloride solutions depends on temperature and chloride concentration. Limestone cements mortars stored in solution with 0.5% chloride at 5°C showed deterioration due to thaumasite formation. At 20°C, however, specimens show no such visible damage.
- The higher the extent of damage due to thaumasite formation, the lower the corrosion resistance of steel rebars in mortar, as indicated by visual observation and LPR measurements.
- The presence of 0.5% chloride in magnesium sulfate solution at 5°C led to higher corrosion rate of steel rebars in limestone cement mortars compared with those exposed to composite sulfate and 2.0% chloride solutions, as indicated by LPR measurements and visual assessment of steel bars.
- At 5°C, the higher the limestone replacement, the higher the deterioration of cement mortars and consequently the higher the corrosion rate of steel rebars.
- 10 % replacement by limestone filler led to increase of chloride diffusion, as indicated by diffusion measurement.

- At 20°C, limestone cement mortars stored in composite sulfate and 2.0% chloride solution led to higher corrosion rate than those in sulfate and 0.5% chloride solution.
- Thaumasite affected areas offered open paths available for rapid chloride increase, as indicated by LPR measurements and visual assessment.
- Reduction in chloride binding capacity of thaumasite affected areas may also contribute in increase corrosion risk, by releasing free chloride in pore solution, as indicated by LPR measurements and XRD analysis (Chapter 4).
- Replacement of CEMI by 50% PFA or 70%GGBS enhanced mortar performance such that specimens subjected to composite sulfate and chloride for 900 days in conditions conducive to thaumasite formation, suffered no visually observed damage.
- Reduction of pH value due to replacement by GGBS and PFA (As indicated by pH measurements of test solution given in chapter 4) seemed have no negative effect on the corrosion resistance. However, it seemed that the pH was high enough to protect steel from corrosion, as indicated by presence of portlandite peaks in XRD patterns for interface samples.
- Replacement by 50% PFA had no positive impact on chloride diffusion in the early exposure period (as indicated by diffusion measurements), but could reduce it at longer exposure, as indicated by LPR measurements and visual assessment of steel bars.
- The high chloride binding capacity of fly ash probably led to reduction in the amount of free chloride available in mortar pore solutions and consequently reduced the corrosion risk as indicated by XRD analysis and corrosion assessment.
- Replacement by 70% GGBS caused significant reduction in chloride penetration.
- Replacement by 50%PFA or 70% GGBS enhanced corrosion resistance of steel rebars in all investigated conditions, probably due to refinement of mortar pore structure, as indicated by obtained results of porosity, permeability, LPR, XRD and visual assessment.

- The results revealed that replacement of up to 50% CEMI with PFA improves the performance of concrete exposed to aggressive environment and in condition conducive to thaumasite formation.
- Higher carbonation, feature of mortars made with PFA or GGBS, seems to enhance the resistance to sulfate attack and corrosion risk, as indicated by carbonation and LPR measurements.
- LPR is a fast and reliable technique for evaluating corrosion of steel rebars in concrete/mortar.
- It appears that 70% GGBS and 50% PFA replacement for CEMI refine the pore structure and reduce the chance of potential corrosion of reinforcing steel.

## **6. TSA and related corrosion risk in the presence of chloride: Overall Discussions**

The discussion addresses the objectives of this current study:

- To investigate the role of chloride and its concentration on thaumasite sulfate attack and its sensitivity to chloride concentrations.
- To investigate the mechanism for any effect played by chloride.
- To investigate the impact of TF on chloride binding capacity.
- To investigate the implications of TSA in the presence of chloride on rebar corrosion risk.
- To study the effect of chloride on performance of fly ash and slag cements in environment prone to thaumasite formation.

### **6.1 TSA in presence of chloride:**

As mentioned in chapter 2, the availability of sulfate, calcium, carbonate and silicate in the presence of water in conditions at low temperature promotes the formation of thaumasite (Crammond, 2003). Previous studies have shown conflicting results regarding the effect of chloride on this process, on the one hand mitigation of attack, but on the others enhancement of the attack.

Open system with 10% limestone replacement and relatively high water to cement ratio at 5°C was selected to be investigated as it showed the greatest extent of attack by thaumasite (Sections 4.2 and 4.3). The effect of chloride concentrations on extent of TSA in the different systems incorporating 10 % limestone filler is shown in Figure 6.1 and 6.2 visually and by mass loss, respectively. By both measures, the presence of 0.5% chloride in magnesium sulfate solution accelerates TSA, while the attack is mitigated at higher chloride concentrations (1.0 and 2.0%) present in sulfate solutions.

Based on the results presented in Chapter 4, in which ion diffusion and CH leaching, pH of test solutions and precipitation-dissolution of some solid



phases are sensitive to the concentration of chloride in sulfate solution, the impact of chloride on TSA is schematically proposed in Figure 6.3 to 6.5 and is discussed below:

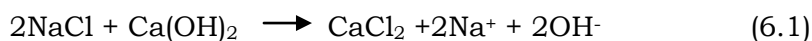
### **6.1.1 Diffusion of sulfate, chloride, magnesium ions, CH leaching and pH change:**

The chemical analysis and pH measurement presented in Chapter 4 indicate that for all the solution at early stage of exposure, leaching of CH from the specimen surfaces leads to an increase in OH and Ca and then the pH. Besides the diffusion of OH and Ca from inside the mortar to the solution, the process also involves diffusion of SO<sub>4</sub>, Mg and Cl from the solution to the mortar.

As Figure 4.107 indicates that the leaching of CH and the consequential OH and Ca ions flow into solutions are sensitive to chloride concentration in solutions, later on the damage in the mortar outer layer caused by sulfate attack.

The effect of low pH of magnesium sulfate solution on sulfate attack is well known process (Gollop and Taylor, 1992). The consequence of penetration by Mg and SO<sub>4</sub> and their interactions with cement paste results in a reduction in the pH of pore solution. When chloride ions present besides magnesium and sulfate ions in test solution, chloride penetrates faster, leading to increase CH leaching and then the pH of pore solution. The amount of CH leaching and the consequential rise in the pH would depend on chloride concentration, in which the higher the chloride concentration in solution, the higher the CH leaching and then the higher to pH.

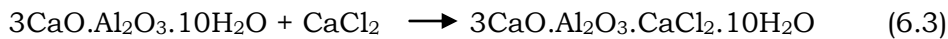
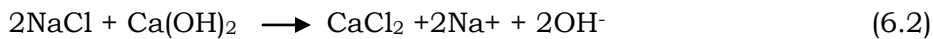
As Figure 4.107 shows, the presence of 0.5% chloride leads to a slight increase in leaching of Ca from CH and pH rise (Figure 4.115). When 2.0% chloride present in solution, however, the penetration of more chloride ions, leads to a rapid increase in the pH, due to higher CH leaching. Saikia et al. (2006) attribute this increase in the pH when chloride present to the release of Na<sup>+</sup> and OH<sup>-</sup> as a result of the rapid reaction between sodium chloride and calcium hydroxide according to equation 6.1.



Besides, these concentration gradients, dissolution- precipitation processes will occur due to the disturbance to the initial thermodynamic equilibrium between the pore solution and the mortar outer layer.

### 6.1.2 Friedel's salt formation

The exposure of cement mortars to magnesium sulfate is known to have destructive effect on the specimens due to the low pH (Liu et al., 2013). When chloride present in addition to sulfate and magnesium ions in solution, the interaction becomes more complicated and appears to depend on chloride concentration. Figure 4.24 and 4.25 indicate that penetration of chloride into the mortar is more rapid than for sulfate. The rapid diffusion of chloride and its interaction with cement paste leads to precipitation of non expansive Friedel's salt (Ekolu et al., 2006). The interactions between sodium chloride and cement paste is given in quotations 6.2 and 6.3 below (Saikia et al., 2006):



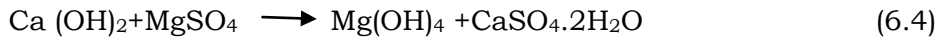
Thus, the higher the chloride concentration, the higher the amount of Friedel's salt formed as shown in Section 4.5.1.

Since, the maintained pH at early exposure period shows dependency on chloride concentration (See Section 6.1.1); this would affect the stability of Friedel's salt. Goñi and Guerrero (2003) point out that Friedel's salt becomes unstable at low pH, which is a value attained when insoluble brucite precipitates at the surface as the XRD results in Figure 4.21 shows. It was also reported by Xu et al. (2013) that Friedel's salt may be transformed to ettringite in presence of sulfate. This agrees with the finding of this study, in which the XRD results in Figure 4.21 showed Friedel's salt was not present in the degraded mortar surface stored in SC5.

The initial rise in pH shown in Figure 4.115 of the SC20 solution appeared from the XRD and SEM, Sections 4.5.1 and 4.6 to benefit the stability of formed Friedel's salt. Therefore, as suggested by Zhang et al. (2013), it is possible that at 2.0% chloride concentration, the amount of Friedel's salt produced could present a physical barrier impeding ingress of chemical specie and it may also result in limiting the availability of aluminates phases free to engage in degrading sulfate bearing products.

### 6.1.3 Gypsum formation

In presence of magnesium sulfate and due to the increase in portlandite dissolution as the temperature decreases, rapid reactions with sulfate and magnesium ions are expected to form gypsum and brucite, both in which as Figure 4.21 shows were found in the degraded materials. The relevant reaction is shown in equation 6.4 (Gaze and Crammond, 2000).



In such conditions (high sulfate concentration), gypsum is reported to form by Bonen and Cohen (1992), Gollop and Taylor (1996) and Santhanam et al. (2001) to be a dominate sulfate product. Since, from Figure 4.21 gypsum was observed in all degraded materials; it is believed to play a role in the deterioration of the surface layer of mortar at early stage of exposure. For its stability, the pore solution would need relatively high Ca and SO<sub>4</sub> ions concentrations and low pH (Zhou et al., 2006). As Figure 4.21 indicates the formation of brucite would offer such a low pH value.

The formation of gypsum would cause damage of the external layer of mortar (Mehta, 1983, Irassar et al., 2003). This observation seems to agree with the early type of deterioration reported in the visual appearance of all attacked mortars. Enhancement of sulfate ingress and acceleration of sample degradation is also believed by Bellmann et al. (2006) to be related to micro-cracking caused by gypsum formation when such high sulfate concentration is involved.

According to visual assessment shown in Section 4.2, this process seems to occur more rapidly in mortar outer layer when 0.5% chloride is present in sulfate solution than in sulfate only solutions. There are two possible scenarios for the enhanced precipitation of gypsum observed in Figure 4.21 and related damage when 0.5% chloride present in solution. The first one is the availability of relatively high Ca concentration in mortar pore solution, due to the relatively high initial leaching of lime as discussed in Section 6.1.1. The high concentrations of sulfate and calcium ions available in mortar pore solution at low pH would promote gypsum formation (Zhou et al., 2006). The second scenario is the possible physical impact of microstructure changes by both rapid decomposition of Friedel's salt and precipitation of gypsum. The absence of Friedel's salt and the deposition of gypsum in the attacked surface layer of SC5 mortar and the presence of Friedel's salt and absence of gypsum in the

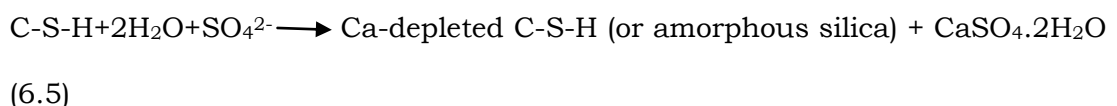
sound core indicated by XRD analysis in Figure 4.25 may support such a process. The rapid propagation of microcracks noted in SC5 mortars result also in exposing further lime to aggressive solution where SC5 mortars showed visual microcracks followed by increase in pH of test solution.

The visual appearance and XRD analysis suggest that presence of 2.0% chloride in solution, however, protects the outer layer of mortars from destructive process of the early gypsum deposition as the conditions for its formation was not attained. As mentioned above, low pH (Zhou et al., 2006) and high sulfate and calcium ions (Bellmann et al., 2006) are required for gypsum to form. In the current study, such chemical conditions were not reached in SC20 mortar pore solution as Figure 4.98 and Figure 4.115 indicate. In addition, the solubility test in Figure 4.121 indicates that gypsum is highly soluble when 2.0% chloride present in solution. The mitigation effect of such high chloride concentration on sulfate attack is reported by Sotiriadis et al. (2013), Zuquan et al. (2007) and Al-Amoudi et al., (1995) to be related to the high solubility of sulfate products in presence of chloride.

#### 6.1.4 C-S-H decalcification

C-S-H can be susceptible to decalcification when high alkalinity of surrounding environment is lost due to the depletion of CH (Bonen and Cohen, 1992). In presence of magnesium sulfate, the consequence of precipitation of brucite described in Section 6.1.5 would cause such a reduction in pH so that ultimately C-S-H would become vulnerable to sulfate attack as Hartshorn et al.(2002), Gaze and Crammond (2000) and Bonen and Cohen (1992) explain. The breakdown of C-S-H gel by magnesium and sulfate ions and the consequence attack is also reported by Hobbs (2003) and Irassar et al. (2003).

Liu et al. (2013) reported that if the pH of pore solution in hydrated cement phases is lower than 11.4, the decomposition of C-S-H will occur and leads to generate silicon and gypsum formation according to the following equation:



Thus, the high pH of SC20 solution, shown in Figure 4.115, protected the CSH from attack as visual observation (Section 4.2) and microstructural analysis (Section 4.6) shows.

### 6.1.5 CaCO<sub>3</sub> solubility

Limestone filler as cement replacement acts as an internal source of carbonate ions in mortar pore solution. The solubility of calcium carbonate was demonstrated in Figure 4.121 to be sensitive to chloride concentrations. The presence of 0.5% chloride in sulfate solutions at both temperatures leads to great increase in solubility and would provide relatively high quantities of carbonate ions in mortar pore solutions. This increase is expected to be even greater in mortar made with cement replaced by 10% limestone filler.

An investigation by Duan and Li (2008) showed that calcite solubility increased as chloride concentration increased up to a certain amount and then decreased. In this study, in which sulfate was also present, the calcite has higher solubility in combined sulfate and 0.5% chloride solution than solution containing combined sulfate and 2.0% chloride, as Figure 4.121 shows.

### 6.1.6 Thaumasite formation

All the results including visual assessment, pH, and chemical analysis of test solutions, SEM/EDX, XRD and IR provide supportive evidence for the sensitivity of the degradation of attack due to TSA to chloride concentrations. Based on the above discussion and proposed interactions given in Figures 6.4 and 6.5, the possible scenario of the role of chloride on thaumasite related attack can be summarised below:

Due to the very slow kinetics of thaumasite formation (Schmidt et al., 2009), usually it would be preceded by formation of conventional sulfate product (Barcelo et al., 2014). Thus, exposure to relatively high magnesium sulfate solution similar to that used in this study would lead to often initial stage attack by gypsum deposition as Bellmann et al.(2006) suggest. A study by Gaze (1997) suggested that some gypsum is required before thaumasite can form. In the current study, the precipitation of gypsum at early stage of exposure indicated by XRD finding in Figure 4.21 is believed to contribute to the later degradation due to thaumasite formation; either by providing more sulfates ions in the pore solution for additional thaumasite formation, as mentioned by Schmidt et al. (2008) and Irassar et al. (2005) or due to the degradation caused by gypsum deposition or both. This would cause opening up of the microstructure of cement mortars at the early stages of attack, which appears to be a prerequisite for thaumasite formation, as reported by

Ramezaniyanpour and Hooton (2013). The importance of such physical attack on the outer layer of the specimens but due to the formation of ettringite on thaumasite formation when sodium sulfate is used as exposure solution, as reported by Schmidt et al. (2009).

The presence of chloride in sulfate solutions results in Friedel's salt which appears to play a role in early attack, depending on its amount and stability. Figure 4.1 suggests that the presence of 0.5% chloride in solution accelerates the early attack, possibly due to both Friedel's salt decomposition and gypsum precipitation shown in Figure 4.21, which is affected by a maintained pH below 11. According to Figure 4.21, Friedel's salt is not stable at such low pH and gypsum formation is favoured. However, the relatively high early Friedel's salt produced and its relatively high stability at the pH when 2.0% chloride is present in solution seems to benefit against sulfate attack. Such a Friedel's salt could present a physical barrier that delays access of chemical species as suggested by Zhang et al. (2013). This would reduce the chances of gypsum formation as noted by Schmidt et al. (2008) and Bellmann et al. (2006) as relatively low sulfate and calcium ions concentrations available in mortar pore solution as Figure 4.98 and 4.99 indicate. This may also result in limiting the availability of aluminates phases free to engage in degrading sulfate bearing products (Tosun-Felekoğlu, 2012, Irassar et al., 2005). It was reported by Irassar et al. (2005) in a study conducted to investigate the effect of C<sub>3</sub>A content of cement on thaumasite formation, that cement with zero C<sub>3</sub>A, such as SRPC and containing limestone filler showed no thaumasite formation which was also supported by Zhou et al. (2006). The formation of gypsum shown by Figure 4.24 in core specimens in sulfate only solution and instead Friedel's salt seen in Figure 4.25 in composite sulfate and chloride specimens may reflect the operator of such a pore blocking effect of Friedel's salt formation.

The silicon and calcium ions generated in pore solution from the decomposition of C-S-H are required for thaumasite to form (Thaumasite Expert Group, 1999, E.F. Irassar et al, 2005, Hobbs, 2003, Grammond, 2003). The attack of C-S-H seen in Figure 4.50 appears to be enhanced when 0.5% chloride is present in sulfate solution, as indicated by massive change in its microstructure and the transformation of C-S-H later towards thaumasite. However, the stability of C-S-H when 2.0% chlorides present in sulfate solution is most likely due to the maintained high alkalinity at early exposure time as Figure 4.66 and 4.35 shows.

An increase in limestone replacement was found to increase the extent of thaumasite attack, which is attributed to the increase of carbonate ions in pore solution as carbonate content increases. The effect of limestone filler replacement on thaumasite formation is well documented by Torres et al. (2003), Torres et al. (2006) and Kakali et al.,(2003) and further confirmed in the current study.

However, the presence of chloride appears to play a similar role but depends on its level in solution, as indicated by solubility test and extent of damage. The solubility of calcium carbonate was found to be sensitive to chloride concentrations in sulfate solution as Figure 4.121 shows. The presence of 0.5% chloride in sulfate solutions leads to relatively large increase in its solubility, which may provide relatively high quantities of carbonate ions in mortar pore solutions, needed for thaumasite formation as reported by Torres et al. (2006). The availability of carbonate ions in pore solution would reduce as the chloride concentration increases, as indicated by the solubility test.

Besides the role of pH on stability and dissolution- precipitation of some important phases as mentioned above, pH has a significant role in thaumasite formation. It is suggested by Collett et al. (2004) and Crammond (2003) that high pH (More than 10.5) is needed for thaumasite formation. Accordingly, such an increase in the pH as observed in the current study (Figure 4.115) would also encourage thaumasite formation. Chloride can increase the pH of pore solution due to its chemical binding with cement paste and the consequent release of hydroxyl ions.

The acceleration effect of 0.5% chloride on precipitation of thaumasite which is the main deterioration product, can be attributed to: (1) Friedel's salt decomposition and gypsum formation (2) Availability of appropriate alkaline solution (3) Availability of significant concentration of carbonates  $\text{CO}_3$  due to high solubility of calcium carbonate (4) Availability of high sulfate and calcium ions (5) Availability of silicate and calcium ions, from the decomposition of the C-S-H. However, the mitigation effect when 1.0 and 2.0% chloride are present in sulfate solution is greatly related to the maintained high pH and stability of Friedel's salt at early exposure stage.

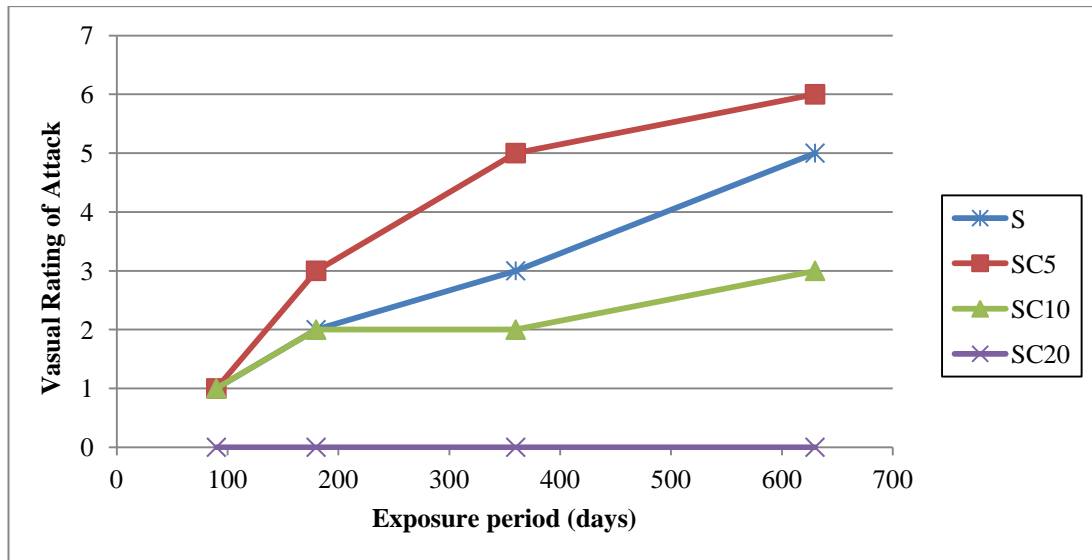


**Figure 6.1.** Evaluation of damage degree as indicated by visual appearance of mortar specimens. [0= No visible damage, 1= minor cracking to corners and edges, 2= moderate damage at corners and edges, 3= severe attack at corners, 4= cracking and spalling, 5= swelling of surfaces, and 6=extensive cracking and swelling].

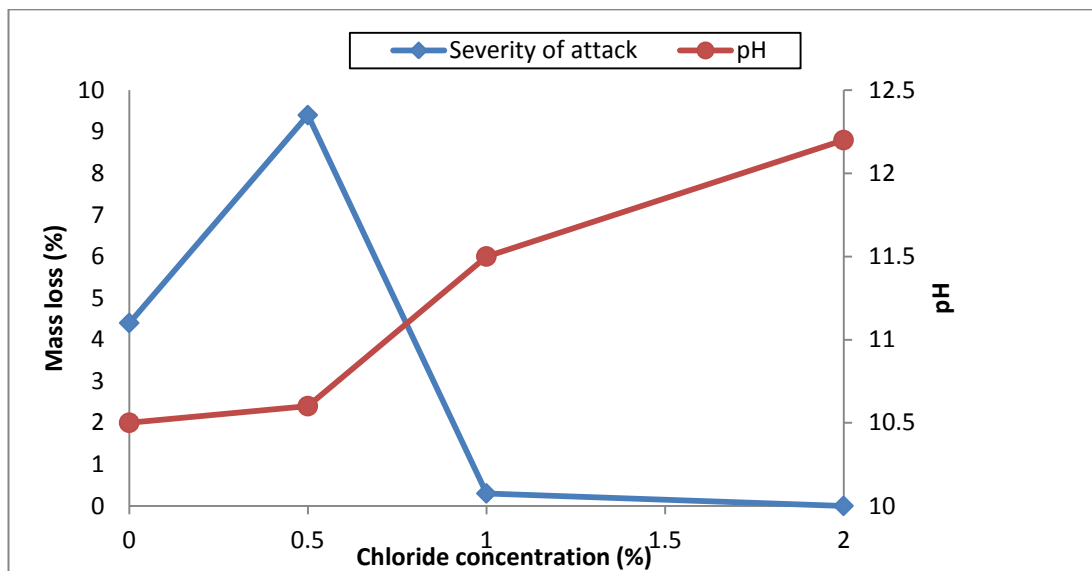


**Figure 6.2.** Effect of chloride level on initial pH change and later severity of TSA of CEMI-LF stored 630 days in solutions at 5°C.



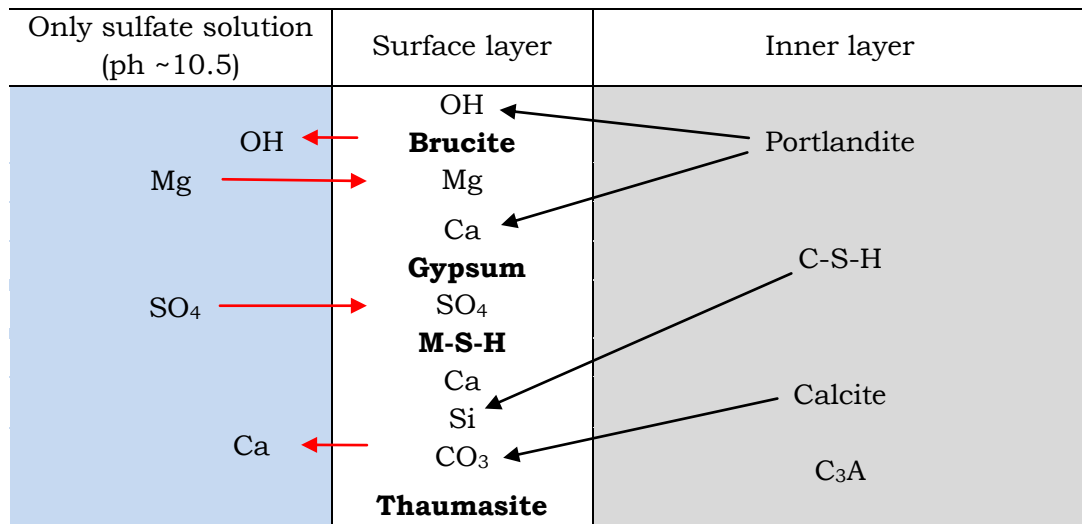


**Figure 6.3.** Scheme for sulfate interaction between limestone cement components and magnesium sulfate solution at 5°C (A modified schematic proposed by Bonen and Cohen (1992)).

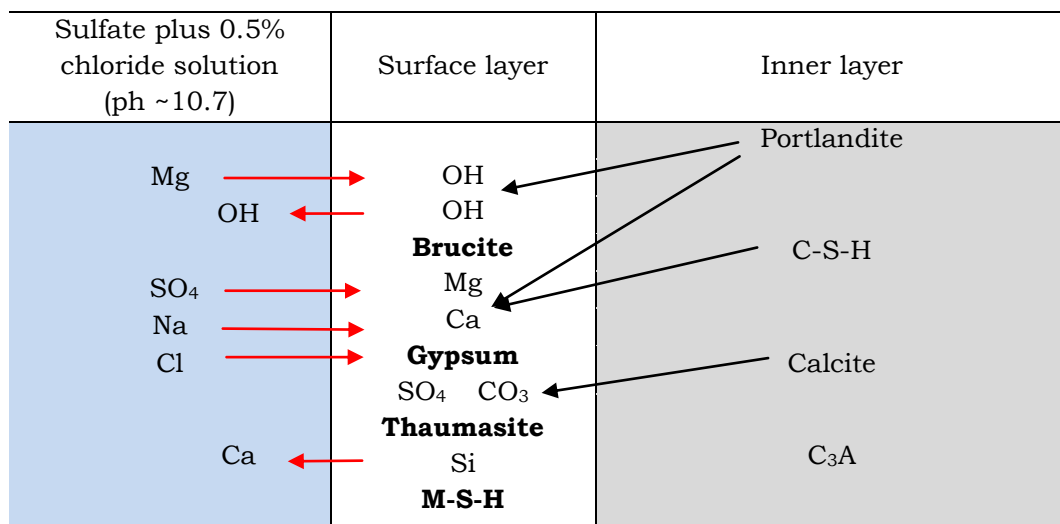


**Figure 6.4.** Scheme for sulfate and chloride interaction between limestone cement components and composite sulfate and 0.5% chloride solution at 5°C.

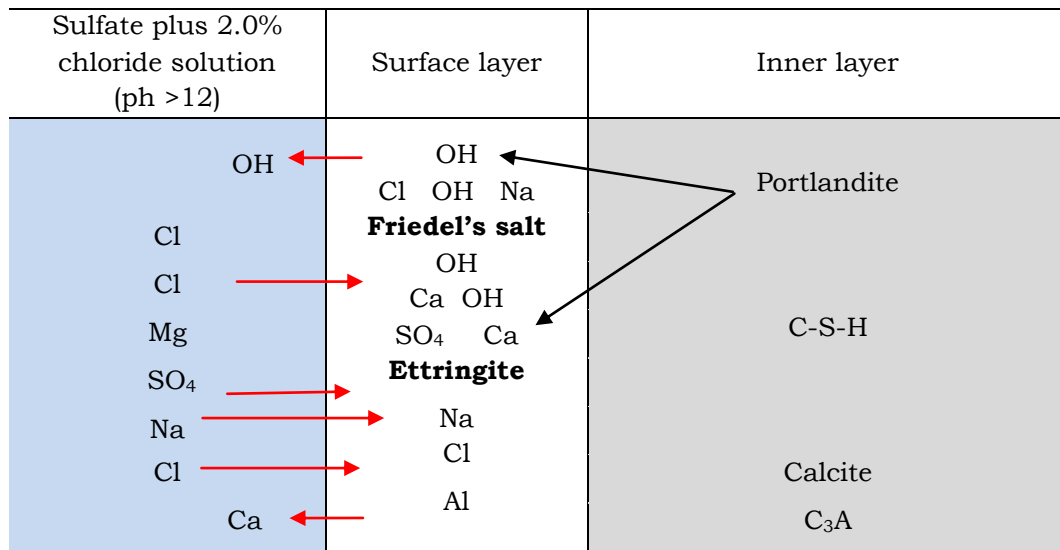


**Figure 6.5.** Scheme for sulfate and chloride interaction between limestone cement components and composite sulfate and 2.0% chloride at 5°C.

## 6.2 The effect of TSA on chloride binding capacity of cement and related corrosion risk

As mentioned in Chapter 2, chlorides react chemically with tricalcium aluminate (C<sub>3</sub>A) or its hydrates to form calcium chloro-aluminate, C<sub>3</sub>A·CaCl<sub>2</sub>·10H<sub>2</sub>O, known as Friedel's salt, and can also physically bind due to its adsorption on the surface of C-S-H. The high ability of cement matrix to bind chloride is known to benefit in reducing corrosion risk of concrete steel reinforcement. As soon as the bound chlorides are released to form free chloride ions in the pore solution of concrete, they would present a corrosion risk similar to the aggressive free chloride ions (Glass and Buenfeld, 2000).

According to Figure 6.6, the relative peak intensity of Friedel's salt, evaluated by XRD analysis in Figure 4.21, in the surface layer of mortars made with CEMI blended with 10% limestone filler is decreased as the extent of thaumasite attack increases, as assessed by mass loss in Section 4.3. The observation of Friedel's salt in the sound core in Figure 4.25, but not in the degraded surface layer indicates its instability in presence of thaumasite.

The C-S-H gel of cement matrix as indicated by microstructural analysis shown in Figure 4.21 is also affected by thaumasite sulfate attack in which the specimen's surface matrix has converted into thaumasite, leading to porous, cracked and permeable matrix as indicated by corrosion results in Section 5.8. This would also result in an increase of  $\text{Cl}^-/\text{OH}^-$  ratio hence increasing the risk of corrosion as reported by Beaudoin et al. (1990) and Kayyali and Haque (1988). The increase of  $\text{Cl}^-/\text{OH}^-$  ratio in pore solution in mortars affected by thaumasite formation should contribute to increased corrosion risk observed in this study, Sections 5.8 and 5.9.

The degradation of concrete/mortar cover due to thaumasite formation aids chloride ingress and a negative impact on corrosion resistance as Figure 5.32 indicates. This can be attributed to; low resistance to chloride diffusion due to the damage inflicted in the matrix that open cracks and flaws as suggested by Wimpenny and Slater (2003) and Slater et al. (2003); and due to increase in free chloride as discussed above.

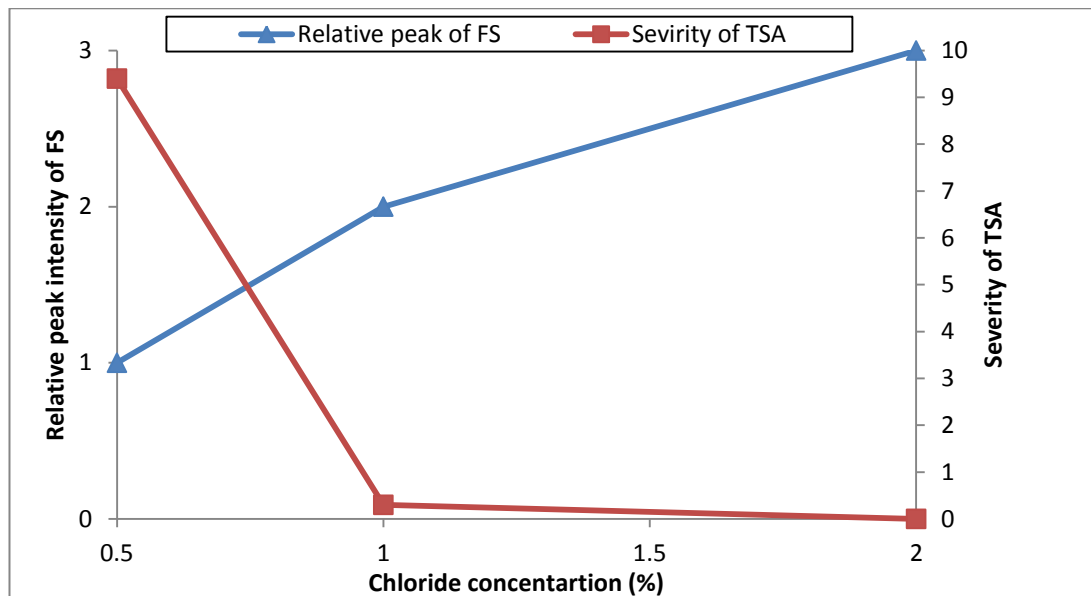


**Figure 6.6.** Severity of TSA (By mass loss) and relative peak height of Friedel's salt (FS) in surface materials for CEMI-LF mortars stored 630 days at 5°C. (Scale of relative peak intensity for FS: 1= low or absence; 2=moderate; and 3= high).

### **6.3 The use of fly ash and slag as cement replacement to prevent TSA in presence of chloride:**

Effectiveness of fly ash and slag cements against sulfate attack is frequently reported (Kandasamy and Shehata, 2014, Veiga and Gastaldini, 2012, Atahan and Dikme, 2011) to be related to the consumption of portlandite, as portlandite is not stable in presence of sulfate ions. Bellmann and Stark (2008) reported that in the absence of calcium hydroxide, the C-S-H has a much lower calcium/silicon ratio and a higher resistance against the formation of thaumasite.

In this study, open systems, in which relatively high water to binder ratio of 0.6 was used to accelerate the interaction, containing 50% PFA or 70% GGBS offered good resistance to TSA up to 630 days in salt solutions. However, microstructural investigations using XRD and SEM revealed that with time these systems could be subject to conventional form of sulfate attack, namely gypsum as all conducive conditions, including low pH, availability of Ca and high concentration of sulfate ions in pore solution, are available for its promotion.

The decalcification of C-S-H appears to be main source of calcium ions in pore solution. Due to the consumption of CH and under exposure to magnesium sulfate solution, the C-S-H gel produced in pozzolanic reaction of slag and fly ash would be subjected to attack by sulfate and magnesium ions to form M-S-H and gypsum as SEM images show in Figure 4.95 and as confirmed by EDX analysis in Figure 4.96 and 4.97.

The delay in the attack is probably attributed to low porosity and permeability (Section 5.3), due to pozzolanic reaction and the consequential portlandite consumption as Figure 4.27 and 4.28 indicate.

Superior performance against sulfate attack was observed where cement mortars incorporated 50% fly ash, in that no visual damage was observed in any samples after 630 days in any test solutions at both temperatures as Figure 4.9 shows. However, as Figure 4.27 indicates the deposition of gypsum in the surface layer of mortar revealed vulnerability eventually to conventional sulfate attack. This was confirmed in 20mm cubes shown in Figure 4.5 and the process may progress to thaumasite sulfate attack as microstructural analysis given in Figure 4.77 shows small traces of thaumasite were also formed in fly

ash mortars at 5°C. A long term laboratory investigation by Abubaker et al. (2014) reported the susceptibility of fly ash concrete to TSA.

The presence of chloride has different effect on performance of fly ash and slag mortars as visually observed in Figure 4.8 and indicated by XRD analysis shown in Figure 4.27 and 4.29. The presence of 0.5% or 2.0% chloride in sulfate solution leads to a further improvement in the performance of PFA mortar samples against sulfate attack. This may be attributed to the high aluminate contents in its composition that provides high capacity for chloride binding. This binding in form of Friedel's salt probably blocks pores and reduces the chance for the destructive interactions between aluminates and sulfate ions as discussed in Section 6.1.2.

CEMI blended with 70% slag specimens also performed well against sulfate attack, they did not show any visual damage within 630 days of exposure to any test solutions at both temperatures. However, microstructure analysis revealed that GGBS specimens would be subjected to conventional form of sulfate attack, as this was also confirmed in Figure 4.95 using 20mm specimens.

Gollop and Taylor (1996) report that the C-S-H gel of slag is subjected to attack by magnesium ions when specimens exposed to magnesium sulfate solution. The consequence are this is to increase the concentration of calcium ions in mortar pore solution, which with sulfate ions at low pH would promote gypsum formation. As chemical analysis of test solution in Section 4.7 shows, the greater reduction in magnesium and sulfate concentrations and the following calcium release observed in sulfate solution of slag specimens compared to fly ash, indicate the higher vulnerability of C-S-H of slag cement to attack than for fly ash C-S-H and this may also explain why slag cement showed earlier damage compared to fly ash mortar, even in the presence of chloride.

The decalcification of calcium silicate hydrate gel of slag was much more extensive than in fly ash as indicated by increase of calcium concentration at early stage of immersion in sulfate solution in Figure 6.7 and later attack by gypsum. The consequent decomposition of C-S-H by Mg would release calcium ions to the pore solution.

However, the microstructure analysis shown in Figure 4.29 of the outer layer of specimens in sulfate only and composite sulfate and 0.5% chloride solution at 5°C also showed clearly gypsum deposition. The extent of attack of 20mm

mortar due to gypsum precipitation was more severe in presence of 0.5% chloride than for only sulfate solution. This may also reflect the further enhancement of C-S-H gel attack of slag cement when 0.5% chloride is present in solution, which provided more calcium available for gypsum precipitation. Once more, the relatively high solubility of gypsum when 2.0% chloride is present in solution seen in Figure 4.121 probably controlled the gypsum formation in the mortar outer layer placed in solution with 2.0% chloride, as discussed above.

As explained above, the presence of 0.5% chloride in sulfate solution negatively affected the performance of 20 mm mortars incorporating 70% slag. Microstructural analysis in Figure 4.95 of damaged surface shows this was related to intensive precipitation of prismatic gypsum crystals around the aggregate and within cement matrix. The decalcification of C-S-H gel by magnesium in regions close to this gypsum is the most probable source of the calcium required. This process appears to have occurred more rapidly when 0.5% chloride is present in solution, which showed early visual deterioration due to gypsum deposition. Attack due to growth of gypsum crystals in presence of such high sulfate concentration was also reported by Bellmann et al. (2006).

High slag replacement level produced secondary C-S-H gel with lower calcium/silica ratio which was capable of bind more alumina in its structure which resulted in reduced ettringite formation, as explained by Gollop and Taylor (1996). In presence of chloride, this would also cause a reduction in the amount of formed Friedel's salt, which may explain why slag exhibited a lower amount of Friedel's salt, as shown in Figure 4.29.

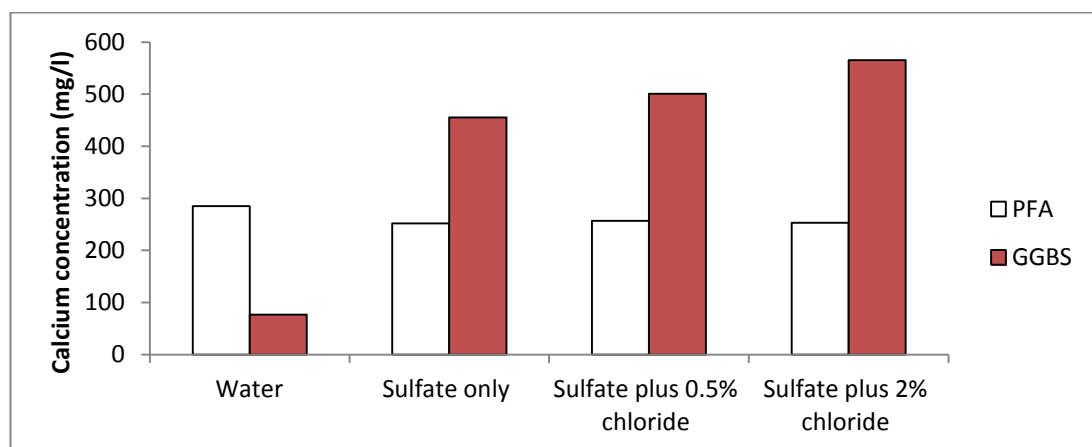


**Figure 6.7.** Calcium concentration in different solutions after 7 days exposure at 5°C.

## 7. Conclusions and recommendations

### 7.1 Overall Conclusions

Most available research reported in the literature concerns the investigation of the effect of chloride on sulfate attack at 20°C, in which ettringite would be the main deterioration product. Furthermore, an extensive literature search identified very few available laboratory studies into the effect of chloride on sulfate attack at low temperatures and under conditions conducive to thaumasite formation. In addition the existing studies appear to give contradictory results with Sotiriadis et al. (2012 and 2013) indicating mitigation of attack, whereas Torres (2004) enhancement of attack.

Concerning the corrosion risk of concrete reinforcement, field investigations led by Wimpenny and Slater, (2003) to propose that this may increase during thaumasite sulfate attack. However, due to the sensitivity of TSA to chloride concentration, the role of chloride concentration on damage of concrete cover due to thaumasite formation and the consequence attack on corrosion risk needs also to be taken into consideration.

Although the use of PFA and GGBS as cement replacement are reportedly effective in delaying or preventing TSA at 5°C, the presence of chloride alongside sulfate at low temperature was found by Sotiriadis et al. (2013) to have a negative effect on the performance of concrete made with these components.

Accordingly, the role of chloride on performance of CEMI, CEMI blended with 10%LF, CEMI blended with 50%PFA and CEMI blended with 70%GGBS mortar specimens subjected for 630 days to combined action of sulfate (0.6%  $\text{SO}_4^{2-}$  as magnesium sulfate) and chlorides (0.5, 1.0 and 2.0%  $\text{Cl}^-$  as NaCl) in terms of thaumasite form of sulfate attack at 5 and 20°C were evaluated.

The experimental results obtained from the current study indicate the complexity of the chemical interactions of chloride at various concentrations. The major findings can be drawn from the obtained results are:

- The impact of chloride on sulfate attack depends on the exposure temperature as it mitigates classical form of sulfate attack at 20°C, but it can enhance the thaumasite form of sulfate attack at 5°C (See Figure 4.8), which is in agreement with the findings of Torres (2004).
- Chloride acts as a catalyst in thaumasite formation. This is confirmed by the absence or low peak of Cl in the SEM-EDX (Figure 4.53) analyses of thaumasite, which supports the finding by Torres (2004).
- The extent of thaumasite sulfate attack (TSA) depends on temperature, carbonate content and chloride concentration, as Figure 4.8 illustrates.
- At low temperature (5°C) and as can be seen in Figure 4.8, the presence of low (0.5%) chloride combined in a DS4 (BRE Ground aggressivity Class) sulfate in ground water can lead to severe damage due to thaumasite formation. The extent of damage decreases as the chloride concentration increases. This is probably due to the complexity of the chemical interactions at various concentrations.
- The extent of damage increases as the carbonate content increases, which is probably because the greater availability of carbonate facilitates more thaumasite formation.
- At ambient temperature (20°C) and as shown in Figure 4.72, the presence of low (0.5%) chloride in sulfate solution can also lead to attack due to thaumasite formation in limestone cement mortars, but with lower damage extent compared to that at 5°C.
- The solubility of calcite is found to be sensitive to chloride concentration (Figure 4.121). Calcite solubility is increased at low (0.5%) chloride concentration leading to greater availability of carbonate ions in the pore solution which results in rapid thaumasite formation. At higher chloride concentration, calcite solubility is reduced, favouring the formation of Friedel's salt (Figure 4.63) which may further reduce chemical ingress/interaction through a physical barrier effect as reported by Liu et al.(2013).
- Early gypsum precipitation (Figure 4.1) under low chloride (0.5%Cl-) conditions is believed to contribute to the rapid thaumasite formation; either by acting as a prerequisite for thaumasite formation, as mentioned by Schmidt et al. (2008) and Irassar et al. (2005) and/or by causing opening up



of the cement microstructure at the early stages of the attack, which would increase the access for reactive ions, as reported by Ramezani pour and Hooton (2013).

- The mitigation effect when high chloride (1.0% and 2.0% chloride) levels combined with high sulfate DS4 solution on TSA can be attributed to; 1) Initial leaching of calcium hydroxide which would raise the alkalinity (Figure 4.115) of pore solution and make the cement hydration products more stable, 2) High gypsum solubility (Figure 4.121), which would cease the negative effect of gypsum formation, 3) Low calcite solubility (Figure 4.121) which would reduce the availability of carbonate ions in pore solution, 4) Formation and stability of Friedel's salt (Figure 4.63) which may further reduce chemical ingress/interaction through a physical barrier effect.
- The presence of low (0.5%) chloride concentration combined in a DS4 (BRE Ground aggressivity Class) sulfate in ground water can also lead to reduction in service life of concrete structures due to the damage to the concrete covering the steel reinforcement by thaumasite formation (Figure 5.1). This would provide increased access for chloride penetration (Wimpenny and Slater, 2003) and a commensurate increase in chloride ions in pore solution, both leading to increased corrosion risk as Figure 5.32 shows.
- The use of slag and fly ash as cement replacements probably delays sulfate attack (Figure 4.9), because of the consumption of calcium hydroxide (Figure 4.27 and Figure 4.29) and pore refinement Figure 5.9. However, concrete made with these cements and exposed to aggressive conditions of DS4 as magnesium sulfate at low temperature would be subjective to conventional form of sulfate attack (Figure 4.83), namely gypsum, rather than TSA, probably due to: 1) Low alkalinity of pore solution (Figure 4.117), 2) The availability of high sulfate ions, 3) The availability of high calcium ions in the pore solution, as a result of C-S-H decalcification 4) The absence of enough carbonate ions in the pore solution.
- In conditions conducive to thaumasite formation, the use of slag and fly ash as cement replacement enhances the physical properties of concrete/mortar against chloride penetration Figure 5.9. Consequently corrosion resistance of concrete reinforcement is increased (Figure 5.36). This enhancement can be attributed to: 1) pore refinement due to pozzolanic reaction; 2) reduction in

chloride diffusion; and 3) increase in chloride binding capacity, particularly in fly ash cement.

- The presence of chloride combined in a DS4 magnesium sulfate in ground water can lead to further enhancement of sulfate resistance of fly ash concrete, probably due to the positive effect of high chloride binding capacity (Figure 4.27) of fly ash cement. However, the presence of chloride enhances lime leaching (Figure 6.7) of GGBS cement, providing more calcium ions required for gypsum precipitation (Figure 4.95). At high chloride concentration (2.0%) and due to high gypsum solubility (Figure 4.121), no gypsum can be formed.

## **7.2 Implications of Results for Research and Engineering**

This research has provided new data on the role of chloride on thaumasite form of sulfate attack. From the engineering point of view, the key findings and implications of this research are as follows:

- Besides increased levels of sulfate ions present in the ground due to the oxidation of pyrite (TEG, 1999) which is proposed (Zhou, 2006) as a primary cause of the deterioration observed in field studies (as found in the M5 motorway bridge foundations), chloride (mainly due to using de-icing salts during winter times) could also have a serious implication on observed deterioration.
- Current specifications (BRE Special Digest 1: 2005), however, do not sufficiently take into consideration the possible adverse effects of chloride ions in groundwater on concrete structures in cold conditions. Since, both chloride and sulfate may be present in ground water at various concentrations depending on de-icing salt run-off, updated standards with regard to the effect of chloride on sulfate attack at low temperature and in conditions conducive to thaumasite formation should be considered.
- The low/non chloride binding capacity of thaumasite means that where TSA has occurred, the reinforcement corrosion is increasingly vulnerable to damage. An additional implication of a poor binding capacity of

thaumasite is that physically adsorbed chloride on C-S-H would be released into the pore solution (because C-S-H can be transformed to thaumasite), which would also lead to increased corrosion risk.

- Due to the reduction of chloride binding capacity of thaumasite-affected concrete and its poor resistance to chloride penetration, the current experimental study supports the recommendation by TEG (1999) that the thickness of TSA affected concrete should be discounted from any consideration of future durability.

### **7.3 Recommendations for Future Work**

According to the results obtained in this research, the following are suggested for further study:

- The assessment of TSA on corrosion resistance was evaluated in this study by a combination of individual assessments by LPR measurements and observation of visual damage. However, monitoring of concrete/mortar deterioration due to thaumasite formation with time by means of electrochemical impedance spectroscopy (EIS) would benefit the determination of the extent of damage due to thaumasite formation on corrosion resistance of concrete reinforcement. Since, several different parameters involved and due to the time limitation, such an application could not be applied in the current study.
- It is important to investigate concrete/mortars with different water to binder ratio in order to generate conclusion about the role of chloride of sulfate attack at low temperature. In the current study, water to binder ration of 0.6 was selected to accelerate chemical diffusion and interaction, thus allowing identification of any potential reactions within a shorter time frame.
- It would be also of great interest to study the role of chloride on performance of SRPC cement in conditions conducive to thaumasite formation, since, it has zero  $C_3A$ .
- Besides experimental data obtained by this study, thermodynamic modelling would help in understanding the role of chloride on sulfate attack in conditions conducive to thaumasite formation at low temperature.
- It would be beneficial if chemical analysis with regards to various ions concentration could be done on extracted pore solutions of concrete/mortar

exposed to combined action of sulfate and chloride in environment prone to thaumasite with time formation, which would further help in understanding the role of chloride ions on TSA. Such an application requires special squeezing equipment which was not accessible.

- Different concentration of chlorides (from 0.1 to 1% Cl) and sulfate solutions should be studied to identify the optimum chloride concentration for thaumasite formation.
- According to BRE (Special Digest 1: 2005), sulfate can be present in ground conditions in different concentrations. This may lead to different interactions with chloride on TSA. Due to the possible availability of SD4 sulfate in aggressive ground conditions and due to the time restriction, SD4 was the only composition selected in this study.

## References

- ABUBAKER, F., LYNSDALE, C. & CRIPPS, J. 2014. Laboratory study of the long-term durability of buried concrete exposed to Lower Lias Clay. *Construction and Building Materials*, 64, 130-140.
- AI-AMONDI, O. S. B., MASLEHUDDIN, M. 1993. THE EFFECT OF CHLORIDE AND SULFATE IONS ON REINFORCEMENT CORROSION. *CEMENT and CONCRETE RESEARCH*, 23, 139-146.
- AL-AMOUDI, O. S. B. 1995. Performance of 15 reinforced concrete mixtures in magnesium-sodium sulphate environments. *Construction and Building Materials*, 9, 149-158.
- AL-AMOUDI, O. S. B., MASLEHUDDIN, M. & ABDUL-AL, Y. A. B. 1995. Role of chloride ions on expansion and strength reduction in plain and blended cements in sulfate environments. *Construction and Building Materials*, 9, 25-33.
- AL-AMOUDI, O. S. B., RASHEEDUZZAFAR & MASLEHUDDIN, M. 1991. Carbonation and corrosion of rebars in salt contaminated OPC/PFA concretes. *Cement and Concrete Research*, 21, 38-50.
- AL-TAYYIB, A. J. & SHAMIM KHAN, M. 1991. Effect of sulfate ions on the corrosion of rebars embedded in concrete. *Cement and Concrete Composites*, 13, 123-127.
- AL-TAYYIB, A. J., SOMUAH, S. K., BOAH, J. K., LEBLANC, P. & AL-MANA, A. I. 1988. Laboratory study on the effect of sulfate ions on rebar corrosion. *Cement and Concrete Research*, 18, 774-782.
- ANDRADE, C. & ALONSO, C. 2001. On-site measurements of corrosion rate of reinforcements. *Construction and Building Materials*, 15, 141-145.
- ARYA, C., BUENFELD, N. R. & NEWMAN, J. B. 1990. Factors influencing chloride-binding in concrete. *Cement and Concrete Research*, 20, 291-300.
- ARYA, C. & XU, Y. 1995. Effect of cement type on chloride binding and corrosion of steel in concrete. *Cement and Concrete Research*, 25, 893-902.
- ATAHAN, H. N. & DIKME, D. 2011. Use of mineral admixtures for enhanced resistance against sulfate attack. *Construction and Building Materials*, 25, 3450-3457.
- BARCELO, L., GARTNER, E., BARBARULO, R., HOSSACK, A., AHANI, R., THOMAS, M., HOOTON, D., BROUARD, E., DELAGRAVE, A. & BLAIR, B. 2014. A modified ASTM C1012 procedure for qualifying blended cements containing limestone and SCMs for use in sulfate-rich environments. *Cement and Concrete Research*, 63, 75-88.
- BARKER, A. P. & HOBBS, D. W. 1999. Performance of Portland limestone cements in mortar prisms immersed in sulfate solutions at 5 °C. *Cement and Concrete Composites*, 21, 129-137.
- BARNETT, S. J., MACPHEE, D. E., LACHOWSKI, E. E. & CRAMMOND, N. J. 2002. XRD, EDX and IR analysis of solid solutions between thaumasite and ettringite. *Cement and Concrete Research*, 32, 719-730.
- BEAUDOIN, J. J., RAMACHANDRAN, V. S. & FELDMAN, R. F. 1990. Interaction of chloride and C · S · H. *Cement and Concrete Research*, 20, 875-883.
- BELLMANN, F., MÖSER, B. & STARK, J. 2006. Influence of sulfate solution concentration on the formation of gypsum in sulfate resistance test specimen. *Cement and Concrete Research*, 36, 358-363.
- BELLMANN, F. & STARK, J. 2007. Prevention of thaumasite formation in concrete exposed to sulphate attack. *Cement and Concrete Research*, 37, 1215-1222.

- BELLMANN, F. & STARK, J. 2008. The role of calcium hydroxide in the formation of thaumasite. *Cement and Concrete Research*, 38, 1154-1161.
- BEN-YAIR, M. 1967 THE DURABILITY OF CEMENT AND CONCRETE IN SEA WATER. *Desalinatan*, 3, 147-154.
- BENSTED, J. 1999. Thaumasite -- background and nature in deterioration of cements, mortars and concretes. *Cement and Concrete Composites*, 21, 117-121.
- BENSTED, J. 2003. Thaumasite--direct, woodfordite and other possible formation routes. *Cement and Concrete Composites*, 25, 873-877.
- BENSTED, J. & SATYA PRAKASH, V. 1976. A discussion of the paper "Thaumasite formation: A cause of deterioration of portland cement and related substances in the presence of sulphates" by J. H. P. Van Aardt and S. Visser. *Cement and Concrete Research*, 6, 321-322.
- BLANCO-VARELA, M. T., AGUILERA, J. & MARTÍNEZ-RAMÍREZ, S. 2006. Effect of cement C3A content, temperature and storage medium on thaumasite formation in carbonated mortars. *Cement and Concrete Research*, 36, 707-715.
- BONEN, D. & COHEN, M. D. 1992. Magnesium sulfate attack on portland cement paste — II. Chemical and mineralogical analyses. *Cement and Concrete Research*, 22, 707-718.
- BROOMFIELD, J. 1997. *Corrosion of steel in concrete understanding, investigation and repair*. London, E & FN SPON.
- BROWN, P., HOOTON, R. D. & CLARK, B. 2004. Microstructural changes in concretes with sulfate exposure. *Cement and Concrete Composites*, 26, 993-999.
- BROWN, P. W., HOOTON, R. D. & CLARK, B. A. 2003. The co-existence of thaumasite and ettringite in concrete exposed to magnesium sulfate at room temperature and the influence of blast-furnace slag substitution on sulfate resistance. *Cement and Concrete Composites*, 25, 939-945.
- BUILDING RESEARCH ESTABLISHMENT. BRE special digest 1: concrete in aggressive ground. 3rd ed. watford: BRE; 2005.
- CHANG, C.-F. & CHEN, J.-W. 2006. The experimental investigation of concrete carbonation depth. *Cement and Concrete Research*, 36, 1760-1767.
- CHENG, T.-P., LEE, J.-T. & TSAI, W.-T. 1990. Corrosion of reinforcements in artificial sea water and concentrated sulfate solution. *Cement and Concrete Research*, 20, 243-252.
- CLAISSE, P. 1988. *The properties and performance of High Strength Silica Fume Concrete*. PhD, Leeds University.
- COLLETT, G., CRAMMOND, N. J., SWAMY, R. N. & SHARP, J. H. 2004. The role of carbon dioxide in the formation of thaumasite. *Cement and Concrete Research*, 34, 1599-1612.
- CRAMMOND, N. 2002. The occurrence of thaumasite in modern construction - a review. *Cement and Concrete Composites*, 24, 393-402.
- CRAMMOND, N. J. 2003. The thaumasite form of sulfate attack in the UK. *Cement and Concrete Composites*, 25, 809-818.
- CRAMMOND, N. J., COLLETT, G. W. & LONGWORTH, T. I. 2003. Thaumasite field trial at Shipston on Stour: three-year preliminary assessment of buried concretes. *Cement and Concrete Composites*, 25, 1035-1043.
- DEHWAH, H. A. F. 2007. Effect of sulfate concentration and associated cation type on concrete deterioration and morphological changes in cement hydrates. *Construction and Building Materials*, 21, 29-39.
- DHIR, R. K., EL-MOHR, M. A. K. & DYER, T. D. 1996. Chloride binding in GGBS concrete. *Cement and Concrete Research*, 26, 1767-1773.
- DHIR, R. K., EL-MOHR, M. A. K. & DYER, T. D. 1997. Developing chloride resisting concrete using PFA. *Cement and Concrete Research*, 27, 1633-1639.

- DHIR, R. K. & JONES, M. R. 1999. Development of chloride-resisting concrete using fly ash. *Fuel*, 78, 137-142.
- DIAMOND, S. 2003. Thaumasite in Orange County, Southern California: an inquiry into the effect of low temperature. *Cement and Concrete Composites*, 25, 1161-1164.
- DUAN, Z. & LI, D. 2008. Coupled phase and aqueous species equilibrium of the H<sub>2</sub>O-CO<sub>2</sub>-NaCl-CaCO<sub>3</sub> system from 0 to 250°C, 1 to 1000bar with NaCl concentrations up to saturation of halite. *Geochimica et Cosmochimica Acta*, 72, 5128-5145.
- EDEN, M. A. 2003. The laboratory investigation of concrete affected by TSA in the UK. *Cement and Concrete Composites*, 25, 847-850.
- EHTESHAM HUSSAIN, S., RASHEEDUZZAFAR & AL-GAHTANI, A. S. 1994. Influence of sulfates on chloride binding in cements. *Cement and Concrete Research*, 24, 8-24.
- EKOLU, S. O., THOMAS, M. D. A. & HOOTON, R. D. 2006. Pessimum effect of externally applied chlorides on expansion due to delayed ettringite formation: Proposed mechanism. *Cement and Concrete Research*, 36, 688-696.
- FREYBURG, E. & BERNINGER, A. M. 2003. Field experiences in concrete deterioration by thaumasite formation: possibilities and problems in thaumasite analysis. *Cement and Concrete Composites*, 25, 1105-1110.
- GARCÍA LODEIRO, I., MACPHEE, D. E., PALOMO, A. & FERNÁNDEZ-JIMÉNEZ, A. 2009. Effect of alkalis on fresh C-S-H gels. FTIR analysis. *Cement and Concrete Research*, 39, 147-153.
- GAZE, M. E. 1997. The effects of varying gypsum content on thaumasite formation in a cement:Lime:Sand mortar at 5 °C. *Cement and Concrete Research*, 27, 259-265.
- GAZE, M. E. & CRAMMOND, N. J. 2000. The formation of thaumasite in a cement:lime:sand mortar exposed to cold magnesium and potassium sulfate solutions. *Cement and Concrete Composites*, 22, 209-222.
- GLASS, G. K. & BUENFELD, N. R. 2000. The influence of chloride binding on the chloride induced corrosion risk in reinforced concrete. *Corrosion Science*, 42, 329-344.
- GLASS, G. K., REDDY, B. & BUENFELD, N. R. 2000. The participation of bound chloride in passive film breakdown on steel in concrete. *Corrosion Science*, 42, 2013-2021.
- GLASSER, F. P., MARCHAND, J. & SAMSON, E. 2008. Durability of concrete — Degradation phenomena involving detrimental chemical reactions. *Cement and Concrete Research*, 38, 226-246.
- GOLLOP, R. S. & TAYLOR, H. F. W. 1992. Microstructural and microanalytical studies of sulfate attack. I. Ordinary portland cement paste. *Cement and Concrete Research*, 22, 1027-1038.
- GOLLOP, R. S. & TAYLOR, H. F. W. 1995. Microstructural and microanalytical studies of sulfate attack III. Sulfate-resisting portland cement: Reactions with sodium and magnesium sulfate solutions. *Cement and Concrete Research*, 25, 1581-1590.
- GOLLOP, R. S. & TAYLOR, H. F. W. 1996. Microstructural and microanalytical studies of sulfate attack. V. Comparison of different slag blends. *Cement and Concrete Research*, 26, 1029-1044.
- GOÑI, S. & GUERRERO, A. 2003. Accelerated carbonation of Friedel's salt in calcium aluminate cement paste. *Cement and Concrete Research*, 33, 21-26.
- HARTSHORN, S. A., SHARP, J. H. & SWAMY, R. N. 1999. Thaumasite formation in Portland-limestone cement pastes. *Cement and Concrete Research*, 29, 1331-1340.

- HARTSHORN, S. A., SHARP, J. H. & SWAMY, R. N. 2002. The thaumasite form of sulfate attack in Portland-limestone cement mortars stored in magnesium sulfate solution. *Cement and Concrete Composites*, 24, 351-359.
- HEINZ, D. & URBONAS, L. 2003. About thaumasite formation in Portland-limestone cement pastes and mortars—effect of heat treatment at 95 °C and storage at 5 °C. *Cement and Concrete Composites*, 25, 961-967.
- HIGGINS, D. D. & CRAMMOND, N. J. 2003. Resistance of concrete containing ggbs to the thaumasite form of sulfate attack. *Cement and Concrete Composites*, 25, 921-929.
- HILL, J., BYARS, E. A., SHARP, J. H., LYNSDALE, C. J., CRIPPS, J. C. & ZHOU, Q. 2003. An experimental study of combined acid and sulfate attack of concrete. *Cement and Concrete Composites*, 25, 997-1003.
- HOBBS, D. W. 2003. Thaumasite sulfate attack in field and laboratory concretes: implications for specifications. *Cement and Concrete Composites*, 25, 1195-1202.
- HOBBS, D. W. & TAYLOR, M. G. 2000. Nature of the thaumasite sulfate attack mechanism in field concrete. *Cement and Concrete Research*, 30, 529-533.
- HONG, S.-Y. & GLASSER, F. P. 2002. Alkali sorption by C-S-H and C-A-S-H gels: Part II. Role of alumina. *Cement and Concrete Research*, 32, 1101-1111.
- IRASSAR, E. F. 2009a. Sulfate attack on cementitious materials containing limestone filler -- A review. *Cement and Concrete Research*, 39, 241-254.
- IRASSAR, E. F. 2009b. Sulfate attack on cementitious materials containing limestone filler — A review. *Cement and Concrete Research*, 39, 241-254.
- IRASSAR, E. F., BONAVENTI, V. L. & GONZÁLEZ, M. 2003. Microstructural study of sulfate attack on ordinary and limestone Portland cements at ambient temperature. *Cement and Concrete Research*, 33, 31-41.
- IRASSAR, E. F., BONAVENTI, V. L., TREZZA, M. A. & GONZÁLEZ, M. A. 2005. Thaumasite formation in limestone filler cements exposed to sodium sulphate solution at 20 °C. *Cement and Concrete Composites*, 27, 77-84.
- JALLAD, K. N., SANTHANAM, M. & COHEN, M. D. 2003. Stability and reactivity of thaumasite at different pH levels. *Cement and Concrete Research*, 33, 433-437.
- JARRAH, N. R., AL-AMOUDI, O. S. B., MASLEHUDDIN, M., ASHIRU, O. A. & AL-MANA, A. I. 1995. Electrochemical behaviour of steel in plain and blended cement concretes in sulphate and/or chloride environments. *Construction and Building Materials*, 9, 97-103.
- JUEL, I., HERFORT, D., GOLLOP, R., KONNERUP-MADSEN, J., JAKOBSEN, H. J. & SKIBSTED, J. 2003. A thermodynamic model for predicting the stability of thaumasite. *Cement and Concrete Composites*, 25, 867-872.
- JUSTNES, H. 2003. Thaumasite formed by sulfate attack on mortar with limestone filler. *Cement and Concrete Composites*, 25, 955-959.
- KAKALI, G., TSIVILIS, S., SKAROPOULOU, A., SHARP, J. H. & SWAMY, R. N. 2003. Parameters affecting thaumasite formation in limestone cement mortar. *Cement and Concrete Composites*, 25, 977-981.
- KANDASAMY, S. & SHEHATA, M. H. 2014. Durability of ternary blends containing high calcium fly ash and slag against sodium sulphate attack. *Construction and Building Materials*, 53, 267-272.
- KAYYALI, O. A. & HAQUE, M. N. 1988. Chloride penetration and the ratio of  $Cl^-/OH^-$  in the pores of cement paste. *Cement and Concrete Research*, 18, 895-900.
- KINOSHITA, H., CIRCHIRILLO, C., SANMARTIN, I., UTTON, C. A., BORGES, P. H. R., LYNSDALE, C. J. & MILESTONE, N. B. 2014. Carbonation of



- composite cements with high mineral admixture content used for radioactive waste encapsulation. *Minerals Engineering*, 59, 107-114.
- KÖHLER, S., HEINZ, D. & URBONAS, L. 2006. Effect of ettringite on thaumasite formation. *Cement and Concrete Research*, 36, 697-706.
- LAWRENCE, C. D. 1992. The influence of binder type on sulfate resistance. *Cement and Concrete Research*, 22, 1047-1058.
- LEE, S. T., HOOTON, R. D., JUNG, H.-S., PARK, D.-H. & CHOI, C. S. 2008. Effect of limestone filler on the deterioration of mortars and pastes exposed to sulfate solutions at ambient temperature. *Cement and Concrete Research*, 38, 68-76.
- LENG, F., FENG, N. & LU, X. 2000. An experimental study on the properties of resistance to diffusion of chloride ions of fly ash and blast furnace slag concrete. *Cement and Concrete Research*, 30, 989-992.
- LIU, J., XING, F., DONG, B., MA, H., PAN, D. Study on the water sorptivity of the surface layer of concrete. *Mater Struct* 2013. DOI 10.1617/s11527-013-0162-x.
- LIU, Z., DENG, D., DE SCHUTTER, G. & YU, Z. 2013. The effect of MgSO<sub>4</sub> on thaumasite formation. *Cement and Concrete Composites*, 35, 102-108.
- LIZARAZO-MARRIAGA, J AND CLAISSE, P. 2009. Determination of the concrete chloride diffusion coefficient based on an electrochemical test and an optimization model. *Materials Chemistry and Physics*.117; 536-543.
- LONGWORTH, T. I. 2003. Contribution of construction activity to aggressive ground conditions causing the thaumasite form of sulfate attack to concrete in pyritic ground. *Cement and Concrete Composites*, 25, 1005-1013.
- LOSER, R., LOTHENBACH, B., LEEMANN, A. & TUCHSCHMID, M. 2010. Chloride resistance of concrete and its binding capacity - Comparison between experimental results and thermodynamic modeling. *Cement and Concrete Composites*, 32, 34-42.
- LOUDON, N. 2003. A review of the experience of thaumasite sulfate attack by the UK Highways Agency. *Cement and Concrete Composites*, 25, 1051-1058.
- LUO, R., CAI, Y., WANG, C. & HUANG, X. 2003. Study of chloride binding and diffusion in GGBS concrete. *Cement and Concrete Research*, 33, 1-7.
- MACPHEE, D. & DIAMOND, S. 2003. Thaumasite in Cementitious Materials. *Cement and Concrete Composites*, 25, 805-807.
- MANGAT, P. S. & MOLLOY, B. T. 1991. Influence of PFA, slag and microsilica on chloride induced corrosion of reinforcement in concrete. *Cement and Concrete Research*, 21, 819-834.
- MARTINEZ-RAMIREZ, S., BLANCO-VARELA, M. T. & RAPAZOTE, J. 2011. Thaumasite formation in sugary solutions: Effect of temperature and sucrose concentration. *Construction and Building Materials*, 25, 21-29.
- MEHTA, P. K. 1983. Mechanism of sulfate attack on portland cement concrete — Another look. *Cement and Concrete Research*, 13, 401-406.
- MEHTA, P. K. & GJØRV, O. E. 1982. Properties of portland cement concrete containing fly ash and condensed silica-fume. *Cement and Concrete Research*, 12, 587-595.
- MEHTA, P. K., MONTEIRO, P.J.M. 2006 *Concrete: Microstructure, Properties and materials*, McGraw-Hill.
- MOHAMMED, T. U. & HAMADA, H. 2003. Relationship between free chloride and total chloride contents in concrete. *Cement and Concrete Research*, 33, 1487-1490.
- MORRIS, W., VICO, A., VAZQUEZ, M. & DE SANCHEZ, S. R. 2002. Corrosion of reinforcing steel evaluated by means of concrete resistivity measurements. *Corrosion Science*, 44, 81-99.

- MOUKWA, M. 1989. Penetration of chloride ions from sea water into mortars under different exposure conditions. *Cement and Concrete Research*, 19, 894-904.
- MULENGA, D. M., STARK, J. & NOBST, P. 2003. Thaumasite formation in concrete and mortars containing fly ash. *Cement and Concrete Composites*, 25, 907-912.
- NAGATAKI, S., OTSUKI, N., WEE, T.H., NAKASHITA, K. 1993. Condensation of chloride ion in hardened cement matrix materials and on embedded steel bars. *ACI Material* 90, 323-32.
- NEVILLE, A. 1995. *Properties of the concrete*, Edinburgh Gate Harkow Essex, PERSON-Prentice Hall.
- NOBST, P. & STARK, J. 2003. Investigations on the influence of cement type on thaumasite formation. *Cement and Concrete Composites*, 25, 899-906.
- PAGE, C. L., SHORT, N. R. & HOLDEN, W. R. 1986. The influence of different cements on chloride-induced corrosion of reinforcing steel. *Cement and Concrete Research*, 16, 79-86.
- PIPILIKAKI, P., PAPAGEORGIOU, D., DIMITROULA, M., CHANIOTAKIS, E. & KATSIOTI, M. 2009. Microstructure changes in mortars attacked by sulphates at 5 °C. *Construction and Building Materials*, 23, 2259-2264.
- PIPILIKAKI, P., PAPAGEORGIOU, D., TEAS, C., CHANIOTAKIS, E. & KATSIOTI, M. 2008. The effect of temperature on thaumasite formation. *Cement and Concrete Composites*, 30, 964-969.
- POUYA, H. S. 2007. *Thaumasite Sulfate Attack (TSA) of Concrete in Aggressive Ground at Different Temperatures*. PhD thesis, The University of Sheffield.
- RAMEZANIANPOUR, A. M. & HOOTON, R. D. 2013. Thaumasite sulfate attack in Portland and Portland-limestone cement mortars exposed to sulfate solution. *Construction and Building Materials*, 40, 162-173.
- SAIKIA, N., KATO, S. & KOJIMA, T. 2006. Thermogravimetric investigation on the chloride binding behaviour of MK-lime paste. *Thermochimica Acta*, 444, 16-25.
- SAKR, K. 2005. Effect of cement type on the corrosion of reinforcing steel bars exposed to acidic media using electrochemical techniques. *Cement and Concrete Research*, 35, 1820-1826.
- SALEEM, M., SHAMEEM, M., HUSSAIN, S. E. & MASLEHUDDIN, M. 1996. Effect of moisture, chloride and sulphate contamination on the electrical resistivity of Portland cement concrete. *Construction and Building Materials*, 10, 209-214.
- SANTHANAM, M., COHEN, M. & OLEK, J. 2006. Differentiating seawater and groundwater sulfate attack in Portland cement mortars. *Cement and Concrete Research*, 36, 2132-2137.
- SANTHANAM, M., COHEN, M. D. & OLEK, J. 2001. Sulfate attack research — whither now? *Cement and Concrete Research*, 31, 845-851.
- SCHMIDT, T., LOTHENBACH, B., ROMER, M., NEUENSCHWANDER, J. & SCRIVENER, K. 2009. Physical and microstructural aspects of sulfate attack on ordinary and limestone blended Portland cements. *Cement and Concrete Research*, 39, 1111-1121.
- SCHMIDT, T., LOTHENBACH, B., ROMER, M., SCRIVENER, K., RENTSCH, D. & FIGI, R. 2008. A thermodynamic and experimental study of the conditions of thaumasite formation. *Cement and Concrete Research*, 38, 337-349.
- SIMS, I. & HUNTLEY, S. A. 2004. The thaumasite form of sulfate attack-breaking the rules. *Cement and Concrete Composites*, 26, 837-844.
- SKAROPOULOU, A., KAKALI, G. & TSIVILIS, S. 2012. Thaumasite form of sulfate attack in limestone cement concrete: The effect of cement

- composition, sand type and exposure temperature. *Construction and Building Materials*, 36, 527-533.
- SKAROPOULOU, A., KAKALI, G., TSIVILIS, S. 2006. A STUDY ON THAUMASITE FORM OF SULFATE ATTACK (TSA) USING XRD, TG AND SEM. *Journal of Thermal Analysis and Calorimetry*, 84, 135-139.
- SKAROPOULOU, A., SOTIRIADIS, K., KAKALI, G. & TSIVILIS, S. 2013. Use of mineral admixtures to improve the resistance of limestone cement concrete against thaumasite form of sulfate attack. *Cement and Concrete Composites*, 37, 267-275.
- SKAROPOULOU, A., TSIVILIS, S., KAKALI, G., SHARP, J. H. & SWAMY, R. N. 2009. Thaumasite form of sulfate attack in limestone cement mortars: A study on long term efficiency of mineral admixtures. *Construction and Building Materials*, 23, 2338-2345.
- SLATER, D., FLOYD, M. & WIMPENNY, D. E. 2003. A summary of the Highways Agency Thaumasite Investigation in Gloucestershire: the scope of work and main findings. *Cement and Concrete Composites*, 25, 1067-1076.
- SOTIRIADIS, K., NIKOLOPOULOU, E. & TSIVILIS, S. 2012. Sulfate resistance of limestone cement concrete exposed to combined chloride and sulfate environment at low temperature. *Cement and Concrete Composites*, 34, 903-910.
- SOTIRIADIS, K., NIKOLOPOULOU, E., TSIVILIS, S., PAVLOU, A., CHANIOTAKIS, E. & SWAMY, R. N. 2013. The effect of chlorides on the thaumasite form of sulfate attack of limestone cement concrete containing mineral admixtures at low temperature. *Construction and Building Materials*, 43, 156-164.
- SOTIRIADIS, K., TSIVILIS, T., KOSÍKOVÁ, J., PETRÁNEK, V. 2013. Long Term Behaviour of Portland Limestone Cement Concrete Exposed to Combined Chloride and Sulfate Environment. The Effect of Limestone Content and Mineral Admixtures *Advanced Materials Research* 688, 185-192.
- STARK, D. C. 2003. Occurrence of thaumasite in deteriorated concrete. *Cement and Concrete Composites*, 25, 1119-1121.
- THAUMASITE EXPERT GROUP. The thaumasite form of sulfate attack: risks, diagnosis, remedial work and guidance on new construction, department of the environment, transport and the regions, london, 1999 (January).
- THOMAS, M. D. A. & MATTHEWS, J. D. 2004. Performance of pfa concrete in a marine environment--10-year results. *Cement and Concrete Composites*, 26, 5-20.
- THOMAS, M. D. A., ROGERS, C. A. & BLESZYNSKI, R. F. 2003. Occurrences of thaumasite in laboratory and field concrete. *Cement and Concrete Composites*, 25, 1045-1050.
- TORRES, S. M. 2004. *The influence of chloride on the thaumasite form of sulfate attack in mortars containing calcium carbonate. PhD thesis*, University of Sheffield.
- TORRES, S. M., KIRK, C. A., LYNSDALE, C. J., SWAMY, R. N. & SHARP, J. H. 2004. Thaumasite-ettringite solid solutions in degraded mortars. *Cement and Concrete Research*, 34, 1297-1305.
- TORRES, S. M., LYNSDALE, C. J., SWAMY, R. N. & SHARP, J. H. 2006. Microstructure of 5-year-old mortars containing limestone filler damaged by thaumasite. *Cement and Concrete Research*, 36, 384-394.
- TORRES, S. M., SHARP, J. H., SWAMY, R. N., LYNSDALE, C. J. & HUNTLEY, S. A. 2003. Long term durability of Portland-limestone cement mortars exposed to magnesium sulfate attack. *Cement and Concrete Composites*, 25, 947-954.

- TOSUN-FELEKOĞLU, K. 2012. The effect of C3A content on sulfate durability of Portland limestone cement mortars. *Construction and Building Materials*, 36, 437-447.
- TSIVILIS, S., KAKALI, G., SKAROPOULOU, A., SHARP, J. H. & SWAMY, R. N. 2003. Use of mineral admixtures to prevent thaumasite formation in limestone cement mortar. *Cement and Concrete Composites*, 25, 969-976.
- VEIGA, K. K. & GASTALDINI, A. L. G. 2012. Sulfate attack on a white Portland cement with activated slag. *Construction and Building Materials*, 34, 494-503.
- VERDIER, J., CARCASSÈS, M. & OLLIVIER, J. P. 2002. Modelling of a gas flow measurement: Application to nuclear containment vessels. *Cement and Concrete Research*, 32, 1331-1340.
- VUK, T., GABROVSEK, R. & KAUCIC, V. 2002. The influence of mineral admixtures on sulfate resistance of limestone cement pastes aged in cold MgSO<sub>4</sub> solution. *Cement and Concrete Research*, 32, 943-948.
- WIMPENNY, D. & SLATER, D. 2003. Evidence from the highways agency thaumasite investigation in Gloucestershire to support or contradict postulated mechanisms of thaumasite formation (TF) and thaumasite sulfate attack (TSA). *Cement and Concrete Composites*, 25, 879-888.
- XU, J., ZHANG, C., JIANG, L., TANG, L., GAO, G. & XU, Y. 2013. Releases of bound chlorides from chloride-admixed plain and blended cement pastes subjected to sulfate attacks. *Construction and Building Materials*, 45, 53-59.
- XU, Y. 1997. The influence of sulphates on chloride binding and pore solution chemistry. *Cement and Concrete Research*, 27, 1841-1850.
- YUAN, Q., SHI, C., DE SCHUTTER, G., AUDENAERT, K. & DENG, D. 2009. Chloride binding of cement-based materials subjected to external chloride environment - A review. *Construction and Building Materials*, 23, 1-13.
- ZHANG, M., CHEN, J., LV, Y., WANG, D. & YE, J. 2013. Study on the expansion of concrete under attack of sulfate and sulfate-chloride ions. *Construction and Building Materials*, 39, 26-32.
- ZHOU, Q., HILL, J., BYARS, E. A., CRIPPS, J. C., LYNSDALE, C. J. & SHARP, J. H. 2006. The role of pH in thaumasite sulfate attack. *Cement and Concrete Research*, 36, 160-170.
- ZUQUAN, J., WEI, S., YUNSHENG, Z., JINYANG, J. & JIANZHONG, L. 2007. Interaction between sulfate and chloride solution attack of concretes with and without fly ash. *Cement and Concrete Research*, 37, 1223-1232.

## Appendix

**Table A. 1.** Concentrations of SO<sub>4</sub>, Cl, Mg and Ca in test solutions of combined CEMI and CEMI-LF specimens at 5°C.

| Test solutions                          | Tem. (°C) | Exposure period (Months) | Ion Concentration (mg/l)<br>(At the end of exposure periods) |                 |       |      |
|---|-----------|--------------------------|--|-----------------|-------|------|
|   |           |                          | Cl   | SO <sub>4</sub> | Mg    | Ca   |
| S                                       | 5         | 3                        | 61.5   | 4995.4          | 1372  | 49.1 |
| S5                                      |           |                          | 3315.2   | 5194.4          | 1070  | 22.9 |
| S10                                     |           |                          | 6607.0   | 4997.1          | 722   | 18.1 |
| S20                                     |           |                          | 15590.2  | 5045.2          | 928.7 | 13.5 |
| <b>Solution renewal after 3 months</b>  |           |                          |  |                 |       |      |
| S                                       |           | 6                        | 75.31  | 4815.9          | 1415  | 94.6 |
| S5                                      |           |                          | 3184.3   | 4435.9          | 1246  | 19.8 |
| S10                                     |           |                          | 8229.5   | 5335.5          | 1335  | 22.3 |
| S20                                     |           |                          | 16888.3  | 5466.6          | 1447  | 27.9 |
| <b>Solution renewal after 6 months</b>  |           |                          |  |                 |       |      |
| S                                       |           | 9                        | 74.0   | 4530.8          | 1349  | 92.9 |
| S5                                      |           |                          | 3232.9   | 4200.3          | 1420  | 35.7 |
| S10                                     |           |                          | 4034.2   | 4980.3          | 1484  | 15.2 |
| S20                                     |           |                          | 15844.7  | 5087.3          | 1566  | 31.1 |
| <b>Solution renewal after 9 months</b>  |           |                          |  |                 |       |      |
| S                                       |           | 12                       | 35.1   | 4548.5          | 1304  | 129  |
| S5                                      |           |                          | 3942.2   | 4406.4          | 1119  | 170  |
| S10                                     |           |                          | 4055.5   | 4840.3          | 1387  | 30.3 |
| S20                                     |           |                          | 15943.3  | 5027.1          | 1462  | 40.2 |
| <b>Solution renewal after 12 months</b> |           |                          |  |                 |       |      |
| S                                       | 18        | 49.6                     | 3536.4   | 890.2           | 224   |      |
| S5                                      |           | 4246.8                   | 3243.1   | 353.7           | 802   |      |
| S10                                     |           | 7930.2                   | 4985.7   | 1623            | 38.8  |      |
| S20                                     |           | 14194.2                  | 5017.4   | 1583            | 49.4  |      |

**Table A. 2.** Concentrations of SO<sub>4</sub>, Cl, Mg and Ca in test solutions of combined CEMI and CEMI-LF specimens at 20°C.

| Test solutions                         | Tem. (°C) | Exposure period (Months) | Ion Concentration (mg/l)<br>(At the end of exposure periods) |                 |        |       |
|--|-----------|--------------------------|--|-----------------|--------|-------|
|  |           |                          | Cl   | SO <sub>4</sub> | Mg     | Ca    |
| S                                      | 20        | 3                        | 65.0   | 5248.8          | 1432.4 | 40.3  |
| S5                                     |           |                          | 3017.6   | 5036.8          | 1012.5 | 27.1  |
| S10                                    |           |                          | 6607.0   | 4997.1          | 722.0  | 18.1  |
| S20                                    |           |                          | 15890.3  | 5245.5          | 966.2  | 18.7  |
| <b>Solution renewal after 3 months</b> |           |                          |  |                 |        |       |
| S                                      |           | 6                        | 63.0   | 5305.4          | 1487.2 | 96.2  |
| S5                                     |           |                          | 3982.3   | 5699.4          | 1524.6 | 42.0  |
| S10                                    |           |                          | 8551.5   | 5617.3          | 1378.5 | 21.5  |
| S20                                    |           |                          | 17787.8  | 5846.2          | 1507.3 | 39.5  |
| <b>Solution renewal after 6 months</b> |           |                          |  |                 |        |       |
| S                                      |           | 9                        | 78.1   | 5150.6          | 1627.1 | 122.1 |
| S5                                     |           |                          | 4034.9   | 5481.0          | 1638.4 | 50.0  |
| S10                                    |           |                          | 8661.1   | 5531.1          | 1622.9 | 33.5  |
| S20                                    |           |                          | 16609.5  | 4994.6          | 1496.8 | 33.1  |
| <b>Solution renewal after 9 months</b> |           |                          |  |                 |        |       |
| S                                      |           | 12                       | 31.4   | 5101.6          | 1466.6 | 109.7 |
| S5                                     |           |                          | 3878.9   | 5028.4          | 1463.1 | 56.2  |
| S10                                    |           |                          | 8073.1   | 5727.6          | 1573.8 | 33.1  |
| S20                                    |           |                          | 16702.4  | 5321.3          | 1508.1 | 28.2  |

**Table A. 3.** Concentrations of SO<sub>4</sub>, Cl, Mg and Ca in test solutions after 180 days exposure of 20mm mortars at 5°C.

| Test solutions | Tem. (°C) | Binder    | Ion Concentration (mg/l) |                 |        |        |
|----------------|-----------|-----------|--------------------------|-----------------|--------|--------|
|                |           |           | Cl                       | SO <sub>4</sub> | Mg     | Ca     |
| S              | 5         | CEMI      | 42.4                     | 867.6           | 1.0    | 796.1  |
| S5             |           |           | 4629.5                   | 1354.2          | 0      | 1409.9 |
| S10            |           |           | 9375.6                   | 1237.5          | 0      | 2163.4 |
| S20            |           |           | 15982.8                  | 2818.1          | 0      | 1441.8 |
| S              |           | CEMI-LF   | 21.9                     | 778.6           | 0.9    | 878.7  |
| S5             |           |           | 5366.3                   | 905.2           | 0      | 1803.1 |
| S10            |           |           | 9367.7                   | 1110.6          | 0.9    | 1842.1 |
| S20            |           |           | 15960.6                  | 2361            | 0      | 1493.4 |
| S              |           | CEMI-PFA  | 25.4                     | 3113.6          | 713.7  | 505.2  |
| S5             |           |           | 3459.9                   | 4623.5          | 1603.1 | 61.7   |
| S20            |           |           | 16618.3                  | 5128.1          | 1526.8 | 60.0   |
| S              |           | CEMI-GGBS | 17.6                     | 2705.5          | 554.9  | 601.9  |
| S5             |           |           | 3977.7                   | 2835.1          | 294.1  | 841.1  |
| S20            |           |           | 16186.1                  | 4461.7          | 589.9  | 821.3  |

**Table A. 4.** Concentrations of SO<sub>4</sub>, Cl, Mg and Ca in test solutions after 180 days exposure of 20mm mortars at 20°C.

| Test solutions | Tem. (°C) | Binder    | Ion Concentration (mg/l) |                 |         |       |
|----------------|-----------|-----------|--------------------------|-----------------|---------|-------|
|                |           |           | Cl                       | SO <sub>4</sub> | Mg      | Ca    |
| S              | 20        | CEMI      | 33.5                     | 4197.0          | 24.8    | 29.3  |
| S5             |           |           | 3386.0                   | 4941.0          | 3167.3  | 29.3  |
| S10            |           |           | 8051.0                   | 5310.0          | 6532.0  | 44    |
| S20            |           |           | 16460.5                  | 4650.6          | 13418.6 | 60.8  |
| S              |           | CEMI-LF   | 20.2                     | 4522.0          | 1729.4  | 55.7  |
| S5             |           |           | 3688.7                   | 5160.6          | 1593.8  | 51.1  |
| S10            |           |           | 8655.8                   | 5433.6          | 1544.5  | 40.6  |
| S20            |           |           | 17461.8                  | 5638.5          | 1235.5  | 46.0  |
| S              |           | CEMI-PFA  | 27.5                     | 4872.1          | 1855.3  | 62.3  |
| S5             |           |           | 4540.7                   | 5354.6          | 1815.5  | 43.6  |
| S20            |           |           | 17999.7                  | 5555.5          | 1792.3  | 78.6  |
| S              |           | CEMI-GGBS | 36.3                     | 3050.4          | 608.5   | 635.8 |
| S5             |           |           | 4472.7                   | 3807.8          | 544.7   | 853   |
| S20            |           |           | 16603.4                  | 4795.7          | 527.2   | 940.6 |



CEMI-LF



CEMI



PFA



GGBS

**Figure A 1.** Photos of phenolphthalein treated mortars.



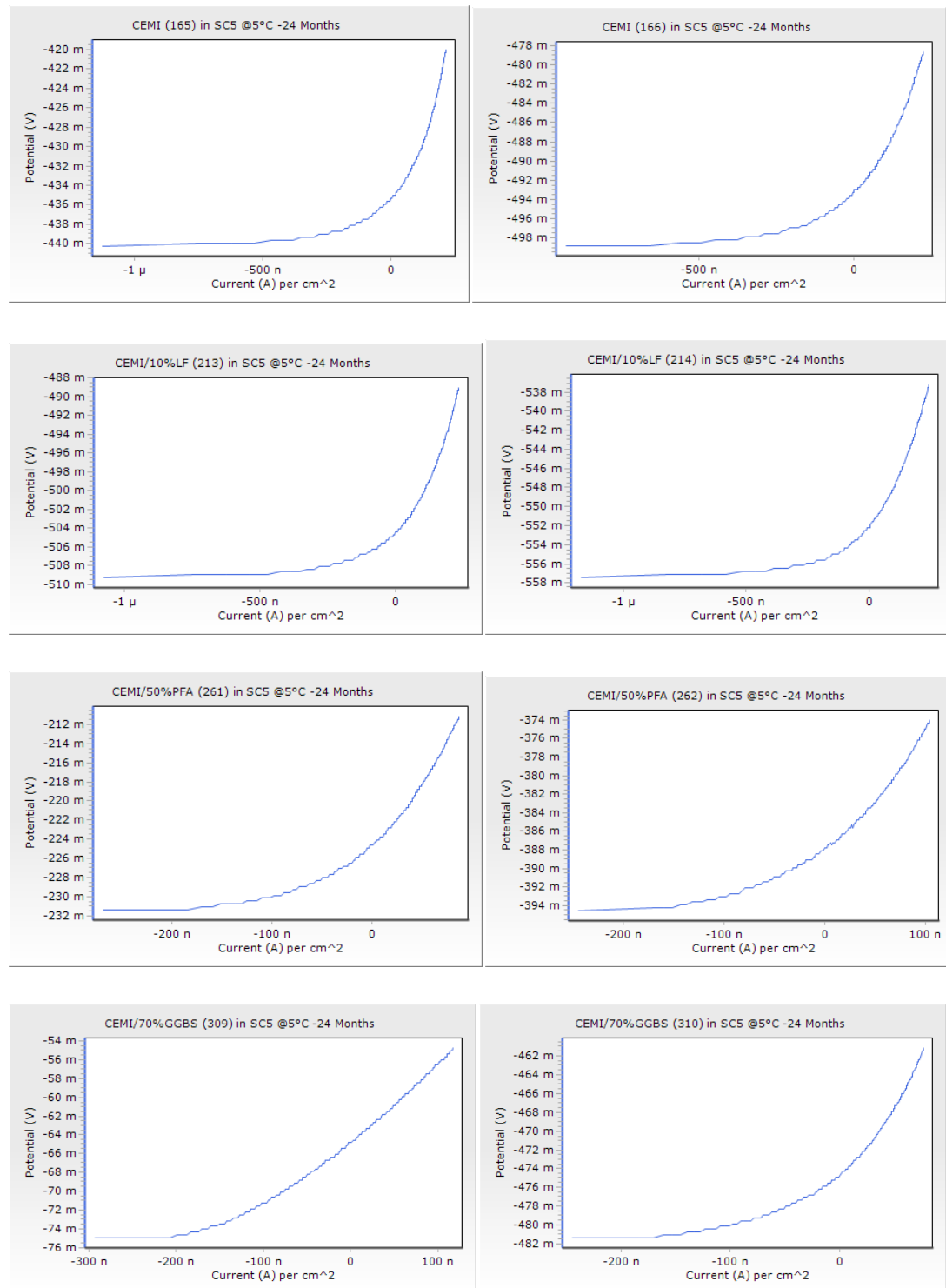


**Figure A 2.** Polarisation curves after 720 days of storage in SC5 at 5°C.

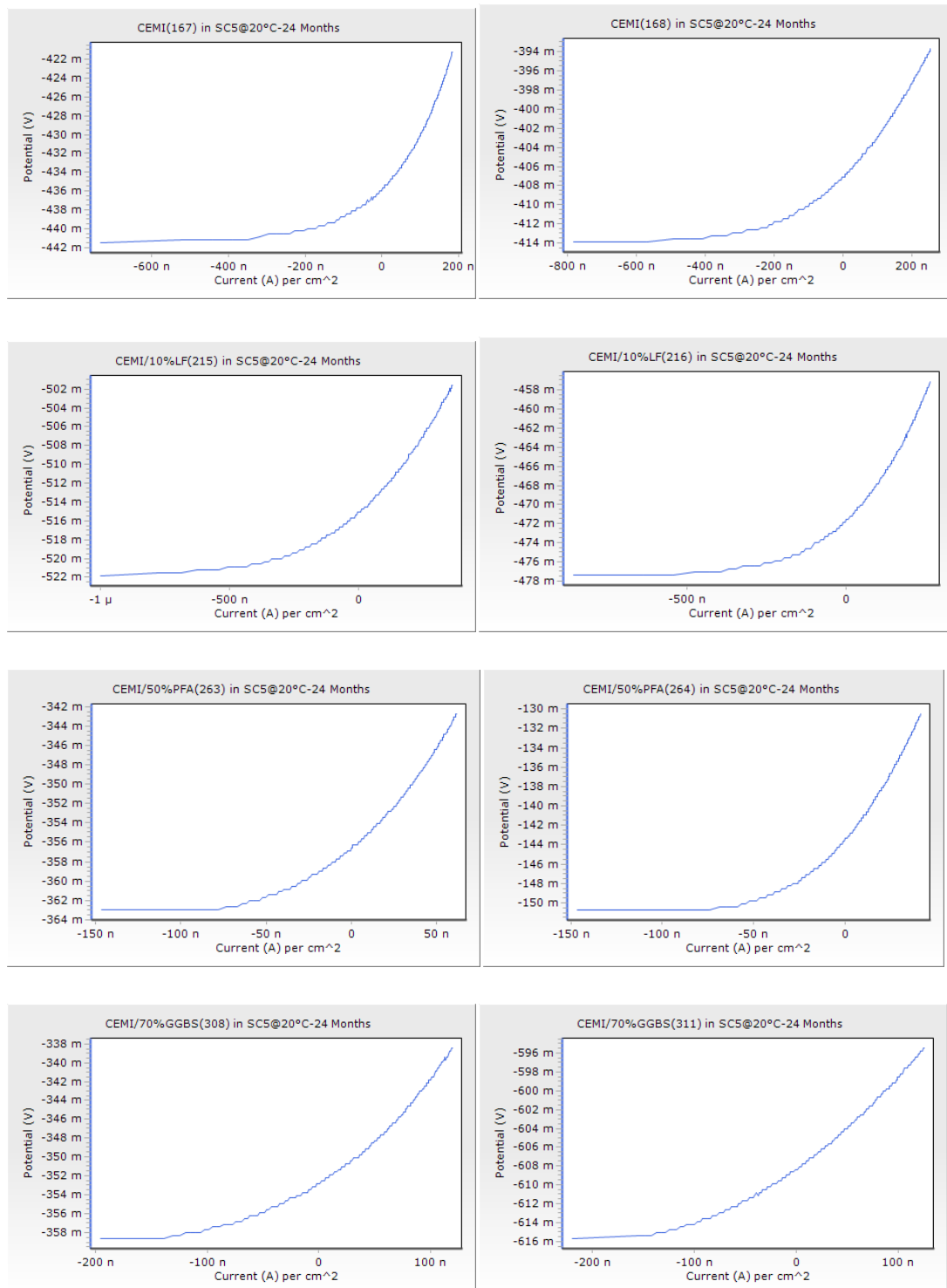


**Figure A 3.** Polarisation curves after 720 days of storage in SC5 at 20°C.

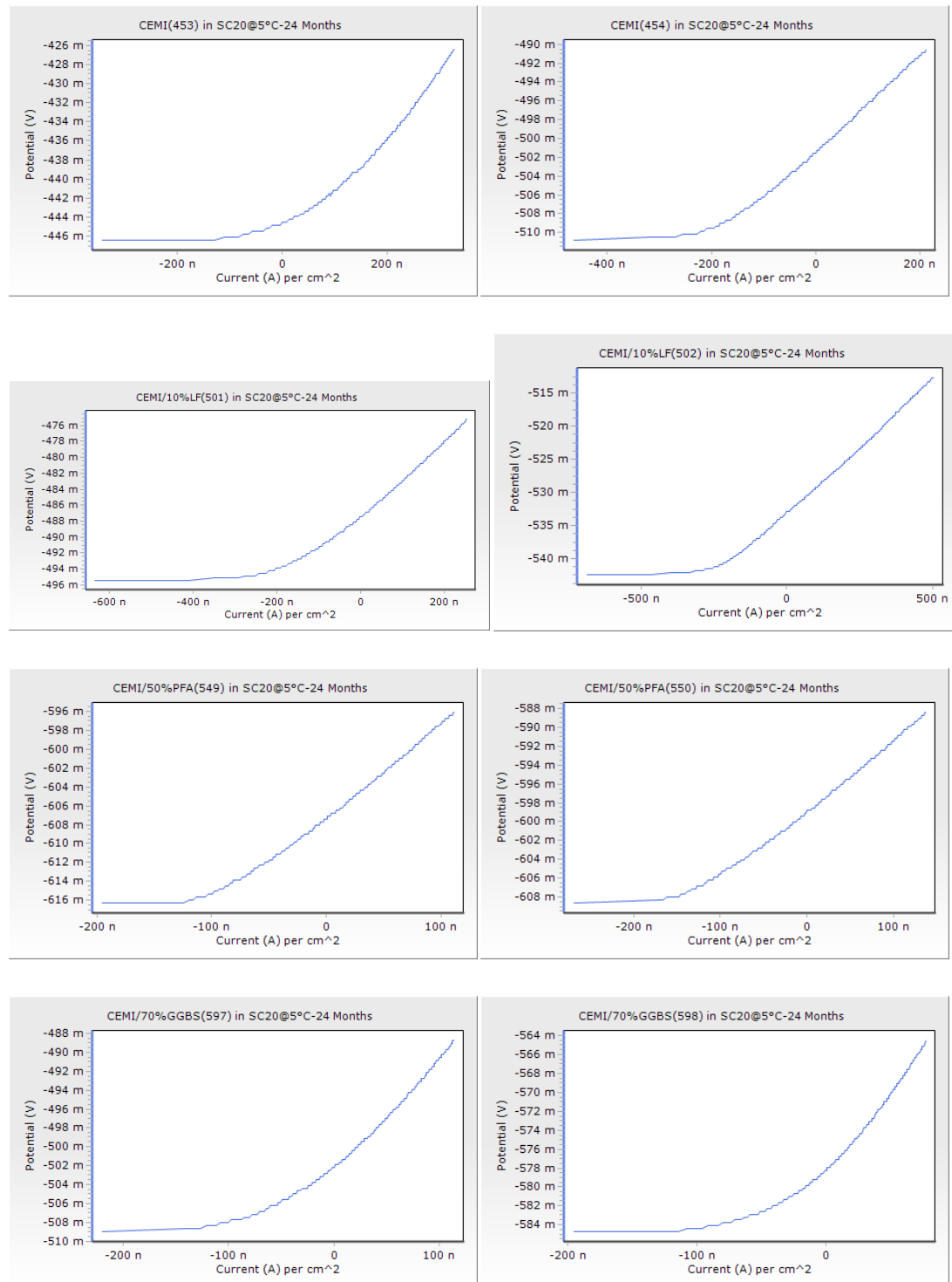


**Figure A 4.** Polarisation curves after 720 days of storage in SC20 at 5°C.

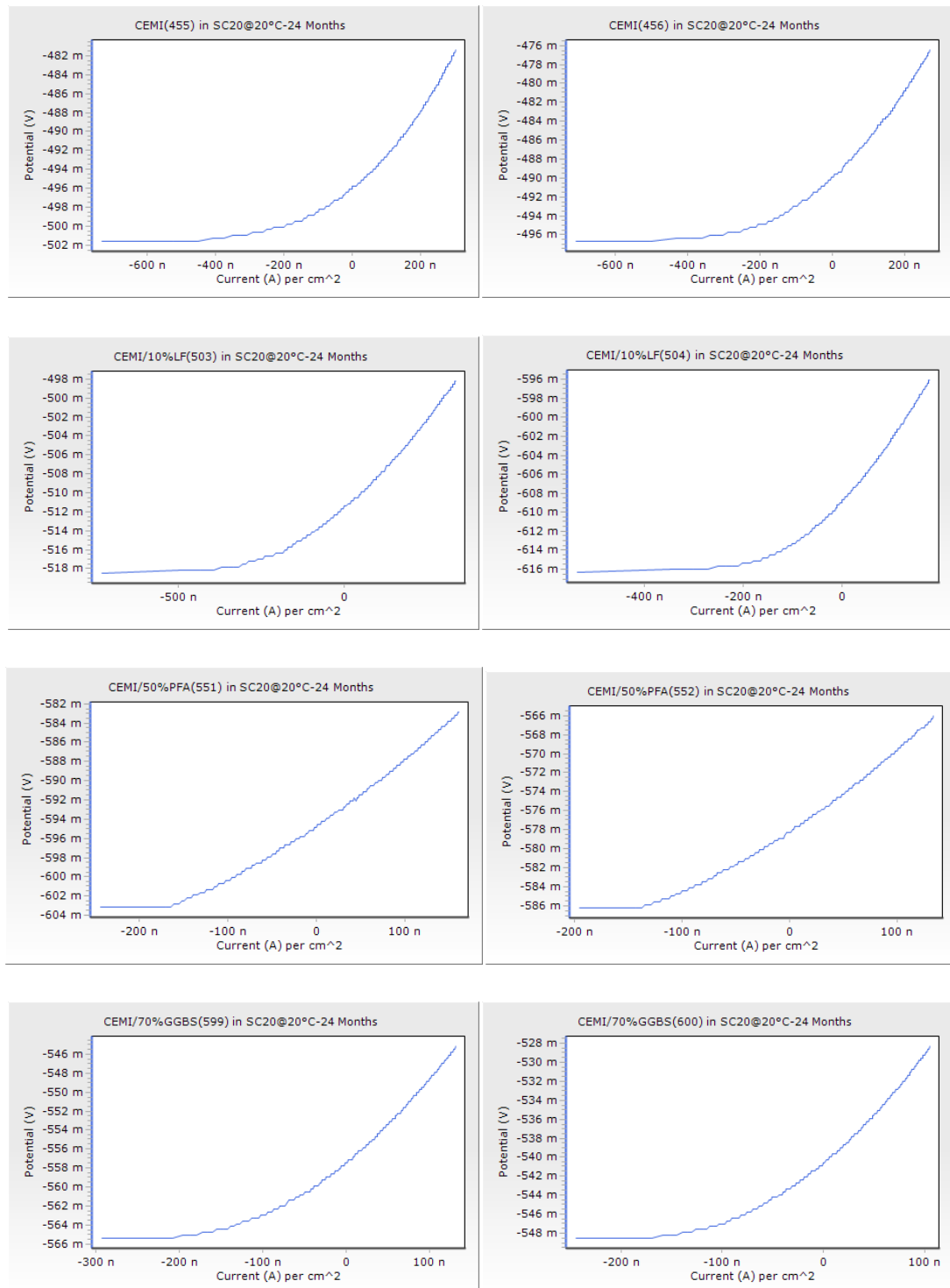


**Figure A 5.** Polarisation curves after 720 days of storage in SC20 at 20°C.

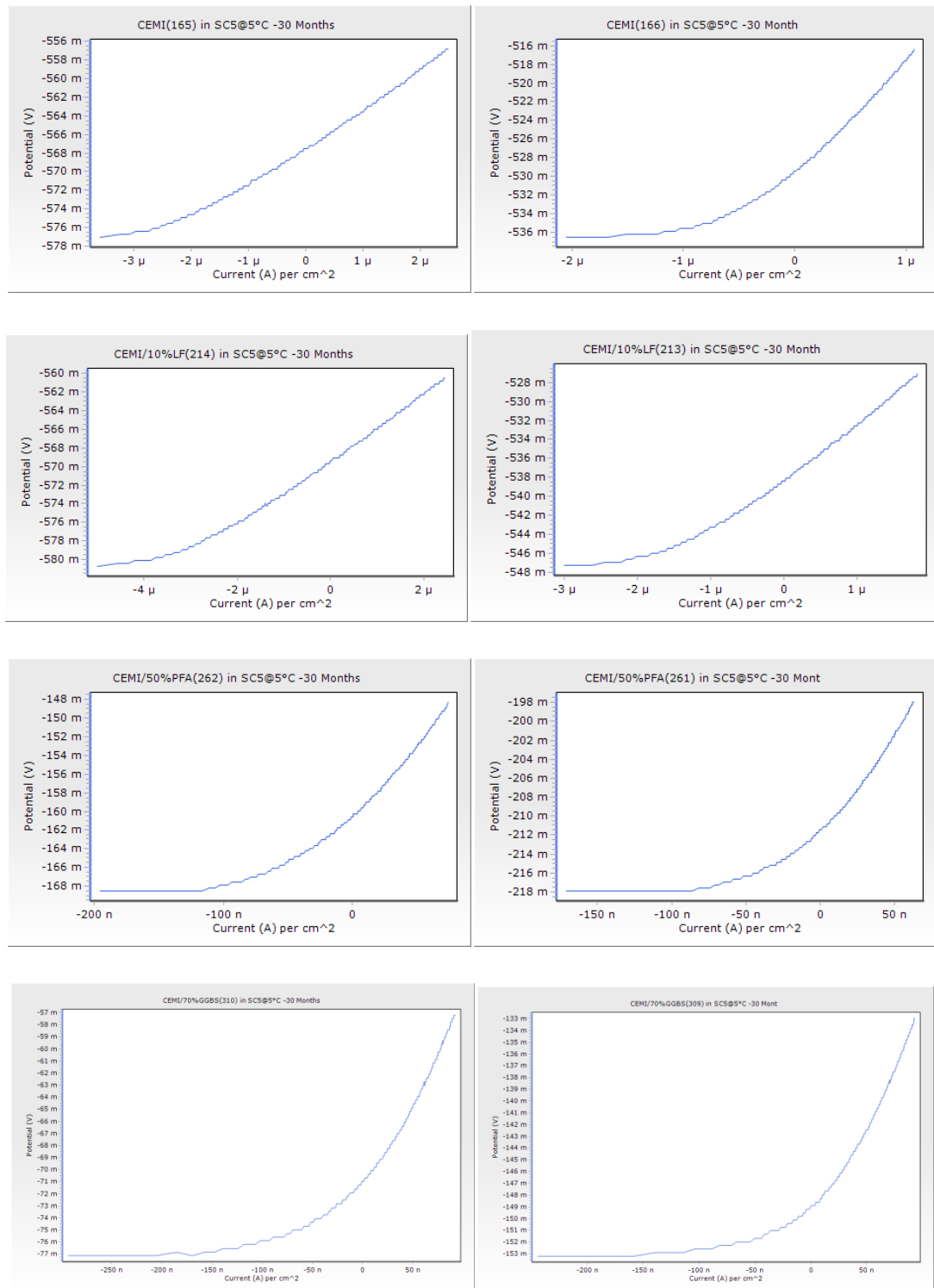


**Figure A 6.** Polarisation curves after 900 days of storage in SC5 at 5°C.

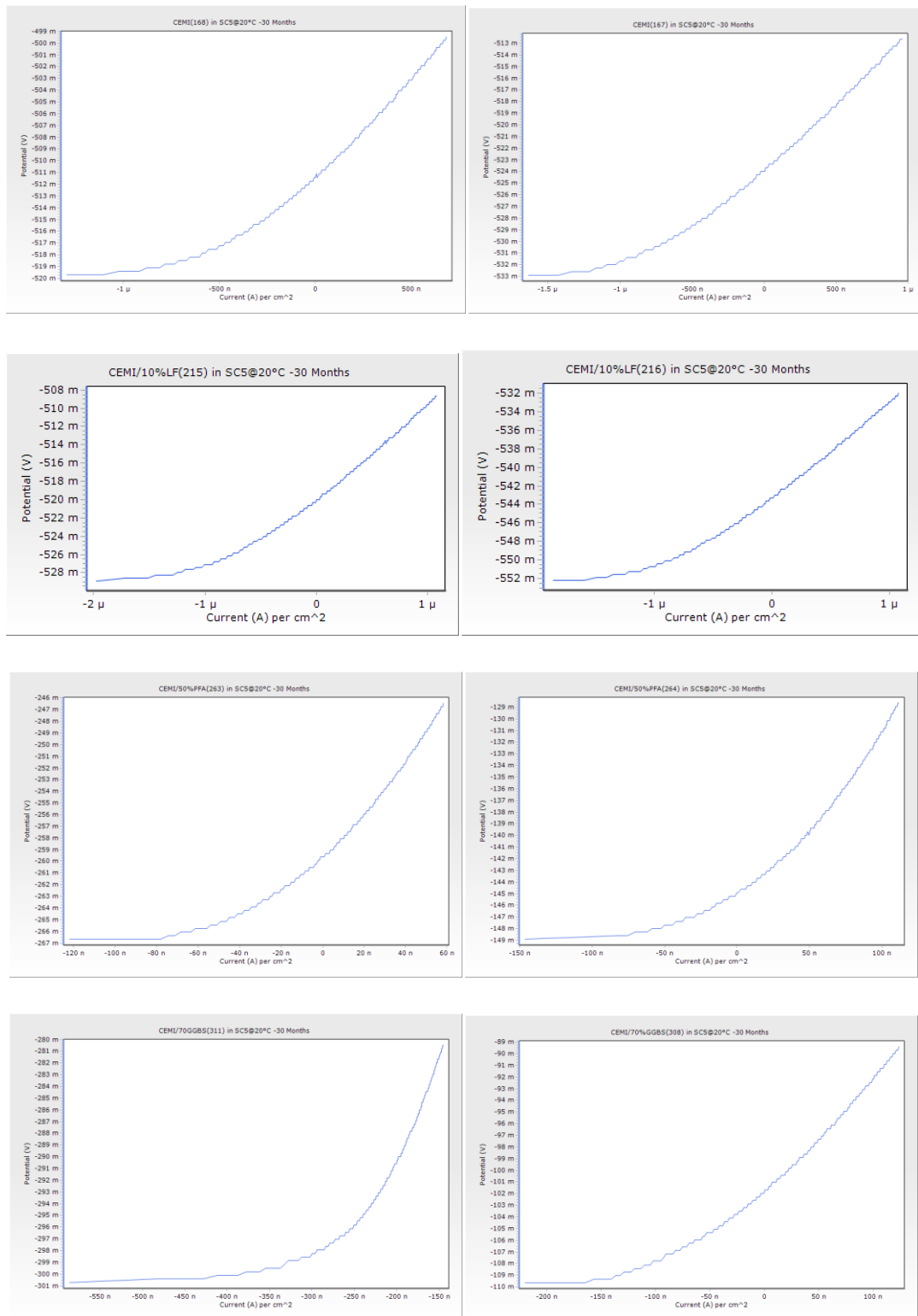


**Figure A 7.** Polarisation curves after 900 days of storage in SC5 at 20°C.

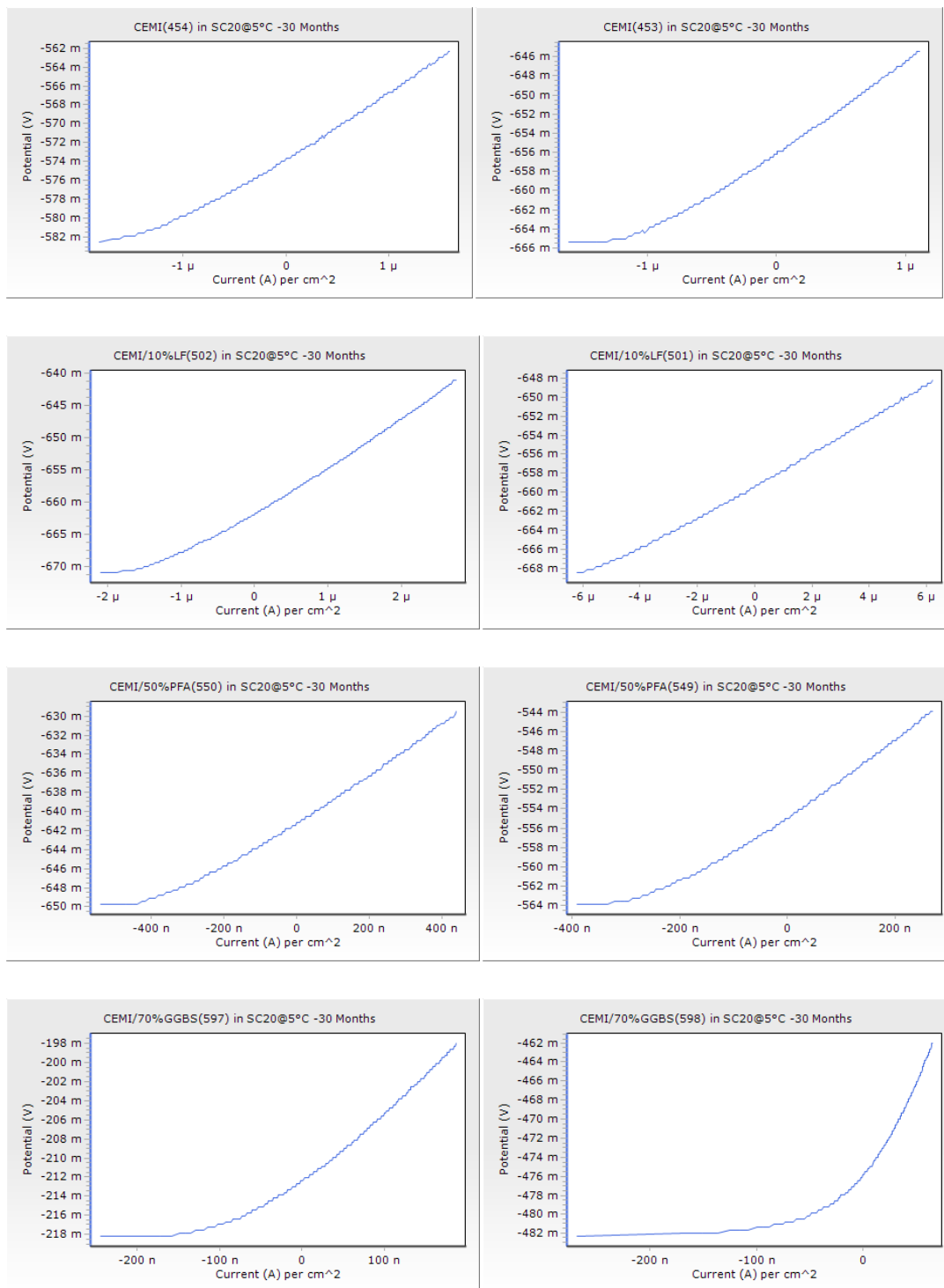


**Figure A 8.** Polarisation curves after 900 days of storage in SC20 at 5°C.

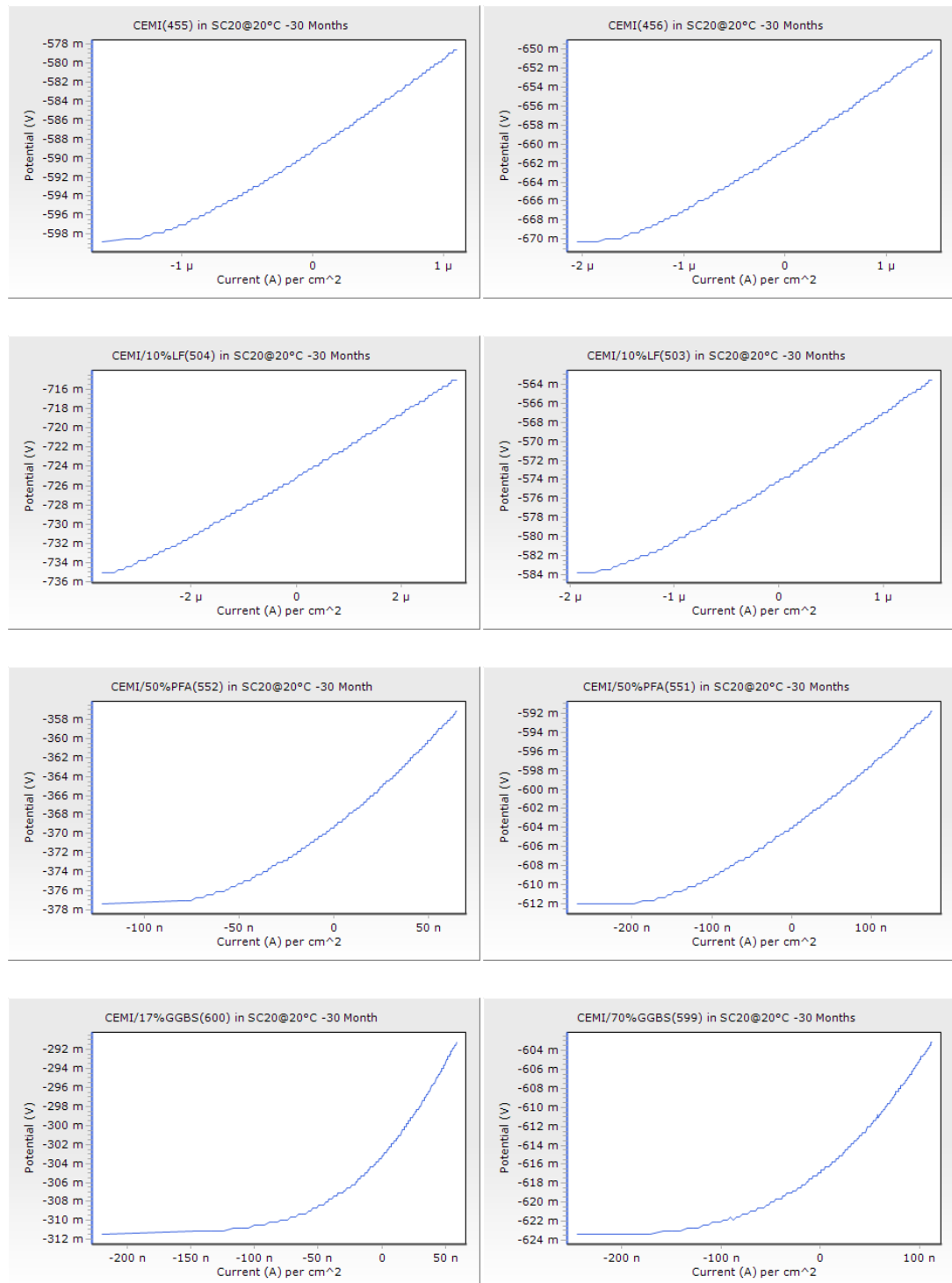


**Figure A 9.** Polarisation curves after 900 days of storage in SC20 at 20°C.